R&D 5003-AN-01

(2)

BASIC MECHANISMS OF DIESEL LUBRICATION CORRELATION OF BENCH AND ENGINE TESTS

Contract No. DAJA 45 85 C0007

Final Report

for

Department of the Army
United States Army Research Development and Standardization Group UK
Edison House, 223 Old Marylebone Road, London NW1 5TH

*****

A F Alliston-Greiner

Dr J A Greenwood

D Cameron

Professor A Cameron
Principal Investigator

March 1991

REPORT DOCUMENTATION PAGE

OMB No 0704-0188
Exp Date Jun 30 1935

1a REPORT SECURITY CLASSIFICATION Unclassified	1b RESTRICTIVE MARKINGS
2a SECURITY CLASSIFICATION AUTHORITY	3 DISTRIBUTION/AVAILABILITY OF REPORT Approved for public release; distribution unlimited
2b DECLASSIFICATION/DOWNGRADING SCHEDULE	
4 PERFORMING ORGANIZATION REPORT NUMBER(S) –	5 MONITORING ORGANIZATION REPORT NUMBER(S) R&D 5305-AN-01
6a NAME OF PERFORMING ORGANIZATION Pembroke College University of Cambridge 6b OFFICE SYMBOL (If applicable)	7a NAME OF MONITORING ORGANIZATION European Research Office USARDSG-UK
6c ADDRESS (City, State, and ZIP Code) Cambridge, CB2 1RF	7b ADDRESS (City, State, and ZIP Code) Box 65 FPO NY 09510-1500
8a NAME OF FUNDING/SPONSORING ORGANIZATION European Research Office USARDSG-UK AR0-E 8b OFFICE SYMBOL (If applicable)	9 PROCUREMENT INSTRUMENT IDENTIFICATION NUMBER 0AJA45-86-C-0007
8c ADDRESS (City, State, and ZIP Code) Box 65 FPO NY 09510-1500	10 SOURCE OF FUNDING NUMBERS PROGRAM ELEMENT NO: 61102A PROJECT NO: 1L161102BH57 TASK NO: 06 WORK UNIT ACCESSION NO: AR
11 TITLE (Include Security Classification) (U) Basic Mechanisms of Diesel Lubrication - Correlation of Bench and Engine Tests	
12 PERSONAL AUTHOR(S) Professor A. Cameron Dr J.A. Greenwood	
13a TYPE OF REPORT FINAL 13b TIME COVERED FROM Dec 85 TO Jan 91 14 DATE OF REPORT (Year, Month, Day) 91 MAR 25 15 PAGE COUNT 226	
16 SUPPLEMENTARY NOTATION	

17 COSATI CODES		
FIELD	GROUP	SUB-GROUP
11	08	
21	07	

18 SUBJECT TERMS (Continue on reverse if necessary and identify by block number)
(U) Oils, (U) Lubricants, (U) Wear, (U) Friction, (U) Surface Roughness, (U) Electrical contact resistance layer (U) Temperature effects

19 ABSTRACT (Continue on reverse if necessary and identify by block number)

The lubrication behaviour of a cylinder liner/piston ring contact in a diesel engine has been simulated in a point contact reciprocating rig. When lubricants containing ZDDP additives are used, electrical contact resistance measurements establish that a thick 'reaction film' quickly forms in the rubbed region, protecting the metal surfaces. Electrical capacitance measurements show that the film thickness can vary from 0.1 to 1 μm: the film appears to be a solid organic polymer with a shear strength of 50-100 MPa.

Using segments of diesel engine cylinder liners from various manufacturers in the reciprocating rig, the changes in surface roughness during the running-in process were monitored. The induction time needed for the formation of the reaction film as well as the coherence of the film was studied as a function of load and temperature (in the range 150 - 250°C).

A theoretical analysis of flash temperatures in reciprocating contacts confirms that these are small under the conditions in this rig, so that the measured temperatures are those actually responsible for the reactions.

20 DISTRIBUTION/AVAILABILITY OF ABSTRACT ☒ UNCLASSIFIED/UNLIMITED ☐ SAME AS RPT ☐ DTIC USERS	21 ABSTRACT SECURITY CLASSIFICATION Unlassified
22a NAME OF RESPONSIBLE INDIVIDUAL Dr. R.E. Reichenbach	22b TELEPHONE (Include Area Code) 071 409 4423 22c OFFICE SYMBOL AMXSN-UK-RA

DD FORM 1473, 84 MAR 83 APR edition may be used until exhausted
All other editions are obsolete

SECURITY CLASSIFICATION OF THIS PAGE
Unclassified

BASIC MECHANISMS OF DIESEL LUBRICATION
CORRELATION OF BENCH AND ENGINE TESTS

Contract No. DAJA 45 86 C0007

Final Report

for

Department of the Army
United States Army Research Development and Standardization Group UK
Edison House, 223 Old Marylebone Road, London NW1 5TH

*****

A F Alliston-Greiner

Dr J A Greenwood

D Cameron

Professor A Cameron
Principal Investigator

March 1991

BASIC MECHANISMS OF DIESEL LUBRICATION CORRELATION OF BENCH AND ENGINE TESTS

Contract No. DAJA 45 86 C0007

OBJECT OF THE WORK

The aim of this project is to produce a method of assessing cylinder liner quality in a laboratory test machine, to reduce the amount of full-scale testing. The possibility of devising a much shorter, but equally effective running-in procedure should also follow.

In order to do this effectively, a study should be made of the type of lubrication encountered in the cylinder liner/piston ring contact. This report seeks to expand the understanding of the role of the anti-wear additive zinc dialkyldithiophosphate (ZDDP) from observations of the action of the additive in the contact forming a reaction film. Measurements of the film thickness are also part of the research.

SUMMARY

The work reported here is in three parts. The first describes the reasons why the high frequency reciprocating (HFR) test apparatus simulates real life conditions. It then describes a new design of the apparatus originally developed at Imperial College London and published in 1981. Electrical contact resistance (ecr) measurements indicated the existence of a thick boundary layer. To confirm this a capacitance technique was developed to measure it. Experiments showed it to be of the order of 1/10 to 1 microns thick, as expected. Using this result together with the friction, the mechanical properties of the layer were determined. This demonstrated the layer had the shear strength of 50-100 MPa, which is typical of organic polymers. The layer was temperature and load dependant.

In the second part the reaction films of commercially available ZDDP additives were studied. The apparatus was then redesigned to accept segments of diesel engine liners. The running-in process was followed by three indicators which were devised in this research. One, the change in the surfaces as shown by

the rounding of the peaks, for which a new computer program was developed. The second was the time, the induction time, taken for the high e.c.r. film to be formed.

Finally, the coherence of this thick film was measured. All these three were dependant on load and temperatures in the range 150-250°C. Five liners, two from Caterpillar OL-5 and OL-6 engines and one each from Cummins NTC-400, John Deere 6404 and Mack T-7 were tested and 9 oils. The conclusion was that this device can clearly distinguish between the liner/oil pairs. To give an order of merit the temperatures must be specified, since the ranking varies with the contact temperature, as would be expected. The decisive temperatures for the different pairs can only be determined by comparing the various rankings as decided by these tests with engine performance. Unfortunately, this was not available, hence only the first part of the programme could be completed.

In the third part, a theoretical study of the temperatures generated in this reciprocal contact device was undertaken. One of the assumptions made in the design of this rig is that, under the conditions of running, the temperature rise in the contact, the temperature flash, was small. It needed a full theoretical analysis to show that this was the case.

In conclusion it may be said that this work has produced a great deal of basic data, especially in the realm of running-in, which will enable the choice of liners and oils to be made with more confidence, once these tests can be compared with the operational data of existing engines.

The title of the whole project is Basic mechanisms of diesel lubrication: correlation of bench and engine tests. Due to a number of reasons no engine tests have been reported to us, so this half of the project could not be attempted. This is regrettable and limits the immediate value of the work. However, much has been found that engine makers and users could apply directly to their products.

ARRANGEMENT OF THE WHOLE REPORT

This report, the final one, is divided into three sections.

Section 1

The first section describes the development of the test rig used for the work. This type of machine is relatively new and has produced evidence of a thick polymer layer being formed on the surfaces of the rubbing contacts over a definite temperature range. It is considered that this layer is a major factor in the effective lubrication of internal combustion engines. The properties of this film, including its thickness, were studied.

This section of the work is self contained and was presented as a paper at the 1987 Leeds-Lyon Symposium. A reprint of the paper is bound at the end of this report.

Section 2

This is in two parts. Part 1 deals with the lubrication characteristics of the Caterpillar liner, designated liner C, and 4 oils, reference numbers AL-15932/33/34/35-L, labelled oils C1-C2-C3 and C4. These were studied in detail and three methods were developed to give numerical values for the running in process. In the second part of the section a number of oils were used with the 6 liners. In all these tests a single ball ended counter surface was used. The reason for this was that there was so much to be learnt with the methods developed in this work to describe the running-in process that attempting to increase the matrix of tests using different piston rings, would have meant the tests would have been spread so thinly that no reliable test data would have been produced. These tests have produced most valuable results, and so have justified the use of the ball ended test piece.

Section 3

There have been criticisms that the reciprocating rig produced temperature flashes of unknown size. A thorough theoretical study was therefore undertaken to find out what the surface temperatures were under these conditions. This work is reported here.

A list of references for each section or part of the work, for convenience, follows that section.

CONTENTS

SECTION 2 THE RUNNING-IN PROCESS: OIL/LINER PAIRS ABCDEF

SECTION 3 TEMPERATURES IN A RECIPROCATING CONTACT

SUMMARY

SECTION 1 - PROPERTIES AND THICKNESS OF ZDDP FILMS

1 OBJECT OF THE SECTION

Earlier work had reported that electrical contact resistance results suggest that oils containing ZDDP additives produced thick films. Resistance measurements are never quantitative, so a capacitance method was needed to measure it.

2 SUMMARY OF SECTION 1

1. A newly designed reciprocating ball-on-flat apparatus is described.
2. Reaction film formation by commercially available ZDDP additives were observed and their thicknesses measured by capacitance during the rubbing process. The film behaviour is related to its composition and the thermal stability and reactivity of the additives.
3. Preliminary observation is made of the running-in process with cast-iron cylinder liners.

3 INTRODUCTION

There have been many observations of reactions between oils containing zinc dialkyldithiophosphate and steel, forming 'varnish-like' films on the metal surface [1-4]. Much about their mode of formation in a contact remains obscure. Monitoring the electrical contact resistance during running is the normal method of detecting their formation [5]. The electrical contact resistance, however, can only give an indication of the effectiveness of the film in reducing solid-solid contact, and cannot give a measurement of film thickness [6]. There has been an attempt to make a quantitative relationship between the degree of asperity interaction and the nominal elastohydrodynamic film thickness for a disc machine contact [7]. This relies on calculating the ehl film thickness.

Measurement of the thickness of reaction films therefore poses a problem. Much work has been done on films already formed on surfaces, either after running in a contact or by dipping a steel plate or 'coupon' in heated oil. The thickness of the resultant film can be determined optically, by scratching the film and observing the shadow cast by a light. Scanning electron microscopy coupled with a chemical analysis system (e.g. Auger Spectroscopy) is also used. Films between 60 nm and 2 μm [8-10] have been reported. The objections to this 'static' study is that the surfaces have to be cleaned before observation, which probably removes some, unknown, amount of loosely bound material. Also the method of film formation with a dipped coupon is different from its formation in a rubbing contact, since the rubbed surfaces take part in the reaction (see below). This is an important but often overlooked consideration.

It has been found that even under conditions of nominally pure rolling, the film in the wear track is far thicker than on the surrounding surfaces [11]. It is believed that the thick film is due to the rubbing process which removes protective oxides and exposes active metal surface,

which in some way promotes film formetion. Usually the rubbing metals are polyvalent such as iron, chromium, etc., which are good catalysts. It is most desirable therefore that any study of the reaction film should be of a film resulting from a rubbing process with carefully controlled contact temperatures (see below). Dipping surfaces into heated oil is much less satisfactory as the resultant film was not formed during the frictional process.

These varnish films are formed by chemical reaction, and so presumably are very temperature sensitive. Hence the temperatures at which the film is formed is of considerable importance and should be known accurately. Furthermore it is well known in accelerated oxidation tests that the reaction mechanism changes with temperature. Hence to study the action of E.P. additives correctly the contact temperatures must be identical in test rig and engine. The problem in most sliding contact bench experiments is that the contact temperature is not known accurately. This is because the contact temperature is made up of a 'bulk' component together with a transient component due to frictional heating. A thermocouple placed near the contact, or embedded in the surface does not pick up this flash temperature, which can be very appreciable [12, 13]. Furthermore where the film is formed in a friction device running at slow speeds to enable the contact temperature to be accurately determined, the rate of contact repetition is wrong. This is discussed further below.

The first study of the formation and simultaneous measurement of a reaction film thickness was using an optical chl device [11]. Temperatures up to 99°C were achieved, and a very reactive oil was used. The optical method demands a semi-reflecting layer on a glass plate, and a very highly polished metal ball, so that the friction system was rather unusual, but the results were of great interest. Next films were observed by a capacitance method in a disc machine, running with a bulk oil temperature of 25°C

[14], but unknown contact temperature. These papers reported increases in the ehl film thicknesses due to additive action of 160 nm and 600 nm. The great disadvantage of the disc machine is that the contact temperatures are difficult to determine with certainty. A variant of the optical method [15] used balls dipped in hot oil and subsequently run in the optical device. Similar results were found.

It seems, therefore, that for a realistic study of the formation of the reaction film, four conditions must be met:

(i) The film must be formed in a rubbing contact.

(ii) Realistic surfaces and materials must be used.

(iii) The temperature of the contact must be known accurately.

(iv) The lubrication conditions should be known.

Many components, and particularly the cylinder liner/piston ring contact function in the 'mixed lubrication regime' - i.e. where there is some contribution from oil viscosity and also some contribution from boundary films. The problem in these cases is sorting out the viscous from the boundary conditions. Therefore in order to make interpretation of film properties straightforward, classical hydrodynamic lubrication should be excluded, so that the lubrication conditions are known to be purely non-viscous.

All these conditions are met in the reciprocating test rig that is described in this report. In order to make measurements of film thickness, the capacitance of the ball/flat contact is to be monitored. Deductions of the film thicknesses are made from the capacitance readings. Thus the distinctive contribution of this work is that thickness measurements are made of reaction films formed by ZDDP during running under carefully controlled conditions, (especially of temperature) and at the correct repetition contact rate.

4 RECIPROCATING RIG

The development of the reciprocating rig first described in [16] has been detailed in the two interim reports [17, 18]. In this section the principle of the machine is described, and then details of the component parts of the rig are given, explaining their function.

In the piston ring/cylinder liner contact (and in any repeating contact device) it is the repetition rate rather than the speed which is important when considering interactions of surface asperities. The protective film formed by additives is completely or partially removed during each contact and must be reformed before the next one: the time available for this is crucial. The rate of reformation depends on the chemical activity of the systems (metals and oil) and of course the temperature - see [19]. Therefore knowing the contact temperature is important. However, in most test devices the speed is high (giving large and unknown flash temperatures due to frictional heating) but the repetition rate is not as in the running engine. The reciprocating apparatus therefore provides a simple device, using actual engine components, of avoiding high flash temperatures (since the sliding velocity is low), but having the correct repetition rate. This means also that the contact temperature can be controlled accurately, simply by controlling the bulk temperature of the test specimens.

4.1 Apparatus

The contact configuration is ball-on-flat, the ball being reciprocated by a Ling Dynamics electro-mechanical 100 W oscillator loaded against a fixed flat (see Figure 1, reproduced from the previous reports). Standard conditions were 34.5 Hz, ± 0.5 mm. The ball is a push-fit into a 0.092" diameter hypodermic tube which holds it in place on the vibrator arm (figure

2). The hypodermic tube provides an easy method of mounting, and also of making electrical connection. Balls used in these studies have been 3/32" diameter bearing balls, and specially produced silver steel 'pins' with radiused ends (radius 4.5 mm), hardened to 450 VHN (45 R_c).

The flat is held in place on the 'boat' (Figure 1) in a clamping arrangement (Figure 2). The 'boat' is prevented from moving horizontally by a strain-gauge transducer (described later). The flats were made from AISI-01 high carbon (0.9 - 1.0%) steel gauge plate, hardened to 750 VHN (60 R_c) and polished with emergy paper and diamond lapping to an initial finish of 0.02 μm cla. The flat was provided with a tapped hole to facilitate electrical connection (dimensions are given in Figure 2).

By making the clamping arrangements for the ball and flat with 'tufnol' (a phenol urea plastic) and also PTFE, electrical isolation of the rig from these parts was readily achieved. This, then, allowed not only for electrical contact resistance to be measured (here isolation does not matter), but also allowed the capacitance of the contact to be measured.

4.2 Electrical Contact Resistance

This is a standard technique for monitoring contact conditions in many test devices [5, 20]. Quite simply, a voltage of approximately 15 mV is applied across the contact by means of a potential divider (see Figure 3), and the contact voltage is observed on an oscilloscope. 'Zero' volts implies that all the voltage drop is across the contact, i.e. that the contact resistance is effectively 'zero' (only a few ohms). '15 mV' on the scope implies no voltage drop across the contact, and therefore a very large or 'infinite' resistance. Its exact value depends on the size of the resistance in the potential divider. In our standard case 'infinite' means > 10^7 Ω.

Because of the way this circuit works, a contact voltage of '7.5 mV' corresponds to a contact resistance of a value equal to the resistance of the potential divider (R_2). Generally, the contact resistance fluctuates, sometimes high and sometimes low (see Figure 4). This gives some indication (qualitative) of the degree of asperity contact [5]. By taking the average of the signal (i.e. putting the signal through a low-pass filter) a continuous record of the 'degree of asperity contact' can be recorded. This was done, and it forms one of the three traces on a chart recorder.

4.3 Contact Capacitance

Capacitance measurements have been made in other friction devices, such as piston ring/cylinder liner [21] and disc/disc [14]. The advantage of this method is that it is possible to make more quantitative estimations of both the amount of asperity contact, and the thickness of the film in the contact. However, the technique does rely on there being little or no asperity contact, since any metal-metal contact shorts out the circuit.

The essential features of our measurement system are given in Figure 5, and are similar to those mentioned above [21, 22]. The ball and the flat become the two 'active' parts of the circuit, their contact capacitance becoming the 'unknown' reactance in a 4-arm bridge circuit. The rest is earthed. Balancing the capacitance with the ball/flat just out of contact gives the value of stray capacitance, which can be deducted from the experimental values. The bridge is a Wayne Kerr B224 transformer ratioarm bridge, with the voltage supplied externally by an oscillator at 2.4 kHz and an amplitude that keeps the contact voltage at about 50 mV. In this way maximum bridge sensitivity is achieved while keeping the voltage low enough to avoid electrical break-down of the film on the contact. The unknown signal is fed into the bridge, and the out-of-balance is also

displayed on a HAMEG 208 storage oscilloscope, together with the friction trace. The bridge can then be balanced at a particular point in the stroke (say mid-stroke), and variations in the capacitance across the stroke can be observed. Metal-metal contact is observed when at particular points in the stroke, the capacitance signal is seen to have a high value, or a "short" (Figure 6).

4.4 Load and Friction Force

The ball is loaded against the flat by means of a 'yoke' and lever (Figure 1), the dead weights being decoupled by a spring. Loads in these experiments were usually between 0.2 kg and 1 kg, sometimes higher. The loads had to be big enough to produce a good friction signal, but not so big that a coherent film did not form. It was found that 1 kg achieved this balance best. Nominal contact pressure therefore range from 1.5 kN/mm^2 to 2.6 kN/mm^2 for the bearing-ball contact.

Horizontal movement of the specimen was restrained by the strain-gauge transducer. This was an aluminium block with a thin leaf section 1 mm thick, acting as a very stiff 'spring'. Strain-gauges glued to the top and bottom surfaces (to provide compensation for bending) pick up the small strains due to the friction force on the flat, and are then amplified. The signal from the amplifier is displayed on the Hameg storage oscilloscope, and also rectified and low-pass filtered to provide an average friction force for the chart-recorder. Since the motion is sinusoidal, the friction trace is a square-wave.

The strain-gauges were calibrated by applying static loads to the aluminium block. The chart-recorder trace was calibrated using a function generator.

4.5 Heating and Temperature Measurement

Heating is by hot air blown into an insulated container surrounding the friction elements. The central section of the rig (that is everything on the small base-plate) is enclosed in a thermally insulated box, which is a metal-fibre sandwich. The box is split in half, and has holes for the vibrator-arm, loading lever, force-transducer, electrical connectors and for hot air to be blown into the box. Air is blown through a tube containing a resistance heater element. The air temperature is raised from supply temperature to box temperature by this process. The hot air outlet is directed to blow just underneath the "boat". The air is from a shop air-line, and a rate of 35 ℓ/min was found suitable.

The temperature of the contact is monitored by two thermocouples. One controls a West 2050 Programmer Controller, which switches the power to the heating element with a 'bang/bang' relay. This thermocouple is kept electrically isolated from the flat by placing it in between the nylon sheets in the specimen clamp (Figure 2), so that it does not provide an earth path which would render capacitance measurement impossible. The other thermocouple is clamped against the flat, but so that the tip is not directly in the path of blown hot air. This records the contact temperature and becomes an input to the chart recorder. The thermocouples are chromel/alumel, and the recording thermocouple is fed to a digital voltage multiplier for display purposes.

The controller can be programmed to supply up to four ramps and four dwells. Typically, contact temperature is maintained at 150°C ± 1°C, and ramp-rates of 5°C/min and 25°C/min are used.

4.6 Cleaning

Cleaning of the entire rig is important. To facilitate this, the central section is made in 18/8 stainless steel so that excess oil can be burned-off and cleaned without harm. It can therefore be thoroughly cleaned when a change of additive is made. Trace amounts of additive seem to make a big difference. The ball and flat specimens are cleaned ultrasonically first in acetone and then in pentane. They are then assembled in the rig carefully, coating them in the oil to be used in the experiment as soon as possible.

4.7 Film Thickness Measurement

Mostly, capacitance readings were taken at mid-stroke, and a typical out-of-balance signal is shown in Figure 7a. The signal is nulled (Fig. 7b) giving a combined capacitance of conductance for the contact.

Film thicknesses are obtained from these capacitance readings by reference to a calibration curve (Figure 8). Calibration was done in the following way. First an unworn flat (initial finish 0.02 μm cla) was coated with a known thickness of amorphous silicon oxide by vacuum depostion at 300°C. The thickness was measured by ellipsometry.

These coated specimens were then used as calibration film thicknesses. A ball was loaded against each flat, with the electrical connections the same as in the experiment. For ease (and because of alignment problems), the ball/flat were not loaded together in the rig, but in a jig to help this alignment. This was particularly important when using balls that had themselves been used in an experiment and had a wear-scar. Contact capacitance was measured as described earlier, and values for a range of film thicknesses and a range of wear-scar sizes were obtained. The

line in Figure 8 has been drawn for a wear scar size of 0.15 mm (diameter), which is typical of these experiments. What is surprising is that the scar size seems to have little effect on the capacitance of the contact. This could be due to misalignment of the contact, even though care was taken to load the coated specimen against the worn part of the ball. There may also be a problem that the ball was not in contact over its entire worn surface, and therefore that the 'nominal' scar size was not actually the size "seen" by the contact. This is confirmed by looking at a profile trace of a worn ball (Fig. 9). The wear scar does not produce a 'flat' on the ball, but rather reduces the curvature and roughens the surface.

The dielectric constant of the oxide film was taken to be 4.0, and that of the reaction film as 2.3 (see below). The calibration line for the reaction film was then obtained by dividing the capacitance values for a given film thickness by the ratio of the dielectric constants.

4.8 Dielectric Constant

The above calibration has assumed that the dielectric constant of the reaction film is the same as that of the un-reacted oil.

It has not been possible to measure directly the dielectric properties of the reaction films formed by ZDDP because of the difficulty in producing sufficient quantities. A search of the literature reveals that measurements have been made of the dielectric constants of mineral oils containing ZDDP [23, 24] and are typically around 2.3 (i.e. the same as the base oil). The capacitance of the base oil (500 Solvent Neutral) in these studies was measured in a simple capacitance cell (Figure 10), and did not change on addition of 1% ZDDP. Thus, in the bulk, the additive does not change the dielectric properties of the oil. Again, no change in the dielectric constant was observed when a sample of oil with 1% ZDDP

was heated to about 250°C and cooled.

From current literature searches, it seems likely that the dielectric constant of the reaction film will not be greatly different from the unreacted additive. In the unlikely worst case of the dielectric constant being as large as 4.0 (c.f. a highly polar polymer) the film thickness would be <u>larger</u> and around twice the value calculated for $\epsilon = 2.3$.

5 REACTION FILMS FORMED BY ZDDP ON STEEL AND CAST IRON

Four different ZDDPs were used in these experiments, incorporated in a 500 Solvent Neutral (500 SN) base oil at a 1% by weight treat level. The four additive oils were designated A to D and details are given in Table 1. The essential difference between the four ZDDPs is the nature of the alkyl groups in the molecule, these are also shown in Table 1. The different alkyl groups give the ZDDPs different thermal stabilities and reactivities, although exact details are not yet available. The base oil and additives were supplied by Castrol Research Laboratories, the additives originating from Exxon and Lubrizol. No details were available about their purity.

The experimental results presented aim to demonstrate some of the features of the method of lubrication with zinc dialkyldithiophosphate additive. Results include observations of film behaviour in the rubbing contact under static and dynamic loading, with varying temperature, stroke and frequency. Additionally, and this is where this apparatus differs from other devices, measurements of film thickness are made during running and at temperatures that are comparable to a running engine. The important point is that the temperatures at which the films are formed is known.

5.1 Film Formation

The standard temperature for experiments was set at 150°C. This is considered to be a typical working temperature for contacts such as cam/tappett and piston ring/cylinder liner - although values much greater than this may be experienced due to transient flash and high sump temperatures. However, it should be noted that the calculated flash temperature in our experiments is only a few degrees, which means that the measured bulk temperature is effectively the contact temperature. It was also found

that 150°C was the optimum temperature for film formation, the additives readily form a reaction film that provides good surface protection.

The first observation was that film formation is rapid. This can be seen in the chart-recording of an experiment for additive C at a constant temperature of 150°C in Figure 11. The load is 1 kg, and the upper trace is the friction force, the lower trace the average electrical contact resistance. Motion was started, and the load was applied. Initially there is an 'induction time' in which no film activity is observed - in this case about 45 seconds. In these first moments of motion a high friction transient is seen, which rapidly settles down to a value just greater than $\mu = 0.1$. This friction transient is associated with the 'induction time' when there is no film activity and therefore little protection of the rubbing surfaces.

Subsequent to the 'induction time the average electrical contact resistance is seen to rise rapidly from a value of almost zero to a value higher than 10 MΩ in about 30 secs to 2 minutes of rubbing (corresponding to 4000 passes or 8 m of sliding). In this time there is a small reduction in the friction force - corresponding to the observed improvement in the coherence of the reaction film. This is seen from the out-of-balance capacitance signal in this period. When the electrical contact resistance is observed to be high over the whole stroke, there is still much evidence of solid-solid contact through the film, manifested by momentary 'shorting out' of the capacitance signal. However, as motion proceeds, these asperity interactions diminish until, in most cases, they vanish. Also in this period, the value of capacitance to 'null' the trace at mid-stroke diminished, indicating that the reaction film thickness increased.

Figure 12 shows another experiment at 150°C, but this time with a variable load. After film formation at the initial load of 0.2 kg, the load was increased in steps of 0.2 kg. The averaged electrical contact

resistance trace reveals that the film was disrupted on two of these load stages (seen from the downward spikes on the trace). But, after the film was disrupted, the contact resistance once again rises rapidly to the high value - the film has re-formed.

So far these observations have been for polished steel specimens, but the same kind of effects were observed for cast-iron cylinder liner specimens. These were plateau honed 0.25% phosphorus flake graphite cast iron with a cla roughness of 1.50 μm. These experiments show the same rapid film formation, although the time taken for appreciable asperity interaction to cease is much larger, if not infinite. A typical trace is shown in Figure 13, for oil B at 150°C and a load of 1 kg (i.e. conditions identical to those in Figure 11). A high electrical contact resistance is formed after about 2 minutes of rubbing, and solid-solid contact is reduced to almost zero within the first 10 minutes of rubbing. A second experiment is shown in Figure 14, and here the film formation takes about 3 minutes, although at the end of this time the amount of asperity interaction was still too great to make capacitance readings.

Cast iron experiments again demonstrate the resistance of the reaction film to load changes. Figure 15 is a variable load experiment at 150°C for oil B. The load is raised in 0.5 kg steps from 0.5 kg to 3 kg. At each load stage, there is a momentary loss of the high electrical contact resistance (e.c.r.), indicating a loss in film protection, but this rapidly heals giving the high e.c.r. again. The capacitance trace reveals that at each load stage solid-solid contact did not fully cease. However, some readings were obtainable, indicating film thickness values of 0.1 to 0.3 μm, which compare favourably with values obtained for the polished steel specimens (0.1 - 1.0 μm). The load stage of 3 kg caused the film to show signs of failure (the high e.c.r. value is greatly reduced).

However, the additive is still effective at loads greater than 3 kg.

Figure 16 is for an experiment with a constant load of 5 kg, at 150°C with oil A. Initial film formation is after about 4 minutes of rubbing, but it then takes about 2 hours for there to be film with an appreciable reduction in solid-solid contact. This is inferred from the amount of 'fur' on the e.c.r. trace gradually reducing over this period.

Returning to the polished steel specimens, experiments have been performed with other initial temperatures from 20°C to 200°C. Two kinds of effect have been observed. The first is that at 20°C there exists what is substantially a hydrodynamic film, since at this temperature the oil is much more viscous than at 150°C, and the additive is not yet reacting. Figure 16 shows the chart recording for an experiment with a constant load of 1 kg using oil B and a 4.5 mm radius pin, with temperatures from 20 - 250°C. Photographs of the electrical contact resistance were taken from the oscilloscope (Figure 18) showing this behaviour. At 20°C there is 'lift-off' in the middle of the stroke (top trace), but no lift-off at the ends of the stroke, which is the hallmark of hydrodynamic lubrication. It should be noted that there is still a high degree of asperity interaction in these conditions. As the temperature is raised to 50°C, there is evidence of some reaction film activity, since there is a non-zero resistance at the ends of the stroke. It is <u>far</u> from being a coherent film, since it is noted that on this scale the resistance 'high' corresponds to only 10 kΩ.

Figure 17 also displays that at 20°C the friction coefficient, μ, is lower than the value after a reaction film is formed. The "hydrodynamic" lubrication gives $\mu = 0.089$, but the pure film gives $\mu = 0.108$. The same effect, although less marked, was observed for the bearing ball sliding (Figure 19): μ rises from 0.088 to 0.095. In both these experiments, a coherent film was not obtained until about 150°C.

The second effect noticed in the variable temperature experiments is slightly different. The same trend in friction force is observed,

but the hydrodynamic action is obscured. This seems to be due to some reaction film formation at the low temperature. This is shown in the results recorded in Figure 20 for a bearing ball sliding, and at the lower load of 0.2 kg. The explanation may lie in the severity of the bearing-ball contact as compared with the radiused pin. The smaller radius gives a larger contact pressure, and therefore greater local asperity pressures which may give temperature effects suitable for film formation.

During motion, the film thickness was found to be nearly constant over the entire stroke, with the main variation being at the ends of the stroke where the velocity reverses. Figure 21 is a photograph of a typical friction and bridge out-of-balance signal taken from the oscilloscope. The bridge signal is very clean, indicating that there is no asperity interaction. It has been 'nulled' at the ends of the stroke, and therefore approximately displays the film 'shape' across the stroke. It should be noted that the bridge separately balances out the capacitance and conductive parts of the 'reactance', so enabling readings of both contact capacitance and resistance.

The film shape is shown better when the signal is 'nulled' at the mid-stroke position (Figure 22). Here the almost uniform film across the stroke is readily observed. The capacitance values at the ends of the stroke are always lower than at the middle. This implies that the film thickness <u>increases</u> at the ends of the stroke - a rather surprising observation, since we would expect the film to be thinner where the velocity is zero. However, if the film is a solid, then this film thickness at the ends of the stroke can be attributed to a kind of 'bull-dozing" effect, as the solid is sheared and pushed to the ends of the contact, and the slider 'rides-up' on the piled-up material.

What is clear is that the film does not act as classical hydrodynamics would require. The velocity varies markedly throughout the stroke, but

but the film thickness appears to be largely unchanged.

5.2 Wear Reduction

From visual obervations of wear scar at various stages of running, it becomes apparent that most of the wear has taken place in the first 1-2 minutes. It is in this period that the reaction film is seen to form. The capacitance observations show that there is little or no solid-solid contact once the reaction film has been formed.

Simply comparing results for the additive oils with results for the base oil alone reveals that while the friction coefficient is roughly the same, the wear is very different. This is displayed in Table 2, where friction coefficients and wear scar diameters for a number of experiments are recorded. The friction coefficient is a very poor indicator of the ability of the reaction film to protect the surfaces. This same effect is shown pictorially in Table 3. The wear reducing action of the additives is very apparent: not only is the wear scar diameter reduced, but also the apparent roughness of the worn surface is lower. The profiles displayed in Table 3 were taken in a profilometer after the ball and flat had been gently rinsed in solvent to remove excess oil. This meant that most of the reaction film was still in place on the surface. The profiles are displaced by about 0.2 - 0.3 μm on the vertical scale of the diagram to give some indication of the relative size of the apparent roughness to the reaction film thickness. At the high load of 1.0 kg, the films were about 0.3 μm thick which was comparable to or greater than the apparent roughness of the wear scar. At the lower load of 0.2 kg, the films were about 0.6 μm thick, and much greater than the apparent roughness of the scar.

It is, of course, this wear reducing ability of the additive that

is important in practice. A photographic record of some results for 5 kg load tests using cast-iron cylinder liner is shown in Figure 23, each picture showing the wear scar on the liner after 2 hours of rubbing. It is immediately obvious that the wear is greatly reduced from the base oil alone by addition of 1% ZDDP. The 'cross-hatch' honing marks were obliterated when the base oil was used, but are still evident after running with additive oil. Figure 24 displays photographs for experiments run for different lengths of time (5 minutes, 2 hours and 4 hours). Here it is quite striking that the wear scars are visually almost the same, indicating that most of the wear seems to have taken place in the first 5 minutes of rubbing.

5.3 Variation of Film Thickness with Load

At a constant temperature (100, 150 or 200°C) with a load of initially either 0.2 kg (bearing ball experiments) or 1.0 kg (for the radiused pins) motion was started. Conditions were allowed to settle down, and then a capacitance reading was taken for the mid-stroke position. The load was then either raised or lowered in steps of 0.1 kg to cover the range 0.2 - 1.0 kg. Each load was applied for 2-5 minutes before a new capacitance reading was taken. This allowed the film to establish itself under the new running conditions. This is termed the dynamic loading of the films.

At the end of the dynamic loading, motion was removed. On all but a few occasions, the film remained in the contact. It was immediately apparent that the film thickness when static was different from the dynamic readings, since the bridge out-of-balance signal changed. The film in the contact was then loaded normally and capacitance readings taken at each load stage.

Although there is some variation in the wear scar size between

each experiment, the calibration curve for deducing the film thickness was used for a typical value of wear scar diameter. The reason for this is that in calibration, the wear scar diameter (for the small sizes in these experiments) did not seem to change the capacitance value significantly. It should be noted that the wear scar on the ball is far from the 'ideal' of a flat on the ball, and is rather a roughened region where the ball contacts the flat. The variations of deduced film thickness against load are shown in Figures 25 - 28, 30 - 33.

Figures 25 - 28 are for bearing-ball experiments at 150°C, the hollow symbols correspond to the dynamic loading, and the solid symbols to the static loading. The first observation is that the film thickness decreases with load. Curves have been drawn on the figures to indicate the general trend. The curve is more nearly a straight line for the static loading, indicating that the film behaves elastically in this condition, confined in the contact. In other words, reduction in film thickness on loading is completely recovered on unloading. Another general feature is that the dynamic film thickness is on the whole lower than the static value. This clearly shows that there is little or no viscous contribution from the film, that it is a solid and is sheared in the contact. The reduction in film thickness with load during motion is probably due to an increased amount of 'smoothing' of the film, the "bull-dozing" effect mentioned in the last section.

The trends of film thickness against load (represented by the dotted lines in these figures) are compared with each other in Figures 29 and 34. There is certainly some difference between the oils in the average film thickness produced, but giving a definite order is difficult since oils B and D are so close to each other. However it does seem that oil C consistently gives the thickest films, and oil A gives the thinnest films. This is probably a reflection of the nature of the alkyl group in the ZDDP, and

will be discussed later.

Figures 30 - 33 differ in that they are for experiments with the radiused pin, not the bearing-ball. Here the same trends are observed as in the previous figures. The main difference is that the deduced film thicknesses are about half the values for the corresponding bearing-ball experiments. The range here is 0.05 μm - 0.25 μm, compared with a range of 0.1 - 0.6 μm. It is not clear whether this is a function of the calibration method with the wear scars, or whether it is a real effect of the radius of the ball. Further work needs to be done to elucidate this effect.

5.4 Variation of Film Thickness with Temperature

Figures 30 - 33 display results of film thickness against load obtained at three different, constant temperatures (100°C, 150°C and 200°C). The variation of film thickness with temperature is not very marked. There does seem to be an increase as the temperature is raised to 200°C, and this is seen most clearly in Figure 31. Values at 100°C are either comparable with those at 150°C, or slightly lower, which would be expected if polymerisation of the film was temperature dependent.

Figure 35 has collected the film thickness values for the experiments reported earlier where the temperature was taken from 20 - 250°C in steps of 25°C. There is a very noticeable change in the trend at around 180°C, where the film thickness drops appreciably. In some cases, above 200°C, the film became disrupted and readings were no longer obtainable. In one experiment, the film failed at 250°C and resulted in a scuff - the friction rose sharply and the noise increased as well. This is shown in Figure 36 for oil A at 1 kg. In this particular case, the film disruption started at about 175°C, and the friction trace was seen to fluctuate as the film began to break down.

In the cylinder-liner experiments, there is a visually noticeable difference between the surfaces run at 50°C, and the surfaces run at 150°C (see Figure 23). This indicates that the ZDDPs have provided a better protection at this temperature. On going to 200°C in separate experiments, there does seem to be a slight reduction in the effectiveness of the additive. This certainly ties up with the observations of electrical contact resistance and friction in these experiments. Figures 37 and 38 show the superimposed e.c.r., friction and temperature traces for the experiments that produced the photographs in Figure 23. Very clearly, the average electrical contact resistance is highest (indicating a thicker and more coherent film) at 150°C. At either 50°C or 200°C, the film quality is noticeably worse. This is most clearly shown with oil B (Figure 37), where there is almost zero e.c.r. at 50°C, and greatly disrupted at 200°C.

5.5 Shear Properties of the Reaction Films

The results presented indicate that the reaction films formed with ZDDP in these experiments did not behave in a viscous manner. The behaviour in the contact is more consistent with a solid polymerised film. Under sliding conditions, the film behaves plastically - as a solid with a constant shear strength. This being the case, deductions about the shear strength should be available from friction force data.

It is assumed that the reaction films have reduced the frequency of metallic contact to such an extent that the contribution of such asperity interaction to the total friction force is negligible. Our results of capacitance measurements show this to be a good assumption. This then means that the friction force measured is due to the shearing of the film itself. The second interim report [18] included a simple calculation of the shear strength of such a film by dividing the friction force in

an experiment by the area of the wear scar - determined by a measurement of the wear scar diameter on the ball. Repeating and extending this calculation for the range of additives gives values of shear strength in the range 50 MN/m^2 to 100 MN/m^2 (Table 4). The shear strengths of the films seem to be roughly comparable.

Workers in the field of thin polymeric films on a hard substrate [29, 30] have suggested a relationship between the measured contact shear force and a shear strength of the film. It has the form:

$$\tau_c = \tau_o + \alpha p$$

where τ_c is the shear strength measured, τ_o is a constant shear strength for the material, α is a constant and p is the contact pressure. It is not clear that our reaction films behave in this way: there is no definite evidence for a τ_o, but there is some indication in our experiments that the reaction films behave in this way, but experimental accuracy at the moment is not enough to decide. Modifications to the sensitivity of friction-force measurement to take this idea further is now being undertaken.

This work was reported to the Leeds Lyon Conference in 1988. A copy of the paper is given at the end of this section, appendix B, page A3.

6 DISCUSSION

The apparatus described here has enabled the reaction film thickness of ZDDP additives incorporated in a base oil to be measured under the four conditions considered necessary in the introduction, namely;

(i) The film formed in a rubbing contact

(ii) Realistic surfaces and materials used

(iii) The temperature of the contact known accurately

(iv) Lubrication conditions known, to be boundary with minimal hydrodynamic component.

These experiments have shown that both temperature and rubbing are necessary for the formation of the reaction films from ZDDP. The second interim report [18] described how no evidence of any reaction film being formed away from the wear scar was found. This was demonstrated there by using x-ray diffraction analysis and looking for the elements in the additive that were expected to appear in the film (namely Zn, P and S). The film formed only where there was rubbing. Recent infra-red studies of rubbed reaction films confirm this observation [25]. Here the important role of temperature in sustaining the reaction of the additive and promoting film formation has been shown. Since the contact temperature is known accurately, conditions under which the film forms have been observed. It appears that the additives can become active at moderately low temperatures (75°C) but that they form the best films in the region of 150 - 200°C. This reflects the thermal stability of the additives. Above 200°C they decompose, and this hinders the formation of the film.

The implication in practice, and particularly in the piston ring/cylinder liner contact, is that the ZDDPs act over a large range of temperature. It is thought that typical liner wall temperatures range from 150 - 250°C (although accurate measurement is absent). At the top of this range,

the ZDDP film is becoming disorientated, and thermal decomposition hinders the anti-wear activity. It should be noted, of course, that the ZDDP additive is never used on its own, and the inclusion of other additives tends to mask the individual contribution [26, 27].

6.1 Film Formation and Wear Reduction

At the onset of rubbing, there was no reaction film in the contact. The observed initial 'induction' time when no film activity was detectable has been reported elsewhere [5], and is probably due to the initial run-in conditions being too severe to sustain a film. However, the subsequent rapid film formation leading to a protective film indicates that these extreme conditions do not last long. It is in the first few minutes that the degree of solid-solid contact is highest, and when most of the wear takes place. This was noted when commenting on the variable time experiments with cast-iron cylinder liners (Figure 24) in the results section. The wear scars are very similar after 5 minutes and after 2 hours. This observation has important implications for the running-in procedures in diesel engines.

Clearly not all the wear takes place in the first 5 minutes, and in the cast-iron experiments it is very evident that asperity interaction continues even for 2 hours of running. This was detected from observations of the capacitance signal being shorted-out at many points. As the experiments proceed, the running-in process continues, and presumably there are significant changes in the surface topography. These observations are the impetus for the next stage of the work, looking at the topographical changes during running in, and the scheme is outlined in the Appendix.

In experiments on the polished-steel specimens as well as on the cast-iron specimens, the reaction film was found to be highly tolerant of changes in operating conditions. This is particularly noticeable in

the variable load experiments. A new load-stage often produced a disruption in the film - evidenced by a sharp drop in the electrical contact resistance, corresponding to a sudden increase in asperities interaction. However, the electrical contact resistance was observed subsequently to rise rapidly to its high value again indicating rapid film re-formation, and the maintenance of anti-wear protection. This is also important in running engines, since conditions in the piston ring contact are seldom steady. The reaction film quickly responds to changes in the contact conditions.

It has long been held that the major importance of an additive such as ZDDP is in wear reduction, and only secondarily in friction reduction. All these experiments have demonstrated this to be the case. The friction coefficient is a bad indicator for the performance of the additive. Here, the base oil alone had a friction coefficient of the same size as base oil + additive, a value around 0.1 in all experiments. The friction coefficient remained at this value, even when all metallic contact had ceased.

6.2 Film Properties

We have observed that the main function of the ZDDP is that of wear reduction. Shearing of the metal surfaces or asperities in the contact is replaced by shearing of this solid reaction film. Although static loading tests on the film formed in the contact shows some elastic behaviour (the film thickness is the same on loading as when unloading), it cannot be the elastic properties that contribute to wear reduction. The film is in gross shearing for most of the contact time, it is only 'static' at the ends of the stroke. It must therefore be the plastic behaviour of the films that is important in the contact, and the way the film is bonded to the surfaces that determines its effectiveness as a wear-reducer. The infra-red studies mentioned earlier [25] indicate that the additive

is strongly bonded to the metal substrate, but that there is a less-strongly held part of the film that is possibly a polymerised layer.

The reaction films formed in these tests were found to be solids, remaining in the contact when motion was removed. They behaved elastically under normal load, and as constant shear strength material under tangential motion. Their plastic behaviour seems to be similar to that of some common extruded polymers such as PMMA and HDPE. The shear strain rates in these experiments are high (of the order 10^6 s^{-1}) and are comparable to the extrusion process. Further experimentation is needed to investigate the shear properties of these films.

It was noted that when the film was loaded dynamically, the film thickness reduced, and also that the film thickness was greater at the ends of the motion (where the velocity is zero) than at mid-stroke. This has been attributed to a "bull-dozing" action of the slider, shearing and pushing the films to the ends of the contact. The slider then rides-up on these heaps of material.

Film thicknesses in these experiments have been deduced to be in the range 0.05 μm - 1.0 μm. These values of thickness are of the same order as films formed by elastohydrodynamic lubrication of concentrated contacts. However, these results have demonstrated that the apparatus functions in the boundary lubrication regime, i.e. that there are no viscous effects. As boundary films, the reaction films are thick, much greater than a 'traditional' boundary film of a few molecular layers. The evidence is that there is a polymerised solid in the contact. The film thickness is generally larger than the surface roughness of the wear scars. At higher loads, the deduced thickness becomes comparable with the roughness. The film remained effective in wear reduction. This remained the case when no film thickness values were obtained (i.e. that film thickness was less than roughness size) with cast-iron liner specimens.

6.3 Effect of Temperature

For the constant temperature of 150°C, it has been observed that there is a variation in the thickness of the reaction film between different ZDDPs used. The four additives can be ranked roughly in the order C, (B/D), A of decreasing film thickness at constant load. Looking at the composition of the additives we see that this trend is reflected in the thermal stability and reactivity of the additives.

Oil C contains a secondary alkyl ZDDP which, when compared with oil A which contains a primary alkyl ZDDP (see Table 1), had a higher reactivity and a lower thermal stability. From this viewpoint, oil C would be expected to react at a lower temperature and to produce thicker films than oil A. This is found to be the case. The placing of oils B and D in the ranking are not clear from the experiments, and as yet details of their relative reactivity and thermal stability are not available. The observation that the nature of the alkyl group affects the thickness of the reaction film formed has recently been indirectly observed using surface analysis techniques [28]. The authors there indicate that while the surface composition for different additives is the same (also indicating a polymerised upper layer on a more tightly held lower layer), the thicknesses are different for different alkyl groups in the ZDDP. Their results tend to the same qualitative picture as deduced here.

The difference in film thickness on going from conditions at 100°C to conditions at 200°C has seemed fairly minimal. If anything, there is a slight increase in the film thickness at 200°C over the value at 150°C or 100°C. This again reflects the reactivity and thermal stability of the additive. Particularly in the polished steel specimens a marked decrease in film thickness was observed at 180 - 200°C, which corresponds to the temperature at which the additive begins to decompose. Together with this film thickness decrease, increased asperity action produces a small increase in wear.

7 CONCLUSIONS

The apparatus described in this report has enabled thickness measurements of reaction films formed by ZDDP during the running process to be made, using capacitance.

The apparatus functions under the four conditions considered necessary in the introduction. Working with these conditions of rubbing contact, realistic surfaces, known contact temperature and known lubrication regime some new features of the formation and thickness of reaction films have been found.

Reaction film thicknesses were deduced to be in the range 0.05 μm - 1.0 μm. These were comparable or greater than the apparent surface roughness of the wear scars.

These film thicknesses are typical of values in the chi regime. Films of this size are not formed by hydrodynamic action, but by polymerisation of the additive on active metal surface produced by rubbing.

Reaction film formation is rapid, taking place in the first few minutes of sliding. The film is continous across the stroke once formed, and remains in the contact when motion is stopped. Film thickness is almost constant across the stroke, being greater at the ends of the stroke due to a piling-up effect.

The reaction films formed in these experiments were found to be solids. They behaved elastically under normal load, and as constant shear-strenght material; under tangential motion. The shear strengths are similar to common extruded polymers such as PMMA and HDPE.

Reaction film thickness and film quality vary according to the temperature of the contact. The films protect the surfaces best in the range 150 - 200°C. The film thickness is affected by the nature of the alkyl group on the ZDDP. Those with a lower thermal stability and higher

reactivity produce the thicker films.

Once formed, the films show a remarkable tenacity and can rapidly respond to fluctuations in load, and hence in contact conditions.

These observations have important implications for the lubrication of engine parts such as cylinder liner/piston ring and in running-in procedures in engines. They also contribute to our understanding of the role of reaction films in boundary lubrication.

The next stage of the research will concentrate on the running-in process using cast-iron cylinder liners. The aim will be to gain a better understanding of what makes a 'good' run-in surface, and particular attention will be made to changes in surface topography. The primary aim is to relate the performance of these test liners to that of the same liners and additives in full-scale tests (see Appendix).

	ZDDP		ANALYSIS	
OIL A	PRIMARY	$-(CH_2)_{3,4}CH_3$	PARANOX 15 Zinc Sulphur	wt% 9 11
OIL B	PRIMARY	$-(CH_2)_{11}CH_3$	PARANOX 16 Zinc Sulphur Phosphorus	wt% 7.7 9.8 7.7
OILC	SECONDARY	$(CH_3)_2\overset{1}{C}HCH_2CH_3$	LUBRIZOL 677A Zinc Sulphur Phosphorus	wt% 8.85 17 8.3
OIL D	ALKYL ARYL	$-(CH_2)_{11}CH_2$ 	LUBRIZOL 1376A Zinc Sulphur Phosphorus	wt% 8.5 12.3 6.4

TABLE 1

DETAILS OF THE ADDITIVES

R 4.5 mm PIN AT 150°C		
	μ	Φ mm
BASE OIL	0.133 0.125	0.497 0.610
OIL A	0.122 0.135	0.159 0.205
OIL B	0.097 0.104	0.116 0.137
OIL C	0.109 0.108	0.155 0.157
OIL D	0.103 0.105	0.145 0.109

TABLE 2

COMPARISON OF WEAR SCAR DIMETERS (Φ) AND FRICTION COEFFICIENTS FOR THE BASE OIL ALONE AND WITH ADDITIVES

	NO ADDITIVE	ADDITIVE A	ADDITIVE B	ADDITIVE C	ADDITIVE D
1.0 Kg					
WORN PROFILES					
FILM THICKNESS µm	NO FILM	0.34	0.34	0.55	0.19
WEAR SCAR DIAMETER mm	0.197	0.126	0.107	0.111	0.150
0.2 Kg					
WORN PROFILES	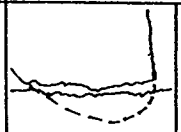				
FILM THICKNESS µm	NO FILM	0.54	0.66	0.62	0.68
WEAR SCAR DIAMETER mm	0.135	0.083	0.084	0.067	0.073

TABLE 3

WEAR PROFILES AND FILM THICKNESSES

R 4.5 mm PIN AT 150°C	
	Shear strength of contact (MPa)
OIL A	41 80
OIL B	54 58
OIL C	58 125
OIL D	45 113

TABLE 4

SHEAR STRENGTHS OF REACTION FILMS

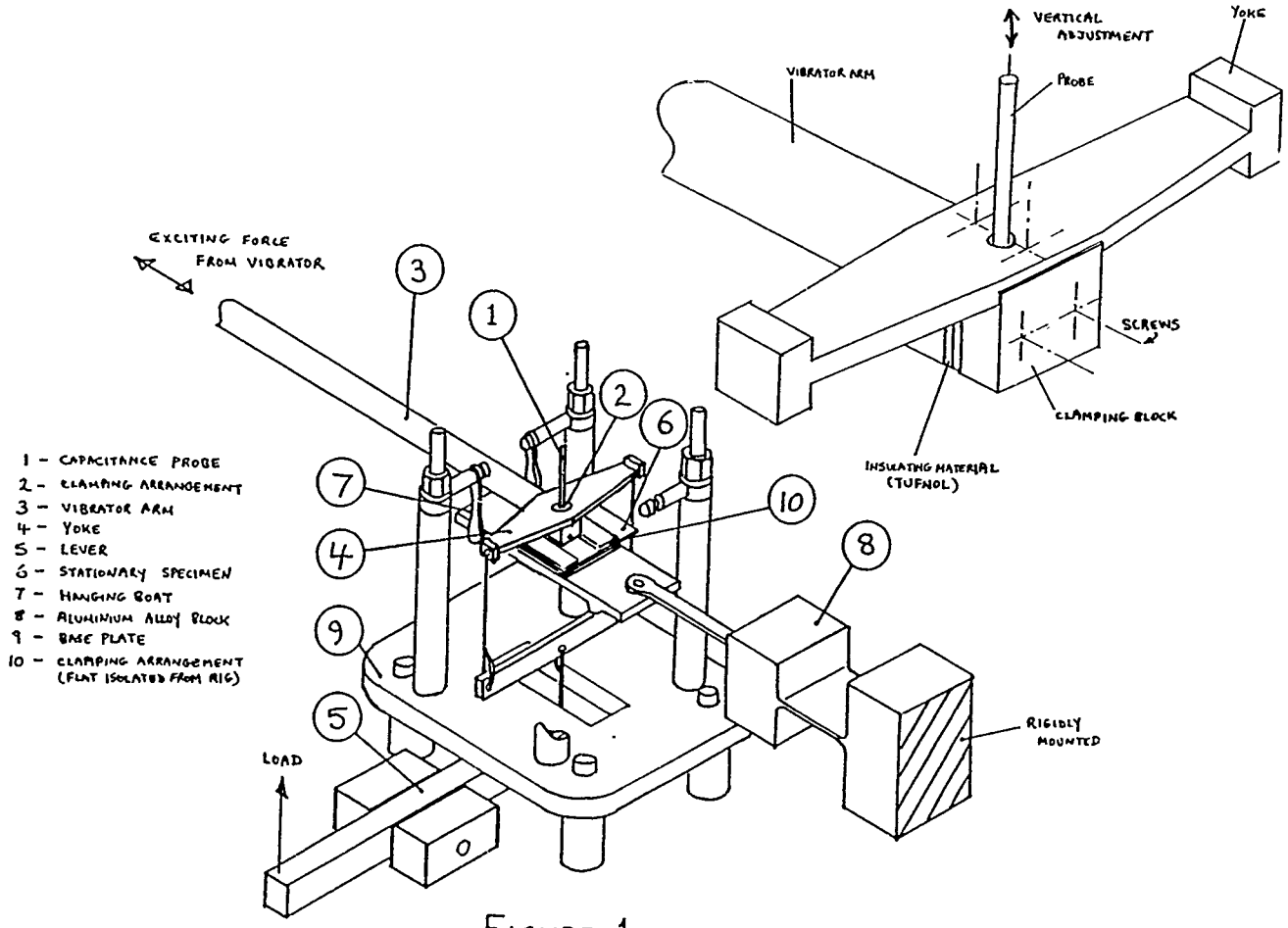

FIGURE 1
RECIPROCATING CONTACT RIG

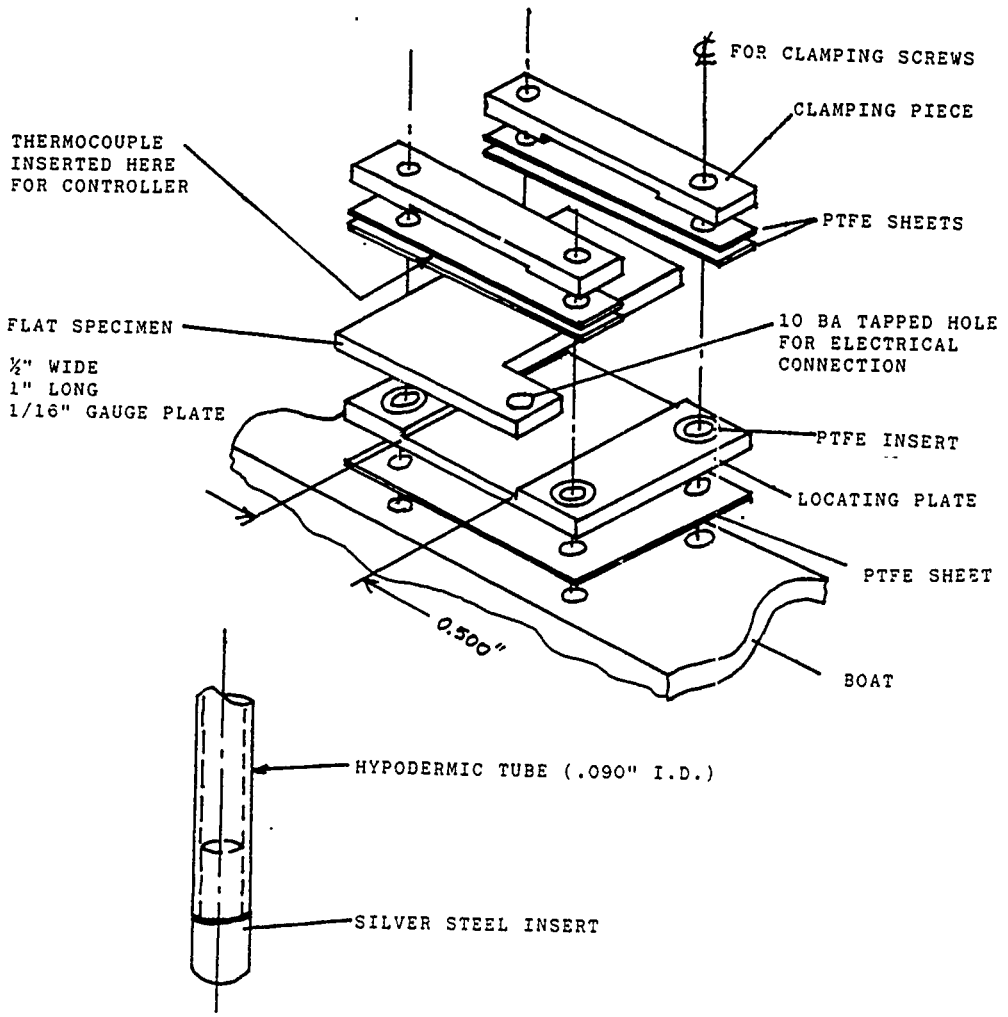

FIGURE 2

DETAILS OF CLAMPING ARRANGEMENT
AND PIN SPECIMEN

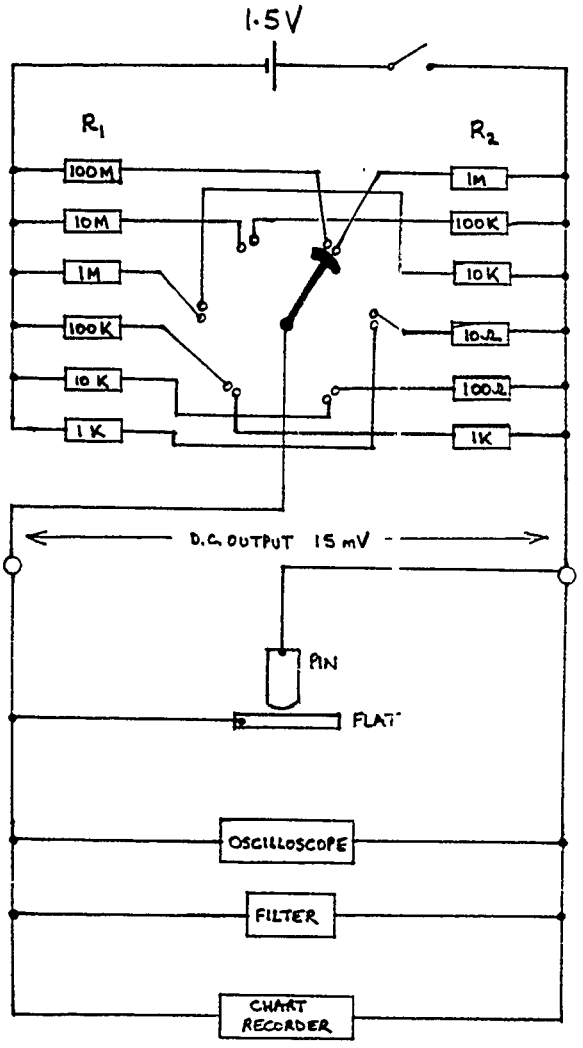

FIGURE 3

FUREY-LUNN TYPE POTENTIOMETER

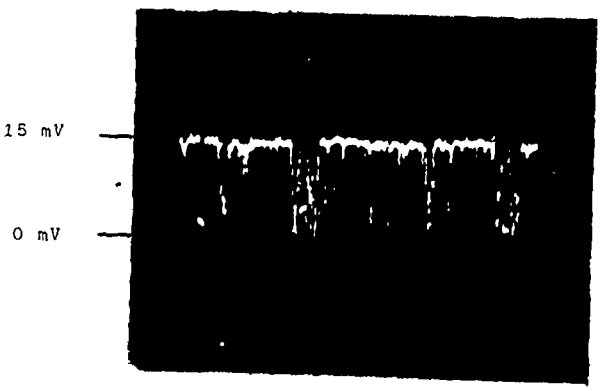

FIGURE 4

TYPICAL CONTACT RESISTANCE PHOTO
FROM OSCILLOSCOPE

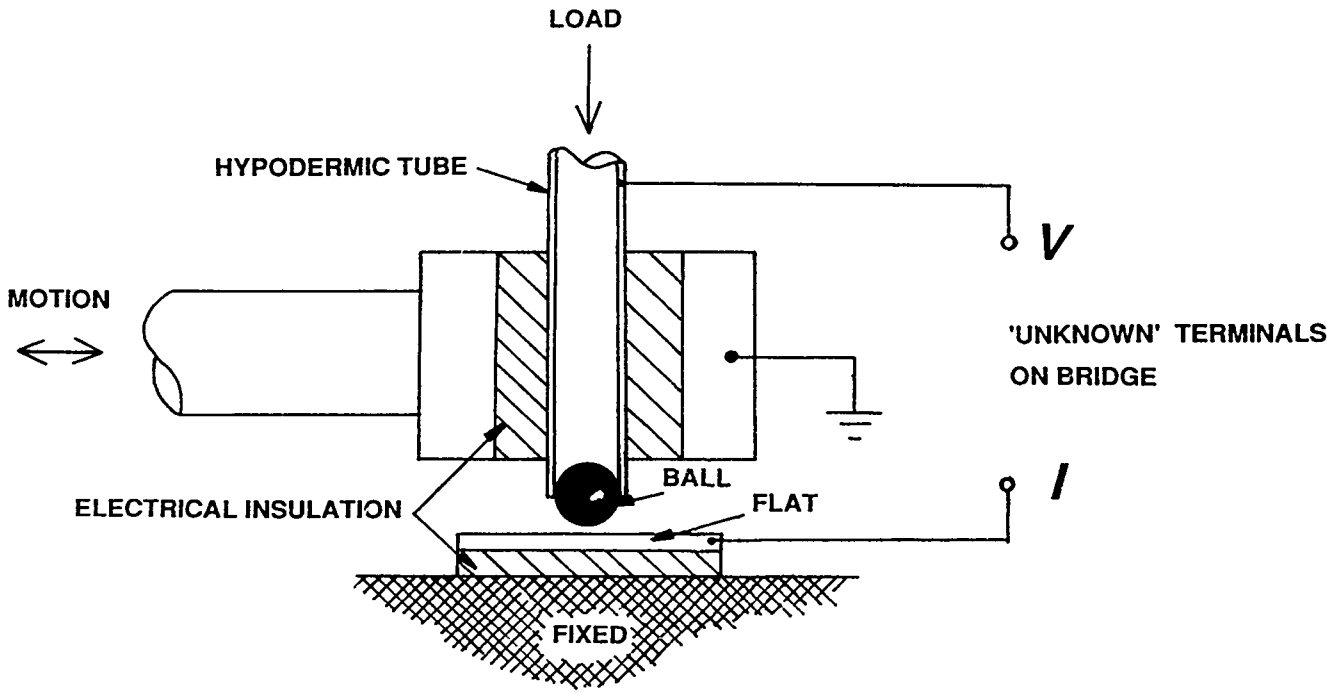

FIGURE 5

CAPACITANCE MEASURING CIRCUIT

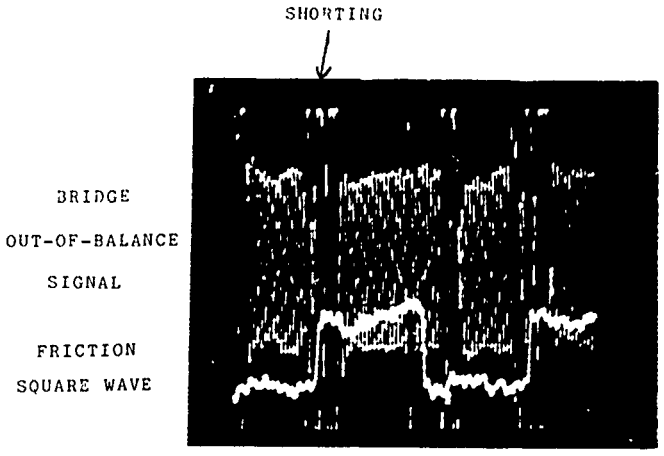

FIGURE 6

FRICTION AND CAPACITANCE TRACES FROM
OSCILLOSCOPE SHOWING SHORTING OF
CAPACITANCE DUE TO METAL-METAL CONTACT

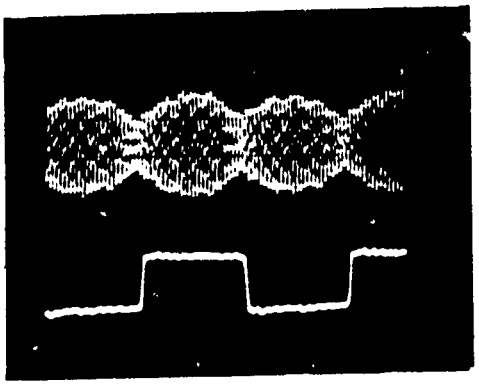

(a)

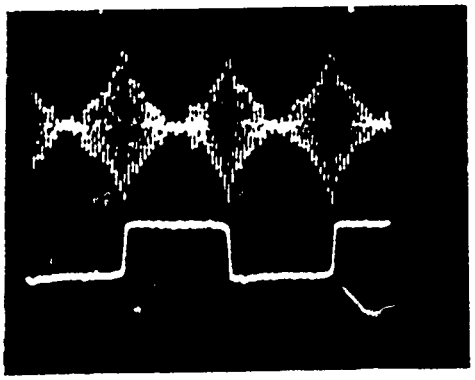

(b)

FIGURE 7

(a) TYPICAL BRIDGE OUT-OF-BALANCE SIGNAL

(b) SIGNAL BALANCED AT MID-STROKE

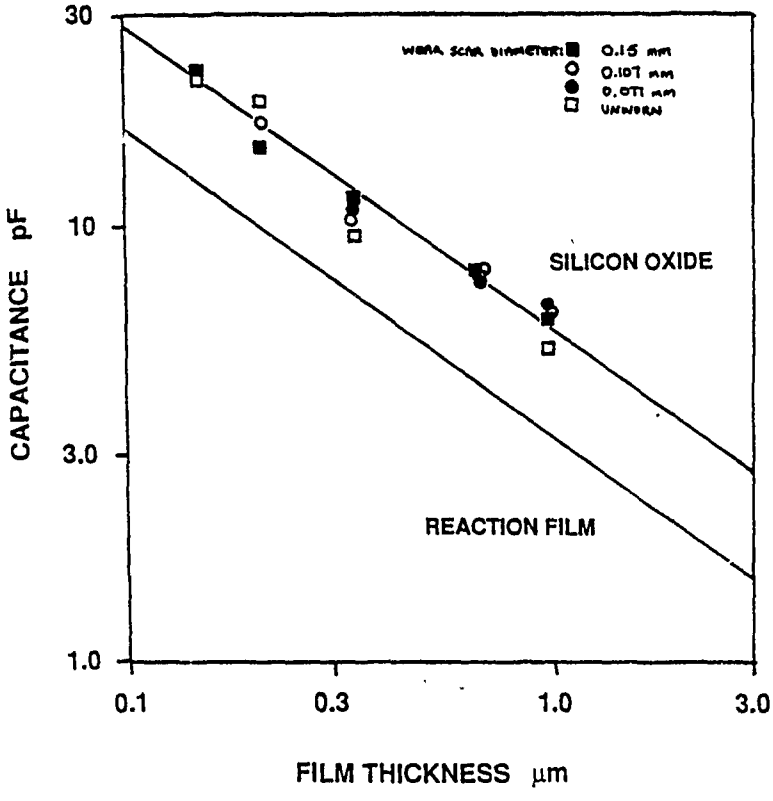

FIGURE 8

CALIBRATION CURVE OF CAPACITANCE
AGAINST FILM THICKNESS

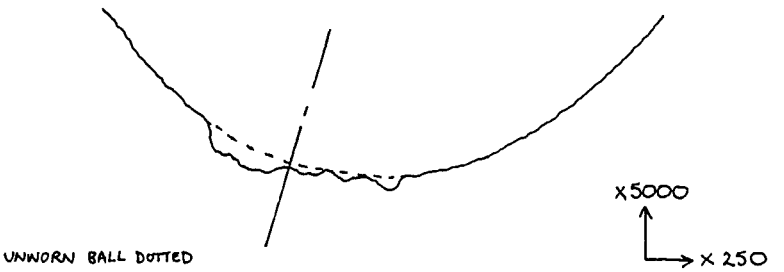

FIGURE 9

WORN PROFILE OF A BALL

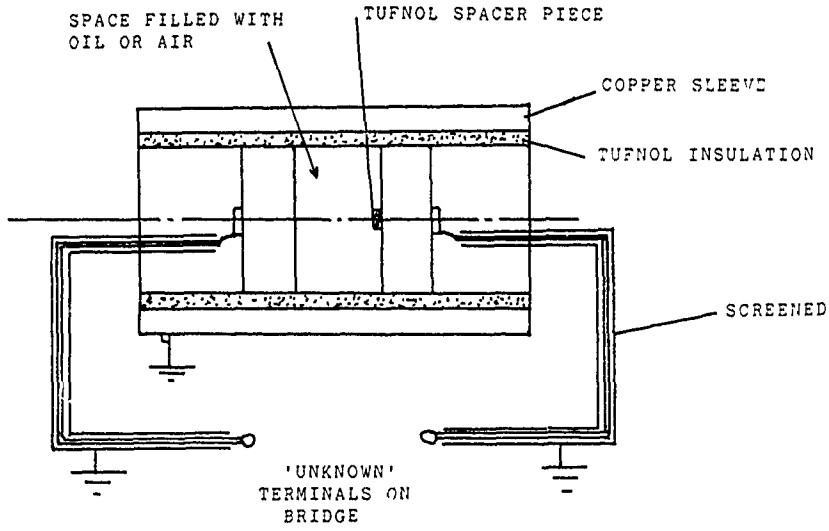

FIGURE 10

CAPACITANCE CELL

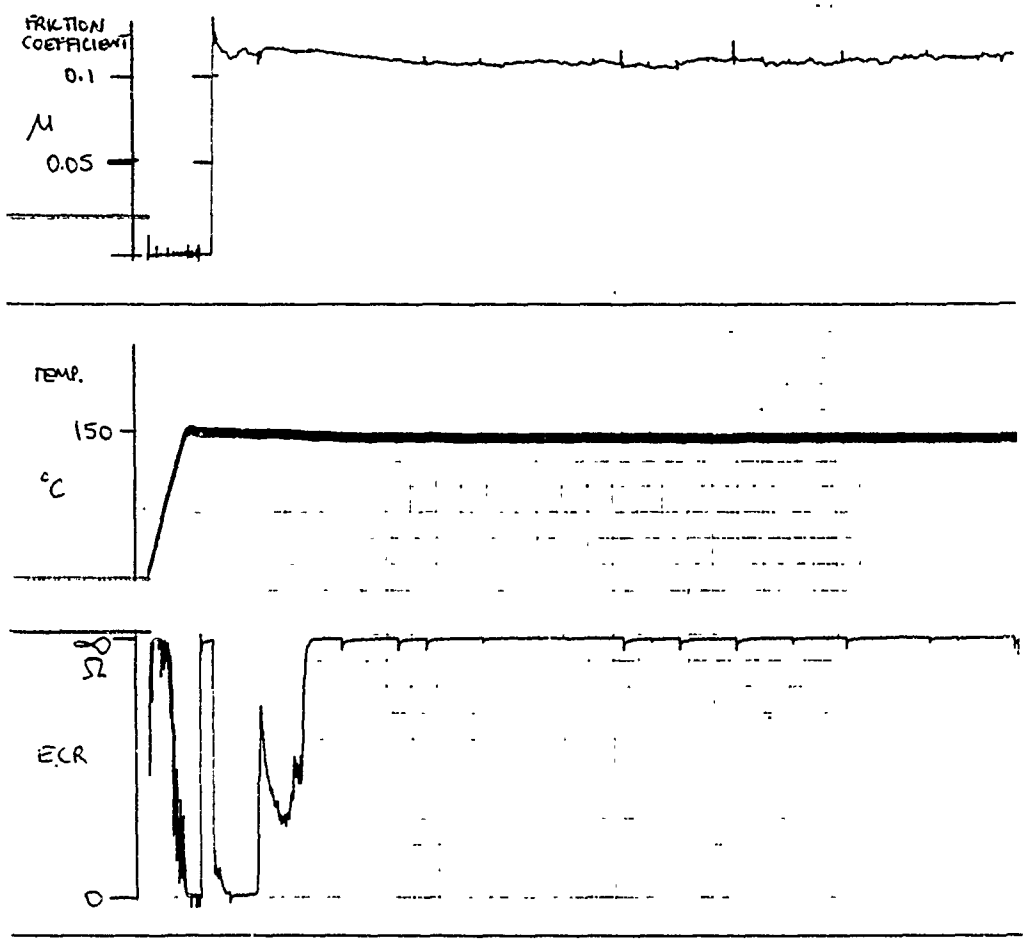

FIGURE 11

FRICTION, TEMPERATURE AND CONTACT RESISTANCE RECORD: CONDITIONS GIVEN

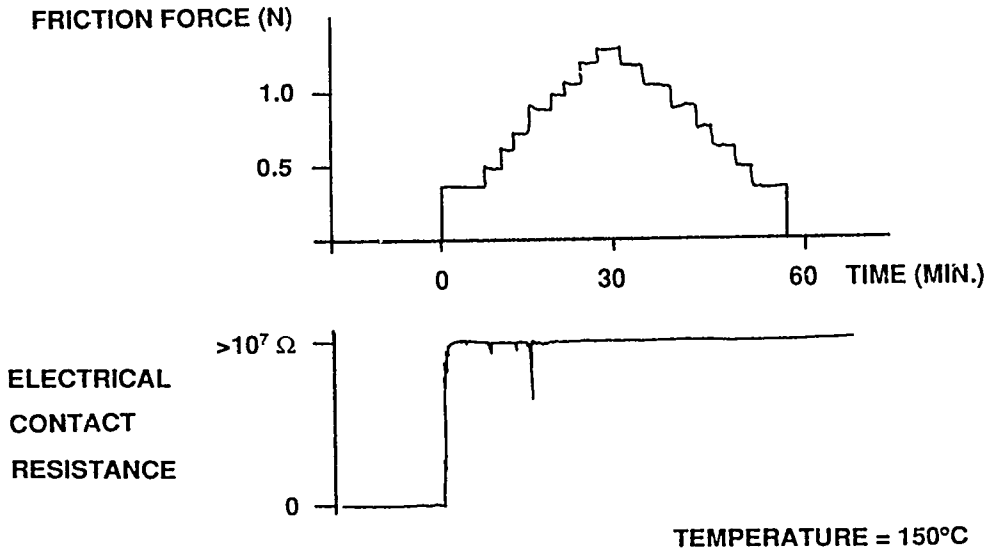

FIGURE 12

VARIABLE LOAD EXPERIMENT

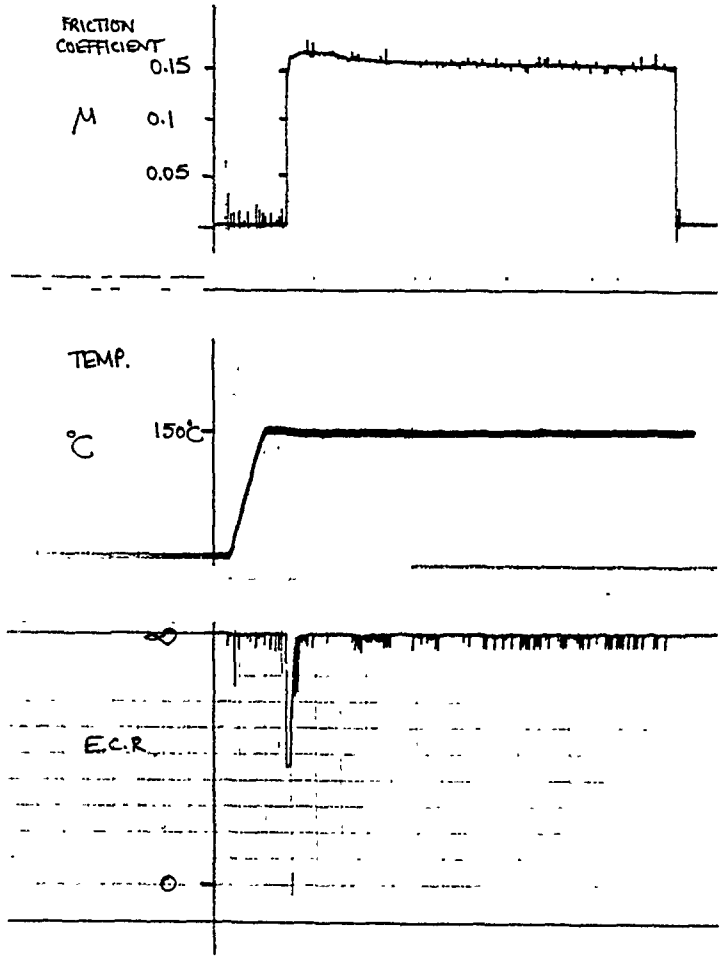
FRICTION
COEFFICIENT
0.15
μ
0.1
0.05
TEMP.
°C
150°C
E.C.R.
500 SN + 1% PARANOX 16
±0.5mm
34.5 Hz
RADIUSED PIN ON CAST IRON

FIGURE 13

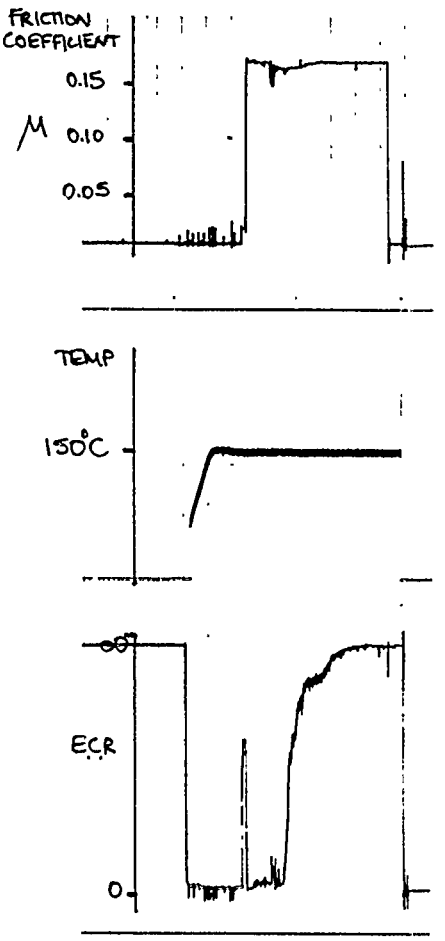

500 SN + 1% PARANOX 16 RADIUSED PIN ON CAST IRON
±0·5 mm
34·5 Hz.

FIGURE 14

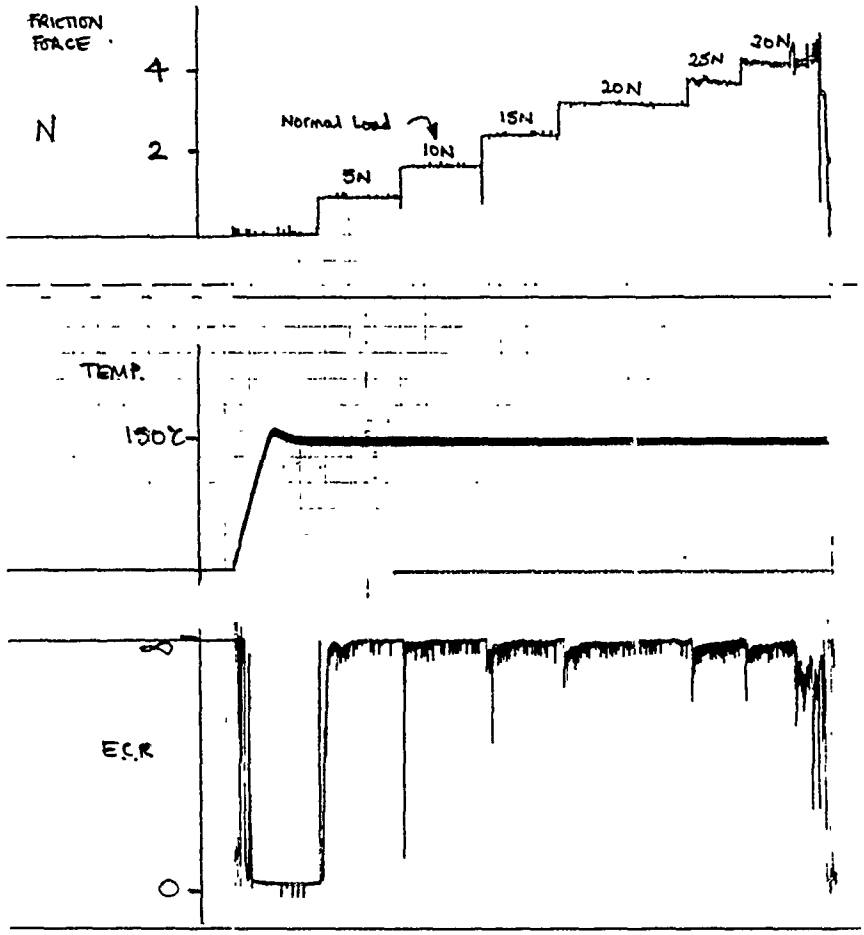

500SN + 1% PARANOX 16 RADIUSED PIN ON CAST IRON
±0.5mm
34.5 Hz

FIGURE 15

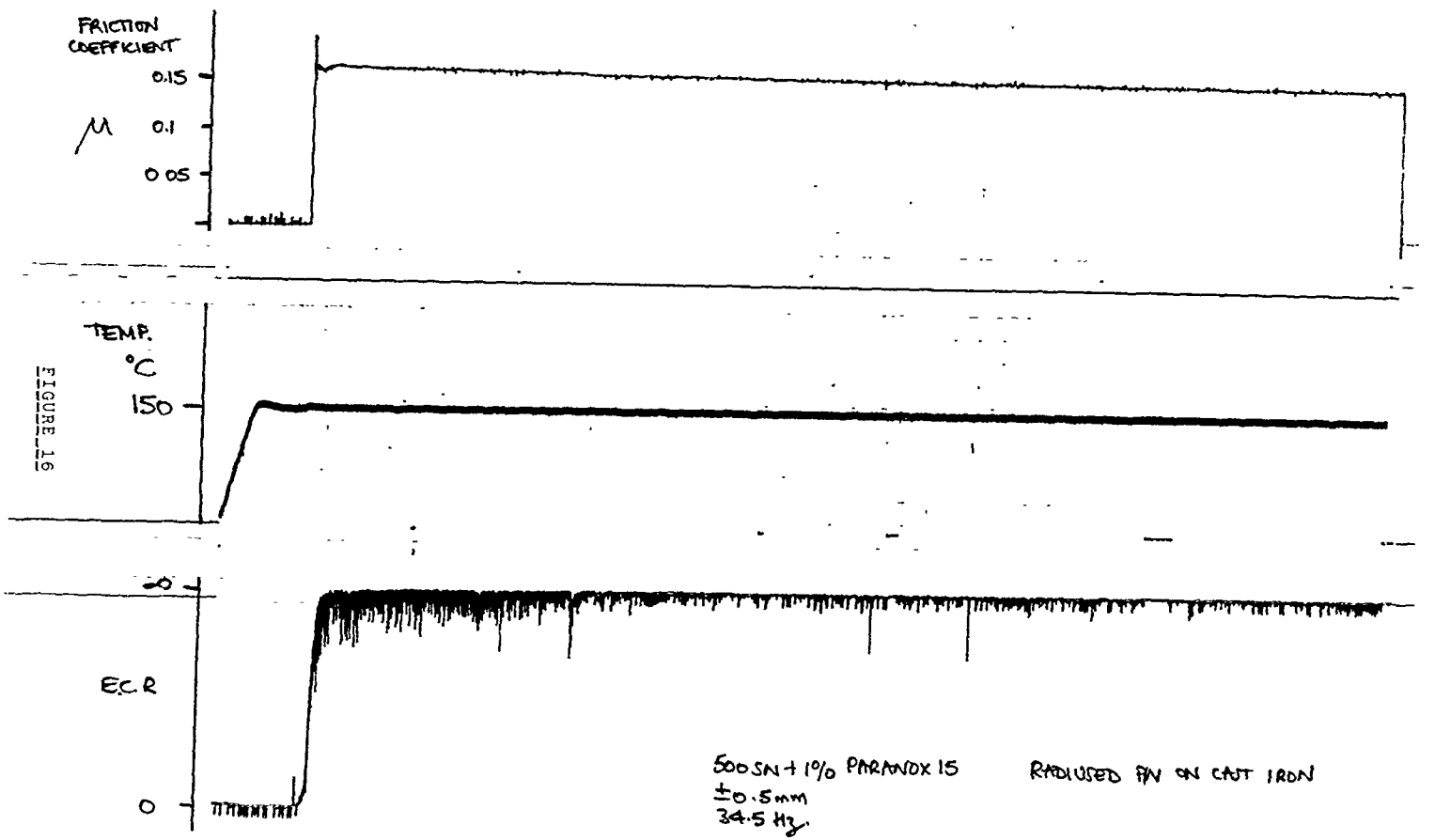
FRICTION COEFFICIENT
0.15
μ 0.1
0 05
TEMP.
°C
150
0
E.C.R
0
500SN + 1% PARANOX 15
±0.5mm
34.5 Hz.
RADIUSED PIN ON CAST IRON

FIGURE 16

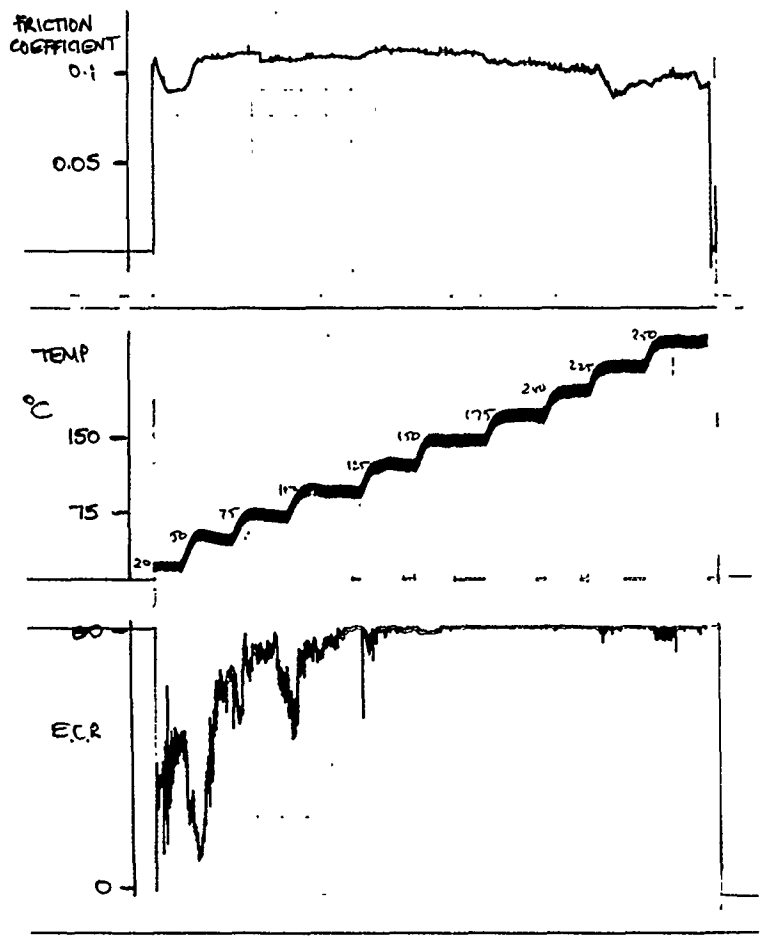

500SN + 1% PARANOX 16 RADIUSED PIN ON STEEL FLAT
±0·5mm
34·5 Hz

FIGURE 17

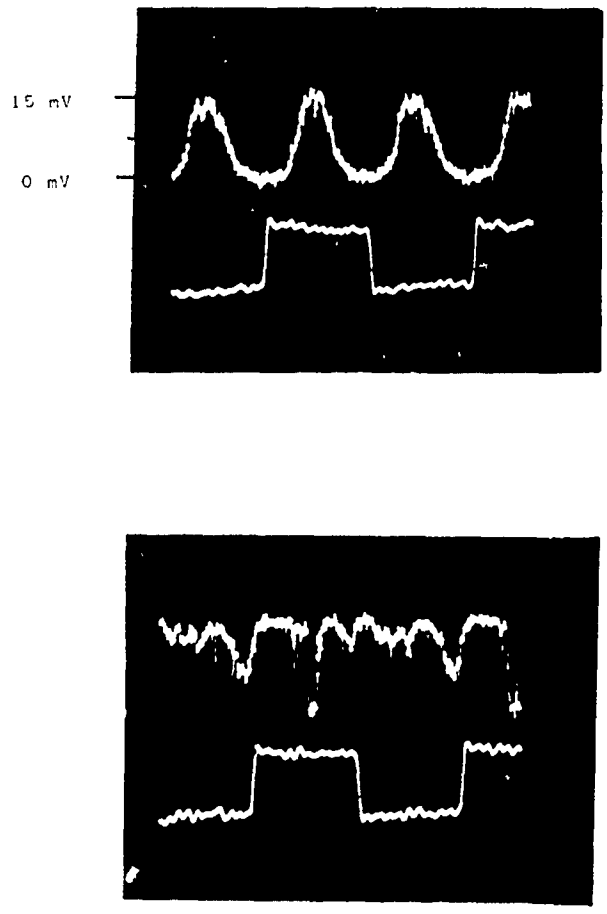

FIGURE 18

FRICTION AND E.C.R. PICTURE
FROM OSCILLOSCOPE, SHOWING 'HYDRODYNAMIC' ACTION

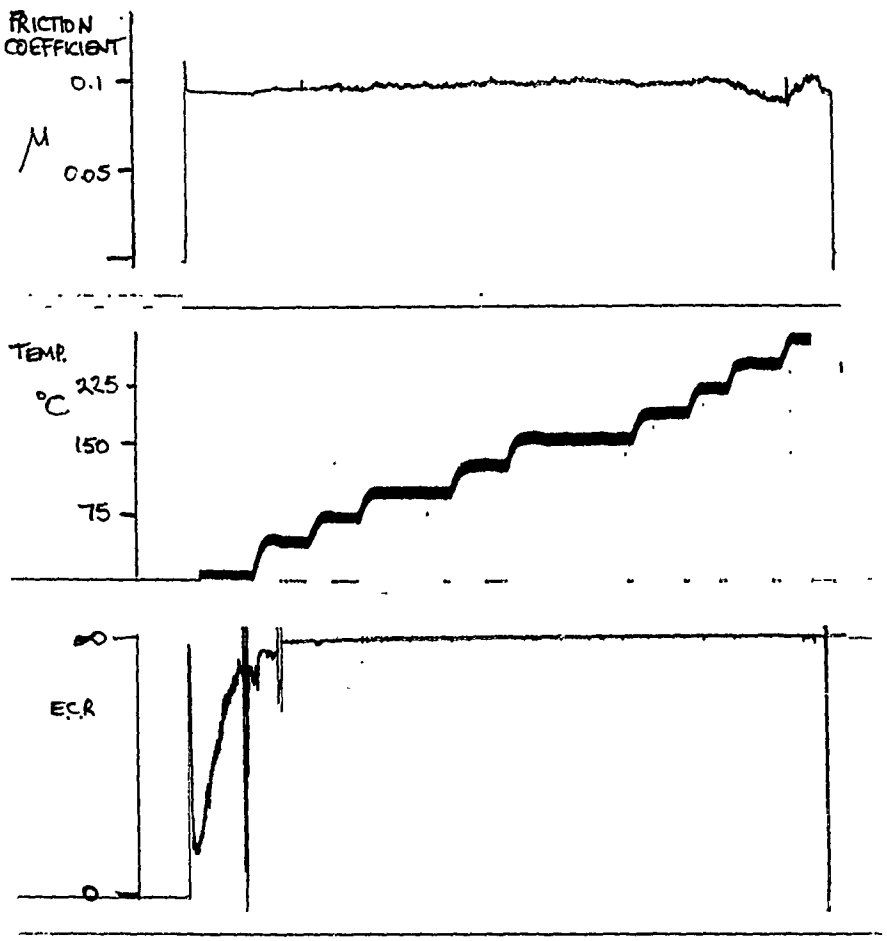

500SN + 1% PARANOX 16 BALL BEARING ON STEEL FLAT
±0.5mm
34.5 Hz.

FIGURE 19

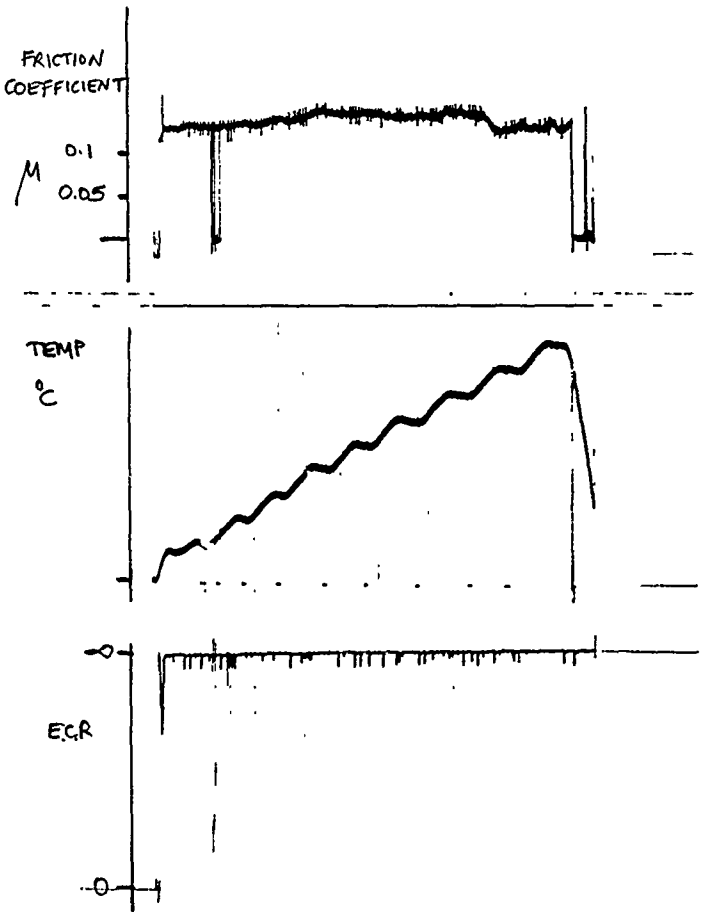

500SN + 1% LUBRIZOL 1376A BALL BEARING ON STEEL FLAT
±0.5mm
34.5 Hz 0.2kg LOAD

FIGURE 20

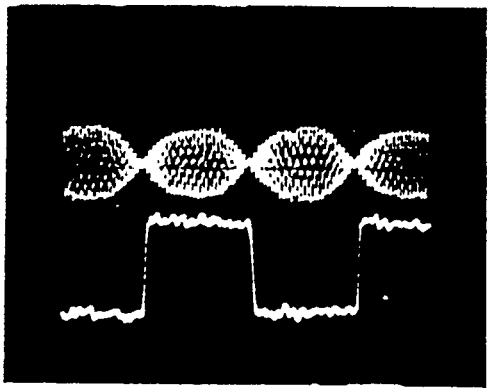

FIGURE 21

BRIDGE SIGNAL 'NULLED' AT ENDS OF STROKE

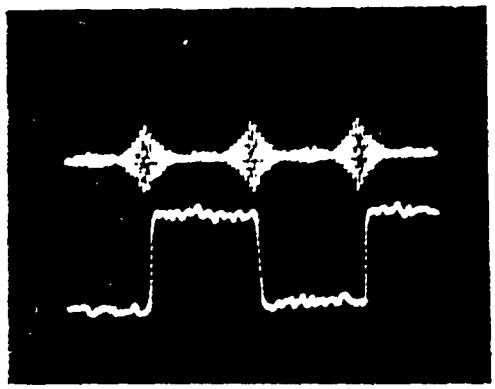

FIGURE 22

BRIDGE SIGNAL 'NULLED' AT MID-STROKE
SHOWING FILM SHAPE

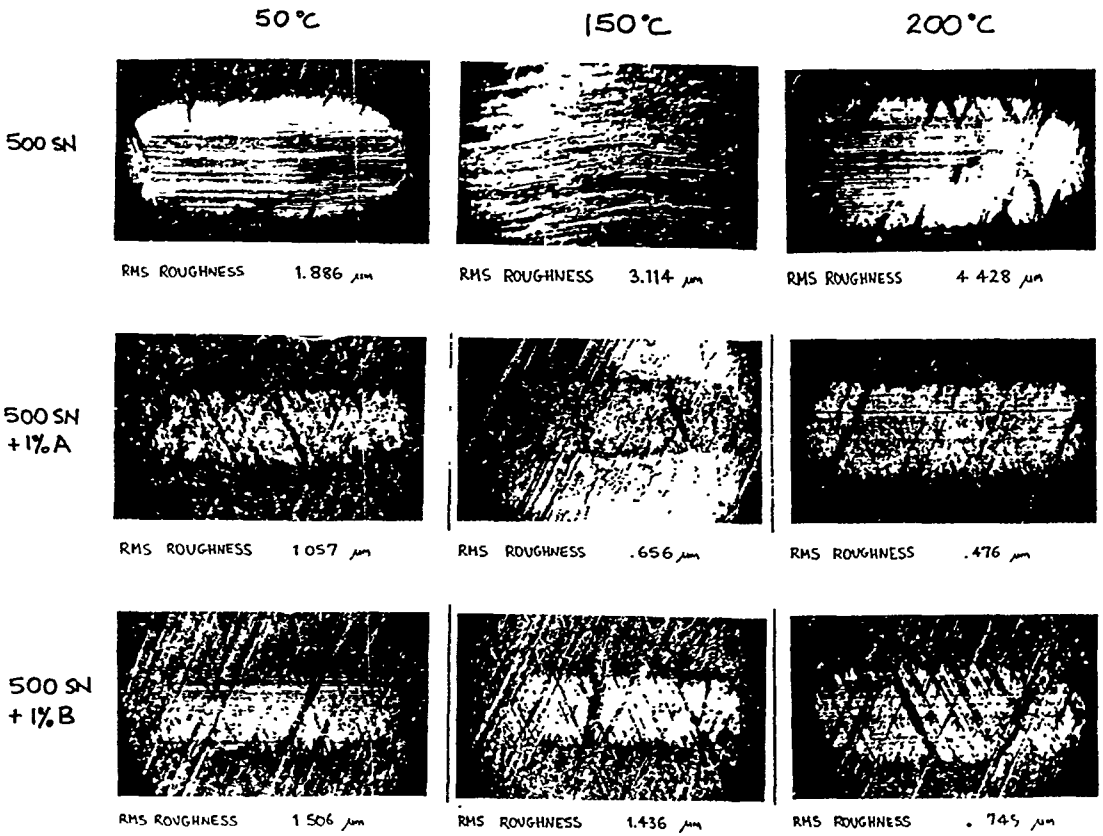

FIGURE 23

CAST IRON PHOTOGRAPHIC WEAR RECORD
AT LOAD OF 5 Kg. VARIBLE TEMPERATURE

UNWORN VALUE
RMS ROUGHNESS 1.510 µm

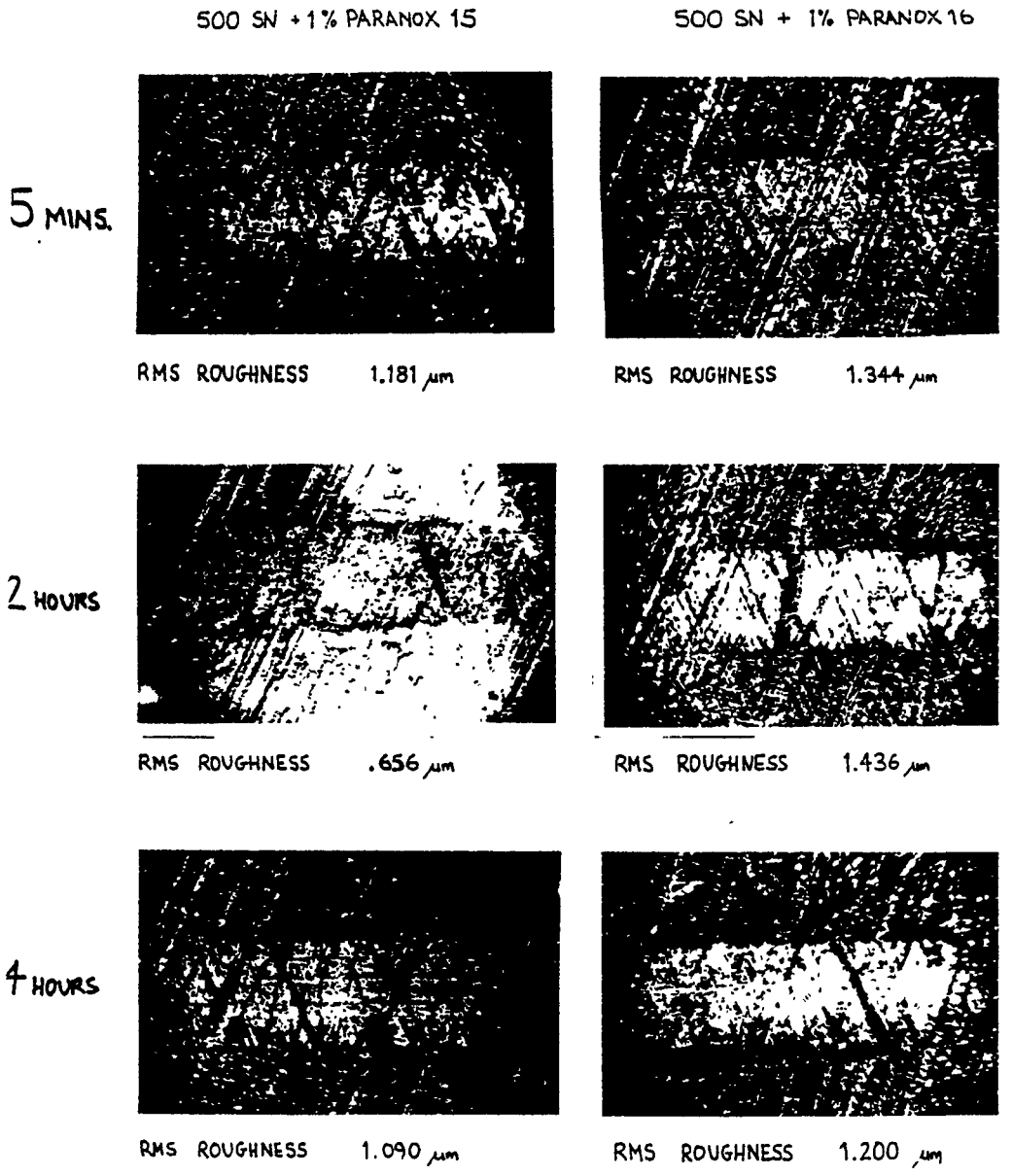

UNWORN VALUE : RMS ROUGHNESS 1.510 μm

FIGURE 24

CAST IRON WEAR RECORD
VARIABLE RUN-IN TIME

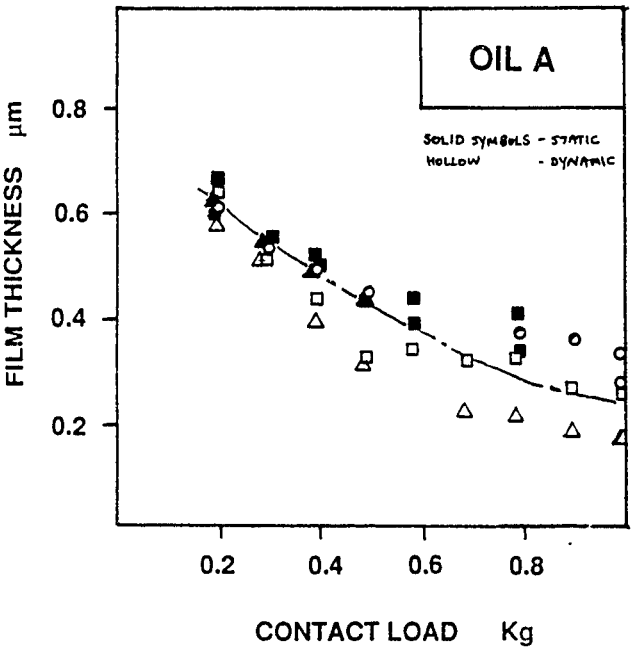

FIGURE 25

OIL A. VARIATION OF STATIC AND DYNAMIC FILM THICKNESS WITH LOAD

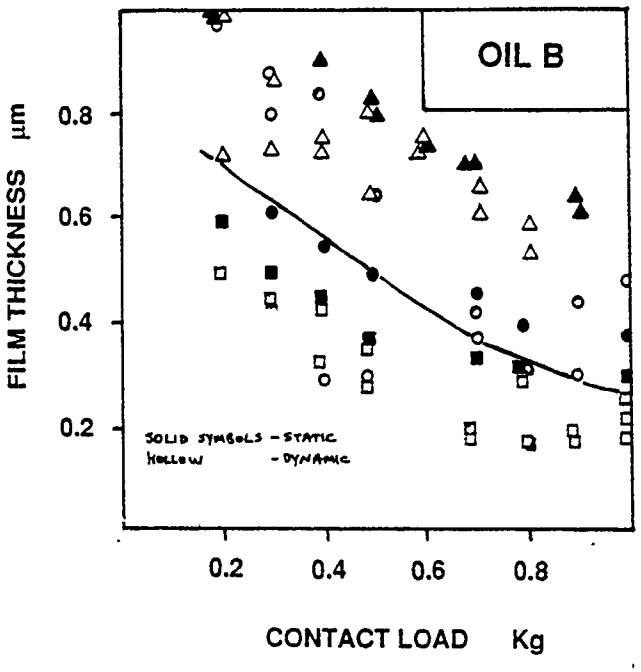

FIGURE 26

OIL B: VARIATION OF STATIC AND DYNAMIC FILM THICKNESS WITH LOAD

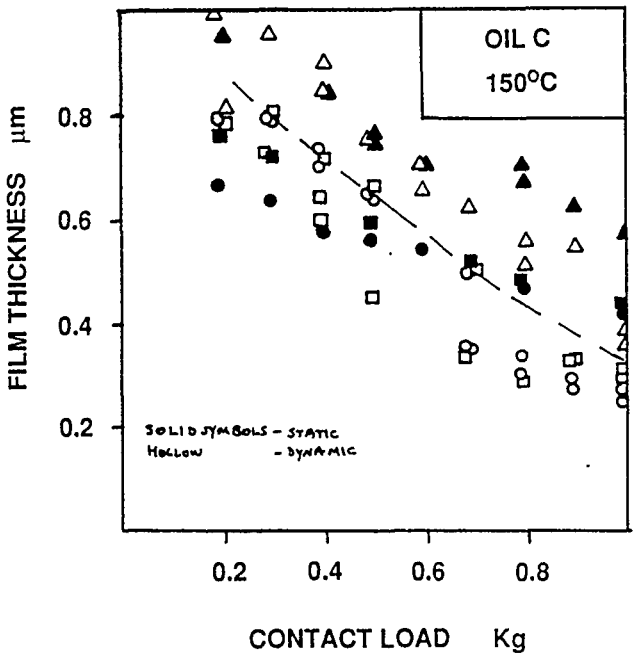

FIGURE 27

OIL C: VARIATION OF STATIC AND DYNAMIC FILM THICKNESS WITH LOAD

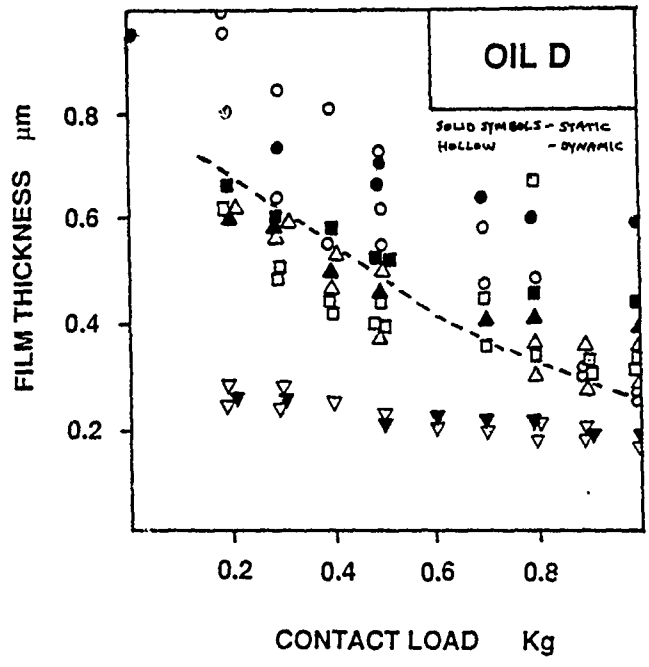

FIGURE 28

OIL D: VARIATION OF STATIC AND DYNAMIC FILM THICKNESS WITH LOAD

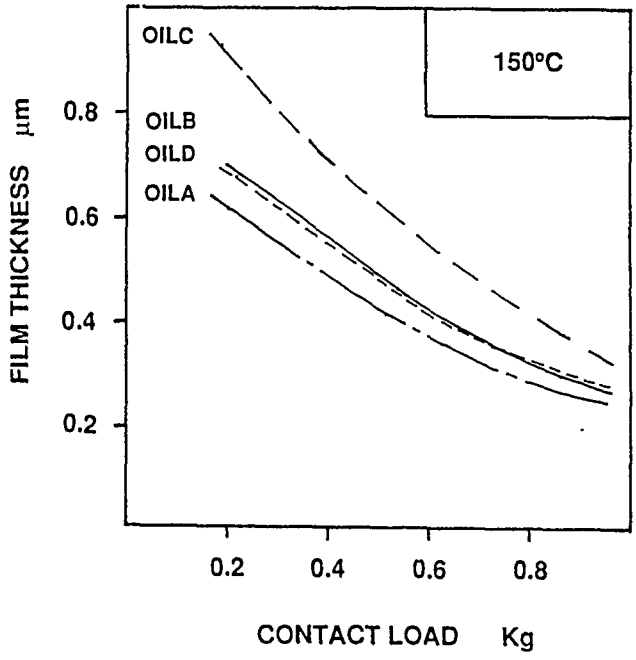

FIGURE 29

COMPARISON OF FILM THICKNESSES BETWEEN
THE OILS - BALL SPECIMENS

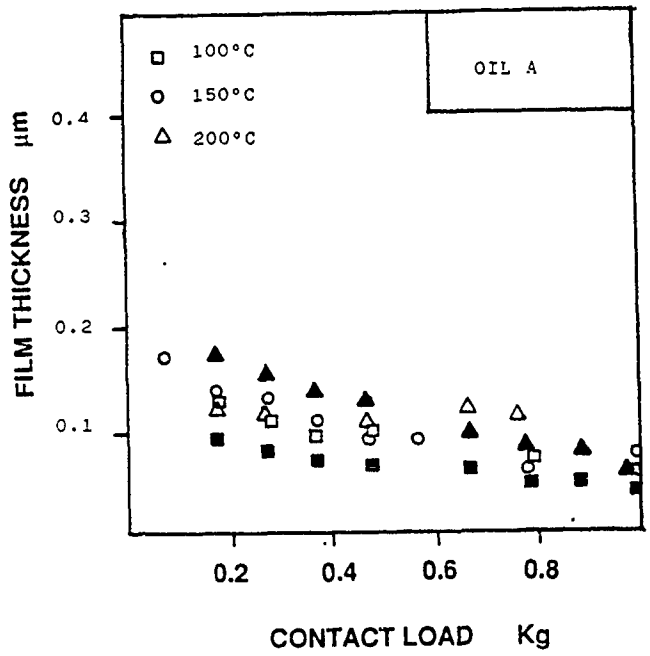

FIGURE 30

OIL A: VARIATION OF FILM THICKNESS WITH LOAD
RADIUSED SPECIMENS

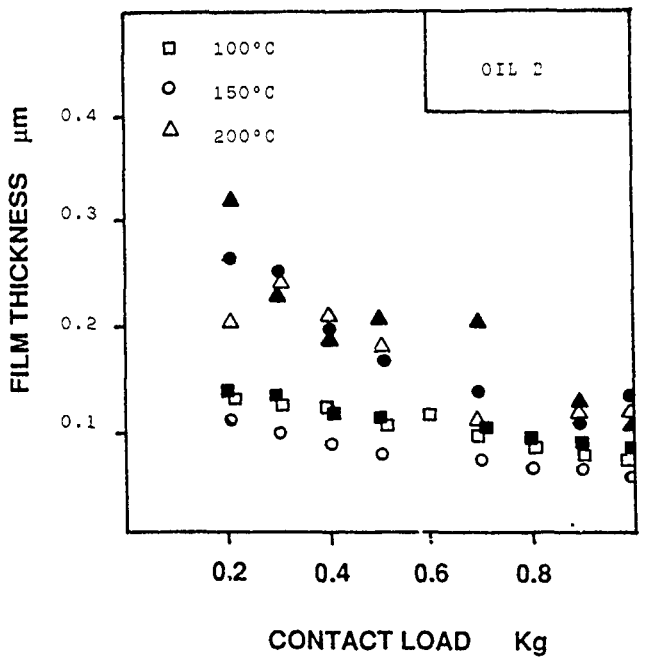

FIGURE 31

OIL B: VARIATION OF FILM THICKNESS WITH LOAD
RADIUSED SPECIMENS

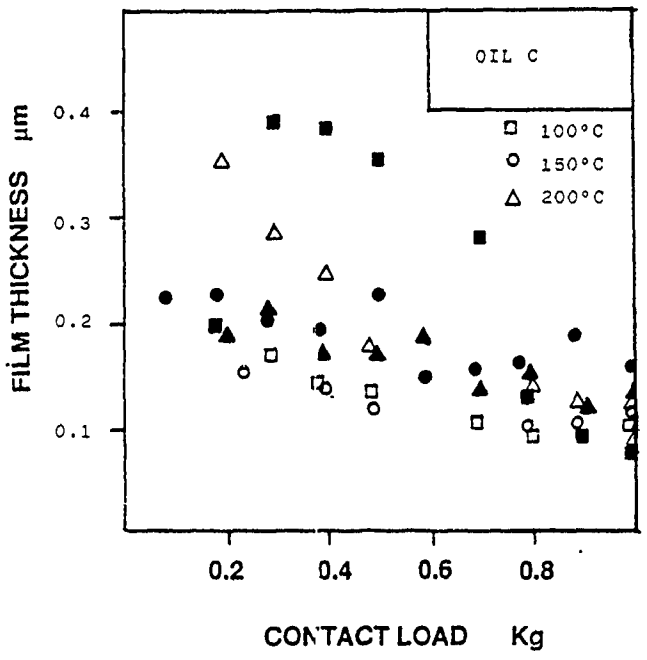

FIGURE 32

OIL C: VARIATION OF FILM THICKNESS WITH LOAD
RADIUSED SPECIMENS

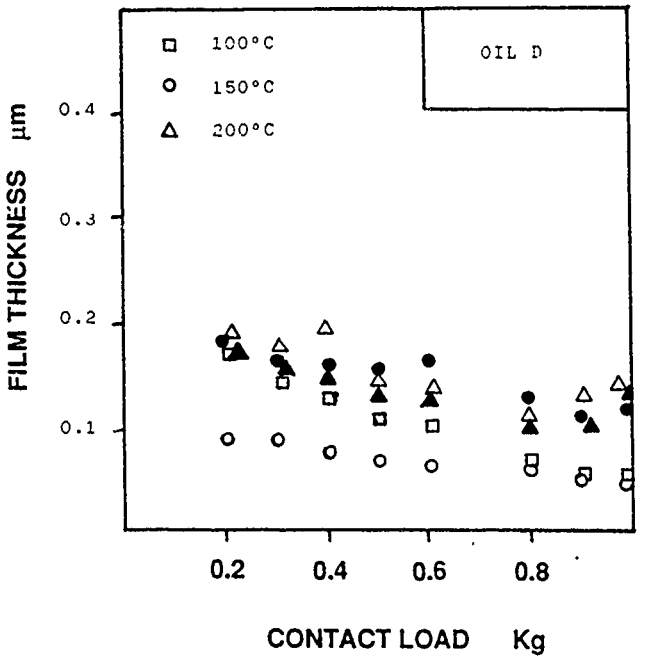

FIGURE 33

OIL D: VARIATION OF FILM THICKNESS WITH LOAD
RADIUSED SPECIMENS

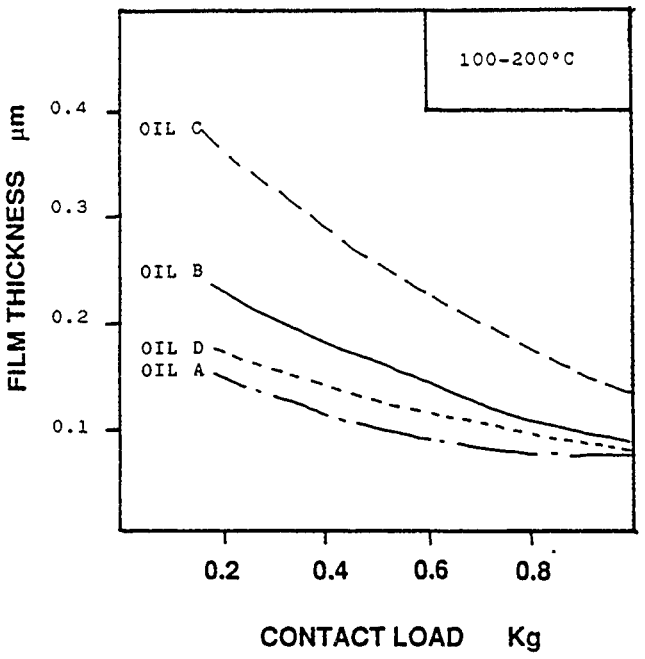

FIGURE 34

COMPARISON OF FILM THICKNESSES BETWEEN THE OILS RADIUSED SPECIMENS

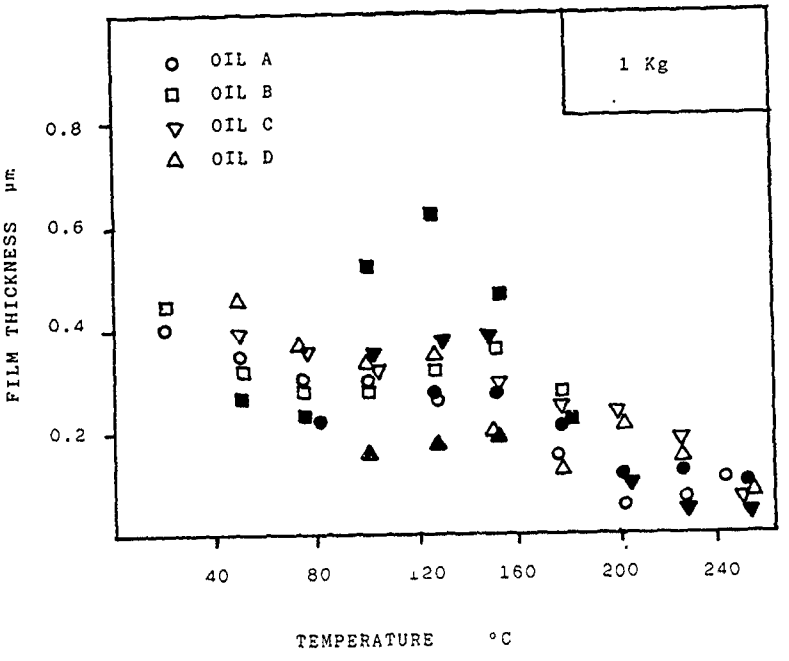

FIGURE 35

VARIATION OF FILM THICKNESS WITH TEMPERATURE
AT A CONSTANT LOAD OF 1 KG

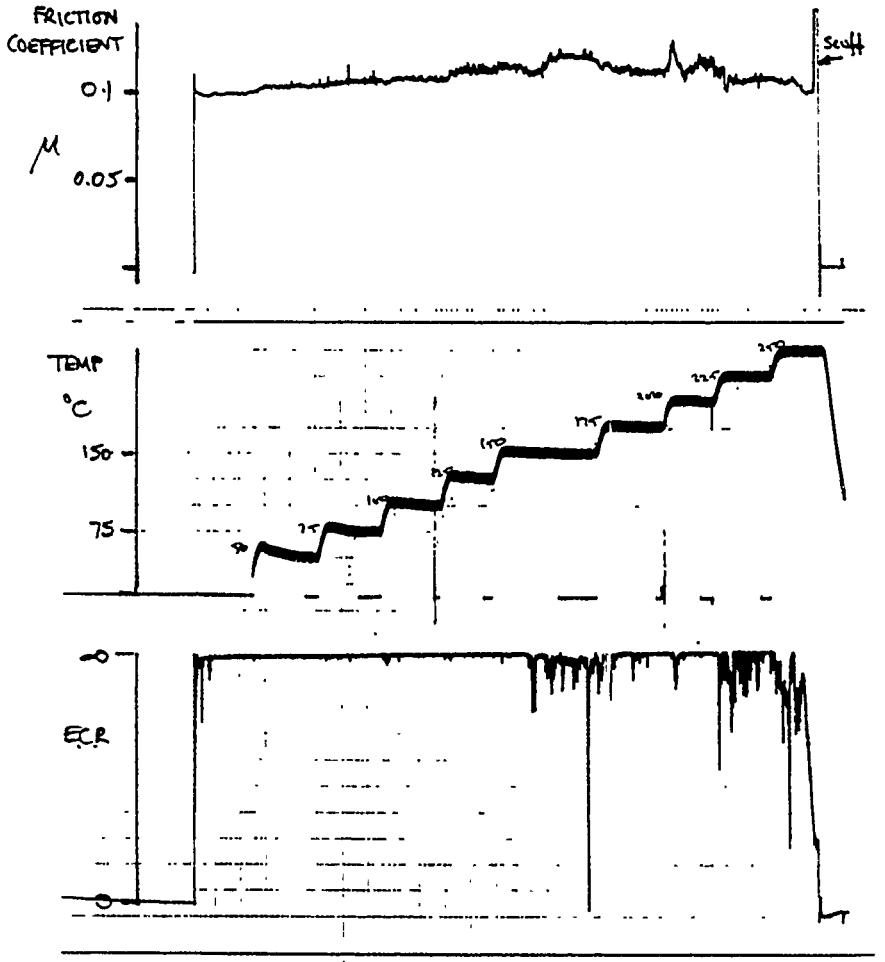
FRICTION
COEFFICIENT
0.1
μ
0.05
Scuff
TEMP
°C
150
75
ECR
500 SN ± 1% PARAFFIN OIL
± 0.5 mm
34.5 Hz
1 kg LOAD

FIGURE 36

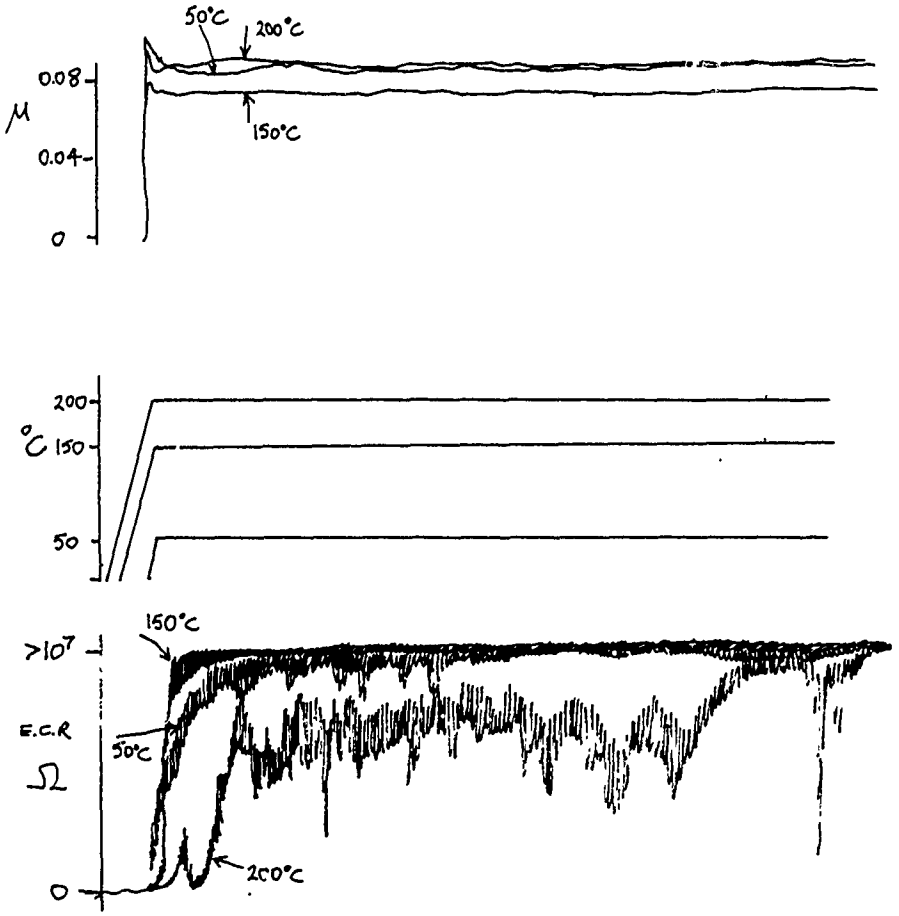

FIGURE 37

CAST IRON EXPERIMENTS AT DIFFERENT TEMPERATURES
OIL A WITH 5 KG LOAD

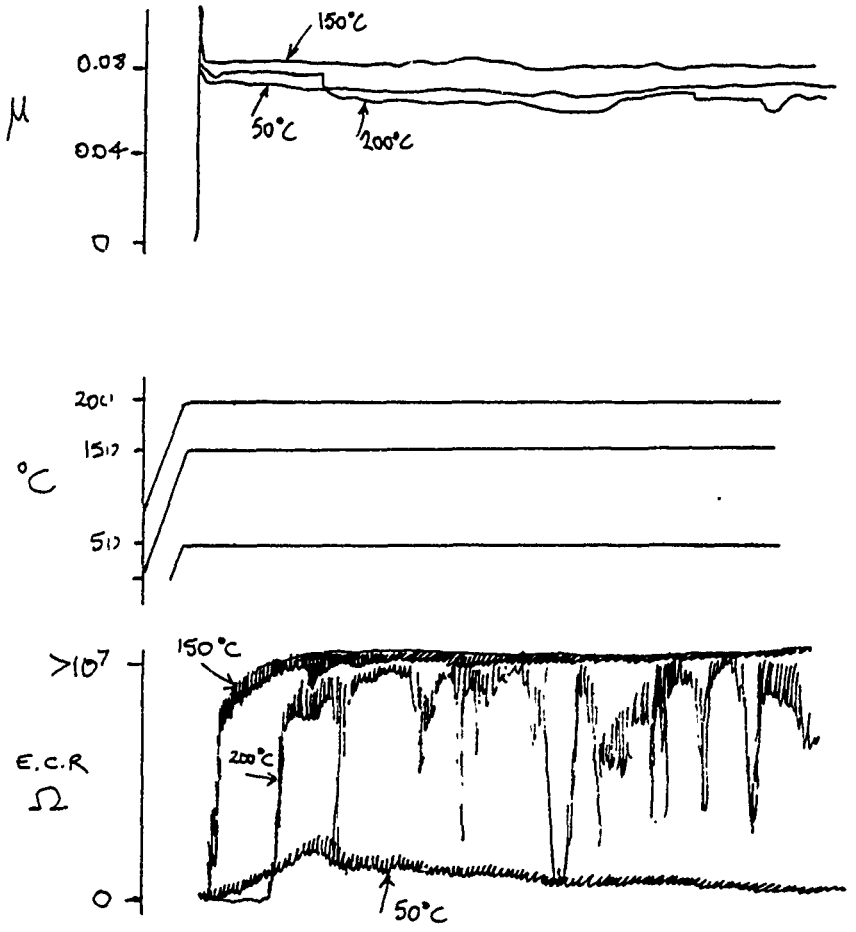

FIGURE 38

CAST IRON EXPERIMENTS AT DIFFERENT TEMPERATURES
OIL B WITH 5 KG LOAD

APPENDIX 1

CIRCUIT DIAGRAMS

Friction Force

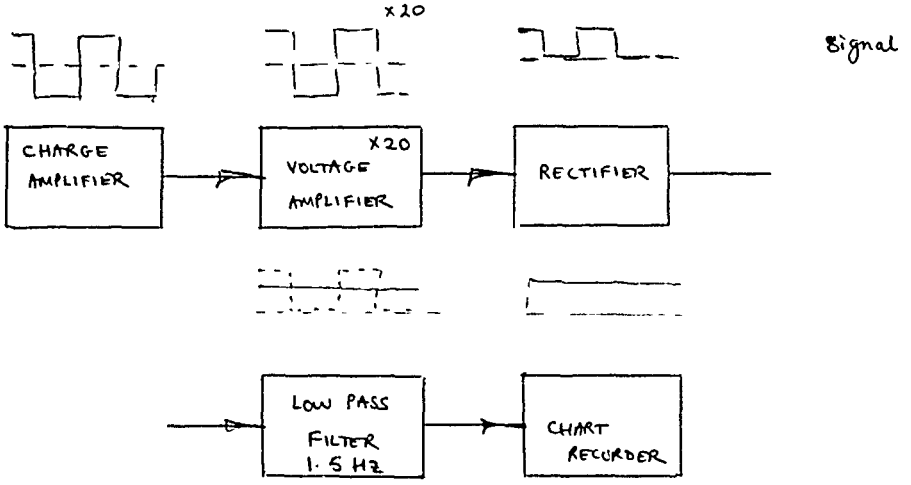

Charge amplifier: high impedance amplifier

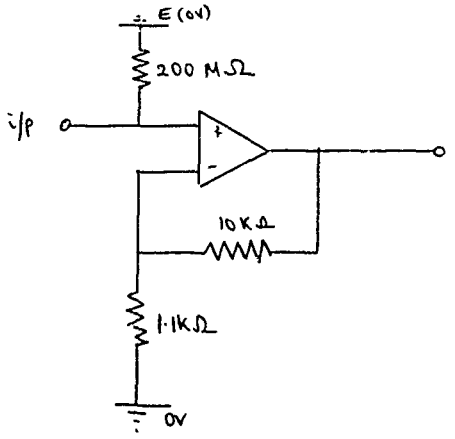

Friction Force (cont'd)

Voltage amplifier (2-stage)

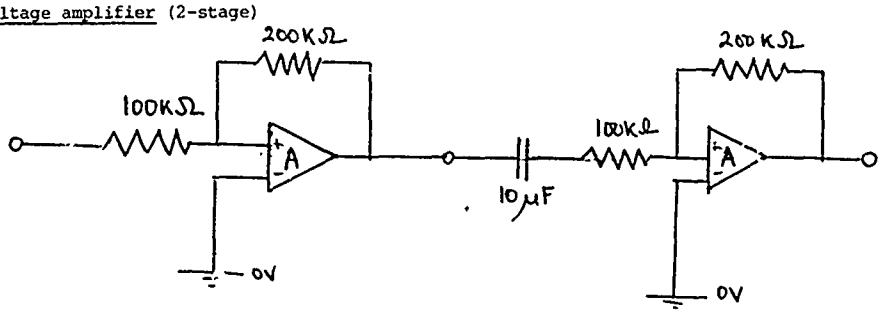

Rectifier

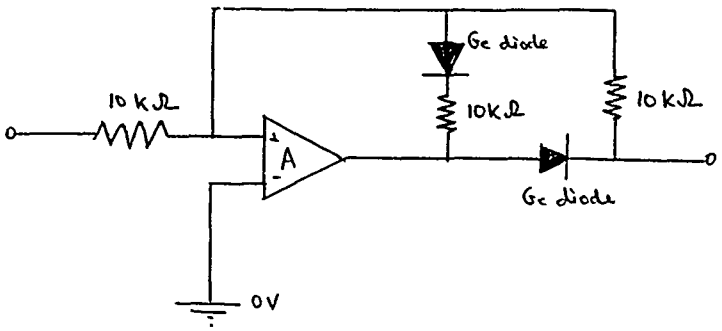

This circuit was used in preference to a single diode rectifier circuit which would not have given a clean rectified signal.

Low pass filter

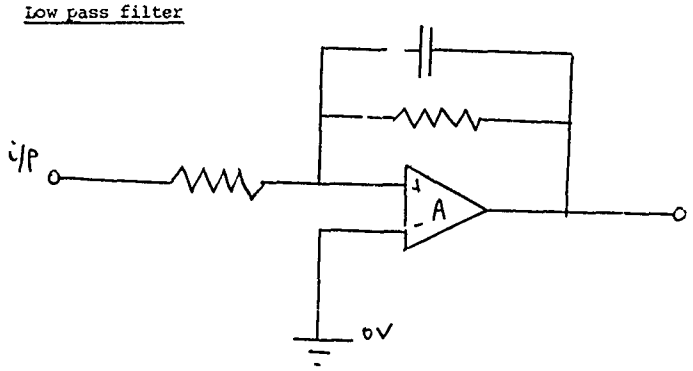

ELECTRICAL CONTACT RESISTANCE

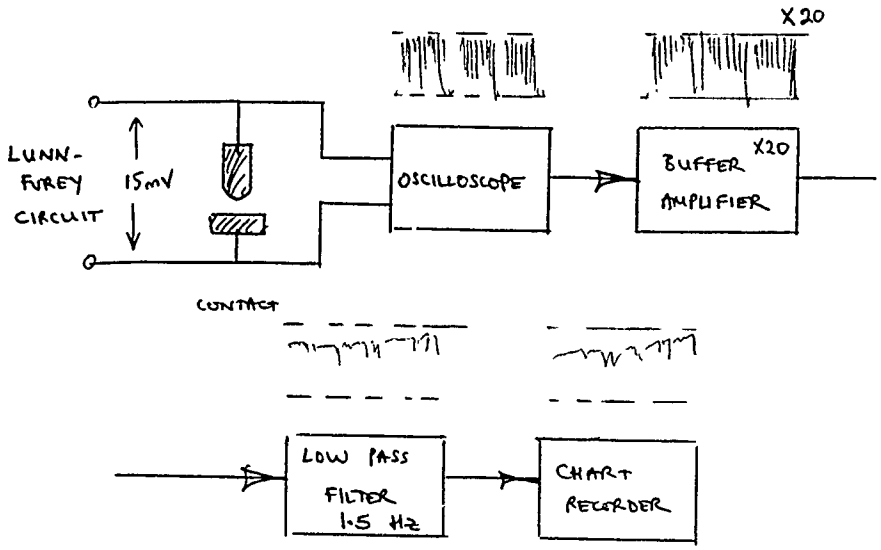

Amplifier and buffer

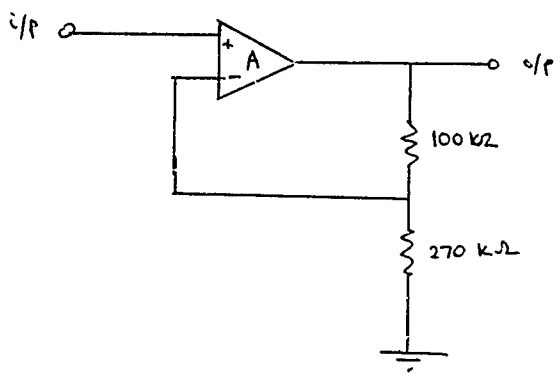

Low pass filter: same as in friction force measurement

REFERENCES

1 KAPSA, Ph, MARTIN, J M, Boundary lubricant films: a review, Trib. Int., 1982, 15, 37-42

2 FUREY, M J, Film formation by an antiwear additive in an automotive engine, ASLE Trans., 1959, 2, 91-100

3 GEORGES, J M, MARTIN, J M, et al., Mechanism of boundary lubrication with zinc dithiophosphate, Wear, 1979, 53, 9-34

4 KASTING, G B, The composition of four-ball wear-scar films formed by crankcase lubricants, ASLE Trans., 1985, 28, 351-357

5 FUREY, M J, Metallic contact and friction between sliding surfaces, ASLE Trans., 1961, 4, 1-11

6 FIENNES, W G, ANDERSON, J C, An analysis of voltage discharge measuremnts in lubrication research, Proc. I. Mech. E., C112/72, 1972, 109-119

7 HIGGINSON, J G, The failure of elastohydrodynamic lubrication, PhD Thesis, Cambridge University, England, 1984

8 SAKAMOTO, T, UETZ, H, FÖHL, J, KHOSRAWI, M A, The reaction layer formed on steel by additives based on sulphur and phosphorus compounds under conditions of boundary lubrication, Wear, 1982, 77, 139-157

9 COY, R C, QUINN, T F J, An application of electron probe microanalysis and X-ray diffraction to the study of surfaces worn under extreme pressure lubrication, Proc. I. Mech. E., 1972, C94, 62-68

10 TONCK, A, MARTIN, J M, KAPSA, Ph, GEORGES, J M, Boundary lubrication with anti-wear additives: study of interface film formation by electrical contact resistance, Trib. Int., 1979, 12, 209-212

11 FOWLES, P E, JACKSON, A, MURPHY, W R, Lubricant chemistry in rolling contact fatigue - the performance and mechanism of one anti-fatigue additive, ASLE Trans, 1980, 24, 107-118

12 BOWDEN, F P, TABOR, D, The friction and lubrication of solids, in Int. Series of Monographs on Physics, Clarendon Press, Oxford, 1986

13 WINER, W O, in Appendix to CZICHOS, H, BECKER, S, LEXOW, J, Multilaboratory tribotesting: results from the Versailles advanced materials and standards programme on wear test methods, Wear, 1987, 114, 109-130

14 SNYDER, F L, TEVAARWERK, J L, SCHEY, J A, Effects of oil additives on lubricant film thickness and traction, SAE Paper No. 840263, 1984

15 JOHNSTON, G, CANN, P M E, SPIKES, H A, A new mechanism of gear and bearing anti-wear additive behaviour. 5th International Colloq. 'Additives for lubricants and operational fluids', Esslingen, 1986, Paper 3.12, 1-10

16 MILLS, T N, CAMERON, A, Basic studies on boundary, EP, and piston-ring lubrication using on special apparatus, ASLE Trans., 1981, 25, 117-124

17 ALLISTON-GREINER, A F, CAMERON, A, GREENWOOD, J A, Basic mechanisms of diesel lubrication correlation of bench end engine tests, 1st Interim Report, January 1986

18 ALLISTON-GREINER, A F, CAMERON, A, GREENWOOD, J A, Basic mechanisms of diesel lubrication, correlation of bench and engine tests, 2nd Interim Report, July 1986

19 BAILEY, M W, CAMERON, A, The effects of temperature and metal pairs on scuffing, ASLE Trans., 1972, 16, 121-131

20 LUNN, B, Epilamen und Mischreibung, ZVDI Berichte, 1957, 20, 41-46

21 HAMILTON, G M, MOORE, S L, The lubrication of piston rings, Proc. I. Mech. E., 1974, 188, 253-268

22 HAMILTON, G M, The hydrodynamics of cam follower, Trib. Int. 1980, 13, 113-119

23 GALVIN, G D, NAYLOR, H, WILSON, A R, The effects of pressure and temperature on some properties of fluids of importance in elasto-hydrodynamic lubrication, Proc. I. Mech. E., 1963, 178, 283-290

24 DYSON, A, NAYLOR, H, WILSON, A R, The measurement of oil-film thickness in EHD contacts, Proc. I. Mech. E., 1965, 180, 119-134

25 CANN, P M E, JOHNSTON, G J, SPIKES, H A, The formation of thick films by phosphorus-based anti-wear additives, Proc. I. Mech. E., Tribology - friction, lubrication and wear fifty years on, C208/87, 1987, 543-554

26 ROUNDS, F G, Additive interactions and their effect on the performance of a zinc dialkyldithiophosphate, ASLE Trans., 1977, 21, 91-101

27 BARCROFT, F T, PARK, D, Interactions on heated metal surfaces between zinc diathyldithophosphates and other lubricating oil additives, Wear, 1986, 108, 213-234

28 MONTEIL, G, LONCHAMPT, J, ROQUES-CARMES, C, Study of anti-wear properties of zinc dialkyldithiophosphates through sliding-induced electronic emission, Proc. I. Mech. E., Tribology - friction, lubrication and wear - fifty years on, C224/87, 1987, 531-536

29 BRISCOE, B J, SCRUTON, B, WILLIS, F R, The shear strength of thin lubricant films, Proc. Roy. Soc. Lond., 1973, A333, 99-114

30 AMUZU, J K A, BRISCOE, B J, TABOR, D, Friction and shear strength of polymers, ASLE Trans., 1977, 20, 354-358

APPENDIX

A BENCH TESTS

This phase of the work (detailed in Item 5 of the work statement C-1) can now begin, following the arrival of samples of engine parts and oils.

It is proposed to investigate the running-in process in the various supplied cylinder liner/piston-ring pairs, together with oils from standard engine tests. The materials were described in Table 1 below. The aim of this work is to try and gain a better understanding of what makes a 'good' surface. This will involve studying not only the run-in surfaces, but also the unworn surfaces, to see what features appear to make running-in and lubrication more favourable.

Table 1: Description of parts supplied

It was found (Jan 1991) that the column headed "Engine" should have read "Engine Test Sequence".

Code	Engine	Oils (Ref. Nos.)
A	Caterpillar OL-5	AL-15930-L
B	Caterpillar OL-6	AL-15931-L
C	Caterpillar 1G2	AL-15932/33/34/35-L
D	Cummins NTC-400	AL-15936-L
E	John Deere 6404	AL-15937-L
F	Mack T-7	AL-15939L

Further details are in Appendix 1 page 23 of Section 2.

1 Experiments at first will be restricted to using cylinder liner/oil pairs with the reciprocating specimen being a ball, not a segment of piston-ring. This is for ease of use.

2 A series of tests will be conducted on the running-in of each cylinder liner/oil pair, along the following lines, depending on experimental results

Run-in for $\begin{matrix}1\\2\\5\\30\\120\end{matrix}$ minutes at 150 - 350°C* and constant load $\frac{1}{5}$ kg.

Conditions of frequency and stroke amplitude will be typical of previous experiments, i.e. 35 Hz and ±0.5 mm. Run-in will proceed in the series of temperatures until lubricant or surface failure is observed. This is detected by a rapid rise in the friction force.

The unworn and run-in surfaces will then be characterised by surface profilometry. Details about changes in various surface parameters - especially the mean curvatures of the asperities - will be recorded. Changes in these parameters can be correlated with observations of how the surfaces ran-in (e.g. the friction force variations; the rate of formation of the reaction film; the 'quality' of the reaction film when formed), as well as to visual, optical and scanning electron microscopic observation of the run-in surfaces.

3 In the case of liner C (see Table 1), where 4 oils are available, a matrix of tests can be performed to attempt to 'rank' the oils in order of 'best performance'. This ranking could be done on a criterion of the amount of wear that takes place, or possibly from the point of view of how various surface parameters are affected. Rankings will be obtained at different temperatures, to see if the lubricant performance changes according to this working condition.

It is hoped that these experiments and observations will substantially add to our understanding of exactly what makes a 'good' run-in surface.

---

*Temperature steps will at first be 25°C but may be increased to 50°C, depending on the observed sensitivity to temperature. Once more the uncertainty of the interfacial ring/liner temperature in running diesels makes itself felt.

PRESENTED AT THE 1987 LEEDS-LYON SYMPOSIUM

Paper VII(i)

The rheology of reaction films formed by ZDDP

A.F. Alliston-Greiner, J A. Greenwood and A Cameron

This paper describes experiments performed in a reciprocating ball-on-flat rig operating in the boundary lubrication regime and at contact temperatures up to 250°C. Measurements of contact capacitance permitted deductions about the thickness of the reaction films formed in the contact by ZDDP additives: a typical value was 0.1 μm, far thicker than a true "boundary film" as normally understood. The shear strength of the reaction films were studied as a function of load, temperature and shear rate. Typical contact conditions were $\bar{p}$ = 500 MPa and shear rate 10^6 s^{-1}. The shear behaviour of the films were similar to those of thin films of organic polymers.

1 INTRODUCTION

Zinc dialkyldithiophosphate (ZDDP) is used commercially as an anti-wear agent in diesel and aut motive engines. By reacting chemically with the sliding metal surfaces a polymerised film is thought to be formed which separates the rubbing surfaces, so reducing wear. In these practical applications the film forms under e.h.l. conditions, but appears to be additional to the usual e.h.l. film as shown by Tevaarwerk et al. [1] and Spikes et al. [2], it has many of the features of a boundary lubricating film as normally understood, except that it is far thicker and is correspondingly more effective in reducing wear.

If the formation is a simple chemical reaction, then it should be possible to study it without the confusing factor of an e.h.l. environment; and in particular to study its formation at slow speeds where the surface temperatures are known with confidence. One might go further and eliminate the rubbing completely - but then the film does not form. Relative sliding appears to be essential for the reaction/polymerisation to occur. The role of the surfaces in this reaction has been studied recently by Kajdas [3] and Monteil [4].

Little is known about the film formation or about its behaviour in the contact itself: particularly it is not known if the film exhibits hydrodynamic properties. Recent work in France [5] has shown how films could be removed after they had been formed in a rubbing contact and transferred to specially prepared surfaces. A reciprocating ball on flat apparatus with a very small amplitude of motion (10 - 30 nm) was used to study the elastic behaviour of the films. On the assumption that the reaction film was polymeric in nature, Briscoe et al [6] deposited thin layers of known organic polymers or built-up Langmuir-Blodgett type films and measured their rheological properties. A ball on flat device was also used but with very low, unidirectional sliding speeds, which were necessary to avoid penetration of the film by the ball.

In this paper work is described using a reciprocating ball-on-flat machine operating in the boundary regime of lubrication at elevated temperatures (up to 250°C). In any practical repeating contact device (such as the piston ring/cylinder liner) it is the repetition rate rather than the speed which is important when considering interaction of surface asperities. The protective film formed by additives is completely or partially removed during each contact and must be reformed before the next one: the time available for this is crucial. The rate of reformation depends on the chemical activity of the systems (metals and oil) and of course the temperature - see Bailey and Cameron [7]. Test devices are either high speed (giving large and unknown flash temperatures), with repetition rates similar to practical systems, or low speed giving repetition rates very much lower. The reciprocating apparatus therefore provides a simple device that avoids high flash temperatures (since the sliding velocity is low), but has the correct repetition rate. This means also that the contact temperature can be known with confidence from the bulk temperature of the test specimens.

Four commercial ZDDPs were used in this work, and observations of film formation and behaviour were made in the contact itself. Conditions of load, temperature and repetition rate were similar to those found in an engine.

2 APPARATUS

The rig (see Figure 1) consists of a 6 mm radiused pin (silver steel, polished and hardened to 450 VHN) loaded against a fixed flat (gauge plate, polished to 0.02 μm c.l.a. and hardened to 750 VHN) and reciprocated sinusoidally by a 100 W oscillator. The standard conditions were 35 Hz frequency and ± 0.5 mm stroke. Lubricant was dripped into the contact at 3-5 ml/hr. The friction force was measured with a strain gauge transducer which restrained the flat from moving. By blowing hot air into an insulated box surrounding the contact, temperatures up to 250°C could be readily obtained.

Electrically isolating the ball and flat from the rest of the apparatus made it possible to monitor not only the contact resistance but also the contact capacitance. Using the contact as the "unknown" reactance in a 4-arm bridge, and

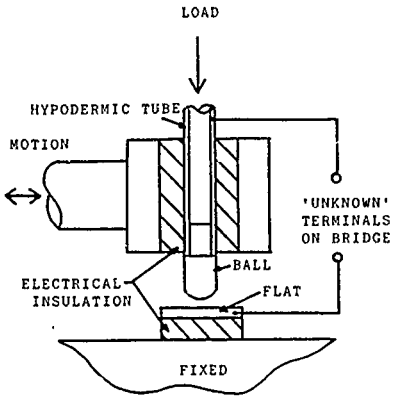

Fig. 1: Contact configuration and measuring circuit

bringing the bridge signal to a null point (displayed on an oscilloscope) meant that values of both capacitance and conductance were obtainable. The rig is described more fully elsewhere [8].

Details of the additives used are given below in Table 1, the ZDDPs being distinguished by the alkyl group on the molecule. Each of the test oils consisted of a 500 Solvent Neutral base oil with 1% by weight of the ZDDP indicated.

	Alkyl radical of ZnDP
OIL A	n-Butyl + n-Pentyl
OIL B	Octyl
OIL C	Methyl iso-butyl Carbinyl
OIL D	Alkyl Aryl (C_{12} or longer)

Table 1: Details of the additives

3 REACTION FILM FORMATION

In these experiments, the formation of the reaction films by the ZDDP additives was rapid. Under a typical load of 1 kg, motion was started and there was an 'induction time' of 15 - 45 seconds in which there was no film activity (as deduced from the low value of electrical contact resistance). In these first moments of motion a high friction transient was seen, which rapidly settled down to give a value of around $\mu = 0.1$. This friction transient was associated with the 'induction time' during which there was no film activity and therefore little protection of the rubbing surfaces.

Subsequent to the induction time the average electrical contact resistance rose rapidly from almost zero to a value higher than 10 MΩ in about 30 seconds to 2 minutes of rubbing. In this time there was usually a small reduction in the friction force - corresponding to the observed improvement in the coherence of the reaction film. This was seen from the bridge out-of-balance signal in this period. When the electrical contact resistance was observed to be high over the whole stroke, there was still much evidence of metallic contact through the film. This was manifested by momentary and repeated 'shorting' of the bridge signal. However, as motion proceeded, these asperity interactions diminished until, in most cases, they vanished. Also in this period, the value of capacitance to null the bridge signal at mid-stroke fell, indicating that the reaction film thickness increased. Once appreciable asperity interaction had ceased, the film thickness did not alter.

A typical bridge out-of-balance signal and friction trace, taken from the oscilloscope, is shown in Figure 2a. The bridge signal here has been nulled at the ends of the stroke. It is immediately clear that there is some variation in the film thickness across the stroke. By nulling the signal and obtaining capacitance values at

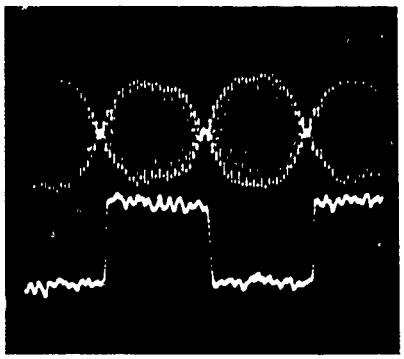

(a) Upper trace, bridge signal balanced at ends of travel.
Lower trace friction force.

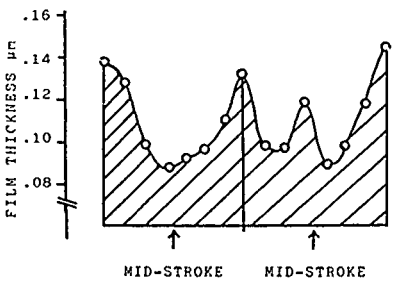

(b) Variation of film thickness in both directions of sliding.

Fig. 2: Film shape in the contact

successive intervals, it was possible to obtain a picture of the variation of the film thickness. This is shown in Figure 2b. The capacitance values at the ends of the travel were always lower than at the middle. This implies that the film thickness increased at the ends. This is an important observation, since the film would be expected to be thinner where the velocity is zero if it were behaving hydrodynamically. Values of the film thickness were obtained by reference to a calibration curve for the contact. The relationship between capacitance and film thickness is not the straightforward inverse proportionality. This arises since for a point contact the capacitance is made up not only of the contribution from the Hertz flat but also the fringe deformed zone around the Hertz area: this second term dominates the capacitance. In this work there was the added complication of a worn ball, so that the area was no longer Hertz area: hence the need for calibration. This was achieved by using deposited silicon oxide films of known thic'ness and dielectric constant, and then relating this to the film of dielectric constant 2.3. This is described by the authors elsewhere [8]. Typical values of film thickness for the four ZDDPs at 150°C and 1 kg load were in the range 0.05 μm to 0.2 μm.

Usually the frequency of motion was 35 Hz, so the maximum velocity (at mid-stroke) was about 100 mm/s. This meant that the shear rates experienced by the film were of the order of 10^6 s^{-1}, but varied sinusoidally across the stroke. The contact pressure at 1 kg was about 500 MPa, based on the wear scar diameter (c.f. 1000 MPa for Hertz conditions). Hence the film was under conditions of pressure, temperature and shear similar to those experienced in running components.

3.1 Nature of Film

In addition to the increase in film thickness at the ends of the stroke, it was observed that the friction was independent of shear rate. As seen from Figure 2a, the friction force was a square wave. If there were viscous or any other rate-dependent properties of the film, this would be reflected in the shape of the friction trace. The shear rate varied markedly throughout the stroke, but the friction force was constant in each direction of sliding. When the motion was stopped, the film remained in the contact and could withstand a normal loading cycle that revealed an elastic-type behaviour. This is termed 'static' loading as opposed to the 'dynamic' tests. A reduction in film thickness on loading was completely recovered on unloading.

The static film thicknesses tended to be greater than the corresponding dynamic thicknesses at the same normal load. A typical example is shown in Figure 3, where the solid symbols are the static loading values. The results are for a ball of radius 1.2 mm instead of 6 mm. These observations lead to the conclusion that the reaction film was not behaving in a viscous manner, but behaved like a plastic. The evidence suggests that there was a polymerised layer of some sort which was sheared in the contact.

3.2 Shear Behaviour

It has been suggested by other workers such as Briscoe [9] and Fein [10] that the shear behaviour

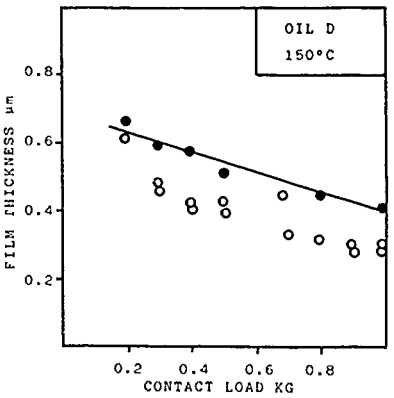

Fig. 3. Comparison between static (solid symbols) and dynamic (hollow symbols) film thickness with load

of the reaction films formed by ZDDP should be similar to that of thin layers of organic polymers such as polymethylmethacrylate (PMMA) and high density polyethylene (HDPE). They state that the shear strength of the contact, τ_c, increased proportionally with the mean hydrostatic pressure, p. The friction coefficient for the shearing film is then given by:

$$\mu = \frac{\tau_c}{p} = \frac{\tau_o}{p} + \alpha \qquad (1)$$

where τ_o and α are constants characteristic of the material being sheared. The existence of this two-term law of friction was first suggested by Deryaguin et al. [11] and theoretical support has been provided by Sutcliffe et al. [12]. They explained the two terms as arising from the motion of one layer of molecules over another. The experimental work of Briscoe at al. [6, 9] has caused the two-term friction law to be taken seriously. Briscoe's studies of the shear strength of polymer films used very smooth surfaces (usually glass) coated with the thin film. This was to ensure film penetration was negligible. Furthermore in order to avoid destroying the carefully deposited films, the sliding speeds were low (up to 0.2 mm/s) which made the shear rate around 10 s^{-1}. This is much lower than in the experiments reported here and far lower than those found in practice.

An advantage of the smooth surfaces used by Briscoe was that the contact pressure could be determined from Hertz theory. In the experiments reported here, the film was formed as the result of a rubbing process. This meant that wear had taken place, and the contact was no longer a ball on flat, but a worn ball. Determining the contact area therefore posed a problem, for which no better solution has been found than to assume that the contact area was simply given by the size of the wear scar.

It was earlier noted that there was little or no metallic contact once a reaction film had been formed. Therefore it was assumed

that the contribution of such contact to the total frictional resistance was negligible. If there was a relationship described by equation (1) then, without needing to know the area of contact (A), it can be re-written as:

$$F = \tau_o A + \alpha W \qquad (2)$$

where F is the measured friction force and W is the normal load. Initial tests indicated the existence of this τ_o and was reported in the abstract. Further studies, however, over a wide load range (50 g - 2 kg) failed to substantiate these results. What was found was that the friction force was directly proportional to the load, i.e. the shear strength was proportional to contact pressure. This is shown in Figure 4.

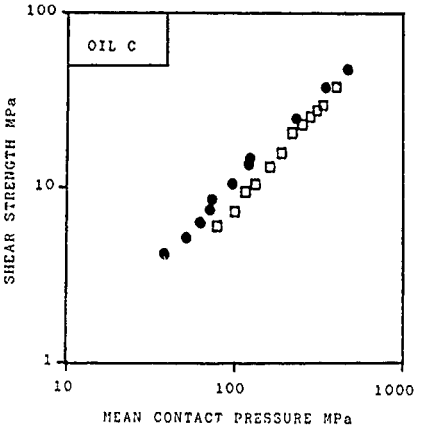

Fig. 4: Variation of shear strength with contact pressure

Replotting these results on linear axes gives lines that go through zero within experimental error. Over the range of experiments carried out with the four additives at temperatures of 100, 150 and 200°C the gradient of the lines were always around 0.1. These results are displayed in Table 2.

	TEMPERATURE °C		
	100	150	200
OIL A	0.08	0.13	0.166
	0.11	0.098	0.093
OIL B	0.098	0.167	0.095
	0.095	0.110	0.100
OIL C	0.094	0.110	0.092
	0.096	0.106	0.114
OIL D	0.100	0.099	0.105
	0.095	0.093	0.106

Table 2: Values of the gradient, , from plots of friction force against contact load

The shear strength of the contact was found to be independent of shear rate. This was shown by three observations. First that the friction force was a square wave, despite the large variations in shear rate in the stroke. Second at a constant amplitude (± 0.5 mm) the frequency was changed, and in a range from 20 Hz - 96 Hz the friction force was independent of frequency. This is shown in Figure 5, which also displays the corresponding variation in the film thickness. As the frequency increases, the film thickness falls (more precisely, the capacitance rises). Third, at a constant frequency (35 Hz) the amplitude was changed: the friction force did not change and the film thickness decreased with increasing amplitude.

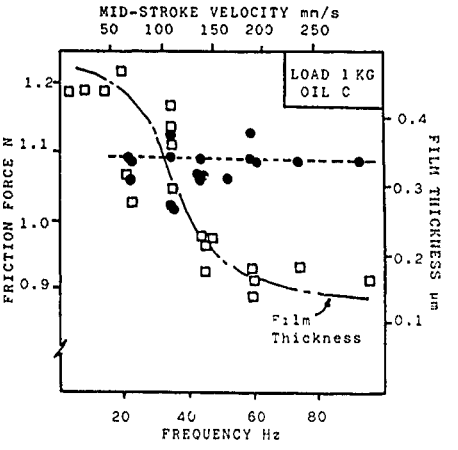

Fig. 5: Variation of friction force and film thickness with frequency

Examining the wear scar on the flat by optical microscopy after an experiment revealed a film in the wear scar and in a region directly around it. This film was easily scratched by a hard scriber as Figure 6 shows. The material around the scar, which could be seen more clearly in an SEM, appeared to be the build-up of worn material that was pushed out of the contact by the slider. Figure 7 is a photograph taken from the SEM of the region at the ends of the travel, showing the lumps of film material. This observation is confirmed by X-ray analysis of the lumps, they contain Zn, P and S which would be expected for film material. Areas well away from the scar had only negligibly small traces of these elements.

Inside the scar there was evidence of not only the deformation of the metal surfaces, but also of film material that itself has been heavily sheared. This is displayed in the SEM photograph of Figure 8. The smeared appearance of the surface, together with the rippled effect at the edge of the scratches shows how the film had been sheared.

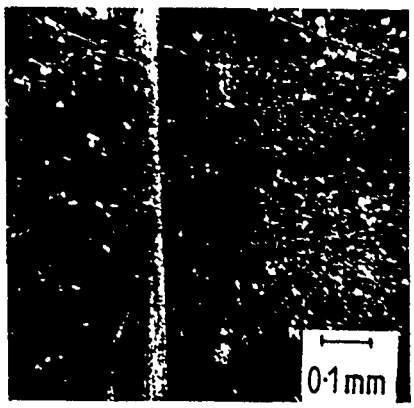

Fig. 6: Optical photograph of the wear scar on a flat showing a scriber mark through the surface film

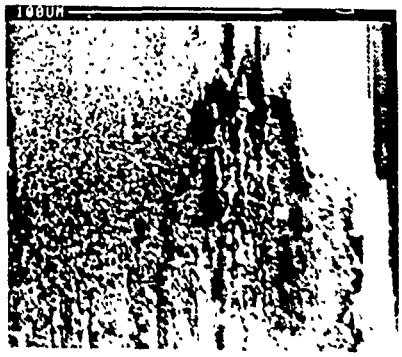

Fig. 7: SEM photograph of surface film at the end of the wear scar on a flat

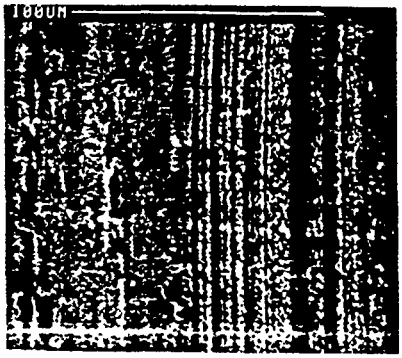

Fig. 8: SEM photograph of surface material in the wear scar on a flat

3.3 Effect of Temperature

The shear strength was found to be slightly dependent on temperature. This was shown most clearly for cases where the temperature was varied during a single test. At a load of 1 kg and starting at room temperature, the temperature was raised in steps of 25°C up to 250°C. The variation in the friction force is shown in Figure 9 for the four additives, and the corresponding changes in film thickness in Figure 10. What can be seen is that once a film was formed (and this sometimes occurred at temperatures

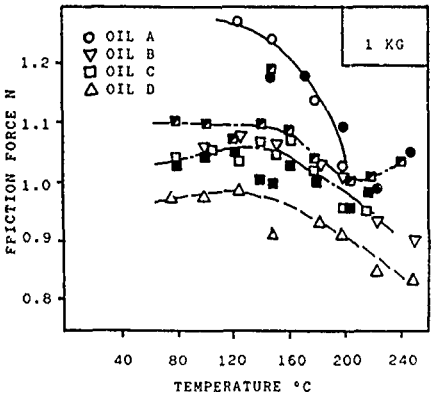

Fig. 9: Variation of friction force with temperature for the four ZDDPs

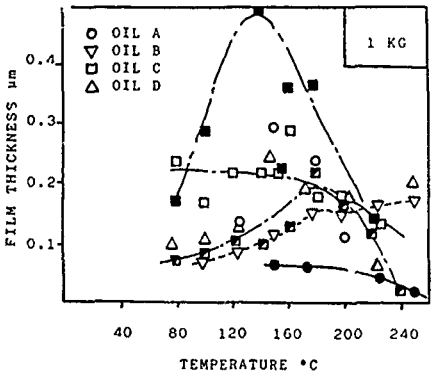

Fig. 10: Variation of film thickness with temperature for the four ZDDPs

lower than 150°C), the shear strength remained fairly constant. At around 160°C - 180°C there was a noticeable drop in the shear strength and this was accompanied by a drop in the film thickness. The friction trace became erratic at temperatures above 200°C, showing that disruption of the film was taking place This was also reflected in the bridge out-of-balance signal which showed signs of film penetration by surface asperities.

4 DISCUSSION

Observation of the changes in film thickness with load, speed and temperature lead to the conclusion that the reaction films formed in this rubbing contact had no obvious hydrodynamic properties. The observations that the static film thickness was greater than the dynamic film thickness at a given load; the film thickness was reduced for increasing shear rate and the film was thicker at the ends of the stroke than at the middle show this. What appears to be happening was that the slider pushed film material before it, having smoothed out the surface, producing a build-up of worn film material at the ends of the stroke. The slider was "bull-dozing" the film into heaps at either end. This was confirmed by optical and SEM examination. The slider, or ball, then rode up on this material as its velocity slowed down to the reversal point, producing the observed increase in film thickness.

During motion there was a balance between film formation and film removal. This was reflected in the decrease in film thickness (while still maintaining no asperity contact) with increasing frequency. The equilibrium film thickness was reduced due to the increase in the repetition rate of the contact. It is the repetition rate that is important in any repeating contact device. The protective film formed by the additives is substantially (or partially in this case) removed during each contact and must be reformed before the next one: it is the time available for this which is important. Arrhenius states that for a chemical reaction the rate is a function of temperature. Therefore for a constant temperature the reaction rate is constant. If the film removal rate increases then the film thickness must decrease accordingly since there is less time for film formation. This again is reflected in the decrease in film thickness and the increase in film penetration observed as the temperature was increased. Film formation appeared to start at a certain temperature, but at the higher temperatures (> 200°C) there was decomposition of both oil and additive, leading to film disruption.

Since the film was in gross shear and at high shear rates ($> 10^5\ s^{-1}$) for most of the contact time, it cannot be the quasi-elastic properties of the film, observed under static conditions, that contribute to the lubrication. Since there was no observed asperity contact in these experiments, the friction force must have been due entirely to the shearing of the metal/film or film/film interface. Shearing of the asperities was replaced by shearing of the polymerised reaction film. In comparing the shear behaviour of these reaction films with that of thin polymer films in other studies, the same pressure dependence on shear strength was found. However the constant shear term, τ_o, described by Deryaguin was not in evidence. The apparatus could function at loads low enough to make the constant shear term readily detectable, although readings at these loads were less accurate. It should be noted that Deryaguin [8] admits the possibility from his experiments that in a certain number of cases in boundary lubrication τ_o could be zero.

The reaction films in these experiments were solids (remaining in the contact when motion was removed) with plastic-like (strain and strain-rate independent, ductile) shear behaviour, with shear strengths proportional to the mean hydrostatic pressure. The constant of proportionality was found to be invariably around $\alpha = 0.1$. This was a value similar to that obtained by Briscoe for HDPE, PTFE and polystyrene [6]. It seems that the dominant property of the ZDDP film was not its intrinsic shear strength, but that the shear strength was highly dependent on pressure. This determined the coefficient of friction, and since no τ_o was detected, then it was found that $\mu = \alpha$. This gave values of μ at around $\mu = 0.1$, typical of boundary lubrication.

5 CONCLUSION

The reaction films formed by ZDDP rubbed on steel in these tests were solid; they behaved elastically under normal load and as plastic-like, strain and strain-rate independent, ductile material under tangential motion. Their shear behaviour was similar to that of thin films of organic polymers such as HDPE, polystyrene and PTFE. Evidence of a two-term friction relationship was not found. Reaction film thicknesses were typically 0.1 μm, far thicker than a true boundary film.

Perhaps the most interesting conclusion of this work is the relation between classical elastohydrodynamic lubrication using lubricants containing ZDDP and the reacted film lubrication described here. In many papers on the lubrication of contacts it seems there is scant realisation that there are two processes at work: one based on surface chemistry and the other on continuum mechanics and lubricant properties.

6 ACKNOWLEDGEMENTS

The authors gratefully acknowledge the funding of the SERC and the US Army Research, Development and Standardisation Group (UK).

References

1 SYNDER, P L, TEVAARWERK, J L, and SCHEY, J A. Effects of oil additives on lubricant film thickness and traction. SAE Paper No. 840263, 1984

2 CANN, P M E, JOHNSTON, G J, SPIKES, H A. The formation of thick films by phosphorus-based anti-wear additives. I.Mech.E. Conf. 'Tribology-friction, lubrication and wear, fifty years on', Paper C208/87, 1987, 543-554

3 KAJDAS, C. On the negative-ion concept of EP action of organo-sulphur compounds, ASLE Trans., 1984, 28, 21-30

4 MONTJIL, G, LONCHAMPT, J, ROQUES-CARMES, C, The study of anti-wear properties of zinc dialkydithiophosphates through sliding-induced electronic emission. I.Mech.E. Conf. 'Tribology - friction, lubrication and

wear, fifty years on', Paper C224/87, 1987, 531-535

5 TONCK, A, KAPSA, Ph., SABOT, J. Mechanical behaviour of tribochemical films under cyclic tangential load in a ball-flat contact. ASME Jnl. Trib., 1986, 108, 117-122

6 BRISCOE, B J, SCRUTON, B, WILLIS, F R. The shear strength of thin lubricant films. Proc. Roy. Soc. Lond., 1973, A333, 99-114

7 BAILEY, M W, CAMERON, A. The effects of temperature and metal pairs on scuffing. ASLE Trans, 1972, 16, 121-131

8 ALLISTON-GREINER, A F, GREENWOOD, J A, CAMERON, A. Thickness measurements and mechanical properties of reaction films formed by ZDDP during running. I.Mech.E. Conf. 'Tribology - friction, lubrication and wear, fifty years on'. Paper C178/87, 1987, 565-572

9 BRISCOE, B J, SMITH, A C. The shear properties of thin organic films. Revs. Deformation Behav. Matl., 1980, 3, 151-191

10 FEIN, R S, A perspective on boundary lubrication. Ind. Eng. Chem. Fundm., 1986, 25, 518-524

11 DERYAGUIN, B V, KARASSEV, V V, ZAKHAVAEVA, N N, LAZAREV, V P. The mechanism of boundary lubrication and the properties of the lubricating film. Wear, 1957, 1, 277-290

12 SUTCLIFFE, M J, TAYLOR, S R, CAMERON, A. Molecular asperity theory of boundary friction. Wear, 1978, 51, 181-192

SECTION 2 - The running in process: oil/liner pairs ABDEF

1. Object of Section 2

The immediate aim of this section is to investigate the running-in process and the role of anti-wear additive films, to provide a performance assessment of the four oils used.

2. SUMMARY

1. A newly designed reciprocating ball-on-flat apparatus is described, differing from the earlier rig in being able to accommodate sections from engine liners.
2. The running-in process is examined using four different oils with the same cast-iron cylinder liner, under different conditions of temperature and load. Measurements are taken of both surface changes to the liner and characteristics of the additive film during rubbing.
3. Relationships between film characteristics and surface changes are investigated and related to oil composition.
4. The four oils are ranked in terms of performance using both film characteristics and surface changes as measures of performance.
5. After the introduction and experimental details, the section divides. Paragraphs 5 to 9 consider in some detail the performance of liner C with 4 oils C1, C2, C3 and C4. Paragraphs 10-13 then report tests on a mixture of oils and liners. Paragraph 14 discusses all the results.

3. INTRODUCTION

The First Annual Report [1] Section 1 examined the formation of reaction films by commercially available zddp additives. Their thickness was measured by capacitance during rubbing and their behaviour under varying conditions of load and temperature studied. A newly designed reciprocating ball-on-flat apparatus was described. Chart recordings monitored the electrical contact resistance, friction force and temperature of the rubbing pair while capacitance readings gave values of film thickness. The wear scar diameter of the steel pin or ball and also visual observation and rms roughness values of the wear scar on the 'flat' were used as indicators of the degree of wear.

After the start of rubbing, films form in a matter of minutes. This is indicated by a rise in the electrical contact resistance (e.c.r.) [2] and a small drop in friction force. The period before film formation is termed the induction period. The e.c.r. rises rapidly at first but takes some time to stabilise - about 10 minutes for a polished steel flat but up to an hour for a cast-iron cylinder liner. This is termed the gradient period. During both induction and gradient periods capacitance readings are shorted out by asperity contact. After the gradient period e.c.r. stabilises and capacitance readings are rarely shorted out, indicating the presence of a thick reaction film that prevents asperity contact. Film thickness can then be measured. The friction force remains stable after the small drop at induction time. Fig. 1 shows a tracing of a typical chart recording.

Film thickness and film 'quality', as measured by the value and stability of the e.c.r., both decreased with increasing load and also as temperature rose above 200°C. Increasing the load once a film has formed results in a sudden drop in e.c.r., indicating disruption of the film, followed by a quick recovery close to its original value of e.c.r. The friction coefficient is similar for base oil

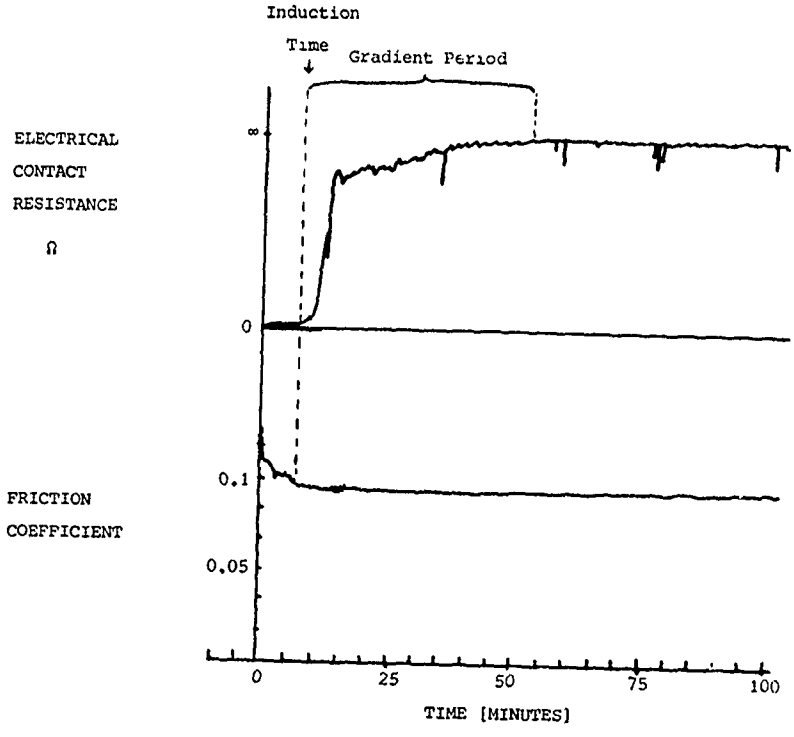

FIG. 1: Typical Chart Recording

Oil C4, Liner C, 5kg, 150°C

and base oil + 1% zddp although the degree of wear indicated by wear scar diameter, visual observation and rms roughness of the flat, all showed considerable wear reduction for base oil + additive. These indicators of wear also suggested that most wear occurs in the early minutes of rubling, particularly during the induction period.

This report examines the running-in process of a cast-iron cylinder liner with four different oils over a period of four hours. The unworn and worn liner surfaces are characterised by surface profilometry, the main parameters of interest being the rms roughness and the peak curvatures. Changes in these parameters are then correlated with how the surface ran-in, particularly the induction time and the film quality, both determined from the e.c.r. chart recording. The oils are then ranked in terms of surface changes, induction time and film quality at different temperatures and loads. Because the majority of wear occurred during the induction period an attempt is made to compare oil performance in terms of surface changes at an early stage. Any differences between the oils in terms of prevention of surface changes during the induction period could be very significant. This quality of the oil is referred to as its initial anti-wear activity.

4. EXPERIMENTAL DETAILS

4.1 Reciprocating Rig

The development of the reciprocating rig first described in [3] has been detailed in the two interim reports [4] [5] and the First Annual Report [1]. This rig was redesigned to take segments of cylinder liner as the lower specimen, the essential difference being the nature of the clamping arrangement. Liner material was available in ½" wide rings cut from a new cylinder liner and these were further cut to produce segments of liner ½" x 3/4". These were of variable thickness according to the particular liner being used. The thicknesses could vary from 1/8" to ½". The reciprocating apparatus therefore, was completely redesigned and the main features are shown in Figure 2. There was no need to isolate electrically the liner segment from the rest of the apparatus, since only the contact resistance was to be monitored during the experiments. This meant that the liner could be clamped up against the cross-bars and the back face of the hanging system (Figure 2), which provided easy accommodation of specimen size differences. The hanging system was supported by leaf springs connected to four upright pillars. Horizontal motion of the hanger was prevented by the piezo-electric force transducer, which gave readings of the reaction, or friction force.

The pin specimen clamp was as described in the First Annual Report, made of 'tufnol' to ensure electrical insulation and enable the contact resistance measurements to be made. A Ling Dynamics 20 Watt shaker was used to drive the pin specimen over the liner and loads were applied by dead weights, via a yoke and pulley system. Oil was drip-fed into the contact region through a hypodermic tube that was incorporated in the pin clamp.

The central part of the rig was 'double glazed' using 'Pyrex' heat-resistant glass tubes of two different diameters. The tubes had slots cut in them, to fit over the force-transducer coupling and shaker arm and to allow hot air to be

blown into the rig space for heating purposes. A Pyrex lid that fitted over the top of the tubes had a hole to allow the oil-feed and electrical connection to the pin specimen to pass through. The heating and temperature controlling arrangements were as described in the First Annual Report.

Waste oil was channelled from the drip-tray under the specimen clamp, to be collected in a beaker and a fume extractor was installed directly over the heated section. The entire rig was manufactured from stainless steel to enable flame cleaning between oil changes. Other crucial parts, such as the oil feed tube and thermocouple were readily replaceable. Specimens were cleaned ultrasonically for 10 minutes, first in acetone and then in pentane before assembly in the rig.

Electrical connections were made to the pin specimen and the rest of the rig, and a resistance switch box as described in the First Annual Report was used to monitor the contact resistance. In these experiments, a resistance 'high' was usually $>10^5$ Ω, two decades less than in the previous experiments for reasons given later. The contact resistance was displayed on a storage oscilloscope, together with the friction signal from the force transducer. A chart kept a continuous record of the average electrical contact resistance (ecr) and friction force as before.

4.2 Materials

The pin specimen is made of silver steel, finished with a 4.5 mm radius, heat treated at 800°C, water quenched, then tempered at 450°C for one hour to 550 VHN. The radiused head is then polished with emery paper and brasso, a commercial household liquid cleaner containing a mild abrasive.

The liner specimen is liner C (Caterpillar 1G2). Surface hardness was 420 VHN, rms roughness 0.9 μm and peak curvature 0.067 μm^{-1}

Four different oils were used in these experiments, designated oils C1 to C4. Details are given in Appendix 1. The essential difference between these oils is the zddp concentration, varying from 0% to 1.4%.

4.3 Surface Analysis

Surfaces were analysed in a profilometer (Ferranti 'Surfcom') and the digitised profile data was processed by a standard computer program to give

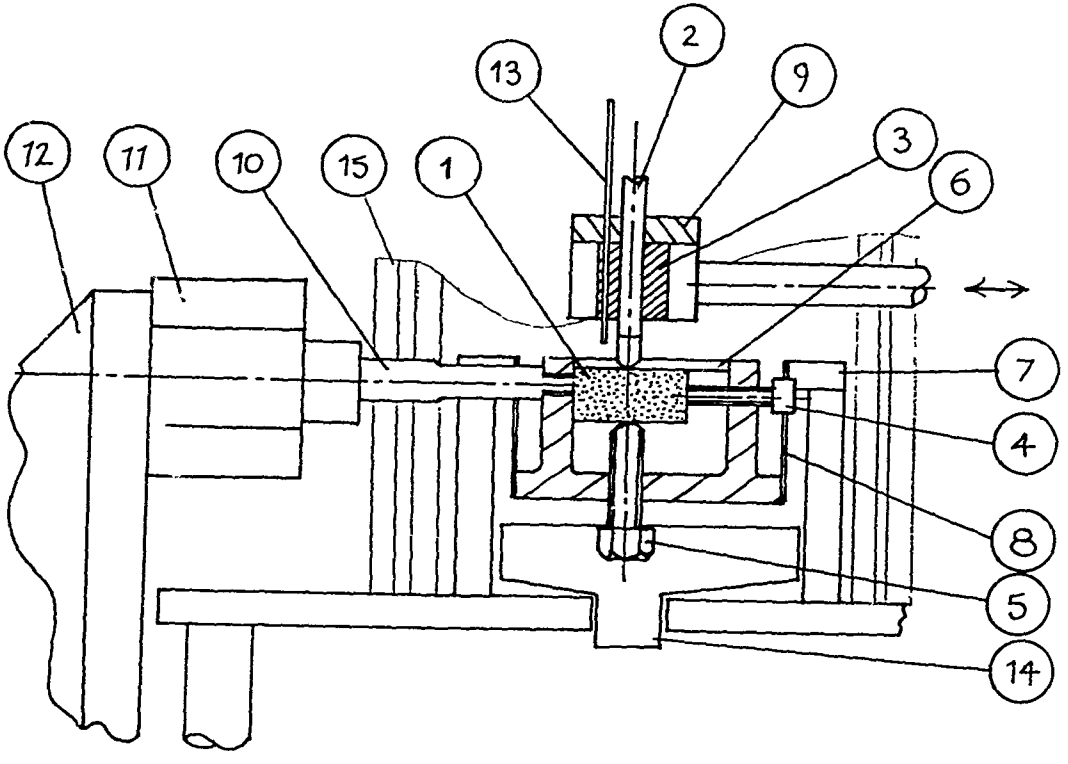

1 Cast-iron specimen
2 Pin specimen
3 'Tufnol' electrical insulation.
4 Horizontal specimen clamp.
5 Vertical specimen clamp.
6 Cross-bar.
7 Supporting pillar.
8 Leaf spring.
9 Loading yoke.
10 Connecting rod.
11 Piezo-electric force transducer.
12 Rigid mounting.
13 Oil feed tube.
14 Oil drip-tray.
15 Pyrex 'double-glazing'.

FIGURE 2 Sectional view of the essential features of the reciprocating rig used for the study of the running-in of cast-iron cylinder-liners.

values of rms roughness and peak curvature. Roughness measurements exhibited considerable variability associated with the manufacturing process. Surface profiles of the unworn liner indicated at least two distributions of honing marks, one set being significantly deeper than the other, but with a lower frequency. The rms roughness varied considerably depending on whether or not such a deep honing mark was present in the profile trace, particularly for measurements of the wear scar rms roughness since the length of profile trace must be less than the length of the wear scar, 1mm. Peak curvatures were calculated by first defining a peak as a point that was higher than its two nearest neighbours and then fitting a curve through these three points. The data sampling interval was set at 2μm for all the readings allowing 500 points along the length of the wear scar. Difficulties in accurately locating the wear scar after short periods of rubbing led to the dumping of 50 of these points at each end of the profile trace. The remaining 400 points at the centre of the profile trace gave more consistent values of peak curvature since they were consistently located within the wear scar. All values of rms roughness and peak curvatures are averages of five profile traces taken in small increments across the wear scar. This attempted to take into account the variations in these parameters across the wear scar and to iron out any freak readings.

4.4 Friction and e.c.r: Film Activity and Coherence

Friction force and e.c.r. are monitored by a chart recorder. The e.c.r. record gives values of induction time, the time at which the e.c.r. begins to rise, and also of film quality. Two measures of film quality are used: '% film activity' and 'coherence'. Both are estimated by eye from the e.c.r. record, and reflect the value and stability of the e.c.r. The % film activity is a measure of film quality from induction time to stop time and is estimated by comparing the area bounded by the e.c.r. trace on the chart recording with the total area of the rectangle given by the axes induction time-stop time and o e.c.r. - ∞ e.c.r. A film activity of 100% would result when the e.c.r. rose to ∞ Ω immediately after the induction time and stayed at this value until the stop

time. The coherence is a measure of film quality after the e.c.r. has stabilised - i.e. after the gradient period. A coherence of 100% would result when the e.c.r. stays at $\infty\ \Omega$ from the end of the gradient period to the stop time. The scale for assessing % coherence is given in Appendix 2.

4.5 Test Conditions

Running-in tests were carried out at 1kg load and 5kg load. The tests at 1kg load were performed at 150°C, 200°C and 250°C, with test duration of 1 min., 5 mins., 30 mins., 1 hour, 2 hours and 4 hours. The tests at 5kg were performed at 150°C and 250°C with test durations of 5 mins., 1 hour and 4 hours.

Standard test conditions were similar to those of the First Annual Report, with reciprocation frequency of 35 Hz and amplitude ± 0.5 mm.

5. THE RUNNING-IN PROCESS, Part 1

5.1 Surface Changes

Changes in the rms roughness and peak curvature of liner C were investigated with oils C1 - C4 over a period of four hours of running-in. Film characteristics - induction time and % film activity - were also measured. The results are summarised in Table 1 (1kg load tests) and Table 2 (5kg load tests). The four oils show similar trends as shown in Figs. 3 - 6 where the surface changes for each oil are shown under different conditions of load and temperature. The first five minutes were marked by a significant decrease in peak curvature and this was followed by a slower fall off for about 40 mins. The rms roughness decreased more slowly, the largest changes occurring in the first 30 mins. to 1 hour, though under severe conditions it continued to fall between 2 and 4 hours. In general a steady value of each parameter was reached after 2 to 4 hours, indicating the completion of the running-in process.

Oils C1, C3 and C4, the three oils containing zddp additives (see Appendix 1), show similar trends as experimental conditions vary, particularly their sensitivity to temperature. For these oils surface changes are minimal at 150°C and 200°C but become much more severe at 250°C. Oil C2, containing a non-zddp additive, shows the reverse trend with less surface changes occurring as temperatures increase from 150°C to 250°C. The affect of load on surface changes is not so clear for any of the oils. In general increasing the load from 1kg to 5kg makes little difference to surface changes unless conditions are severe i.e. high temperature for C1, C3 and C4 or low temperature for C2. Certainly the ability of an additive film to protect the liner surface under the conditions tested is much more dependent on temperature than on load. Considering both rms roughness and peak curvatures changes from Figs. 3-6, the severity of conditions can be ranked for each oil.

C1 $250°C > 200°C > 150°C$

C2 $150°C > 200°C > 250°C$

C3 $250°C > 150°C \geq 200°C$

C4 $250°C > 150°C \geq 200°C$

OIL	1 MINUTE		5 MINUTES		30 MINUTES		1 HR		2 HRS		4 HRS	
1 C1	.790	no fa*	.685	2.5 min	.992	5 min	--	3 min	.785	12 min	.514	13 min
	.0700	0%	.0499	2%	.0682	80%	--	95%	.0566	90%	.0279	45%
5 C2	.944	no fa	.837	no fa	.641	15 min	.691	13 min	.500	15 min	.576	9 min
	.0491	%	.0304	0%	.0389	2%	.0407	80%	.0291	~ 70%	.0263	75%
0 C3	.856	1 min	.839	2 min	.936	1.5 min	.792	1.5 min	.690	2.5 min	.763	1.5 min
	.0663	10%	.0644	35%	.0606	95%	.0619	98%	.0570	95%	.0505	95%
°C C4	.925	no fa	.729	5 min	.756	21 min	.735	20 min	.754	22 min	.877	16 min
	.0705	0%	.0627	0%	.0608	30%	.0601	80%	.0508	85%	.0537	95%
2 C1	.768	no fa	.848	no fa	.716	--	.589	9 min	.629	5 min	.541	2 min
	.0607	0%	.0510	--	.0514	30%	.0158	50 %	.0269	55%	.0349	90%
0 C2	.677	no fa	.830	no fa	.876	no fa	.837	10 min	.574	20 min	.867	15 min
	.0542	0%	.0351	0%	.0506	0%	.0466	80%	.0398	60%	.0328	75%
0 C3	--	no fa	.734	2 min	--	2 min	.988	2 min	.828	1.5 min	.710	1.5 min
	--	0%	.0584	5%	--	95%	.0590	95%	.0578	90%	.0517	99%
°C C4	--	no fa	1.028	2 min	.868	2 min	.893	3 min	.886	8 min	.773	4.5 min
	--	0%	.0741	60%	.0690	90%	.0700	90%	.0625	90%	.0334	75%
2 C1	.829	no fa	.758	no fa	.673	6 min	.692	5 min	.576	6 min	.513	4.5 min
	.0601	0%	.0364	0%	.0383	40%	.0403	50%	.0189	55%	.0166	70%
5 C2	.945	no fa	.931	no fa	.751	7 min	.889	25 min	.885	18 min	.927	24 min
	.0535	0%	.0565	0%	.0545	50%	.0516	90%	.0476	90%	.0456	80%
0 C3	.912	no fa	.769	1.5 min	.836	1 min	.577	1.5 min	.448	1 min	.869	1.5 min
	.0770	0%	.0657	35%	.0601	85%	.0212	80%	.0271	70%	.0263	40%
°C C4	.809	no fa	.824	no fa	.612	15 min	.782	no fa	.774	7 min	.458	4.5 min
	.0538	0%	.0565	0%	.0391	40%	.0196	0%	.0503	85%	.0239	15%

* no fa = no film activity

DATA PRESENTED IN THE FOLLOWING FORM:

RMS Roughness (μm)	Induction Time
Mean Peak Curvature (μm^{-1})	Percentage Film Activity

TABLE 1: Results from running-in experiments with liner C at a load of 1 kg.

		5 MINUTES		1 HOUR		4 HOURS	
150°C	C1	0.646	No f.a.*	0.894	12	0.581	6
		0.0400	0%	0.0370	40%	0.0247	70%
	C2	0.796	No f.a.	0.693	43	0.566	27
		0 0566	0%	0.0175	0%	0.0441	80%
	C3	0.938	3	0.858	4.5	0.851	3
		0.0574	5%	0 0605	80%	0 0406	95%
	C4	0.817	No f.a.	0.708	15	0.568	8
		0.0625	0%	0.0644	90%	0.0507	90%
250°C	C1	0.760	4.5	0.735	6	0.065	11
		0.0401	0%	0.0115	1%	0.0096	5%
	C2	0.857	No f.a	1 045	50	0.759	21
		0.0610	0%	0.0355	0%	0.0469	50%
	C3	0.874	4	0 393	2.5	0.752	5
		0.0518	3%	0.0279	2%	0.0400	30%
	C4	0.822	No f.a	0 570	5	0.428	5.5
		0.0409	0%	0.0471	70%	0.0240	50%

* No. f.a. = No Film Activity

DATA PRESENTED IN FOLLOWING FORM:

Roughness [μm]	Induction Time [mins]
Average Peak Curvature [μm^{-1}]	% Film Activity

TABLE 2: Results from Running-In Experiments at 5kg Load

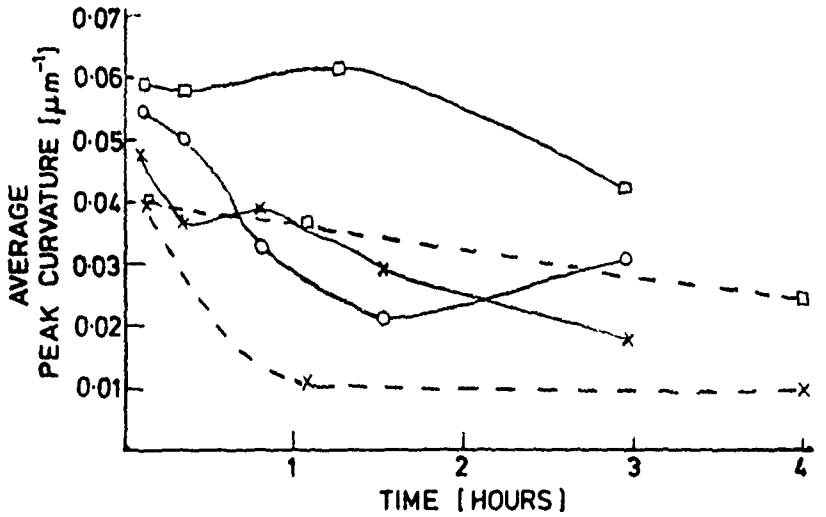

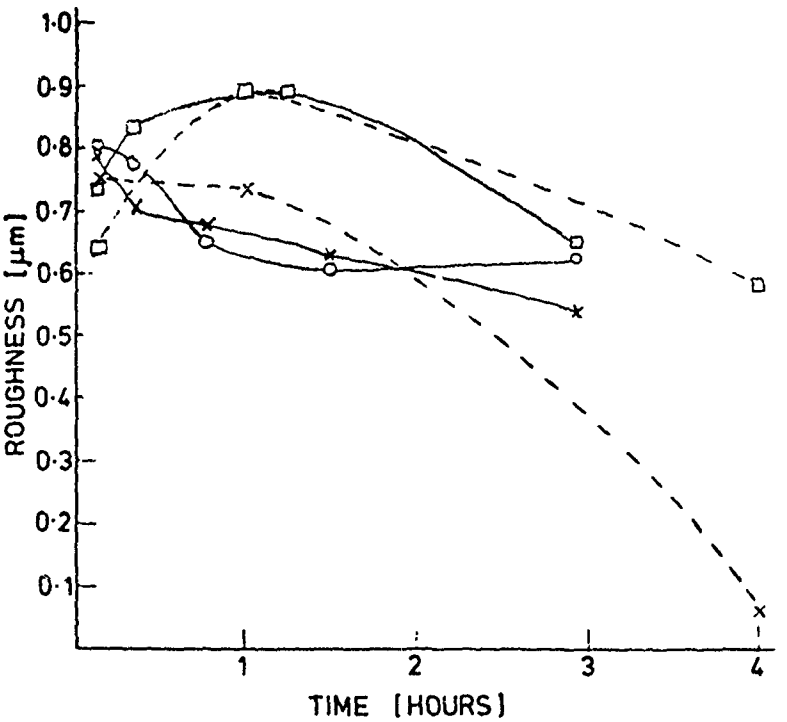

FIG. 3: Oil C1, Surface Changes

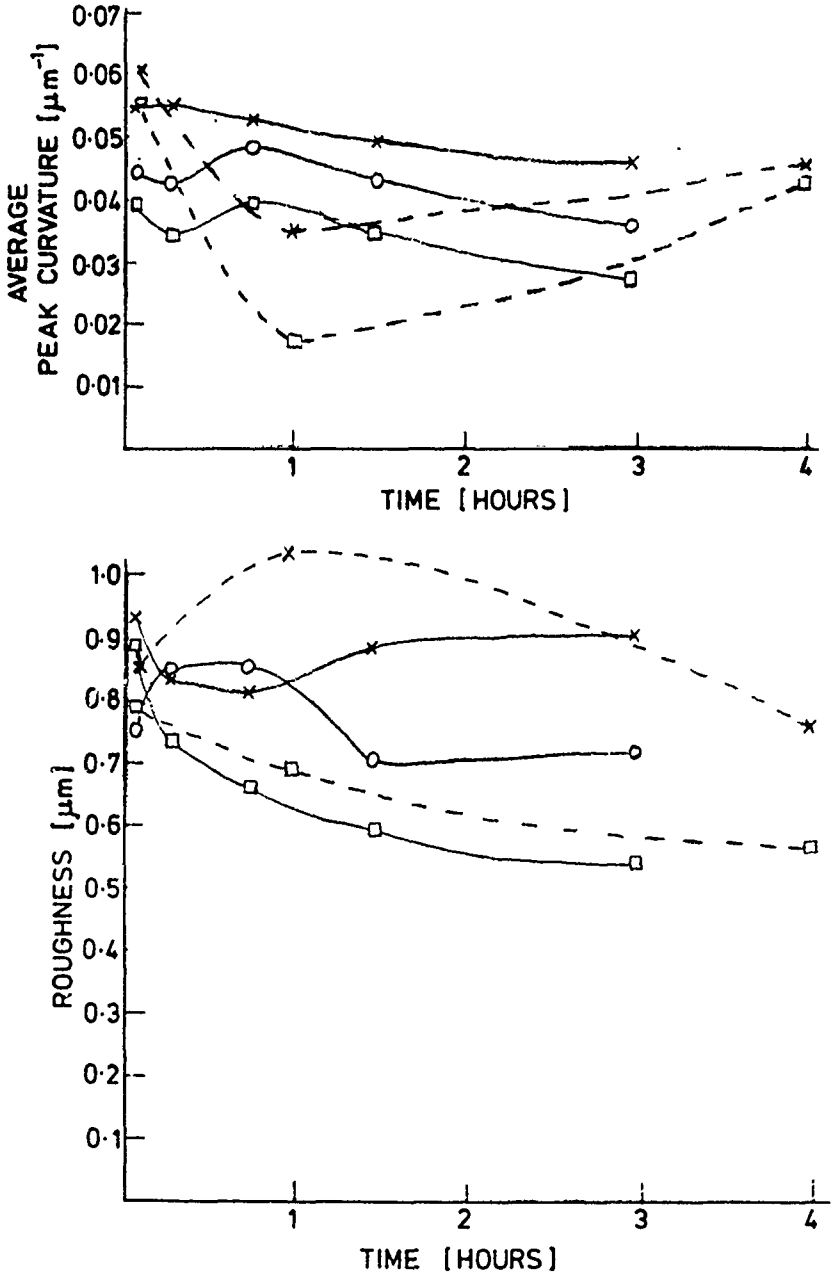

FIG. 4: Oil C2, Surface Changes

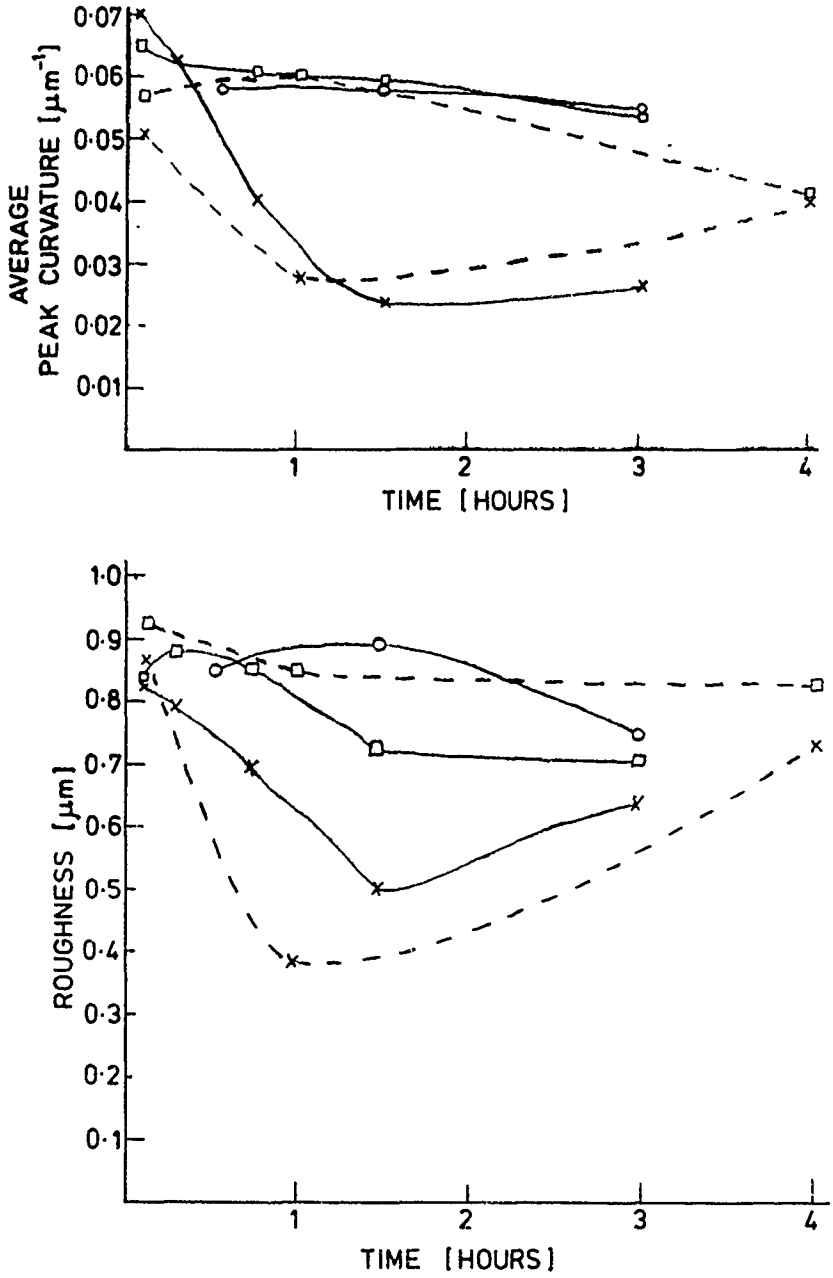

FIG. 5: Oil C3, Surface Changes

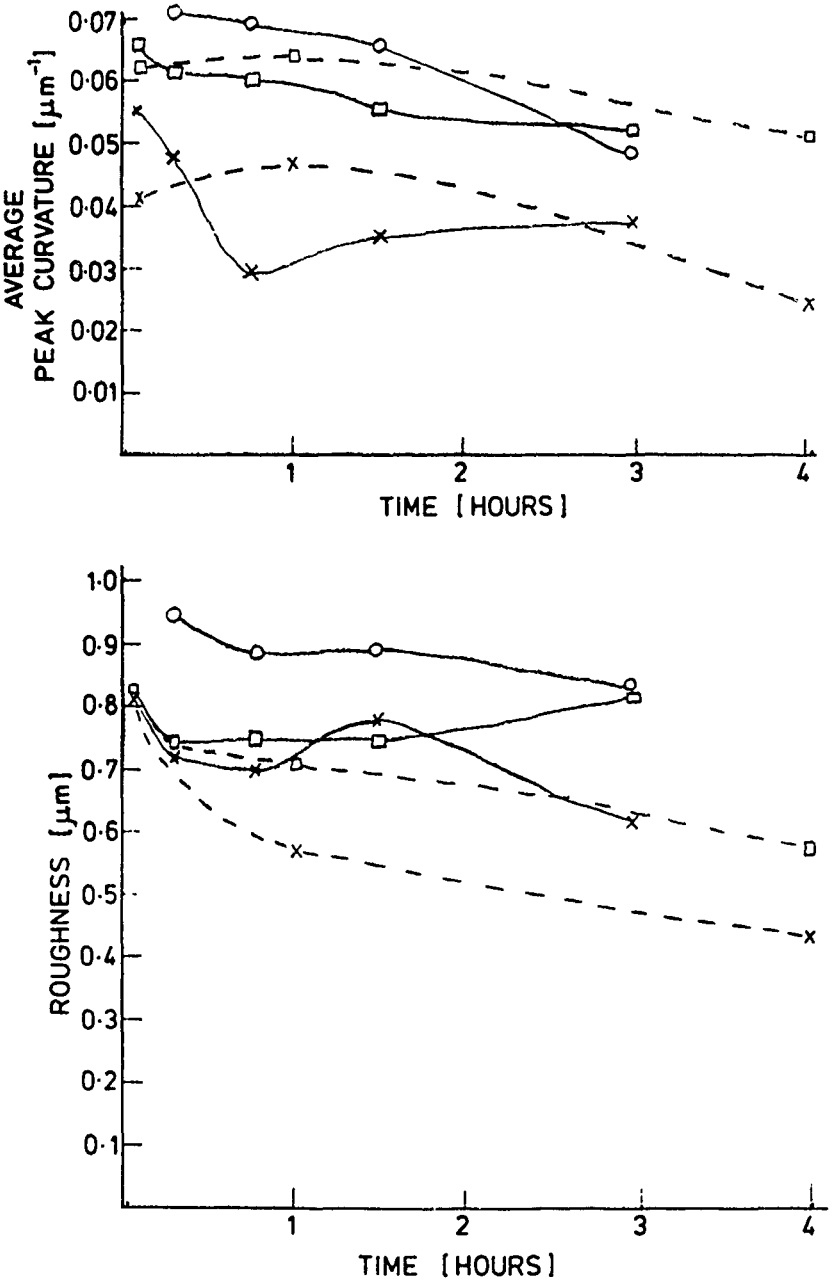

FIG. 6: Oil C4, Surface Changes

These results confirm the observation that zddp films decompose as temperatures rise above 200°C. The First Annual Report noted that film thickness decreased significantly for zddp additive films as temperatures increased from 200°C to 250°C.

Figs. 7-11 compare the performance of the four oils, in terms of preventing surface changes, at each experimental condition. Considering both parameters of surface changes together from Figs. 7-11, the performance of the four oils can be ranked for each experimental condition.

1kg	150°C	C1, C3, C4 > C2
	200°C	C3, C4 > C2 > C1
	250°C	C2 > C3, C4 > C1
5kg	150°C	C3, C4 > C1, C2
	250°C	C2 > C3, C4 > C1

The improvement in performance of oil C2 with temperature is very clear. Oils C3 and C4 appear to have comparable performance at each condition. They contain 0.5% zddp and 1.4% zddp respectively. Oil C1's performance is comparable with the other zddp oils only at the least severe condition for zddp additive films - 1 kg 150°C. At higher temperatures and the higher load performance is poor. This may reflect the very low concentration of zddp in oil C1, less than 0.1%. This suggests that zddp concentration in oil C1 is too low for good overall performance and that the higher concentration in oil C4 compared to oil C3 does not produced improved performance.

5.2 Induction Time

Induction time is the time at which the e.c.r. begins to rise, indicating the formation of a thick additive film. Table 3 summarises the results of induction time measurements for the four oils at each different experimental condition.

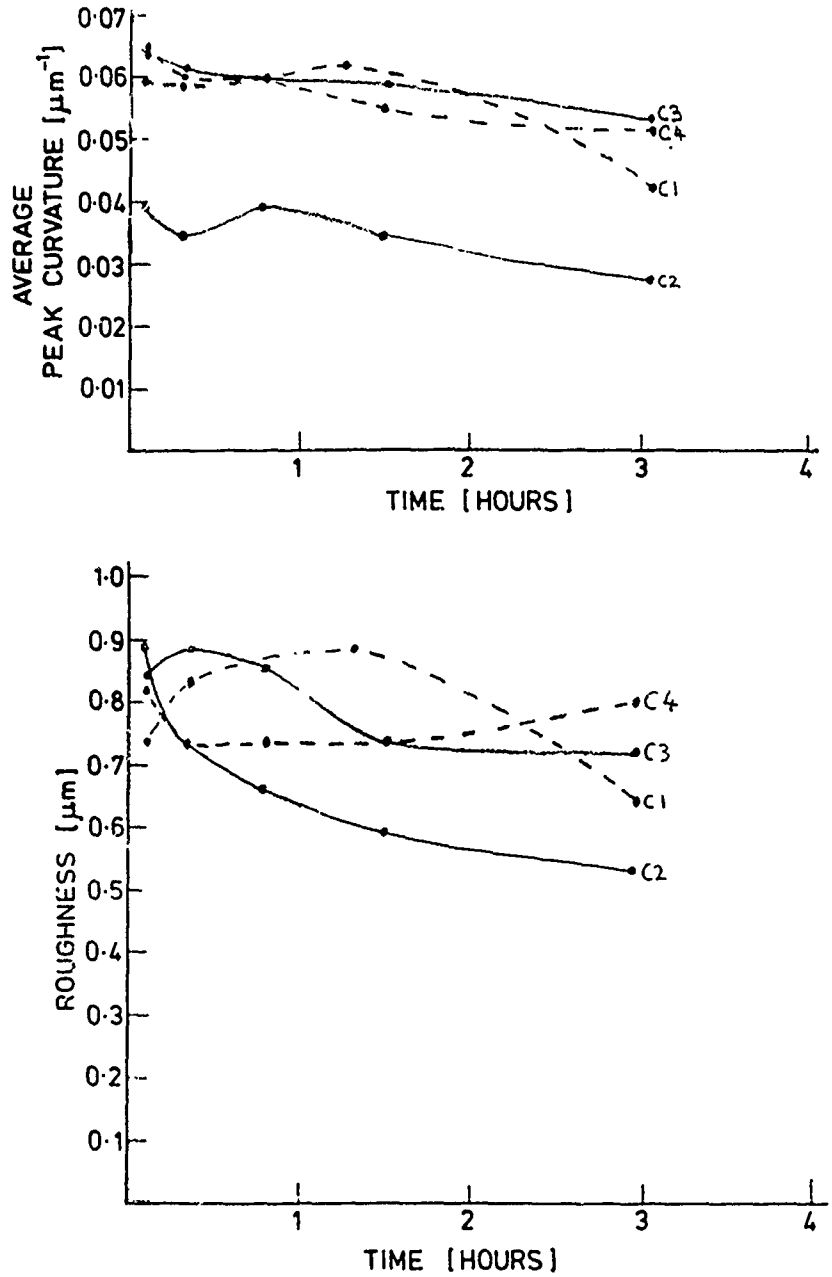

FIG. 7: 1 kg, 150°C. Comparison of all Oils in terms of Surface Changes

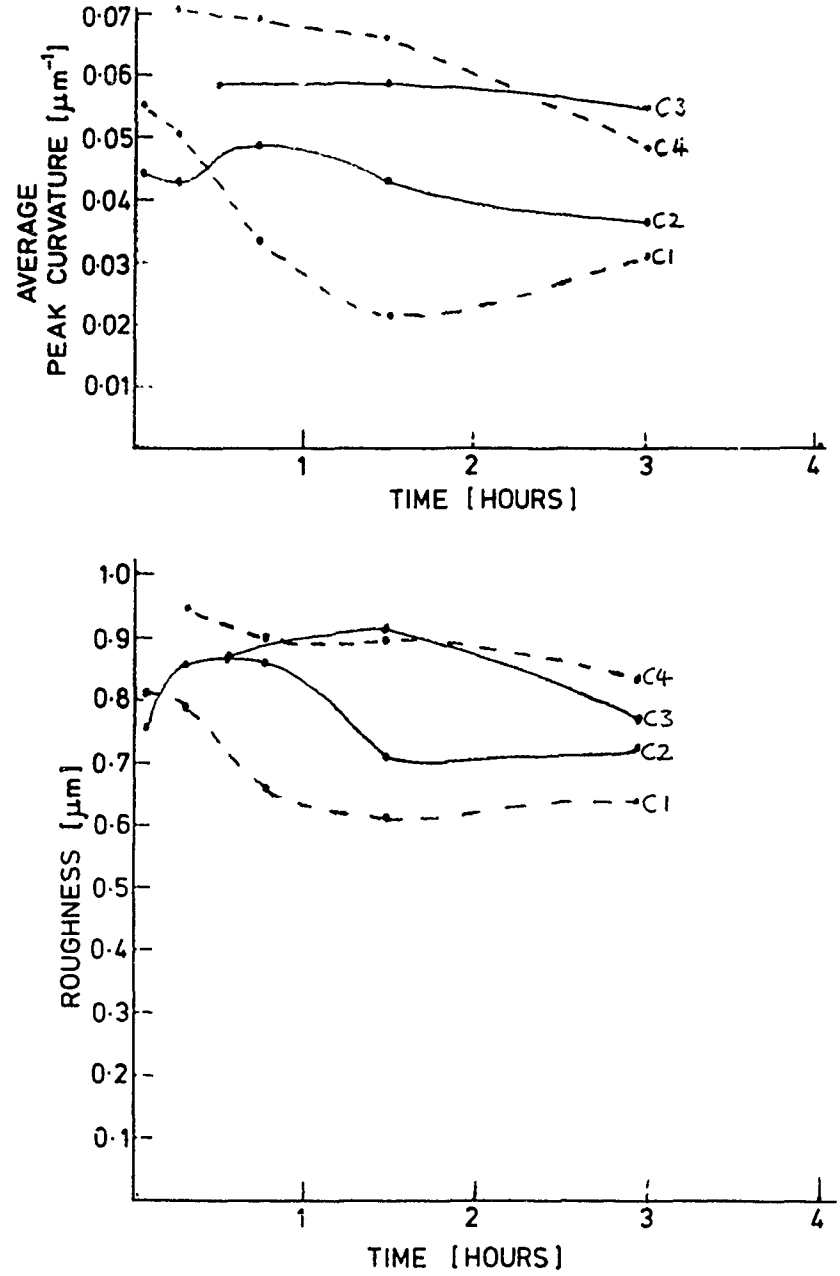

FIG. 8: 1 kg, 200°C. Comparison of all Oils in terms of Surface Changes

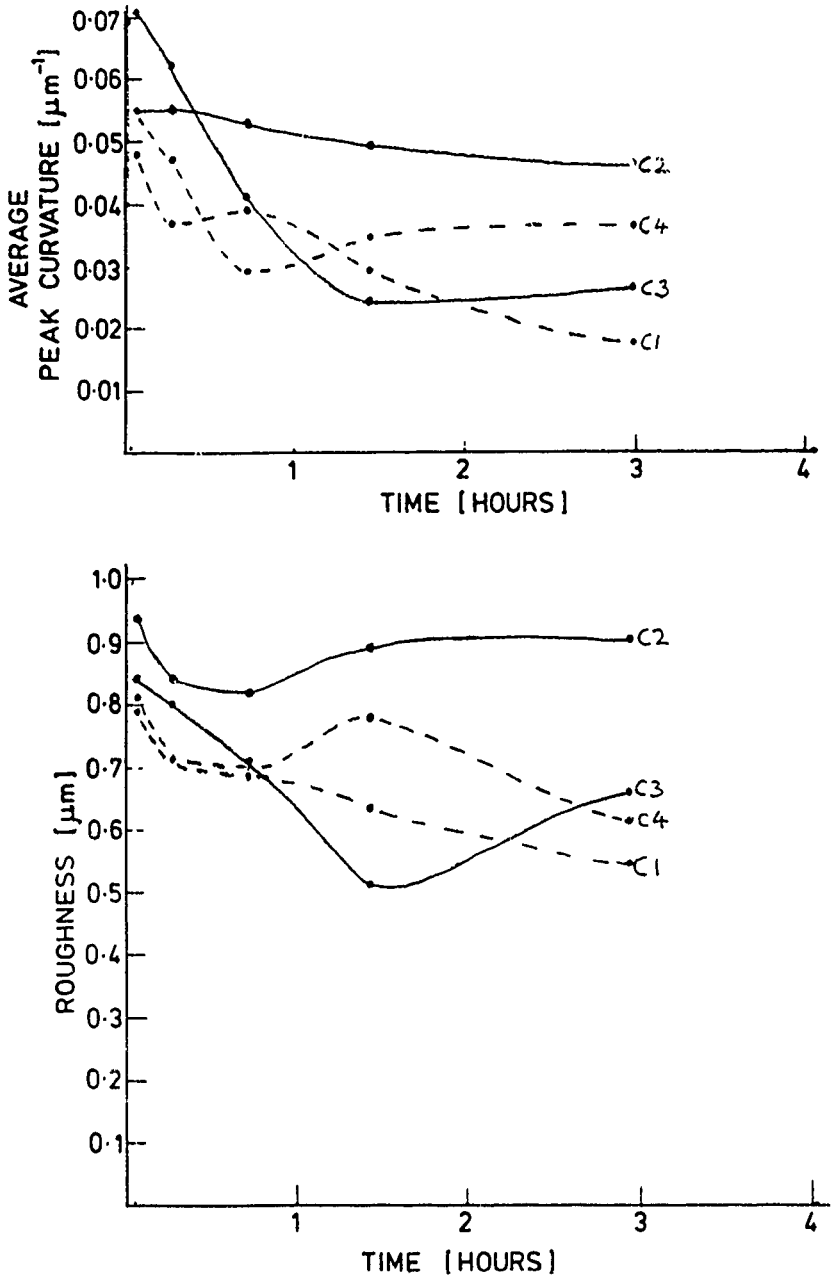

FIG. 9: 1 kg, 250°C. Comparison of all Oils in terms of Surface Changes

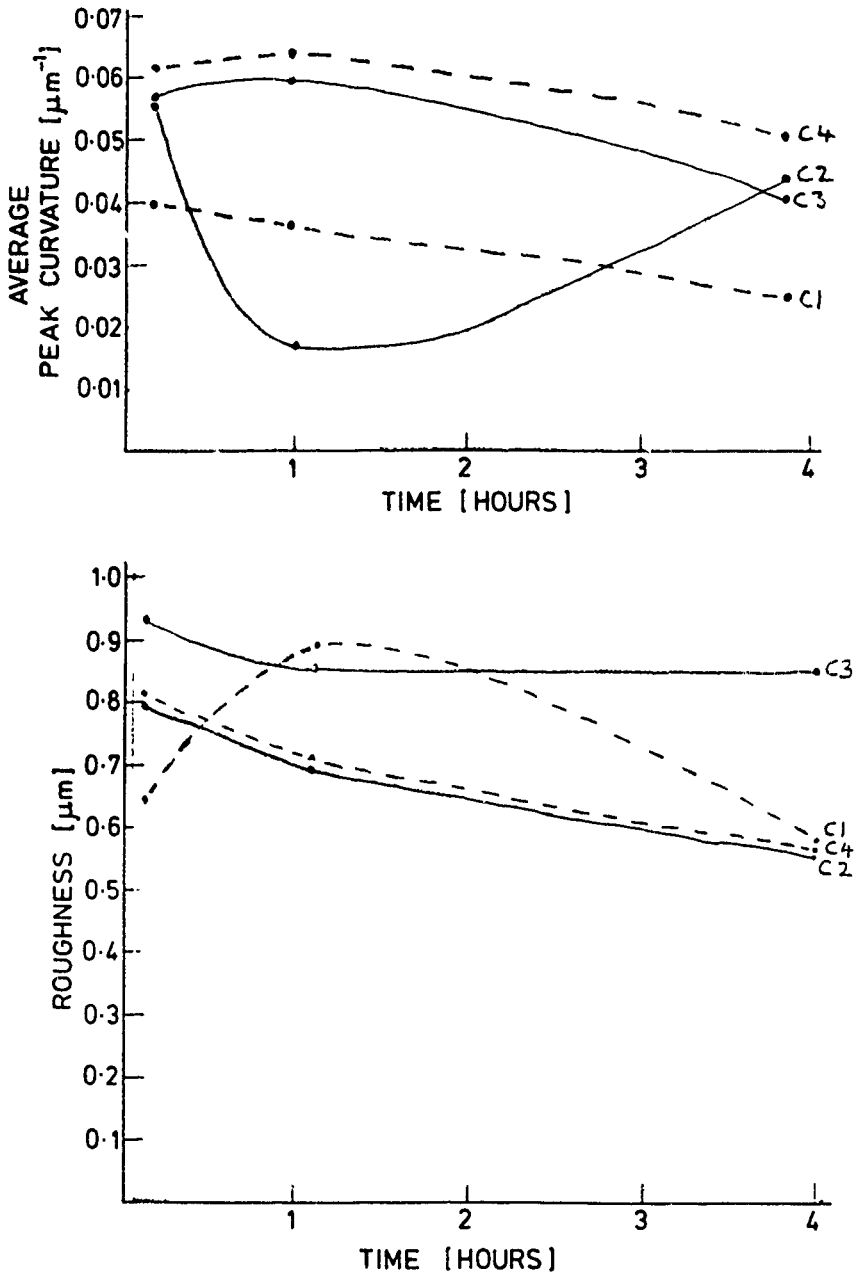

FIG. 10: 5 kg, 150°C. Comparison of all Oils in terms of Surface Changes

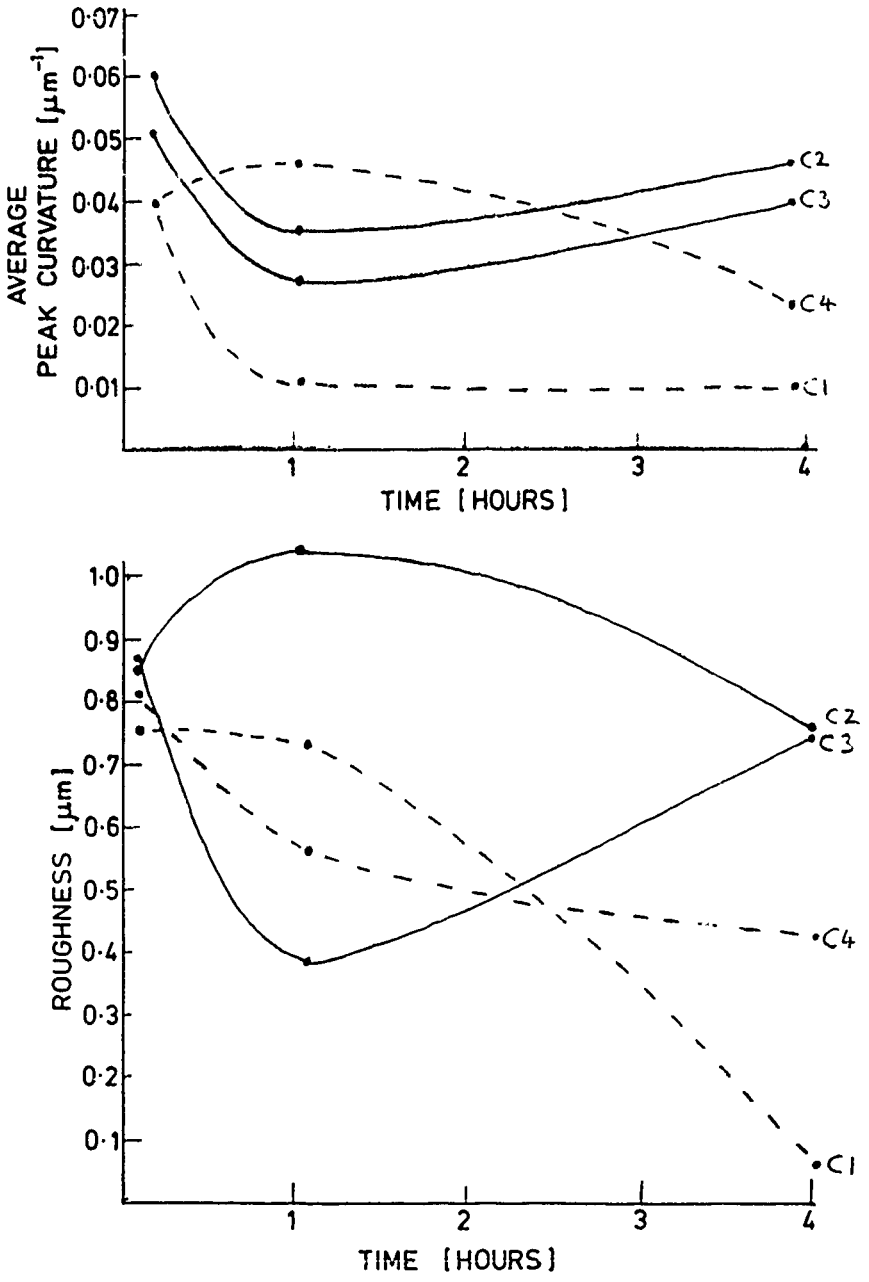

FIG. 11: 5 kg, 250°C. Comparison of all Oils in terms of Surface Changes

	150°C		200°C	250°C	
	1 kg	5 kg	1 kg	1 kg	5 kg
C1	7.1	9	5.3	5.4	7.2
C2	13	35	15	18.5	35.5
C3	1.7	3.5	1.8	1.3	3.8
C4	6.8	11.5	3.9	8.8	5.3

Table 3: Induction Times [in minutes]

The ranking of the four oils remains consistent under the different conditions, although oil C4 shows considerable variability.

Induction time ranking: C2 > C1, C4 > C3

Increasing temperature appears to reduce slightly the induction time for zddp oils C1, C3 and C4, oil C4 showing this most clearly. Conversely oil C2, the non-zddp oil, shows a slight increase in induction time as temperature increases. Increasing load increases the induction time for oils C1, C2, and C3, especially oils C2 and C3 where the induction time at 5kg load is double that at 1kg load. However oil C4 shows a reduction in induction time at the higher load. An increase in induction time with load would be expected since:-

Film formation rate = film reaction rate - film removal rate

Film removal rate will be increased by increased load, delaying film formation.

The role of induction time in the running-in process was investigated by comparison with surface changes. The First Annual Report noted that most surface changes occurred in the first few minutes and concluded that 'most of the wear' took place during this time. Figs. 3-6 of this report also indicate significant surface changes during this time, though not necessarily 'most of the wear'. The induction time marks the end of this high wear rate period, so it would be expected to correlate with the surface changes that occur after 5 to 30 minutes of running-in - the longer the induction time, the greater the surface changes. Fig. 12 examines the relationship between induction time and peak curvature

changes at 1 kg load. For Fig 12(a) the peak curvatures at 5 mins. and 30 mins. are averaged to give values at the averaged time of 17.5 mins, at which time the differences in induction time may be most evident, differences in film anti-wear activity being mostly eliminated. Fig. 12(b) looks at the relationship between final run-in peak curvature (averaged for 2 and 4 hours) and induction time, with shaded areas representing the induction time values from Fig. 12(a) - this allows easy comparison between surface changes at induction time and surface changes once running-in is complete.

Fig. 12(a) shows that differences between the oils are evident after 17.5 mins. of running-in. Oil C4's variability of induction time is very clear, but oils C1, C2 and C3 are fairly well grouped, and these groupings do follow the expected trend. Oil C3, with the shortest induction time, shows the least surface changes at 17.5 mins., while oil C2, with the longest induction time shows the most. However considering trends within each oil grouping it is clear that this is not the whole story. Oil C2 shows this particularly: as temperature rises from 150°C to 250°C induction time lengthens, yet surface changes reduce. Similarly oil C1's induction time is relatively constant as temperatures change, yet surface changes vary considerable. This provides good evidence that the initial anti-wear activity, during the induction period, is not constant, showing the same temperature sensitivity trends noted in the oil rankings in terms of run-in surface changes - namely for oil C1 anti-wear activity is reduced as temperature increases while for oil C2 it increases (see section 5.1).

Fig. 12(b) compares the oils film anti-wear activity Oil C3 performs well except at 250°C when its additive film is clearly not protecting the surface well. Oil C2 demonstrates good film performance, allowing a drop of only about 0.01 μm^{-1} in peak curvature from induction time to run-in time. Oil C1's additive film performance is generally not so good, allowing a drop of about 0.02 μm^{-1} in peak curvature over this period. In general it does seem that the differences between the oils in terms of surface changes after running-in are evident already at induction time and that this may be due to differences in initial anti-wear activity as well as in induction time.

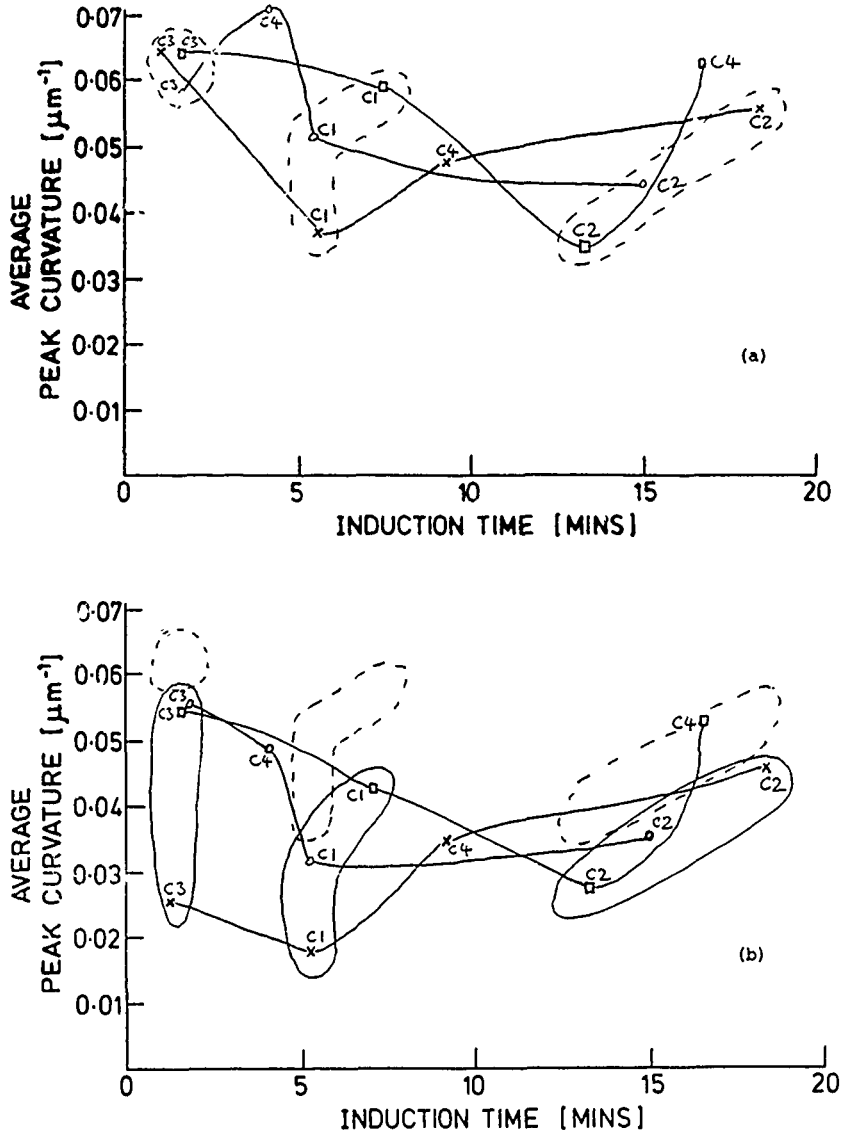

FIG. 12: The Effect of Temperature on Average Induction Time and Surface Changes (1 kg load tests)

□ 150°C
○ 200°C
× 250°C

(a) Peak curvatures after 17½ mins and average induction time.

(b) Peak curvatures after 3 hours and average induction time.

Table 4 compares the oils ranking for peak curvature changes at 5 mins with their ranking after running-in, to examine the differences in initial anti-wear activity. Data from the 5kg load tests are used since the higher wear rate results in greater differences after 5 mins. of running-in, and in most cases delays induction time till after 5 mins., eliminating film anti-wear activity. Run-in time values of peak curvature are the averages of the 1 hour and 4 hour values.

	C1		C2		C3		C4	
	PK. CURVATURE	RANKING	PK. CURV.	RANKING	PK. CURV.	RANKING	PK. CURV .	RANKING
150°C 5 mins	0.0400	4	0.0566	3	0.0574	2	0.0625	1
Av60+240 mins	0.0309	= 3	0.0308	= 3	0.0506	2	0.0576	1
250°C 5 mins	0.0401	4	0.0610	1	0.0518	2	0.0409	3
Av60+240 mins	0.0106	4	0.0412	1	0.0340	3	0.0356	2

Table 4: Comparison of Oil Rankings at 5 Mins. and at Run-in Time.

Table 4 gives clear evidence that the major differences between oils in terms of peak curvature drop at run-in time are the result of differences in the initial anti-wear activity. The change of ranking of oil C2 with temperature is particularly clear.

Any effect of differences in induction time upon final surface changes appears to be minimal compared with the differences in initial anti-wear activity. Taking surface changes as a measure of wear, and so of performance, it seems that induction time is not a good characteristic to use for ranking the performance of these four oils.

5.3 Coherence

Film quality was measured by assessing the value and stability of the e.c.r. trace, firstly from induction time to stop time - the % film activity - and secondly after the e.c.r. has stabilised, after the gradient period - the % coherence. Unlike induction time the gradient period was found to be very

variable when a test was repeated with the same oil at the same experimental conditions. This made it impossible to established a fixed % film activity for a particular oil at a particular condition. However film quality after the gradient period, measured by % coherence, did give consistent results. Tables 1 and 2 give results of % film activity. The % coherence values are the average of the % film activity values after 60 mins. of running-in. Appendix 2 gives the scale of measurement. Table 5 gives % coherence values for the four oils at the different experimental conditions.

	150°C		200°C	250°C	
	1kg	5kg	1kg	1kg	5kg
C1	77	55	65	58	3
C2	75	80	72	87	50
C3	96	87	95	63	16
C4	87	90	85	50	60

Table 5: % Coherence

The zddp oils, C1, C3 and C4, show a reduction in coherence as temperature rises from 150°C to 250°C while oil C2, the non-zddp oil, shows an increase in coherence for the 1kg load tests. Load increases do not significantly affect coherence at 150°C, except for oil C1, while a similar load increase at 250°C does reduce coherence. These trends are in broad agreement with the surface changes trends noted earlier, indicating that coherence may be a good indicator of performance in terms of prevention of surface changes.

The relationship between coherence and changes in peak curvature is examined in detail in Figs. 13-18. Figs. 13-15 examine the effect of temperature at constant load while Figs. 16-18 examine the effect of load at constant temperature. In each case the first figure (i.e. Figs. 13 and 16) looks at the relationship between run-in peak curvature and coherence. The second (Figs. 14 and 17) between peak curvature at induction time and coherence, and the third (Figs. 15 and 18) the relationship between % drop in peak curvature from

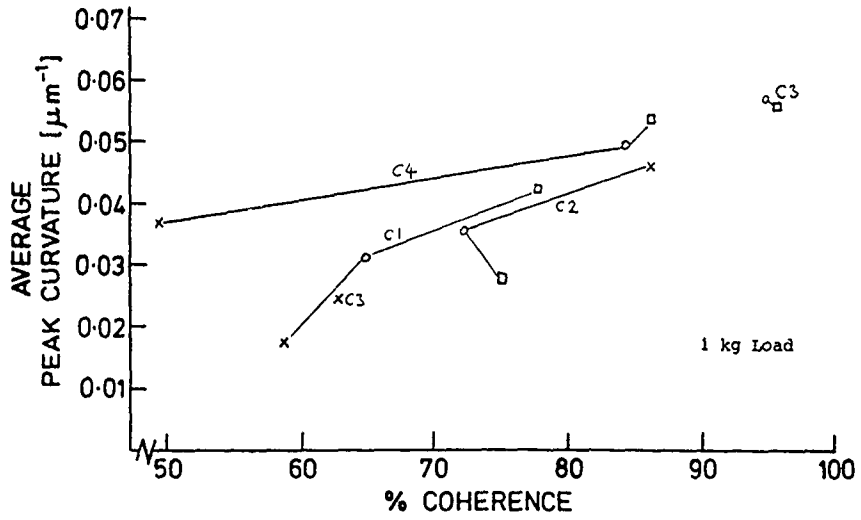

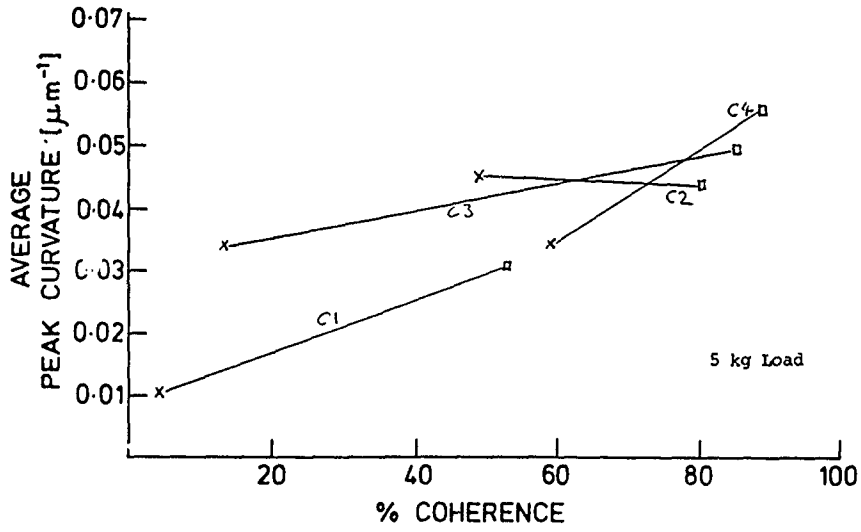

□ 150°C
○ 200°C
× 250°C

FIG. 13: The Effect of Temperature on Coherence and run-in Peak Curvature

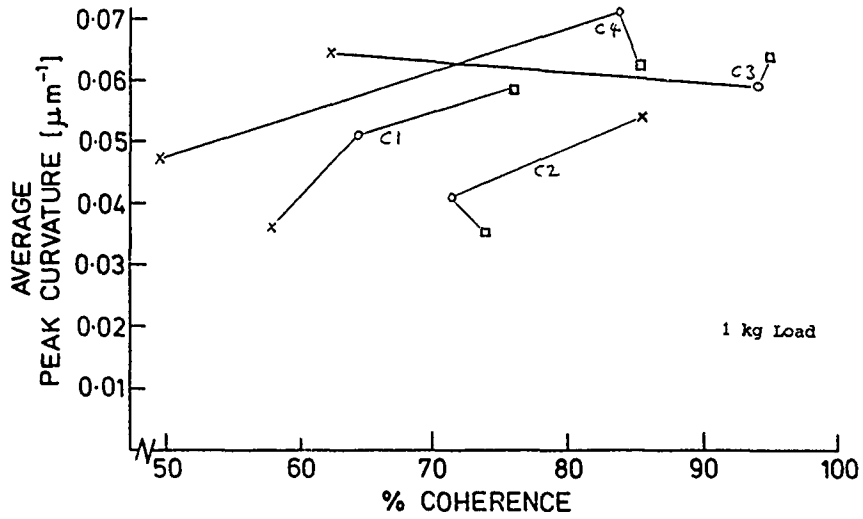

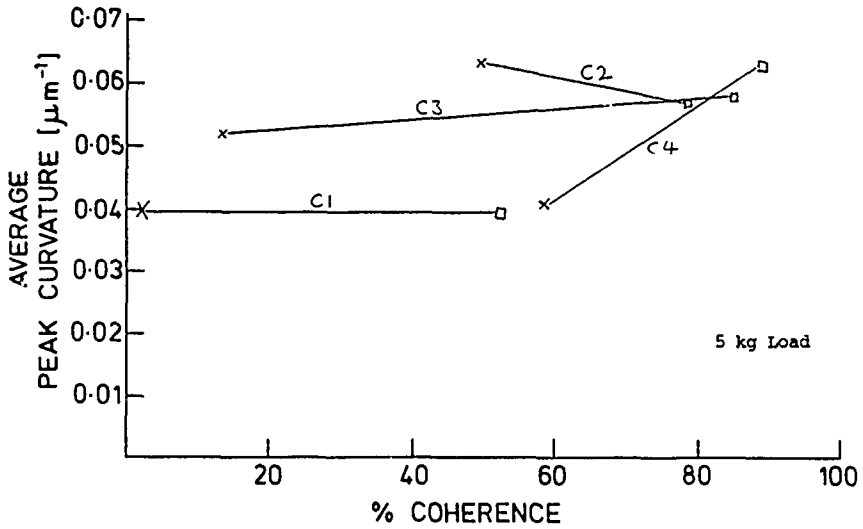

□ 150°C
o 200°C
x 250°C

FIG. 14: The Effect of Temperature on Coherence and Peak Curvature at Induction Time

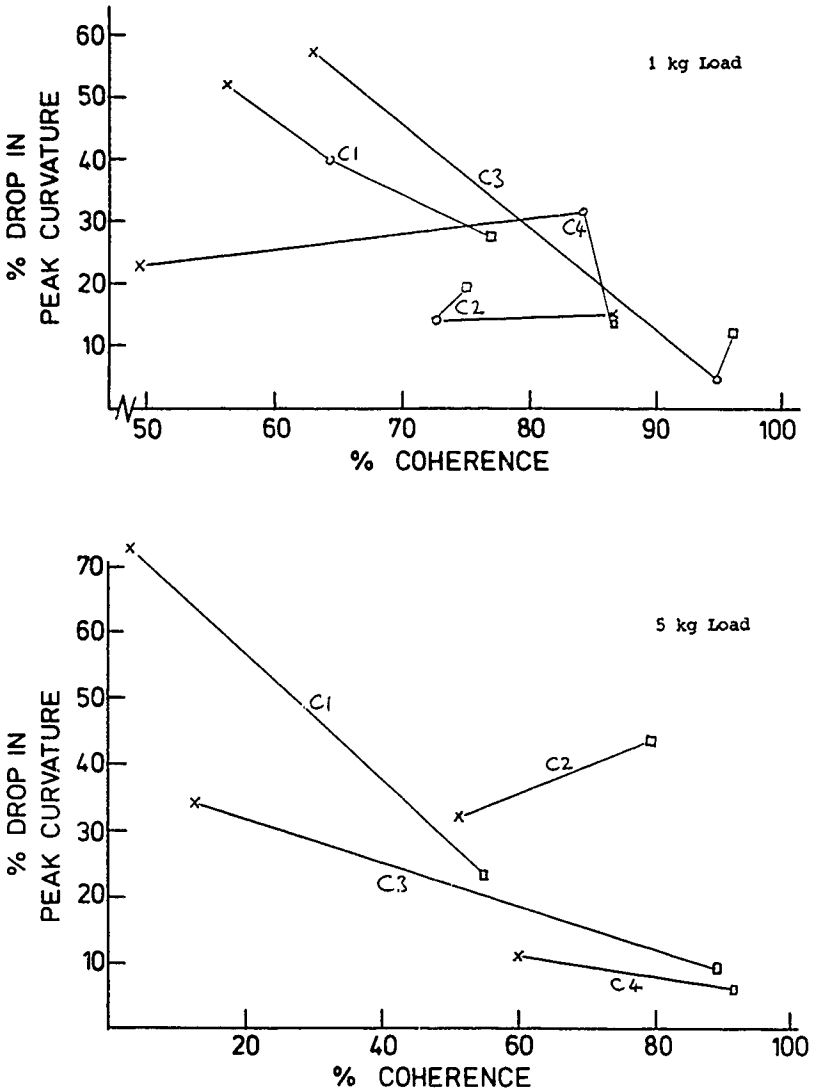

□ 150°C
o 200°C
× 250°e

FIG. 15: The Effect of Temperature on Coherence and % Drop in Peak Curvature from Induction Time to Run-In Time

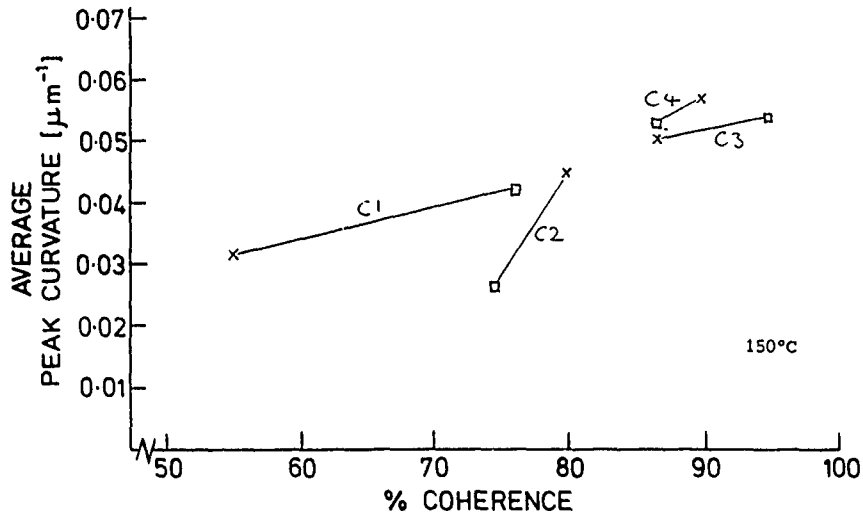

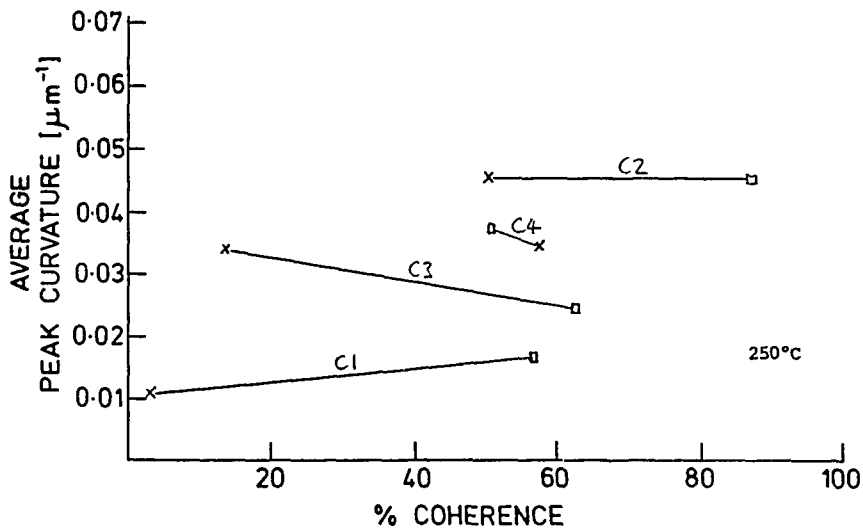

□ 1 kg
× 5 kg

FIG. 16: The Effect of Load on Coherence and Run-In Peak Curvature

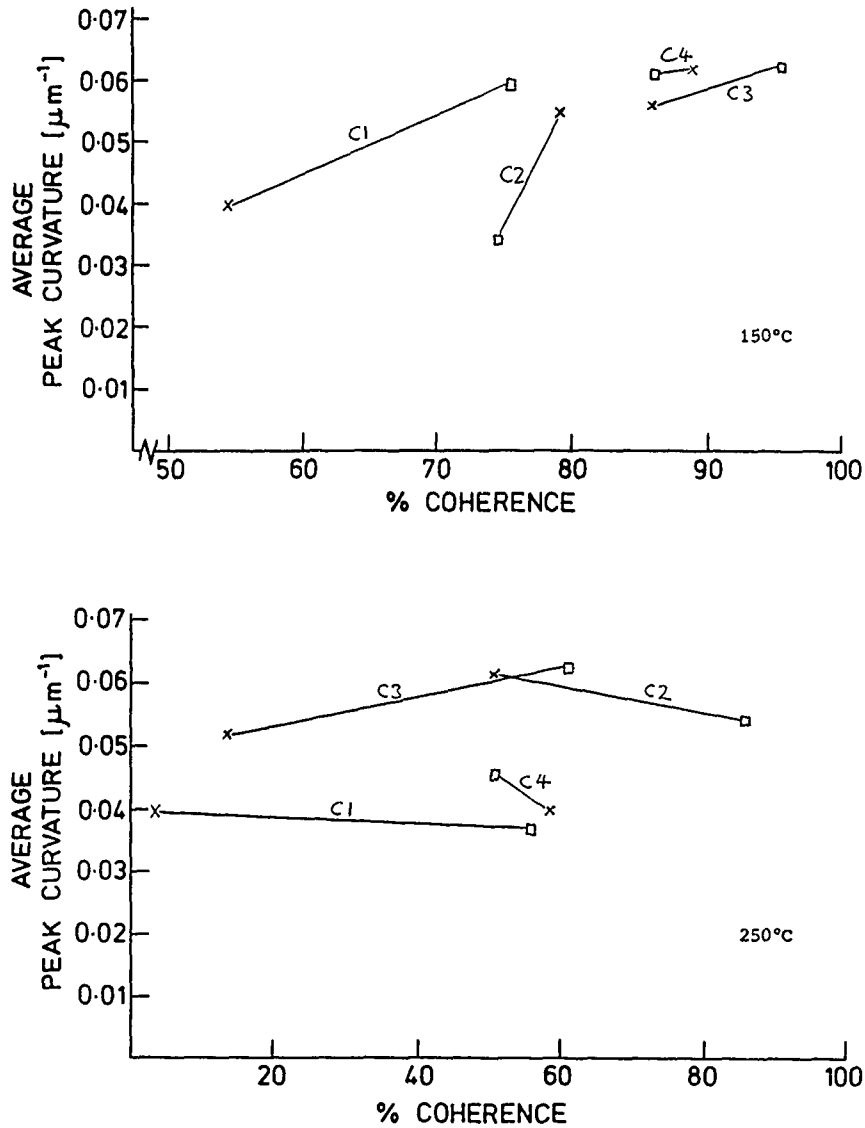

□ 1 kg

X 5 kg

FIG. 17: The Effect of Load on Coherence and Peak Curvature at Induction Time

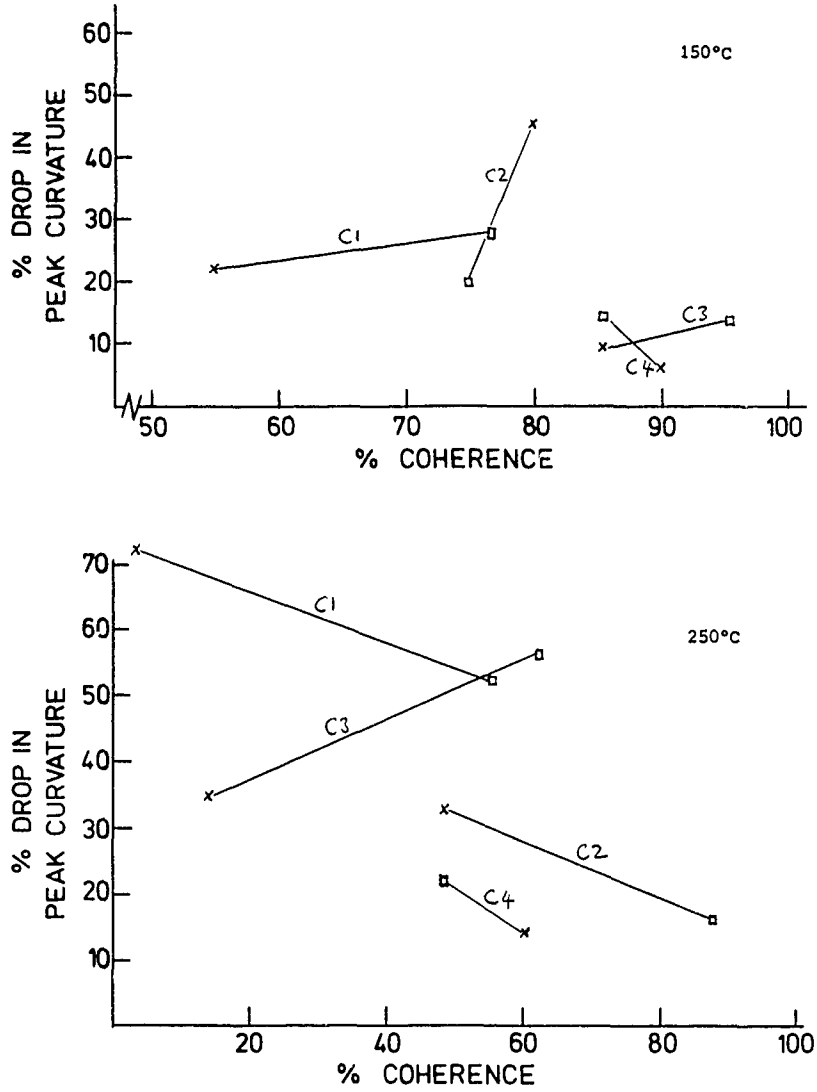

□ 1 kg
× 5 kg

FIG. 18: The Effect of Load on Coherence and % Drop in Peak Curvature from Induction Time to Run-In Time

induction time to run-in time and coherence. In this way any relationship shown between run-in peak curvature and coherence is split into two components representing initial anti-wear activity and film anti-wear activity. The peak curvature at induction time is an estimate based upon the most appropriate values available. For 1kg load it is the average peak curvature of 5 mins. and 30 mins., giving a value at the averaged time of 17.5 mins., while for the 5kg load the 5 mins. values for peak curvature are used.

Fig. 13 examines the relationship between run-in peak curvature and coherence at constant load. The results support the contention that coherence is a good measure of oil quality in terms of prevention of surface changes - high coherence is associated with least change in peak curvature. However Table 4 showed that the majority of differences in peak curvatures between oils were already evident before induction time, so coherence may be associated with initial anti-wear activity rather than film anti-wear activity.

Fig. 14 examines the relationship between peak curvatures at induction time and coherence at constant load. The results indicate that there is a correlation at 1kg load, but not at 5kg load. Fig. 15 then looks at the relationship between % drop in peak curvature from induction time to run-in time and coherence and this indicates that coherence is associated with film quality - high coherence giving a smaller % drop in peak curvature. This suggests that coherence is a measure of both film anti-wear activity and initial anti-wear activity.

Fig. 16 examines the relationship between run-in peak curvature and coherence at constant temperature. The results indicate a correlation at 150°C but not at 250°C. Fig. 16, 250°C does show very clearly the rankings of the oils in terms of both peak curvature and coherence but increasing load reduces coherence without significantly reducing run-in peak curvature. Fig. 17 shows that this pattern is established by the induction time with high coherence being associated with high peak curvature at 150°C but not at 250°C. Fig. 18 shows that film behaviour is quite different with an association at 250°C but not at 150°C, demonstrating the load tolerance of additive films at 150°C compared with at 250°C.

These results indicate that generally coherence is a good measure of surface protection, but there are three areas in which no association is found: at 5kg at induction time (Fig. 14), at 250°C at induction time (Fig. 17) and at 150°C during film activity (Fig. 18). The first two involve the more severe conditions during induction time and it may be that a maximum wear rate is reached due to the constant severe conditions. Fig. 18, during film activity, indicates that increasing load at 150°C does reduce coherence without increasing surface changes. This suggests that the additive film is squashed by the increased load, and this results in a lower coherence, but is still of sufficient strength to protect the surface. At 250°C (Fig. 18) the films strengths is reduced by the higher temperature so that increased load affects both coherence and surface protection.

6. DISCUSSION

The apparatus described here has enabled differences in oil performance to be established based upon the degree of surface changes produced during running-in. The effect of load and temperature on oil performance is also clearly demonstrated. Measurements of the e.c.r. have been shown to give values of oil quality that correlate well with oil performance in terms of surface changes. The importance of the first few minutes of running-in, before film formation, has been shown and oil anti-wear activity during this period has been shown to correlate with the additive film anti-wear activity. A correlation of these results with oil composition has also been attempted. The main object of this project was to compare the assessment of oil performance in this experimental rig with assessment in engine tests, but this has not been possible as the US Army have not produced any engine test data.

6.1 Surface Changes

Peak curvature and rms roughness measurement have indicated differences in wear severity during running-in. Rms roughness values were found to be less consistent due to honing variability, so peak curvature changes were used in determining correlations with oil characteristics. An increase in load from 1kg to 5kg was found to have little effect on surface changes for all the oils. However temperature had a very significant effect. For oils C1, C3 and C4, containing zddp, surface changes were minimal at 150°C and 200°C but become more severe at 250°C. This agreed with film thickness measurements from the First Annual Report, thickness decreasing as temperature rose above 200°C. Conversely oil C2, containing a non-zddp additive, showed less surface changes as temperature rose from 150°C to 250°C.

Rankings in terms of prevention of surface changes were obtained for each experimental condition. Oils C3 and C4 showed the best performance at 150°C and 200°C while oil C2 was the best at 250°C. Oil C1 performed well only at 1kg, 150°C, giving the worst performance at the other conditions. The ranking of the

zddp oils, C1, C3 and C4 seems to be linked to their zddp concentration. Oil C1 has ≈ 0.1% zddp, oil C3 ≈ 0.5% zddp and oil C4 ≈ 1.4% zddp. The poor performance of oil C1 is probably due to a slow film reaction rate, produced by low zddp concentration, such that any increase in severity of conditions from the optimum for zddp oils, 1kg 150°C, results in a significantly thinner film and loss of surface protection. However oils C3 and C4 are very similar in their performance even though oil C4 has considerably more zddp. This is probably due to differences in the metal detergent inhibitors [7,8]. Oil C1 and C3 have similar inhibitors and oil C3, with a higher zddp concentration, shows the fastest induction time, and better surface protection. If oil C4 had a similar inhibitor it would be expected to give a faster induction time than oil C3, and better surface protection. In fact in this case oil C4 would protect the surface too well and not allow running-in. The inhibitor it does have seems to lengthen the induction time allowing a significant degree of surface changes in these first few minutes, allowing running-in to occur. Tests carried out in the First Annual Report with base oil + 1% zddp with no inhibitor show very fast induction times, film coherences of 100% and no significant surface changes after 4 hours of running-in. This indicates the importance of inhibitors in significantly reducing zddp activity allowing some running-in to occur at high concentration of zddp.

6.2 Induction Time

The induction time has been found to be a consistent characteristic of an oil. For the zddp oils C1, C3 and C4 temperature increases slightly reduce induction time while for oil C2 induction time is slightly increased at higher temperature. Load increases from 1kg to 5kg tend to increase induction time, doubling it for oils C2 and C3.

Film formation rate = film reaction rate - film removal rate. The film reaction rate depends upon both anti-wear additive concentration and interference/competition between the additive and detergent inhibitor, and it is the relative importance of the latter that changes with temperature. Load

increases increase the film removal rate, delaying induction time until further running-in has occurred, reducing the severity of contact conditions.

No clear relationship was found between induction time and surface changes after 17.5 mins. of running-in, indicating that the intital anti-wear activity of the oils might be very different. This was confirmed by comparing surface changes rankings at 5 mins with run-in surface changes rankings. The results indicated that the major differences in surface changes after running-in were produced before induction time, and so by differences in the initial anti-wear activity of the oils.

These results suggest that induction time is not the best characteristic by which the performance of an oil should be assessed [9]. However it may still have great importance in an engine test where the additive film fails and a fast recovery is essential. This could be established by comparing engine test data for oils C3 and C4, both of which perform well in terms of protecting the surface, but they differ markedly in induction time and this may affect their engine performance.

6.3 Coherence

The coherence, a measure of the value and stability of the e.c.r., was found to be a consistent characteristic of an oil under fixed conditions. For zddp oils, C1, C3 and C4, coherence was generally highest at 150°C and 200°C, becoming much lower at 250°C, while for oil C2, the non-zddp oil, coherence increases with temperature from 150°C to 250°C. These trends match the surface changes trends. However load increases tend to reduce coherence signficantly whereas surface changes were found to be largely unaffected by load.

Detailed examination of the relationship between coherence and surface changes showed that at constant load there is a good correlation as temperature varies and this correlation is evident for surface changes before induction time as well as surface changes from induction time to run-in time. Coherence appears to be a good measure of oil quality during both these periods suggesting a

similar anti-wear action both before and after induction time. These results can be related to the equation,

Rate of film formation = rate of reaction - rate of film removal

The rate of reaction increases with temperature until thermal degradation begins at about 200°C and this increases rapidly above 200°C resulting in an overall decrease in the rate of reaction, and a reduction in mechanical strength, leading to a reduction in film thickness and consequently greater wear. Increased load increases the rate of film removal and so reduces film thickness but at 150°C the mechanical strength of the film is high and this thinning has little affect on the protecting ability of the film. At 250°C thermal degradation reduces the film strength and any reduction in film thickness due to load then results in considerably more wear.

An electronic method of assessing coherence would be valuable. At the moment it is done by eye which has, obviously, severe limitations.

7. CONCLUSION

Measurements of surface changes during running-in show significant difference in the performance of the four oils. Contact temperature effects performance considerably, oil C2 improving as temperature rises from 150°C to 250°C while the performance of oils C1, C3 and C4 decreases. Load increases from 1kg to 5kg generally have little effect on surface changes. Oil performance rankings based upon peak curvature changes vary with temperature,

150°C - 200°C	C3, C4 > C1, C2
250°C	C2 > C4, C3 > C1

These trends were related to oil composition, oils C1, C3, and C4 contaning zddp performing well at the lower temperatures while oil C2, containing a non-zddp additive performed best at the higher temperature. Higher concentrations of zddp gave better oil performance but the presence of inhibitors can reduce zddp anti-wear activity considerably allowing running-in to occur when otherwise the zddp would protect the surface too well.

From the e.c.r. recording two consistent oil characteristics can be found, induction time which can be obtained directly and coherence, assessed by eye. Induction time was not found to be a good measure of oil performance in terms of surface changes, but did seem related to zddp concentration and inhibitor type in the same way as surface changes. Higher zddp concentration gives shorter induction times but inhibitors can significantly lengthen it. Induction time was only slightly effected by temperature, but increased considerably under load increases. Oils are ranked: C3 < C1, C4 < C2 by induction times.

Coherence is a good measure of oil quality, correlating well with surface changes both before and after induction time. This suggests that anti-wear activity before induction time is essentially similar to anti-wear activity after the additive film has formed. This is confirmed by the observation that the major differences in surface changes after running-in occur before induction time.

The temperature trends for surface changes and coherence for the zddp oils matches the trends for film thickness reported in the First Annual Report.

Unfortunately, the wear performance of these oils in actual engine tests is not known. Data from single-cylinder tests designed to assess the oils in terms of their tendency to form undesirable piston deposits show that oils C3 and C4 failed, suggesting that oils that form a thicker and more effective anti-wear film were the ones that also produced more deposits.

Table 6 summarises the rankings of the oils in terms of induction time, coherence and peak curvature changes before and after induction time. Only comparison with engine test data can determine the relative importance of induction time rankings and surface changes rankings.

		1kg	150°C	1kg	200°C	1kg	250°C	5kg	150°C	5kg	250°C
	C1	7.1	77	5.3	65	5.4	58	9	55	7.2	3
		12.8	28.4	24.5	39.6	44.8	52.4	41.0	22.8	40.9	73.6
	C2	13	75	15	72	18.5	87	35	80	35.5	50
		48.8	20.2	36.7	15.4	18.1	16.0	16.5	45.6	10.0	32.5
	C3	1.7	96	1.8	95	1.3	63	3.5	87	3.8	16
		7.8	13.9	13.4	6.6	7.2	57.6	15.3	11.8	23.6	34.4
	C4	16.8	87	3.9	85	8.8	50	11.5	90	5.3	60
		8.8	15.4	-5.6	33.0	29.5	22.4	7.8	7.8	39.7	13.0
R	C1	2	3	3	4	2	3	2	4	3	4
A		3	4	3	4	4	3	4	3	4	4
N	C2	3	4	4	3	4	1	4	3	4	2
K		4	3	4	2	2	1	3	4	1	2
I	C3	1	1	1	1	1	2	1	2	1	3
N		1	1	2	1	1	4	2	2	2	3
G	C4	4	2	2	2	3	4	3	1	2	1
		2	2	1	3	2	2	1	1	3	1

DATA PRESENTED IN FOLLOWING FORM:

INDUCTION Time [mins]	COHERENCE %
% drop in	% drop in
Pk.curv. 0 - $\frac{5}{17}$ mins	Pk.curv. $\frac{5}{17}$ - 240 mins

RANKINGS IN TERMS OF BEST PERFORMANCE:

- Shortest induction time
- Greatest coherence
- Lowest % drop in Pk.curv. 0 - $\frac{5}{17}$ mins
- Lowest % drop in Pk.curv. $\frac{5}{17}$ - 240 mins

TABLE 6: Data Summary and Rankings

APPENDIX 1

Oil Details

OIL	BASE OIL	ZDDP	METAL DETERGENT INHIBITOR	TEST PERFORMANCE
C1	Mineral Oil	<0.1% primary alkyl	calcium suphonate	Pass
C2	Mineral Oil	no zddp unidentified phosphorus anti-wear agent	calcium suphonate	Pass
C3	Mineral Oil	0.5% primary alkyl(a mixture of Paranox 15 and 16)	barium suphonate	Fail
C4	Mineral Oil	1.4% primary alkyl(a mixture of Paranox 15 and 16)	calcium/magnesium nitrogen-type	Fail

It was found (January 1991) the list of engine specimens should have been headed "Engine Test Methods" and not simply "Engines".

A new list can now be made. In it the first column gives the label as supplied (A,B,C....). The next is the official name of the oil, where known [REO is short for Reference Engine Oil]. Then come the test sequence and its purpose and the engine used in the test.

OIL	TEST	PURPOSE OF TEST	ENGINE
A, REO 212	OL5	Piston Deposit Control	Cat 3406 400HP
B, "	OL6	Sump oil degradation	"
C,	1G2	Deposit control	Cat 1 Y73
D, REO 217/86		Crown land deposit and cylinder wear	Cummins NTC 400
E, REO 217	6404	300 hours. Wear	John Deere 6404
F, REO 212/84	Mack T7	Soot. Wear not noted	Mack EM6. 285HP

APPENDIX 2

COHERENCE MEASUREMENT SCALE

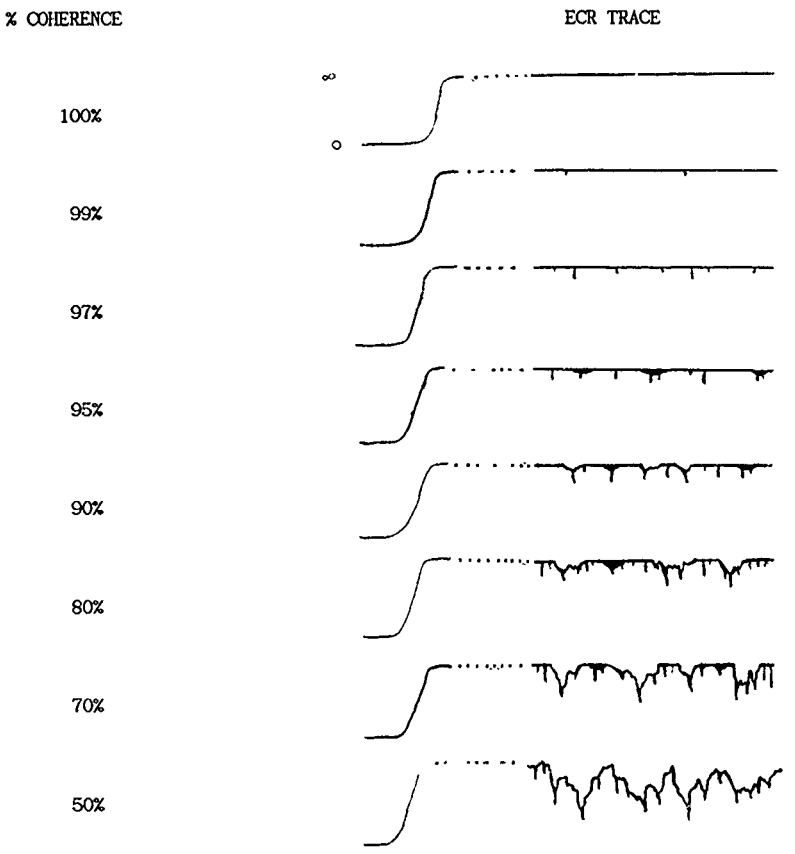

9. REFERENCES

1. ALLISTON-GREINER, A.F., CAMERON, A., GREENWOOD., J.A., Basic mechanisms of diesel lubrication, correlation of bench and engine tests. 1st Annual Report, August, 1987.
2. FUREY, M.J., Metallic contact and friction between sliding surfaces. ASLE Trans. 1961, 4 , 1-11.
3. MILLS, T.N., CAMERON, A., Basic studies on boundary, EP, and piston-ring lubrication using a special apparatus. ASLE trans. 1981, 25, 117-124
4. ALLISTON-GREINER, A.F., CAMERON, A., GREENWOOD, J.A. Basic mechanisms of diesel lubrication, correlation of bench and engine tests. 1st Interim Report, January 1986.
5. ALLISTON-GREINER, A.F. CAMERON, A., GREENWOOD, J.A., Basic mechanisms of diesel lubrication, correlation of bench and engine tests 2nd Interim Report,July 1986.
6. LUNN, B, Epilamen and Mischreibung, ZVDI Berichte, 1957, 20, 41-46.
7. ROUNDS, F.G., Additive interactions and their effect on the performance of a zinc dialkyldithiophosphate. ASLE trans. 1977, 21, 91-101.
8. SPIKES, H.A., CAMERON, A., Additive interference in dibenzyldisuphide extreme pressure lubrication. ASLE trans. 1974, 17, 283-289.
9. MARTIN, J.M., GEORGES, J.M., MEILLE, G., Boundary lubrication with dithiophosphates: influence of lubrication on wear of the friction interface steel/cast-iron. Wear of Materials, Glaesser, W.A. and Ludema, K.C. eds., 1977, 289-297.

THE RUNNING-IN PROCESS: Part 2

10 Introduction

Running-in experiments were repeated with oil/liner pairs ABDEF following the same experimental design as with liner C. The same test rig was used, test conditions were 150°, 1kg, 150°C, 5kg, 250°C, 1kg, 250°C, 5kg, and test durations were of 5 minutes, 1 hour and 4 hours. Surface analysis and measurements of film characteristics were as before.

Liner characteristics varied considerably in terms of hardness, rms.roughness and peak curvature. Details are given in composition; this is also summarised in the Appendix. Running-in tests were divided into two groups: fixed pairings and mixed pairings. The fixed pairing tests used each liner with its appropriately matched oil, eg. liner A with oil A, and the aim of these tests was to examine the performance of each pair and to compare them. The mixed pairing tests used different combinations of liner and oil at the fixed conditions of 150°C, 1kg. These tests attempted to separate performance differences due to liner surfaces from differences due to oil composition.

11 Fixed oil/liner pairs

11.1 Surface changes

Changes in the rms.roughness and peak curvature of each liner were investigated with the appropriate paired oil over a period of four hours of running-in. Film characteristics, induction time and coherence, were also measured. The results are summarised in Tables 7 and 8. Surface changes for the five oil/liner pairs show similar trends as indicated in Figs. 19-23 where surface changes are shown under different conditions of load and temperature. At 150°C surface changes were minimal but became much more severe at 250°C . Load increases had less significant effect, though generally the 5kg load tests do show slightly greater surface changes than the 1kg load tests. These results confirm those from the running-in tests with liner C where 3 ZDDP oils, oils C1, C3 and C4, showed similar behaviour. Fig. 21 shows that oil/liner pair D undergoes very severe surface changes under all test conditions, presumably due to the softness of the liner D(VHN 200).

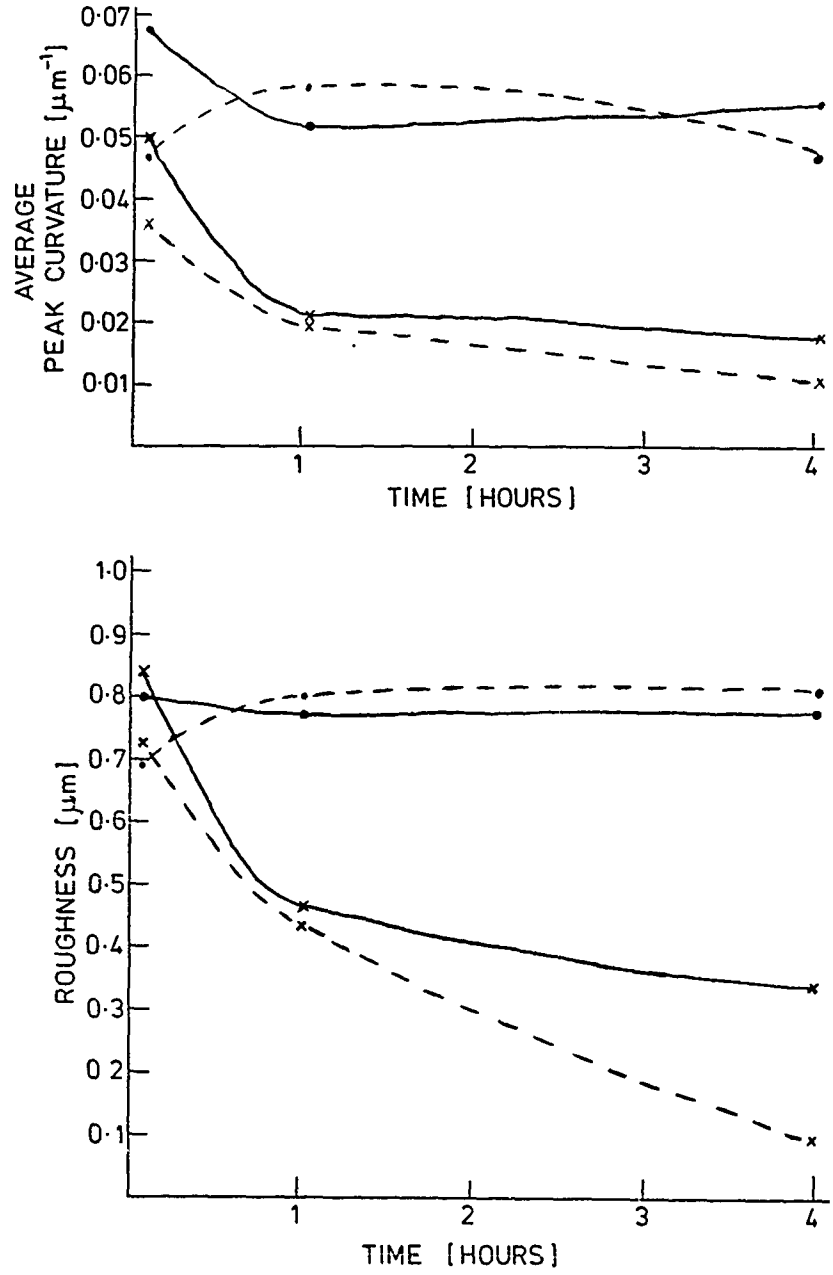

Fig.19: Surface changes, oil/liner pair A.

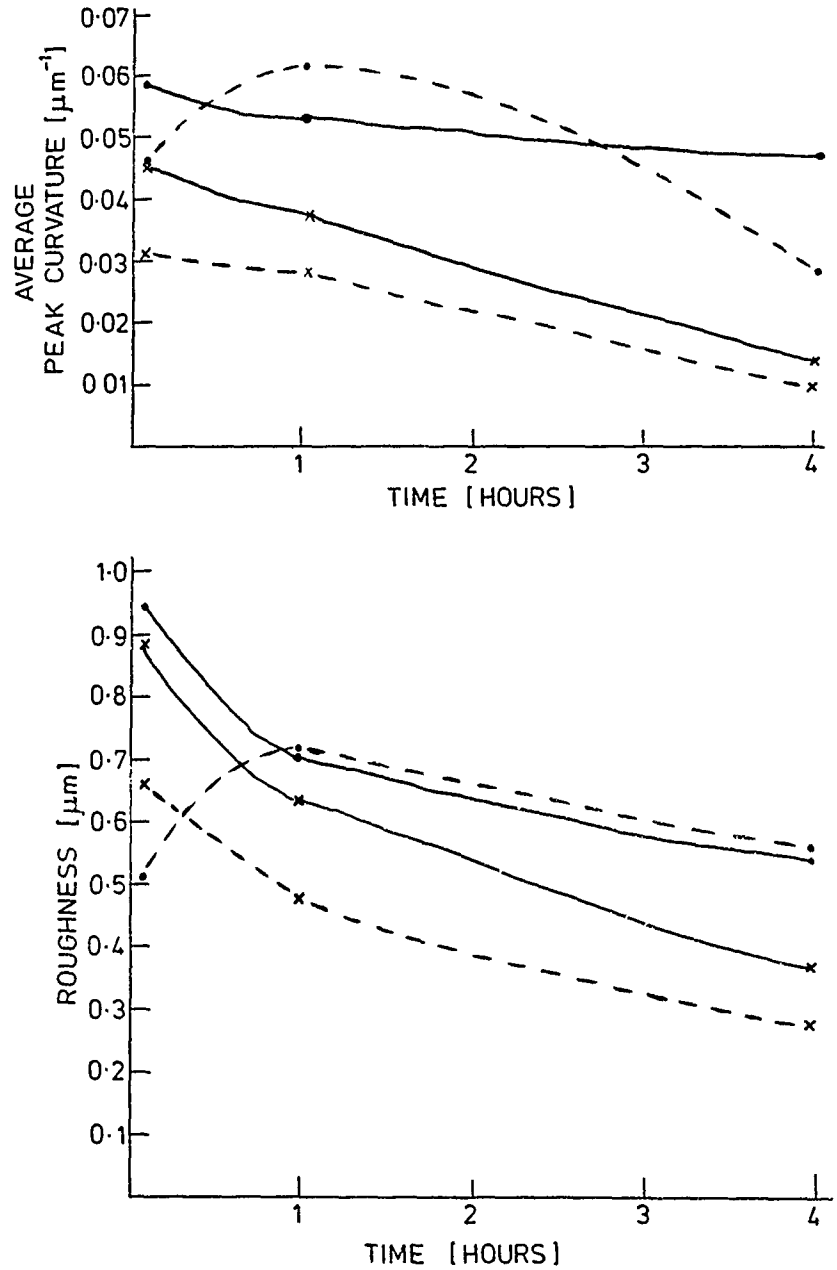

Fig.20: Surface changes, oil/liner pair B.

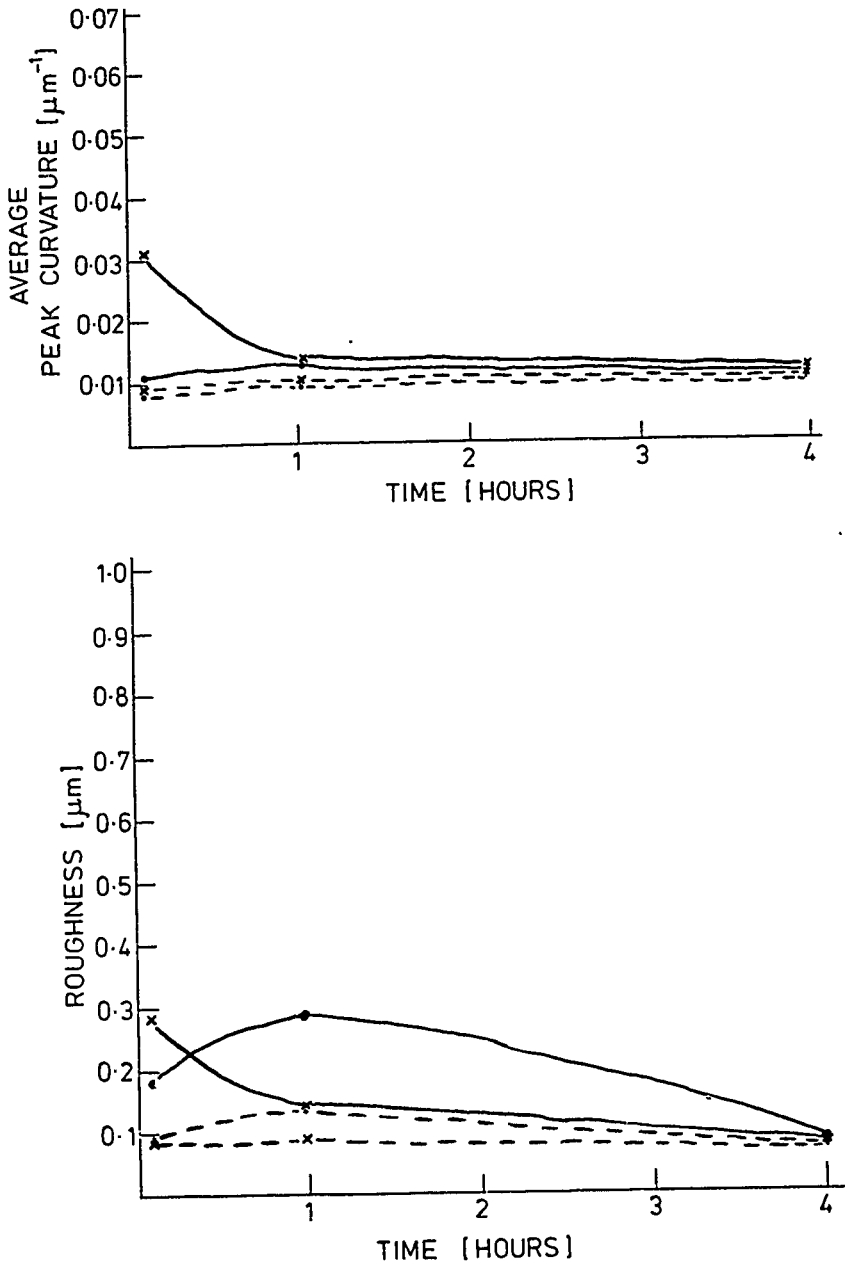

Fig. 21: Surface changes, oil/liner pair D.

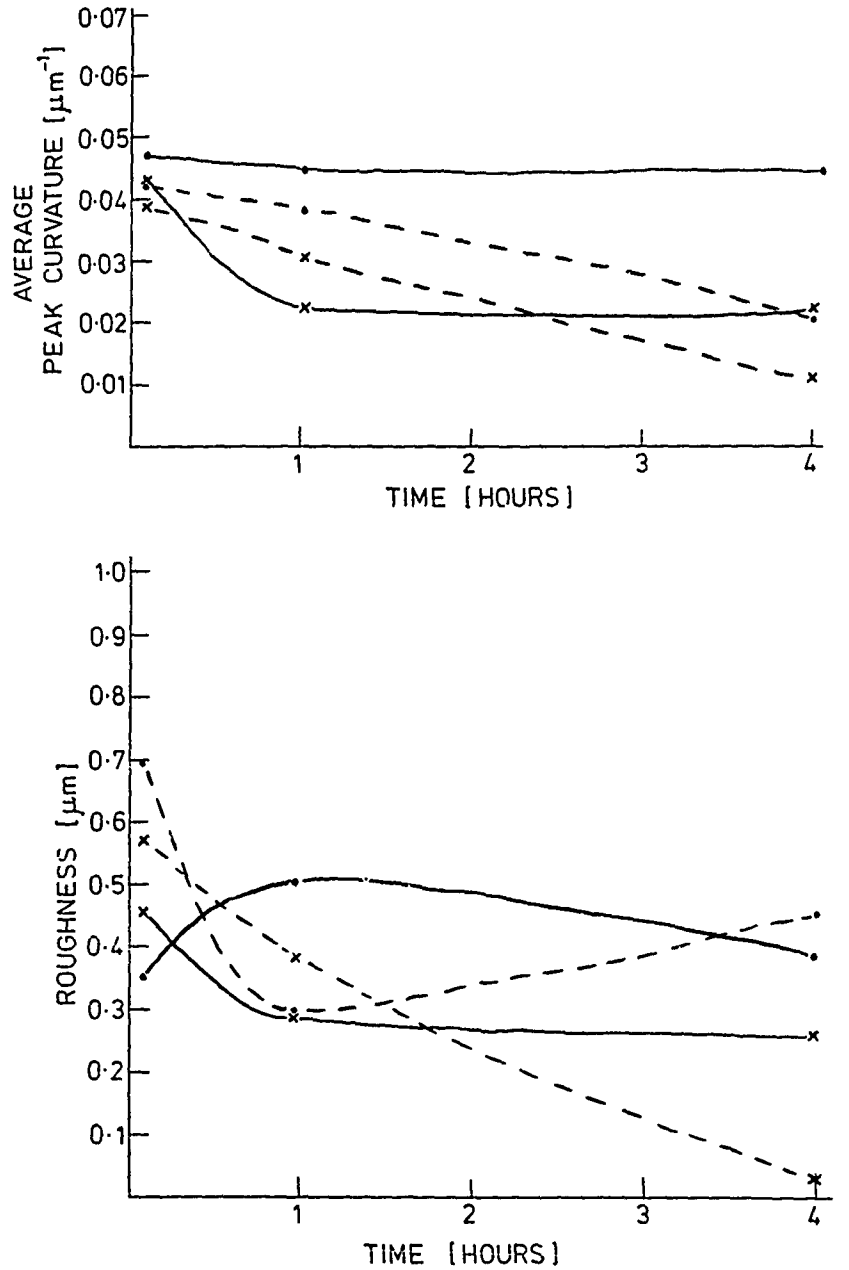

Fig.22: Surface changes, oil/liner pair E.

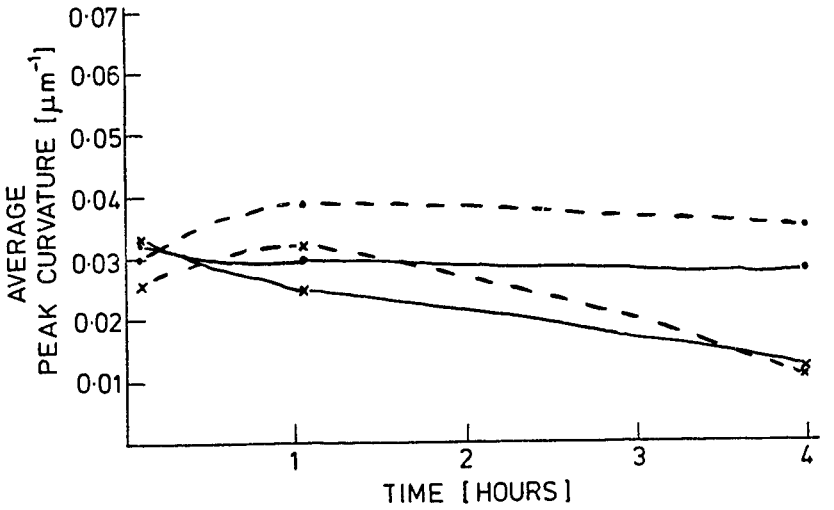

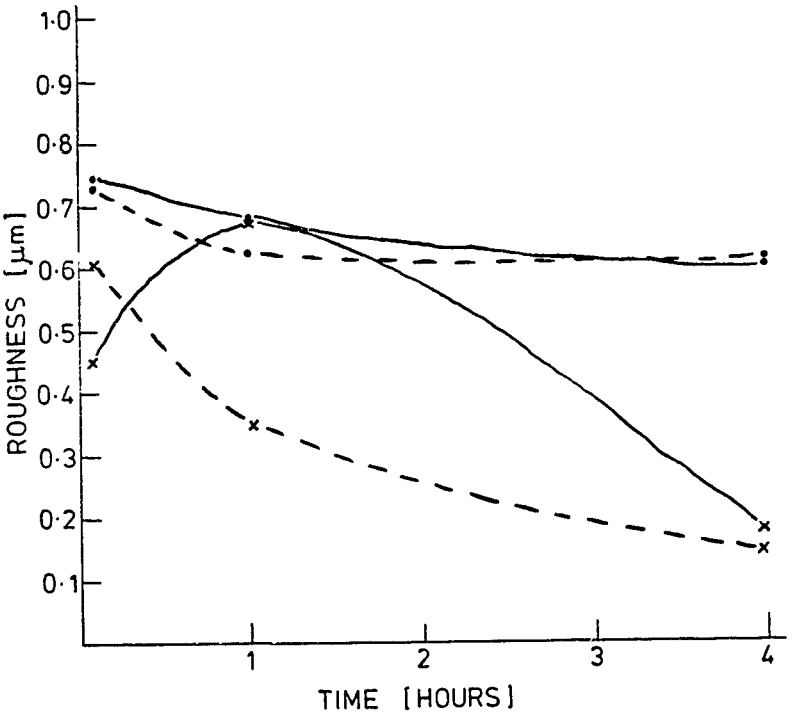

• 150°C —— 1kg

× 250°C - - - 5kg

Fig.23: Surface changes, oil/liner pair F.

Considering both rms.roughness and peak curvature changes from Fig.s 19-23 the severity of conditions can be ranked for all pairs: 150°C, 1kg≤150°C, 5kg<250°C, 5kg.

Figs 24-27 compare the performance of the five oil/liner pairs, in terms of prevention of surface changes, at each experimental condition. These figures clearly show the severity of conditions ranking indicated above, but due to differences in initial surface parameters of the five liners, a performance ranking of the five pairs cannot be directly obtained. The effect of liner hardness may be indicated in the performance of liners D and A. Pair D, with the softest liner (VHN 200) always performs poorly, as noted above.

		5 MINUTES	1 HOUR	4 HOURS
150°C	A	0.803 no fa*	0.774 25	0.774 25
		0.0677 0%	0.0518 70%	0.0554 95%
	B	0.941 no fa*	0.707 19	0.537 10
		0.593 0%	0.0536 80%	0.0474 95%
	D	0.179 3	0.290 3	0.075 2
		0.0116 0%	0.0133 90%	0.0115 80%
	E	0.352 0.5	0.507 0.5	0.382 0.5
		0.0474 0%	0.0453 98%	0.0445 97%
	F	0.750 2	0.686 2.5	0.60.9 1
		0.0326 0%	0.0306 97%	0.0282 97%
250°C	A	0.846 no fa*	0.465 6	0.340 9
		0.0499 0%	0.0213 60%	0.0180 95%
	B	0.883 4	0.629 3	0.365 6
		0.0458 0%	0.0377 80%	0.0141 80%
	D	0.287 2	0.147 1	0.085 6
		0.317 0%	0.0139 80%	0.0123 75%
	E	0.460 0.5%	0.287 1	0.254 1
		0.0436 0%	0.0233 90%	0.0224 85%
	F	0.454 1.5	0.681 2	0.178 1
		0.0338 0%	0.0252 98%	0.0119 80%

* no fa = no film activity

Data presented in the following form:

rms.roughness (μm) $_{-1}$	induction time (mins.)
peak curvature (μm^{-1})	% coherence

Table 7: Results of running-in tests with liners ABDEF and paired oils at 1kg load.

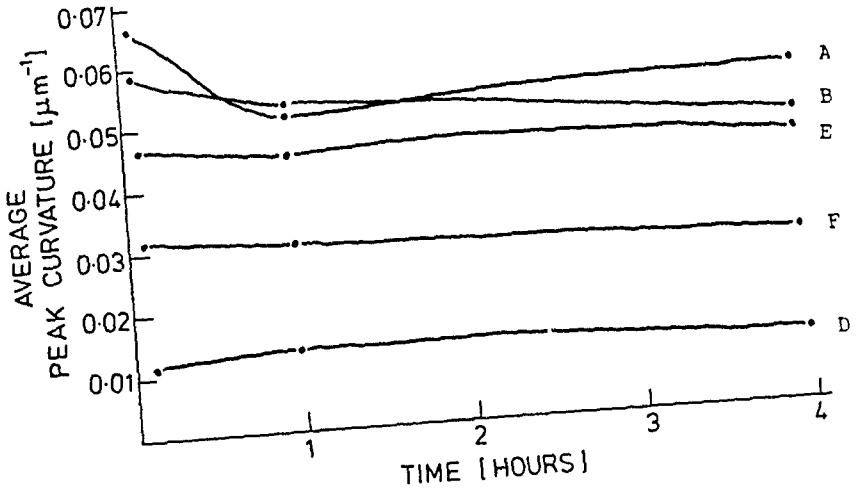

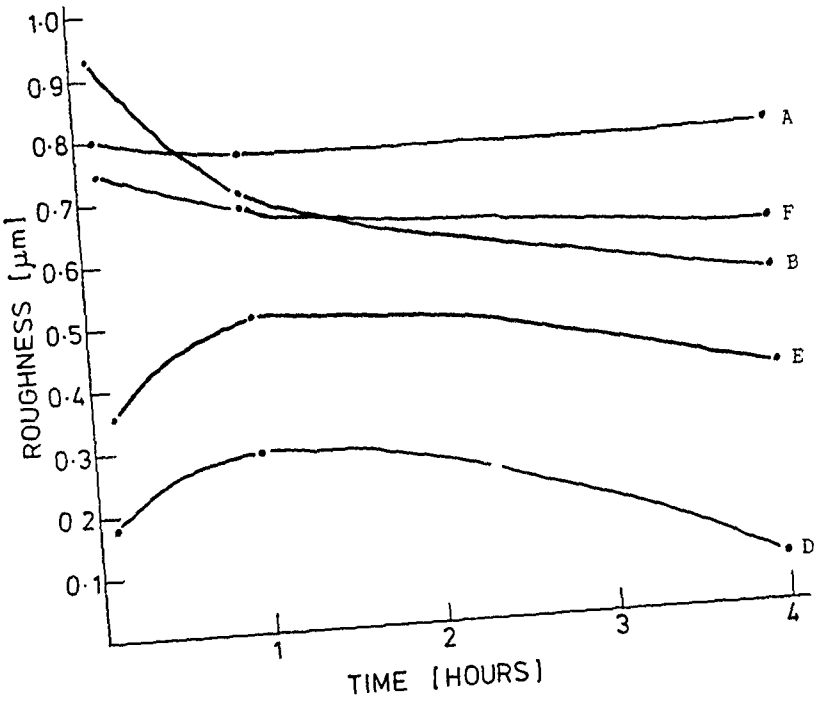

Fig.24: Surface changes at 150°C,1kg , all oil/liner pairs

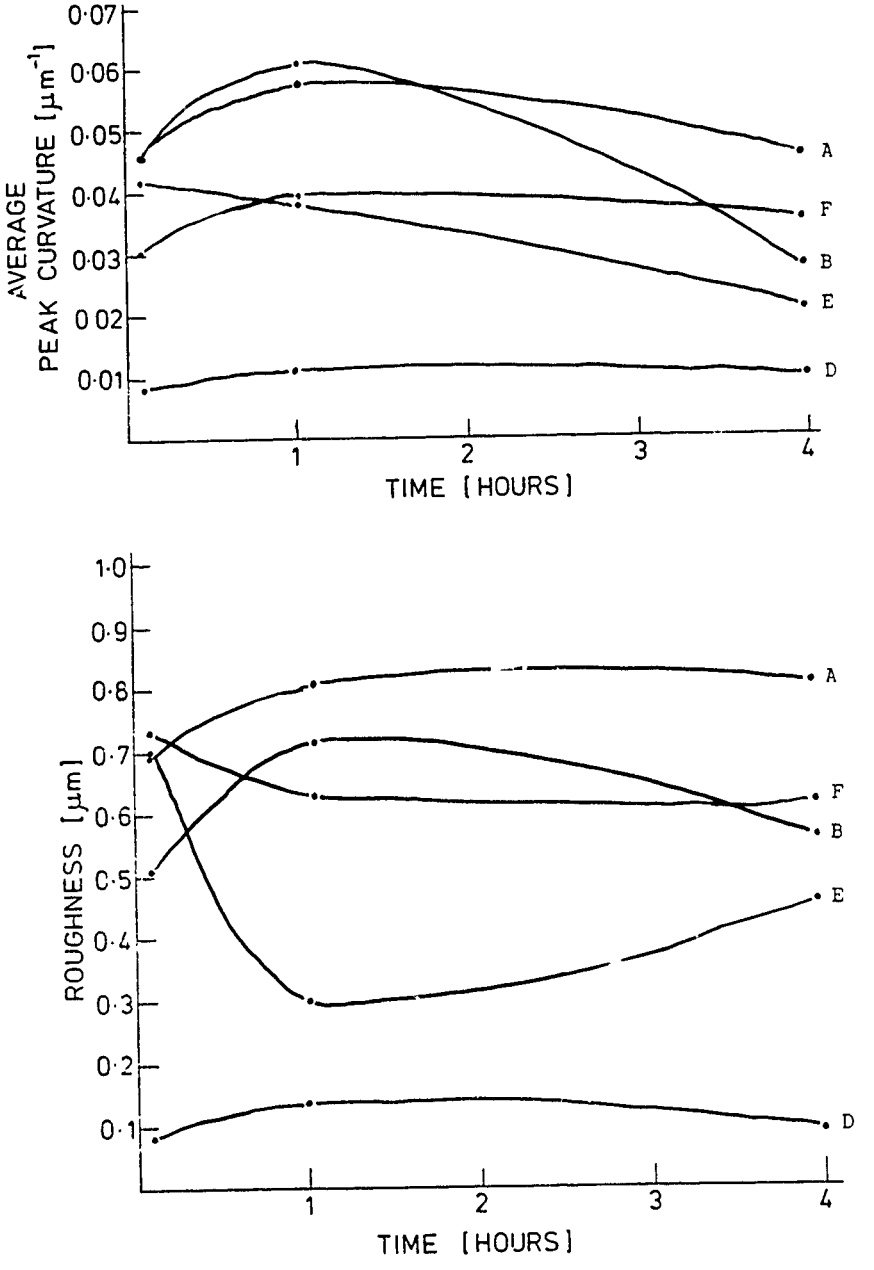

Fig.25: Surface changes at 150°C, 5kg , all oil/liner pairs

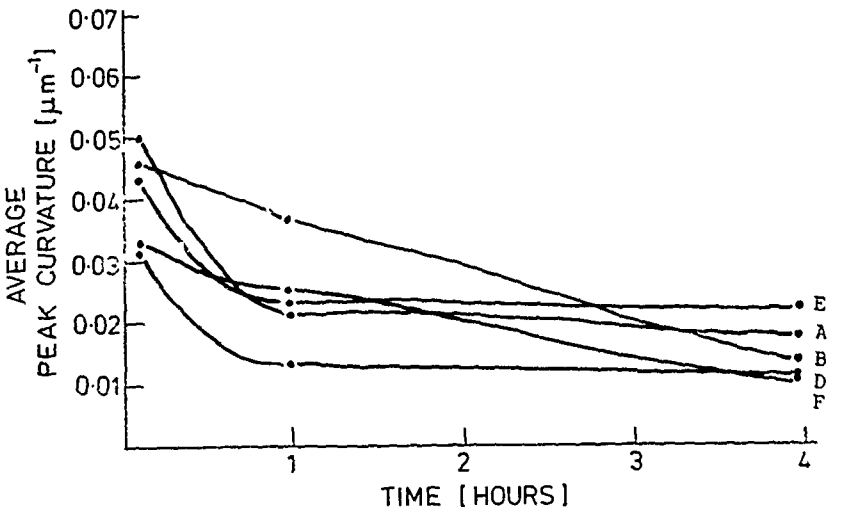

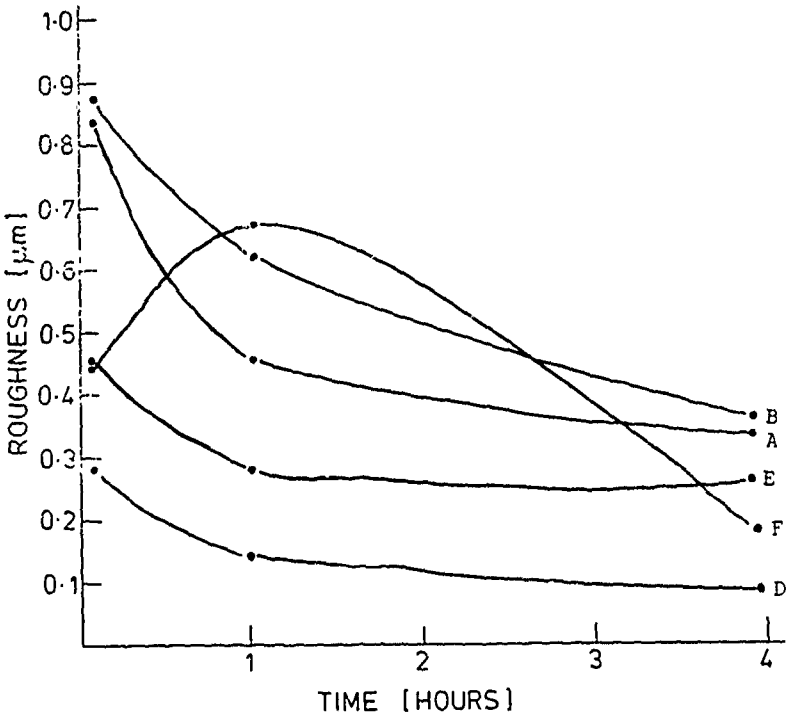

Fig. 26: Surface changes at 250°C, 1kg , all oil/liner pairs

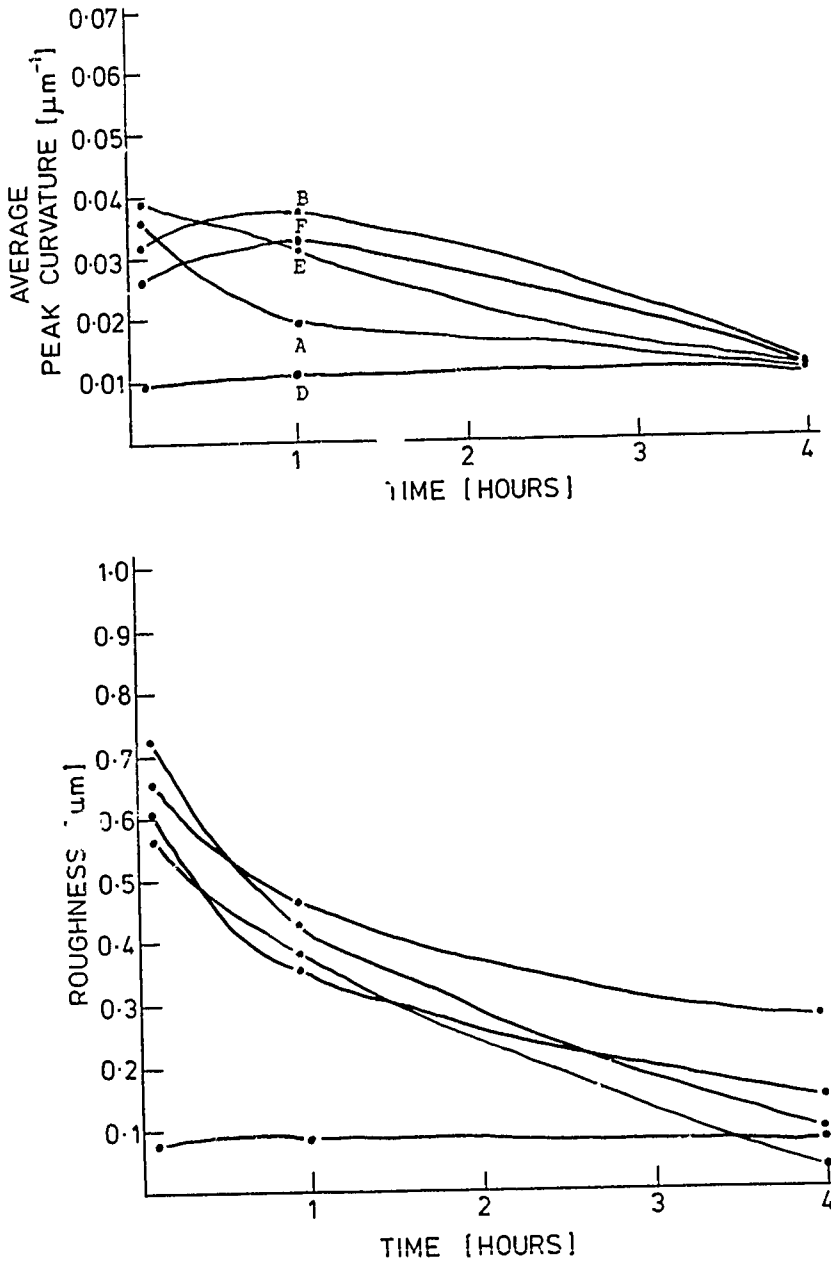

Fig. 27: Surface changes at 250°C, 5kg, all oil/liner pairs

		5 MINUTES		1 HOUR		4 HOURS	
150°C	A	0.690 0.0469	no fa* 0%	0.806 0.0583	13 60%	0.804 0.0460	8 70%
	B	0.504 0.0466	no fa 0%	0.718 0.0620	14 70%	0.556 0.0283	13 60%
	D	0.080 0.0085	no fa 0%	0.143 0.0109	1.5 90%	0.092 0.0102	11 25%
	E	0.697 0.0427	1.5 0%	0.296 0.0382	5 90%	0.452 0.0208	1 75%
	F	0.735 0.0306	3.5 0%	0.632 0.0394	4 85%	0.620 0.0352	4 90%
250°C	A	0.731 0.0360	no fa 0%	0.436 0.0196	- -	0.093 0.0104	20 50%
	B	0.659 0.0317	no fa 0%	0.474 0.0283	- 85%	0.093 0.0108	20 50%
	D	0.081 0.0096	no fa 0%	0.087 0.0110	6.5 30%	0.079 0.0115	6 20%
	E	0.575 0.0395	3 0%	0.387 0.0310	- -	0.037 0.0117	4 20%
	F	0 617 0.0263	2 0%	0.357 0.0326	4 40%	0.149 0.0117	3.5 75%

* no a = no film activity

Data presented in the following form:

rms.roughness (μm)	induction time (mins.)
peak curvature (μm^{-1})	% coherence

Table 8: Results of running-tests with liners ABDEF and paired oils at 5kg load.

Liner A is the next softest liner (VHN 390) but initially has the greatest peak curvature and rms. roughness, and so might be expected to show a greater degree of surface changes as conditions become more extreme. This does appear to be the case: at 150°C line A still has the greatest values of peak curvature and rms.roughness after running-in while at 250°C surface changes are more severe for liner A than for liner B (VHN 450) and liner B has the greatest values of surface parameters after running-in.

Table 9 shows the % drop in peak curvature for each oil/liner pair over the four hour running-in period at each experimental condition. Pair D is omitted since wear is severe at all conditions.

	150°C, 1kg	150°C, 5kg	250°C, 1kg	250°C, 5kg
A	26.0	38.5	75.9	86.1
B	35.1	61.3	80.7	85.2
E	25.3	65.1	62.4	80.4
F	31.4	14.3	71.1	71.5

Table 9: Total % drop in peak curvature during running-in

The values indicated in Table 9 suggest the following performance ranking for the five pairs:

150°C, 1kg: E>A>F>B>D

150°C, 5kg: F>A>B>E>D

250°C, 1kg: E>F>A>B>D

250°C, 5kg: F>E>B>A>D

On this basis pair E shows the best performance at 1kg load, pair F at 5kg. Pair A performs well at 150°C but less well at 250°C. In general performance ranking is:

F≥E>A>B>D

To compare surface changes before induction time with those after induction time, Table 10 shows the % drop in peak curvature during the first five minutes and the % drop in peak curvature from five minutes to four hours. Pair D is again omitted.

	% drop in peak curvature 0-5 mins.			
	150°C, 1kg	150°C, 5kg	250°C, 1kg	250°C, 5kg
A	9.5	37.3	33.3	51.9
B	18.8	36.2	37.3	56.6
E	20.5	28.4	26.8	33.7
F	20.7	25.5	17.8	36.0
	% drop in peak curvature 5-240 mins			
	150°C, 1kg	150°C, 5kg	250°C, 1kg	250°C, 5kg
A	18.2	1.9	63.9	71.1
B	20.1	39.3	69.2	65.9
E	6.1	51.3	48.6	70.4
F	13.5	-15.0	64.8	55.5

Table 10: % drop in peak curvature before and after induction time

Firstly we can see differences in how initial anit-wear activity and film anti-wear activity are effected by changing conditions. Initial anti-wear activity, as indicated by the % drop in peak curvature in the firs five minutes, is similar at 150°C, 5kg and 250°C, 1kg, approximately midway between the least severe condition, 150°C, 1kg, and the most severe condition, 250°C, 5kg. Film anti-wear activity, as indicated by the % drop in peak curvature from five minutes to four hours, is mainly affected by temperature with performance at 150°C, 5kg being similar to that at 150°C, 1kg, and 250°C, 1kg performance similar to that at 250°C, 5kg. Table 10 also indicates similar initial anti-wear activities for pairs A and B and also for pairs E and F. This may be due to similarities in the initial surface parameters: liners A and B have similar high values of rms.roughness and peak curvature compared to those of liners E and F (see Appendix 1).

11.2 Induction time

Table 11 shows average induction times for the five oil/liner pairs under different experimental conditions. The ranking of the induction times is also shown.

	150 °C				250 °C			
	1kg	ranking	5kg	ranking	1kg	ranking	5kg	ranking
A	25	5	10.5	4	7.5	5	20	5
B	14.5	4	13.5	5	4.3	4	9	4
D	2.7	3	6.3	3	3.0	3	6.3	3
E	0.5	1	2.5	1	0.8	1	3.5	2
F	1.8	2	3.8	2	1.5	2	3.2	1

Table 11: Average induction times (minutes)

Pairs D, E and F show the trends expected from the results of running-in tests with oils C1 to C4 and liner C, namely that temperature does not significantly affect induction time while increasing the load from 1kg to 5kg doubles the induction time. Pairs A and B do not show such clear trends but do suggest a faster induction time at the higher temperature.

The ranking of induction times seem fairly consistent across the different experimental conditions; in terms of fastest induction time: E>F>D>B>A

Pairs A and B are similar in having long induction times while pairs E and F have short induction times. This may be due to the differences noted above in the initial surface parameters: liners A and B with greater values of rms.roughness and peak curvature may need more running-in before the thick ZDDP film can build.

11.3 Coherence

Table 12 shows average % coherence values for the five oil/liner pairs at different experimental conditions.

	150 °C, 1kg	150 °C, 5kg	250 °C, 1kg	250 °C, 5kg
A	95	70	95	50
B	95	60	80	50
D	80	25	75	20
E	97	75	85	20
F	97	90	80	75

Table 12: Average % coherence

The experimental conditions can be ranked in terms of severity, the more severe the conditions the lower the coherence:

150°C, 1kg<250°C, 1kg<150°C,5kg<250°C, 5kg

This ranking does not match that of surface changes noted in Table 9 where 150°C,5kg is less severe than 250°C, 1kg. This ranking is however shown in Table 10 for % drop in peak curvature in the first five minutes, suggesting a link between film coherence and initial anti-wear activity.

Pair D gives the lowest values of coherence throughout, presumably due to the high wear rate resulting from the softness of liner D. Pair F gives the highest coherence at the 5kg load conditions, agreeing with the % drop in peak curvature data in tables 9 and 10 where pair F shows least surface changes of all pairs at high load. The relationship between coherence and changes in peak curvature is examined in detail in Figs. 28-31, Figs. 10 and 19 showing the relationship between peak curvature at five minutes and coherence and Figs. 30 and 31 the relationship between % drop in peak curvature from five minutes to four hours and coherence. This attempts to show any relationship between firstly initial anti-wear activity and coherence (Figs. 28 and 29) and secondly film anti-wear activity and coherence (Fig.s 30 and 31). Pair D has been omitted as peak curvatures drop to their run-in values almost immediately even at the least severe conditions.

The trends are similar for all oil/liner pairs. Figs. 28 and 29 show that a constant temperature load increases reduces both coherence and peak curvature at five minutes. It is also clear that at constant load the higher temperature reduces coherence and peak curvature at five minutes. This clearly indicates a correlation between initial anti-wear activity and the coherence of the ZDDP film formed after induction time. Figs. 30 and 31 show that at constant load the higher temperature both reduces coherence and increases the % drop in peak curvature from five minutes to four hours. This indicates a correlation between coherence and film anti-wear activity. However at constant temperature load increases reduce coherence without necessarily a corresponding increase in % drop in peak curvature, eg. Fig. 31 pair F.

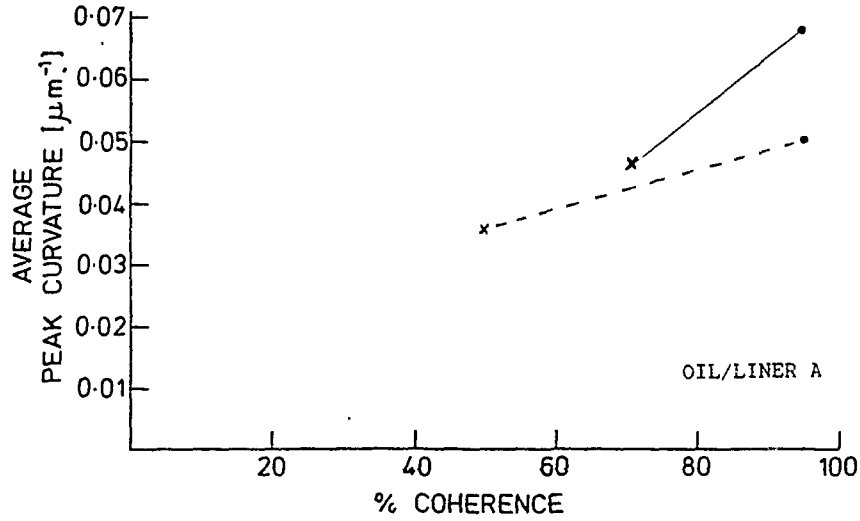

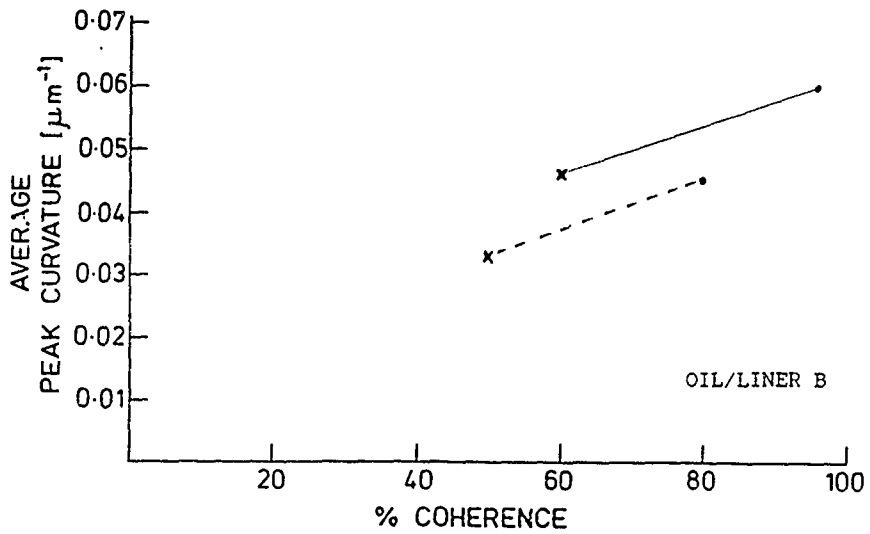

• 1kg ——150°C

× 5kg ---250°C

Fig. 28: Coherence and peak curvature after 5 mins. of running-in.

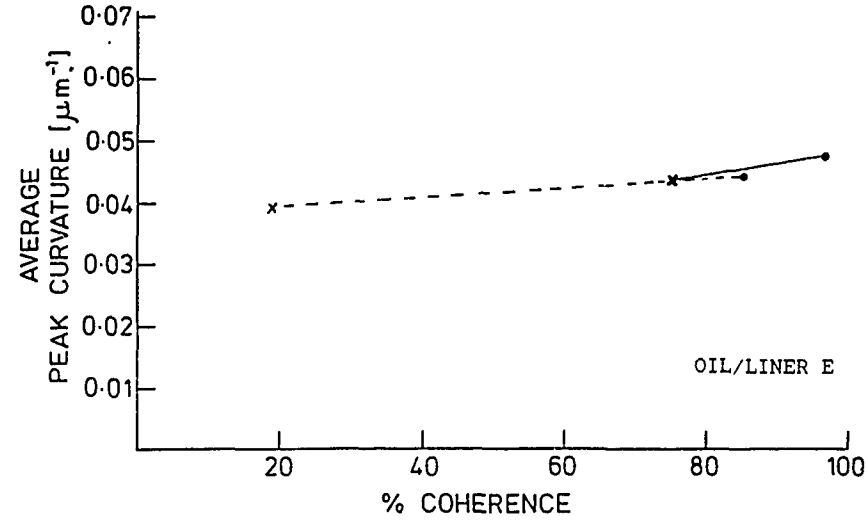

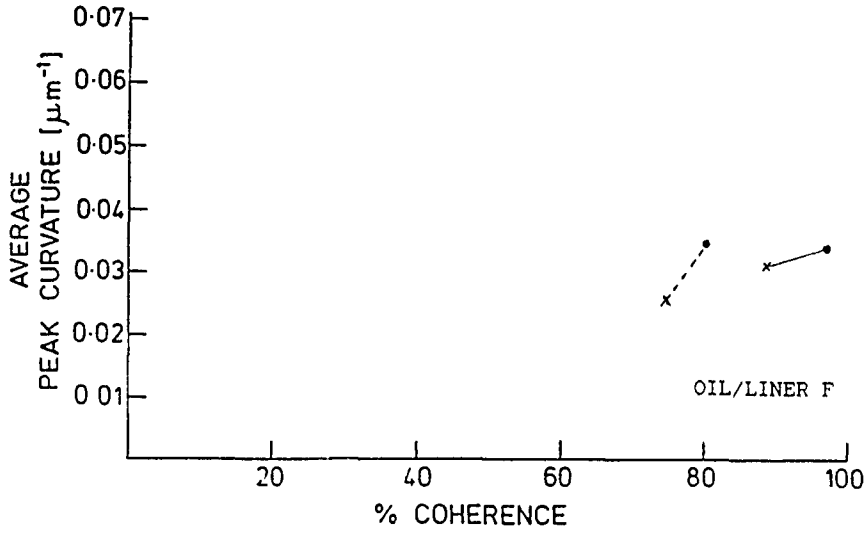

• 1kg —150°C

x 5kg ---250°C

Fig. 29: Coherence and peak curvature after 5 mins. of running-in.

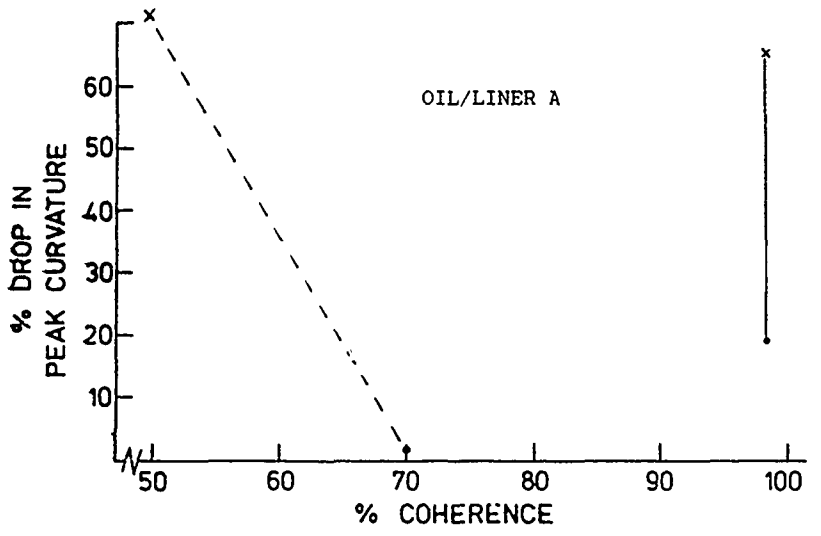

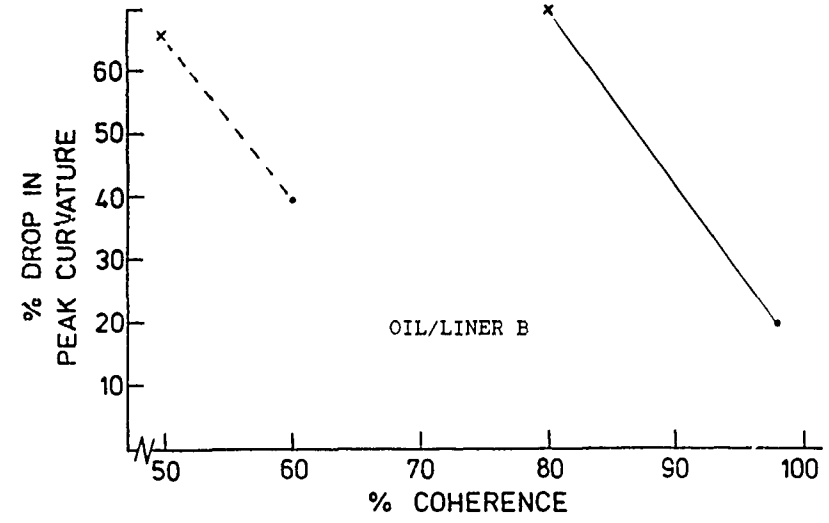

• 150°C ——1kg

× 250°C ---5kg

Fig.30 : Coherence and % drop in peak curvature from 5 - 240 mins.

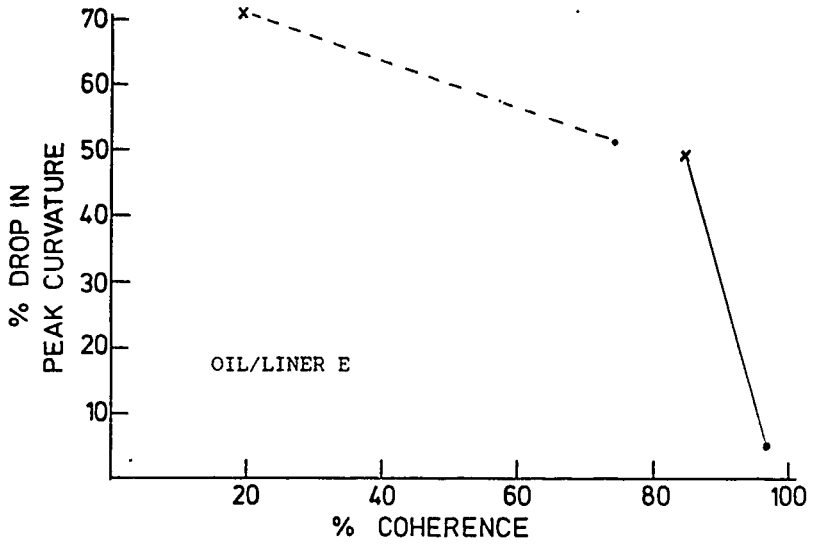

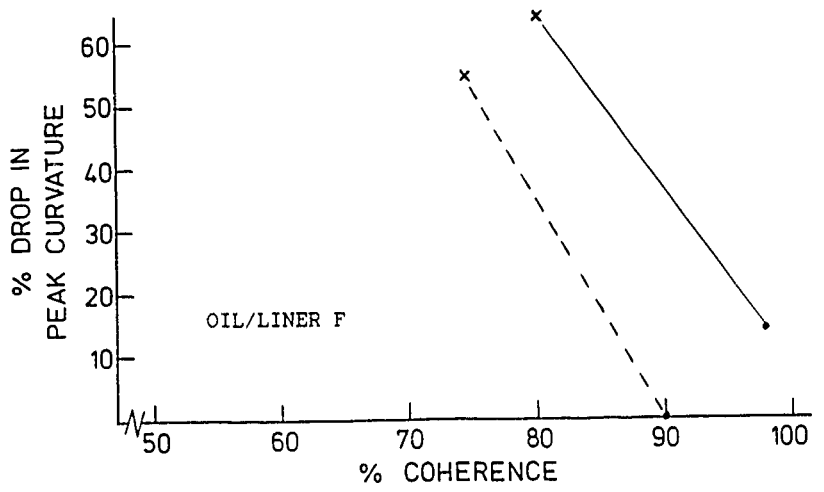

• 150°C ——1kg

X 250°C ---5kg

Fig.31: Coherence and % drop in peak curvature from 5 - 240 mins.

11.4 Summary

Table 13 summarises the rankings of oil/liner pairs ABEF in terms of best performance for induction time, % coherence, initial anti-wear activity (% drop in peak curvature in the first five minutes) and film anti-wear activity (% drop in peak curvature from five minutes to four hours).

	150	C,1kg	150	C, 5kg	250	C, 1kg	250	C,5kg
A	4	=3	3	3	4	1	4	=2
	1	3	=3	=1	3	=2	3	=3
B	3	=3	4	4	3	=3	3	=2
	2	4	=3	3	4	4	4	2
E	1	=1	1	2	1	2	2	4
	=3	1	2	4	2	1	1	=3
F	2	=1	2	1	2	=3	1	1
	=3	2	1	=1	1	=2	2	1

KEY:

Induction time.	% coherence
% drop in Pk.C 0-5 mins.	% drop in Pk. C 5-240 mins.

Table 13 Summary of rankings in terms of best performance

On these criteria pairs E and F perform better than pairs A and B. This may well be due to liners E and F having low initial values of rms.roughness and peak curvature. The good performance of pair F at 5kg may well result from the low initial peak curvature of liner F, allowing the higher load to be more evenly spread across the asperities.

12 MIXED OIL/LINER PAIRS

12.1 Surface Changes

Changes in the rms.roughness and peak curvature of liners ABCDEF were investigated over a period of four hours of running-in, using a variety of oils with each liner. Liners A and C were run-in with each of the five oils, ABDEF, liner A with a high value of initial rms.roughness and peak curvature, liner C with lower values. The results for liner C could then be compared with the previous running-in data for liner C with oils C1, C2, C3 and C4. Oils A and D were tested on all liners, oil A with the longest induction time, oil D with a much shorter induction time. By comparing the performance of liner A with liner C and oil A with oil D it was hoped that differences in performance due to initial liner surface parameters could be distinguished from differences due to oil composition. Standard experimental conditions were fixed at 150°C, 1kg load.

Tables 14 and 15 summarise the running-in data for all oil/liner combinations tested. Figs. 32-37 show the changes in surface parameters during running-in for each of the six liners, comparing the performance of all oils tested on each liner. The performance ranking of oils in terms of prevention of surface changes is given as follows:

Liner A: ABEF > D

Liner B: A > D > B

Liner C: AB > DEF

Liner D: A > D

Liner E: A > E > D

Liner F: ADF

A general oil performance ranking does seem evident:

A ≥ B > EF ≥ D

OIL	LINER	5 MINUTES		1 HOUR		4 HOURS	
A	A	0.803 0.0677	No F.A.* 0%	0.0774 0.0518	25 70%	0.774 0.0554	25 95%
	B	0.973 0.0621	No F.A. 0%	0.992 0.0677	14 85%	0.996 0.0657	14 85%
	C	0.738 0.0666	No F.A. 0%	0.937 0.0643	12 90%	0.793 0.0608	17 95%
	D	0.500 0.0425	2 0%	0.258 0.0253	1.5 80%	0.174 0.0217	2.5 85%
	E	0.558 0.0521	2.5 0%	0.659 0.0546	3 97%	0.575 0.0455	2 99%
	F	0.659 0.0372	5 0%	0.534 0.0308	3.5 98%	0.517 0.0276	3 97%
B	A	0.776 0.0611	No F.A. 0%	0.940 0.0600	15 0%	0.783 0.0571	4 95%
	B	0.941 0.0593	No F.A. 0%	0.707 9.0536	19 80%	0.537 0.0474	10 95%
	C	0.606 0.0598	No F.A. 0%	0.780 0.0595	6 98%	0.581 0.0583	6 99%

* No F.A. = no film activity

DATA PRESENTED IN FOLLOWING FORM:

rms.roughness (μm)	induction time (mins.)
peak curvature (μm^{-1})	% coherence

Table 14: Results of running-in tests at 150°C, ''g, for oils A and B with various lines

OIL	LINER	5 MINUTES		1 HOUR		4 HOURS	
D	A	0.931 0.0590	2 0%	0.755 0.0545	2 100%	0.552 0.0424	2 98%
	B	0.999 0.0590	2 0%	0.722 0.0587	2 96%	0.685 0.0497	2 97%
	C	0.572 0.0614	1 0%	0.604 0.0555	1.5 99%	0.620 0.0466	1 95%
	D	0.179 0.0116	3 0%	0.290 0.0133	3 90%	0.075 0.0115	2 80%
	E	0.654 0.0499	0.5 0%	0.304 0.0431	0.5 99%	0.732 0.0337	0.5 99%
	F	0.610 0.0347	1 0%	0.553 0.0355	1.5 98%	0.550 0.0276	1.5 98%
E	A	0.613 0.0560	2 0%	0.831 0.0523	2 96%	0.737 0.0549	2 95%
	C	0.569 0.0561	1.5 0%	0.675 0.0509	2 90%	0.505 0.0441	2.5 95%
	E	0.352 0.0474	0.5 0%	0.507 0.0453	0.5 98%	0.382 0.0445	0.5 97%
F	A	0.904 0.0558	No F.A.* 0%	0.811 0.0554	7 0%	0.856 0.0532	4 95%
	C	0.584 0.0536	No F.A.* 0%	0.682 0.0587	5 90%	0.534 0.0418	4 5 95%
	F	0.750 0.0326	2 0%	0.686 0.0306	2.5 97%	0.609 0.0282	1 97%

* No F.A. = no film activity

DATA PRESENT IN FOLLOWING FORM:

rms.roughness (μm)	induction time (mins.)
peak curvature (μm^{-1})	% coherence

Table 15: Results from running-in tests at 150°C, 1kg for oils D, E and F with various liners.

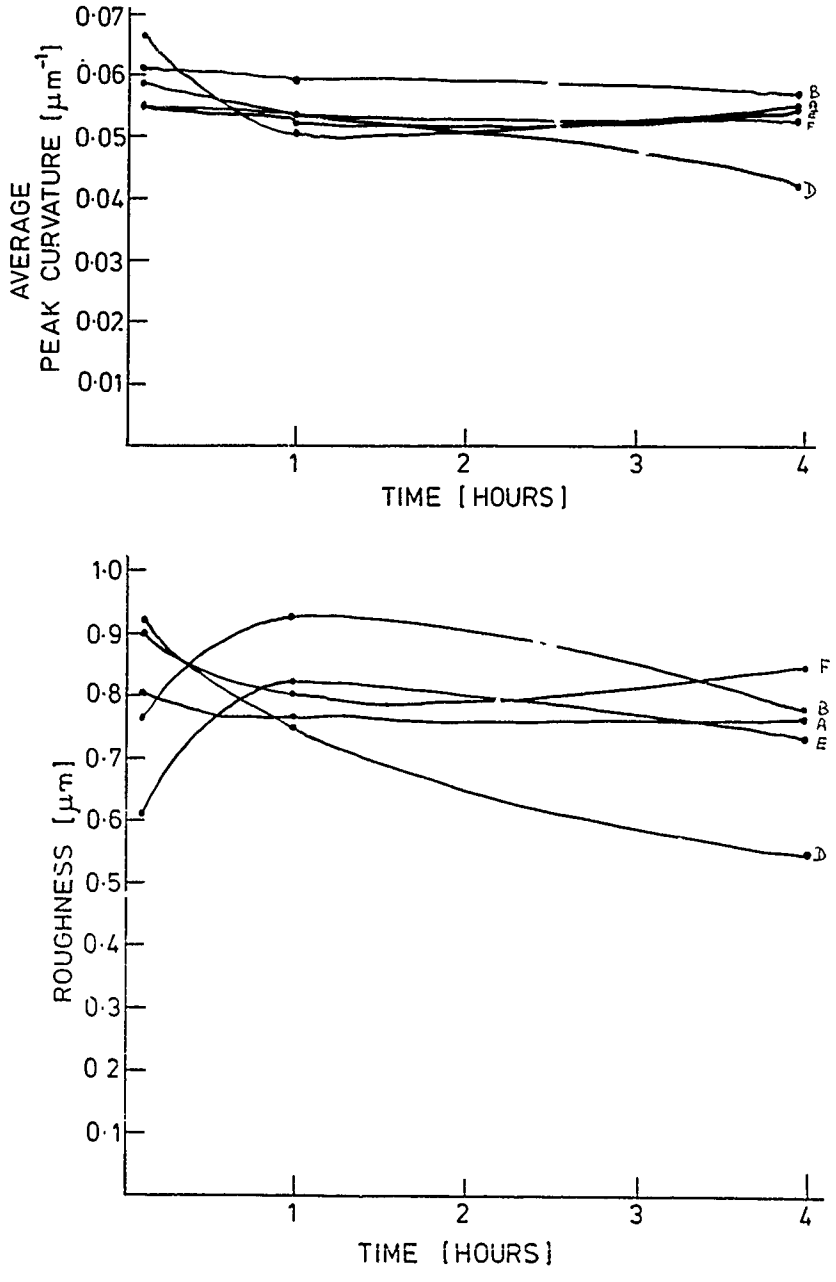

Fig.32: Liner A, surface changes at 150°C, 1kg, oils ABDEF

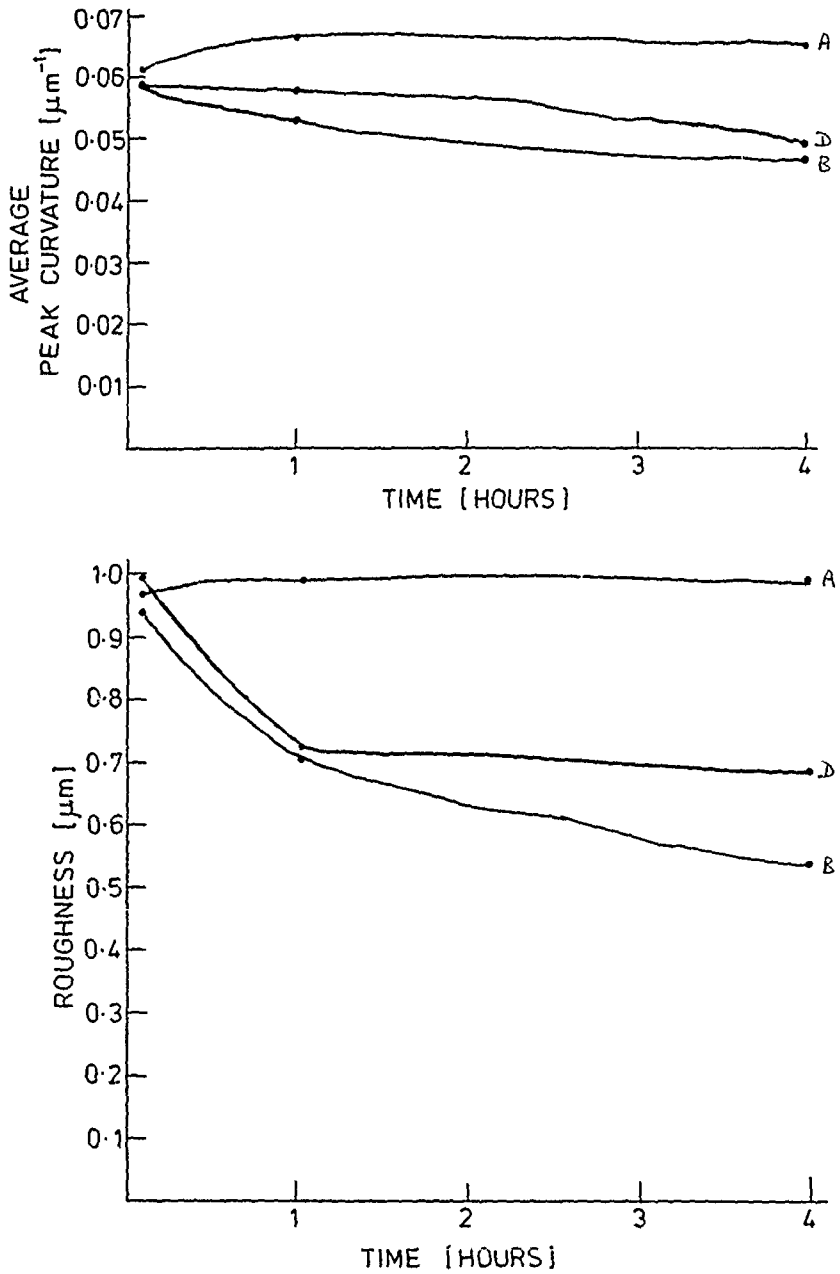

Fig 33: Liner B, surface changes at 150°C, 1kg, oils ABD

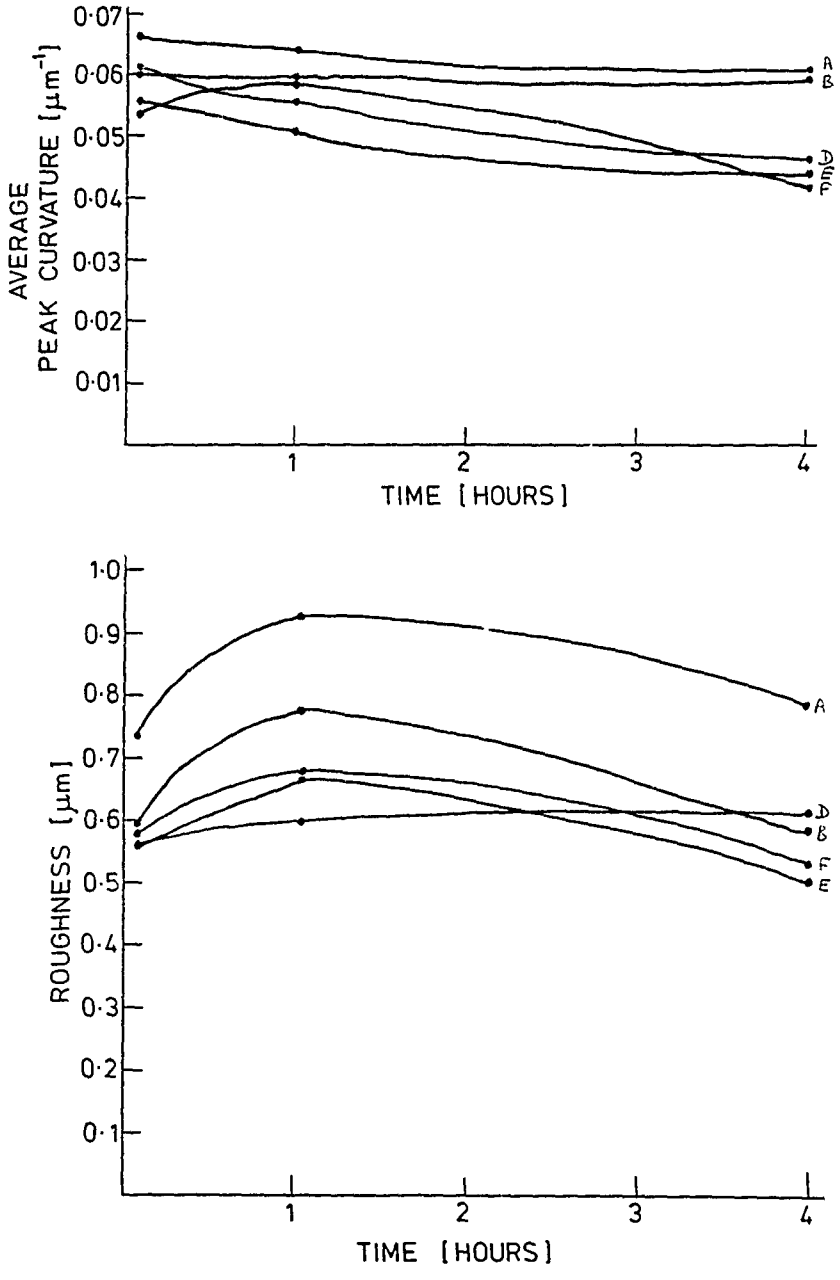

Fig.34: Liner C, surface changes at 150°C,1kg ,oils ABDEF

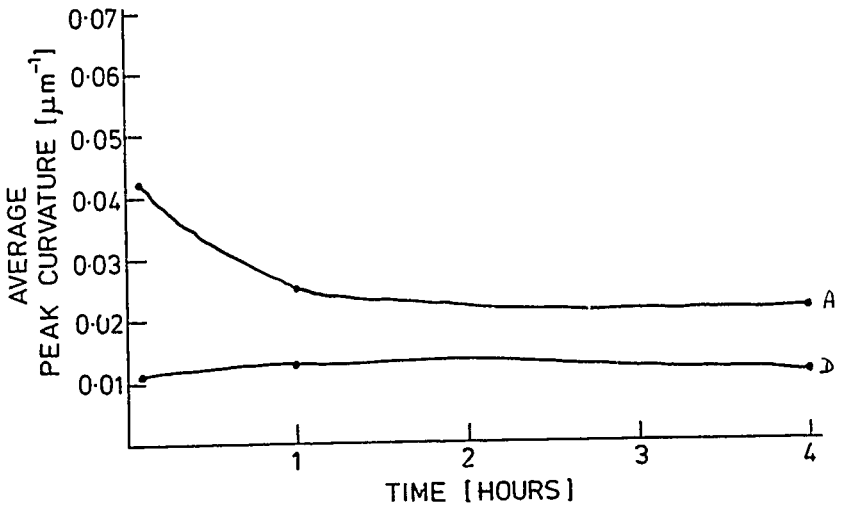

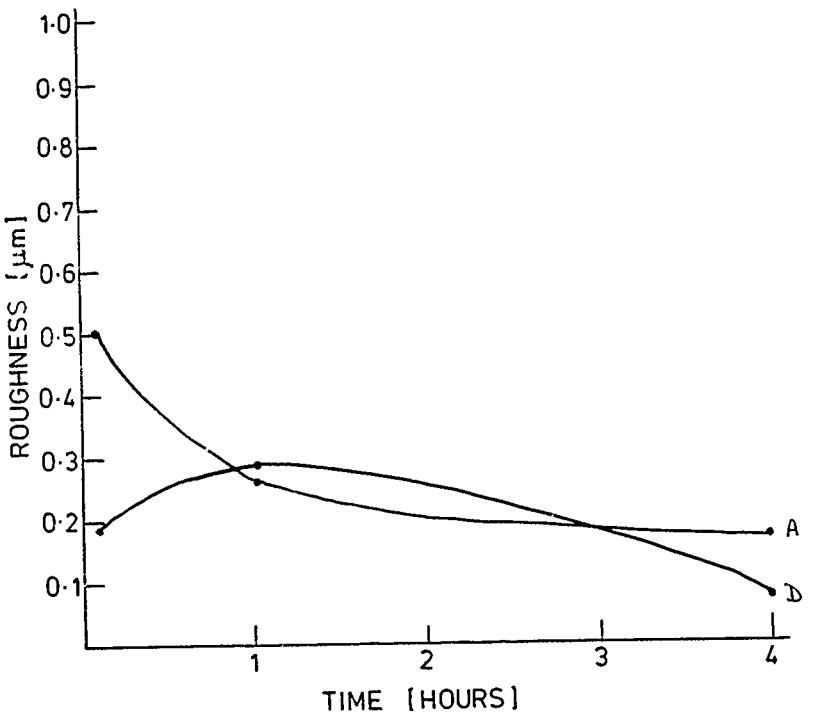

Fig.35: Liner D, surface changes at 150°C, 1kg .oils AD

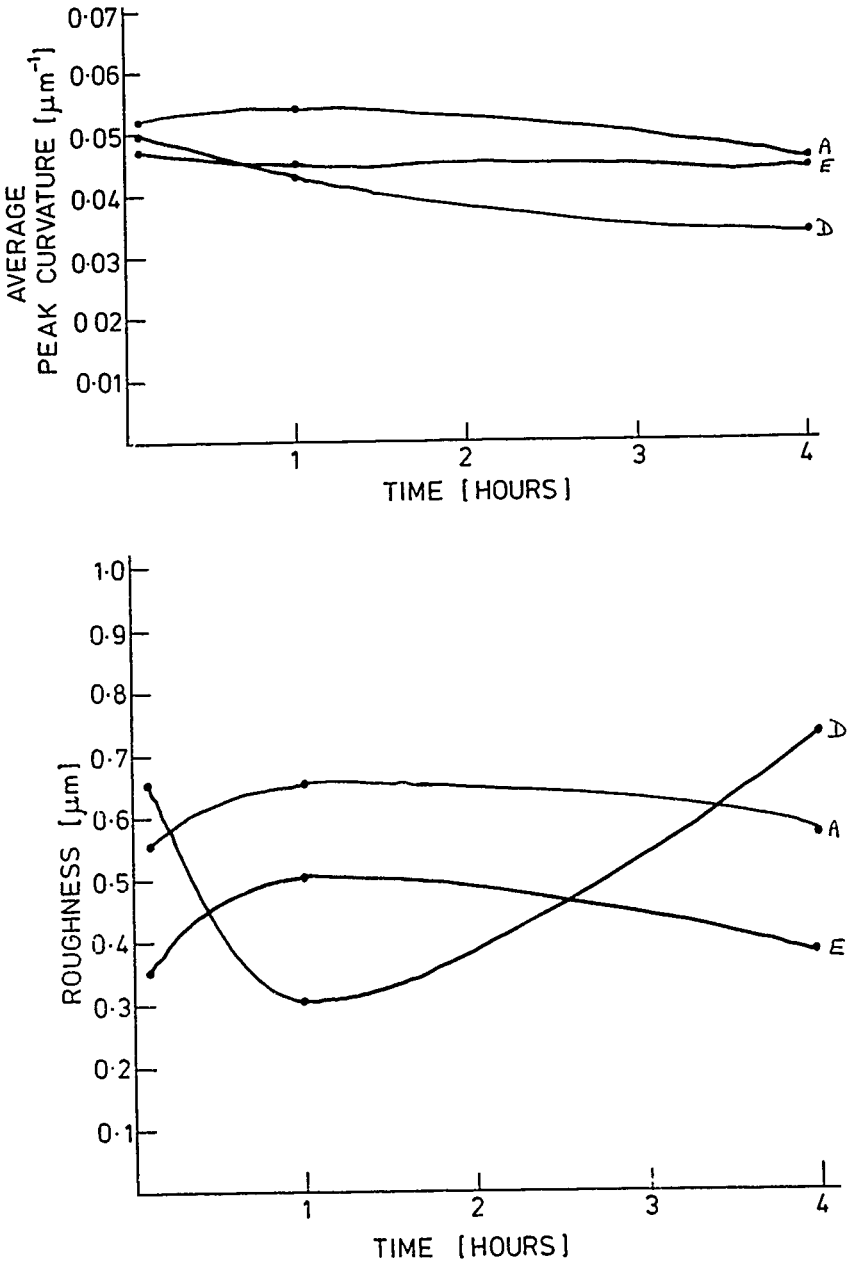

Fig 36: Liner E, surface changes at 150°C, 1kg, oils ADE

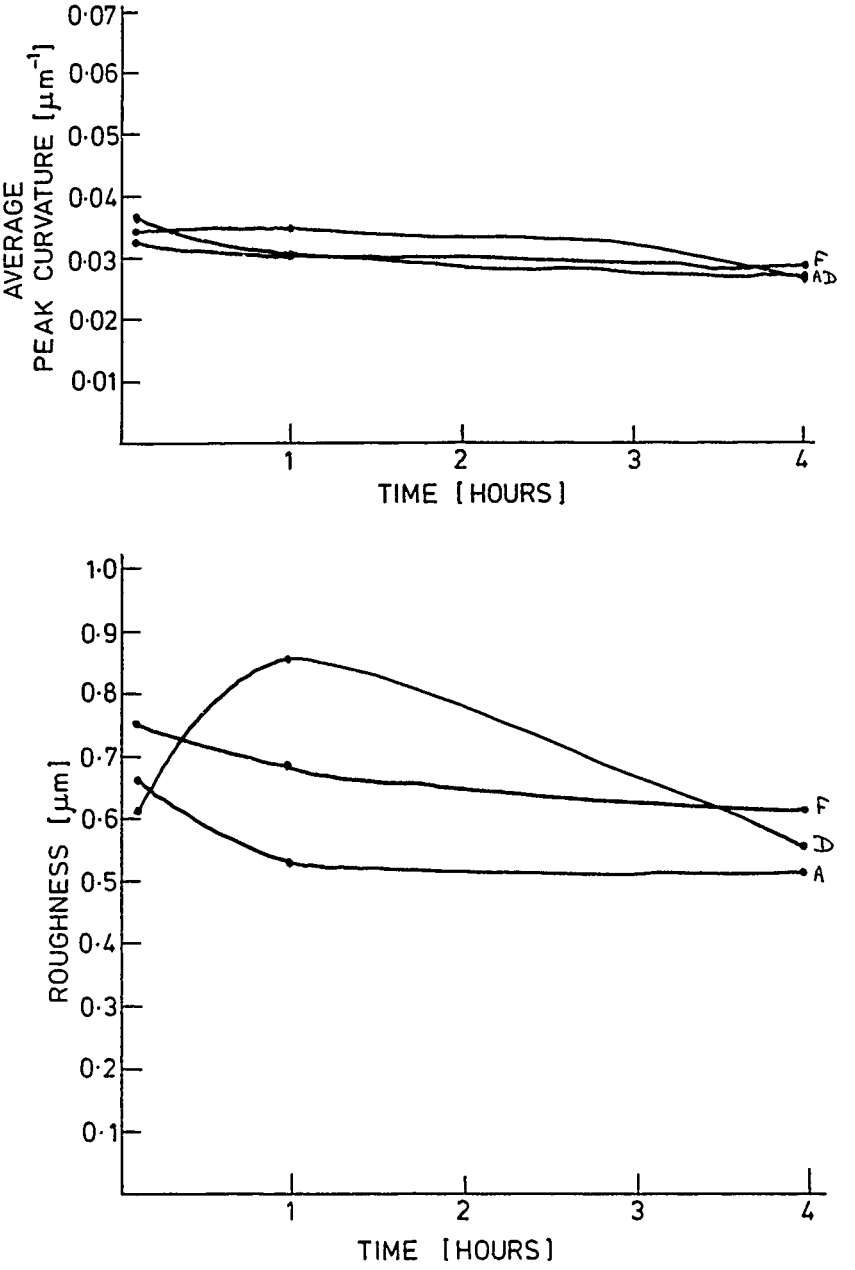

Fig.37: Liner F, surface changes at 150°C,1kg ,oils ADF

Table 16 gives % drop in peak curvature data both before induction time (0-5 minutes of running-in) and after induction time (5-240 minutes of running-in)

% drop in peak curvature 0-5 minutes							
	liner	A	B	C	D	E	F
oil							
A		9.5	14.9	1.8	33.5	12.6	9.5
B		18.3	18.8	11.8	----	----	----
D		21.1	19.2	9.4	81.8	16.3	15.6
E		25.1	----	17.3	----	20.5	----
F		25.4	----	20.9	----	----	20.7

%drop in peak curvature 5-240 minutes							
	liner	A	B	C	D	E	F
oil							
A		18.2	-5.8	8.7	48.9	12.7	25.8
B		6.5	20.1	2.5	----	----	----
D		28.1	15.8	24.1	0.9*	32.5	20.5
E		2.0	----	21.4	----	6.1	----
F		4.7	----	22.0	----	----	13.5

* running-in has been completed after 5 minutes

Table 16: % drop in peak curvature before and after induction time.

Comparing liners A and C it is clear that liner C performs better than liner A during the first five minutes for all oils. However, from 5 to 240 minutes the performance of liner C is only better than liner A for oils A, B and D. On the whole no clear liner performance ranking is evident though D consistently performs badly and there is some evidence to suggest that liners with lower values of surface parameters perform better than those with higher values.

Comparison of oil performance does indicate clearer results, especially for oils A and D. Oil A seems to have particularly good initial anti-wear activity, performing better than the other oils on all liners in the first five minutes and performing better than oil D on all liners except F from 5-240 minutes.

12.2 Induction time

Table 17 shows average induction times for all oil/liner combinations tested.

LINER / OIL	A	B	C	D	E	F
A	25	14	14.5	2	2.5	3.8
B	9.5	14.5	6	-	-	-
D	2	2	1.2	2.7	0.5	1.3
E	2	---	2	-	0.5	-
F	5.5	-	4.8	-	-	1.8

Table 17: Induction time (mins.) for all oil/liner combinations

Clearly induction time is not a characteristic exclusively of oil or liner but rather a combination of the two. Induction time rankings for oils and liners are as follows:

Oils: $D \leq E < F < B \leq A$

Liners: $ED < F < C < B \leq A$

Measurements of induction time with liner D were somewhat confused as the black liner coating gave an initial e.c.r. reading of $\infty\ \Omega$ which quickly dropped to 0Ω as it was worn away in the first minute of running-in.

The ranking of liners for induction time suggested a correlation with initial surface parameters, liners with high initial values of rms.roughness and peak curvature giving the longest induction times. To examine this possibility all liners were ground and polished so that peak curvatures were all 0.0150 $\pm$ 0.0030 μm^{-1} and rms.roughness values were all 0.050 $\pm$ 0.010 μm. Table 18 shows induction times for oils A and D on these liners.

LINER / OIL	A	B	C	D	E	F
A	0.9	1.3	1.4	0.1	2.1	2.6
D	1.1	0.6	1.0	1.6	0.7	1.2

Table 18: Induction tims (mins.) for ground and polished liners

Clearly induction times are faster on these liners, the greatest difference being shown with oil A on liners A, B and C, the liners which had the highest initial values of surface parameters before grinding and polishing.

The importance of induction time in the running-in process is not at all clear, if indeed there is any importance. The comparison between oils A and D is particularly striking in this respect. Table 16 indicated that oil A prevents surface changes to a much greater extent than oil D, yet Table 17 shows that oil D has a consistently faster induction time after the first five minutes of running-in for liners A, B and C, oil A has not produced a thick film, whereas oil D produces a thick film after 1-2 minutes but still allows more surface changes than oil A. This indicates that firstly oil A has a particularly high initial anti-wear activity, and secondly that this may result in delaying induction time since the surface is well protected and takes longer to wear down enough to accommodate a thick film.

12.3 Coherence

Table 19 shows % coherence values for all oil/liner combinations tested.

LINER / OIL	A	B	C	D	E	F
A	95	85	95	85	99	97
B	95	95	99	--	--	--
D	98	97	95	80	99	98
E	95	--	95	--	97	--
F	95	--	95	--	--	97

Table 19: % coherence for all oil/liner combinations

There is little to distinguish the performance of oil/liner combinations in terms of % coherence at 150°C, 1kg load. However liners E and F, with the lowest initial values of surface parameters, do give the highest coherence values.

Liner D gives the lowest coherence values, associated with the high wear rate due to its softness. Certainly there is no clear difference between oils A and D in their coherence values, again suggesting that the better performance of oil A over oil D may be due to better initial anti-wear activity rather than better film activity.

12.4 Summary

To some degree it has been possible to distinguish the affect of initial surface parameters from that of oil composition in the running-in process. A general oil performance ranking based upon surface changes and largely independent of liner type, seems evident:

$$A \gtrsim B > EF > D$$

A general ranking of induction time for the oils has also been possible, and this is almost exactly the reverse of the performance ranking for the oils:

$$D \lesssim E < F < B \lesssim A$$

This supports the suggestion that good performance in terms of prevention of surface changes may result in delayed induction time since the surface takes longer to wear down enough to support a thick film. Performance differences may thus reflect differences in initial anti-wear activity rather than film anti-wear activity, a suggestion supported by the similarity of coherence values for all oils, indicating similar film anti-wear activities.

No clear performance ranking for the liners was possible perhaps due to the relatively mild conditions of 150°C, 1kg load. However, liner D performed poorly both in terms of allowing severe surface changes and having a low coherence value. This presumably is due to the low value of hardness for liner D (VHN 200). Liner C, with lower values of initial surface parameters than liner A, performed consistently better than liner A in the first five minutes of running-in and from 5-240 minutes for oils A, B and D. This suggests that lower initial values of surface parameters may improve performance.

A ranking of induction time for liners was possible:

$$E, D < F < C < B \lesssim A$$

This follows the ranking of initial rms.roughness for the liners, other than liner D whose rms.roughness quickly drops in the first few minutes of running-in. Grinding and polishing of liners with high initial rms.roughness values dramatically reduced induction times for oil A. This supports the suggestion that the induction of a thick film occurs once a certain load bearing area is produced and also that good initial anti-wear activity could therefore lengthen the induction period.

Liners E and F, with the lowest initial surface parameters, showed the greatest values of coherence but performance in terms of prevention of surface changes was not significantly better than the other liners, except liner D. This may be due to the mild conditions, 150°C, 1kg load, allowing all liners except liner D to perform well.

13.0 DISCUSSION

13.1 Surface changes

The fixed pairing tests indicated a general performance ranking in terms of surface changes of:

$$F \gtrsim E > A > B > D$$

The mixed oil/liner combination tests ranked the performance of oils in terms of surface changes as:

$$A \gtrsim B > EF > D$$

and the performance of liners as:

$$C > A > D \quad \text{and} \quad BEF > D$$

Clearly the oil performance ranking does not match the general performance ranking for the fixed oil/liner pairs. The performance ranking of liners, though somewhat unclear, does seem closer to that of the general ranking for the fixed

oil/liner pairs, and this seems to relate to the initial surface parameters of the liners:

Hardness:	BE > F > C > A > D
rms.roughness:	AC > B > D > F > E
Peak curvature:	A > B > C > D > E > F

The poor performance of oil/liner pair D could be due to either the low hardness value of liner D or the consistently poor performance of oil D. The good performance of oil/liner pairs E and F compared with pairs A and B must be mainly due to their low initial values for rms.roughness and peak curvature, combined with relatively high values of hardness, since oils A and B tended to out-perform oils E and F. This certainly seems to indicate that liners manufactured with low values of rms.roughness and peak curvature may need less running-in than those with higher values. There is also some evidence that the severity of wear in the first few minutes is considerably lower for these liners.

13.2 Induction Time

The ranking of induction times for the fixed oil/liner pairs was consistent under all experimental conditions:

$$E < F < D < B < A$$

The mixed pairing tests ranked induction times for oils and liners:

oils:	$D \lesssim E < F < B \lesssim A$
liners:	$ED < F < C < B \lesssim A$

As the induction time rankings for oils is very similar to that for liners it is not possible to establish which is mainly responsible for the ranking given by the fixed oil/liner pairs. Grinding and polishing of liners with high values of initial rms.roughness did dramatically reduce the induction times for oil A, but it is also clear that these are major differences in induction time for oils with the same liner and that these may be linked to differences in the initial anti-wear activity of the oils, induction time being greater for oils that

protect the surface well since it may then take longer for the surface to run-in enough to support a thick film. While induction time may be an indication of initial anti-wear activity there is little evidence to suggest that it has an important role in the running-in process.

13.3 Coherence

The fixed pairing tests at 150°C, 1kg indicated a performance ranking in terms of coherence as:

EF > AB > D

The mixed pairing tests suggested that under these relatively mild experimental conditions all the oils gave similar coherence values. The liners however did provide a definite performance ranking:

EF > ABC > D

This ranking matches that of the fixed oil/liner pairs suggesting that under these conditions it is differences in the liners that is predominately responsible for differences in values of coherence. This ranking also matches the general ranking for surface changes given above, which, as previously noted, matches the rankings of initial rms.roughness and peak curvature for the liners, with the exception of liner D. High values of coherence are associated with good performance in terms of prevention of surface changes and these seem to be related to low initial values of rms.roughness and peak curvature for liners with hardness values between 390 VHN and 470 VHN.

Lack of accurate and detailed information about oil compositions has prevented an examination of the role of oil composition in the performance of differences of the oils.

14. CONCLUSIONS OF RUNNING-IN TESTS

The final aim of this project was to produce, using a laboratory test machine, a method of assessing the quality of oil/cylinder liner pairs which correlates with engine performance, so reducing the amount of full-scale engine testing. Segments of cylinder liner were tested in a reciprocating ball-on-flat

apparatus. Changes in rms.roughness and peak curvature over the four hour running-in period provided the primary method of assessing the quality of oil/liner pairs. The electrical contact resistance (e.c.r.) of the rubbing pair was continually recorded, providing information about the additive film formed after rubbing was initiated. The ecr recording gave two parameters which could be used as a measure of oil/liner quality: induction time, the time at which the additive film forms (indicated by a sharp increase in the ecr.) and coherence, a percentage measure of the magnitude and stability of the ecr after it has reached a steady state. These two parameters were found to be characteristic of a particular oil/liner pair under particular experimental conditions.

Good performance in these tests could then be designed in three ways Firstly, in terms of surface changes: oil/liner pairs with least surface changes over the four hour running-in period perform the best. Secondly, in terms of induction time: oil/liner pairs showing the shortest induction time perform the best. Thirdly, in terms of coherence: oil/liner pairs showing the greatest coherence perform the best. Performance rankings were obtained for each of these three measures of quality at different temperatures and contact loads. However it was realised that performance in these terms could in fact be too good and not allow running-in to occur e.g. 1% ZDDP, with no inhibitors present, at 150°C, 1kg load can give an induction time of less than one minute, coherence of 100% and virtually no surface changes after four hours of rubbing. It was hoped that comparison with engine performance data would establish the optimum performance levels in this test machine but this data has not been made available, leaving the final aim of this project unachieved.

Relationships between surface changes, induction time and coherence were examined and also the affect of temperature and load on each. These results were then related to cylinder liner characteristics (hardness, initial rms.roughness and peak curvature) and oil composition (ZDDP concentration and metal detergent inhibitor type) in an attempt to examine the role of each factor in the running-in process. Unfortunately little information was available about oil composition.

Surface changes -

Both rms.roughness and peak curvatures decreased over the four hour running-in period. Under mild conditions, eg. 150°C, 1kg load, rms.roughness and peak curvature values stabilized after about one hour, while under more severe conditions, eg 250°C, 5kg load, running-in might not be complete until after 3-4 hours of rubbing. In general there was a good correspondence between drop in peak curvature and drop in rms roughness but honing marks caused considerable variability in rms.roughness readings so changes in peak curvatures were used to evaluate the degree of surface changes.

Load increases from 1kg to 5kg produced slightly greater surface changes but temperature was found to be the most important factor. For ZDDP oils, all those tested except oil C2, 150°C and 200°C produced best results, with surface changes being much greater at 250°C. Oil C2 performed best at 250°C. The rankings of oils C1 to C4 on liner C, in terms of surface changes, was the same after 5 minutes of rubbing as after 4 hours and since the thick additive film tended not to form till after 5 minutes, this indicated differences in initial anti-wear activity, as opposed to film anti-wear activity.

Induction time -

Induction time varied considerably between oils and oil/liner combinations, depending on initial rms.roughness of the liner as well as on ZDDP concentration and inhibitor type. Increasing load from 1kg to 5kg tended to approximately double the induction time while temperature usually had little affect. No relationship was found between surface changes and induction time. Indeed there was some evidence to suggest that a long induction time might be associated with good initial anti-wear activity and so good overall performance, contrary to the original assumption that a short induction time indicated good performance.

Coherence -

The coherence of a thick additive film was found to be a consistent characteristic of a particular oil/liner combination, and was found to be affected by load and temperature in much the same way as surface changes.

increased load reduced coherence as did high temperature (250°C) for the ZDDP oils. There is strong evidence to suggest a relationship between the coherence value and the degree of surface changes both before and after induction time, performance rankings based on coherence closely matching performance rankings based on surface changes. In the case of oils C1 to C4 these performance rankings related well to additive type and concentration.

While the overall aim to match these bench test results with engine test results has not been accomplished, due to lack of engine test data, it is clear that the test machine used does allow detailed examination of the running-in process and, in particular, measurement of the *induction time*, the time at which thick film formation occurs, and measurement of the *coherence*, the quality of the thick film formed.

15.APPENDIX 1

Liner characteristics, liners ABDEF

Liner	Hardness (VHN)	rms.roughness (μm)	Peak curvature (μm)
A	390	0.900	0.0750
B	470	0.820	0.0730
D*	200	0.700	0.0640
E	470	0.510	0.0600
F	430	0.650	0.0410

* surface covered with a black coating

Oil characteristics, oils ABDEF

OIL	
A	Primary alkyl ZDDP (1.5% Paranox 16,0.4% Paranox 15)
B	Primary alkyl ZDDP (1.5% Paranox 16)
D	No details
E	No details
F	Primary alkyl ZDDP (1.5% Paranox 16,0.3% Paranox 15)

SECTION 3 - Surface temperatures due to a reciprocating heat source

SUMMARY

The object of this part is to carry out a theoretical analysis of surface temperatures due to a reciprocating heat source. This has confirmed and quantified the original belief that the reciprocating rig provides a convenient method of studying friction and wear in which the surface temperatures are known accurately because the additional flash temperatures are small.

1.1 INTRODUCTION

It is well-known that when a body slides under a (frictional) heat source, the contact surface becomes, locally and for a very short time, very much hotter than the bulk temperature of the solid. These temperatures may be measured directly using an infra-red microscope if one of the sliding pair is made of glass or sapphire (e.g. Turchina, Sanborn and Winer, 1974), or by using the thermo-electric effect between dissimilar metals to make the sliding pair its own thermocouple; but more normal techniques using embedded or trailing, sliding, thermocouples fail because of the localised nature of the temperature rise: the hot zone is frequently only microns thick, and rarely extends more than a millimetre behind the source.

Accordingly, it is often necessary to rely on theoretical estimates of these 'flash' temperatures. Fortunately, at least for a single, well-defined, contact area (such as a square or a circle) moving rapidly, there is a simple formula for the maximum flash temperature

$$\theta_{max} = \frac{2}{\sqrt{\pi}} \cdot \frac{q}{K} \cdot \left[\frac{\alpha d}{V}\right]^{\frac{1}{2}} \qquad (1)$$

where q is the rate of heat supply per unit area, K is the thermal conductivity, α the thermal diffusivity, d the length of the source in the sliding direction, and V the sliding speed. Blok (1937), Jaeger (1942), and Archard (1959) all made contributions to the mathematical and physical basis of this result, and elaborate analyses, such as that by Jaeger and by many later authors, have only showed, either deliberately or involuntarily, the

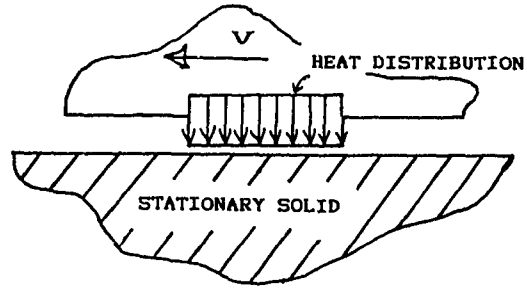

(a)

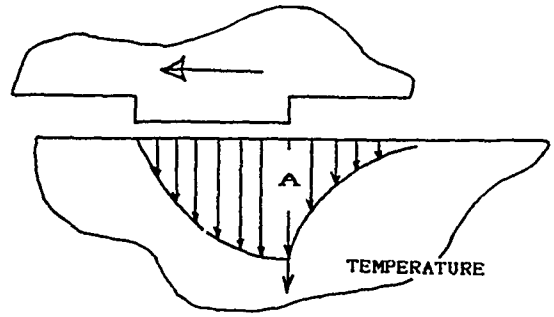

(b)

FIGURE 1 Moving sources of heat. (a) Source represented by a plane bump on a moving semi-infinite solid, lower semi-infinite solid stationary. (b) Flash temperature due to the passage of the slider, a maximum at the rear of the source.

value of Blok's equation.

Temperatures in a Reciprocating Contact

The usual sliding contact moves with a steady, uni-directional velocity. This means that each point on the stationary surface receives heat only when the moving source is above that point, and is subsequently unheated. This is shown in Figure 1a, and the corresponding temperature distribution for the Blok solution in Figure 1b. The point A begins to receive heat when the slider first arrives and stops receiving heat when the back of the slider has passed: the maximum temperature is seen at the rear of the source. The slider, on the other hand, sees a constant heat input from the friction in the contact and can, therefore, be treated as a stationary source on a semi-infinite solid.

In reciprocating contact, the picture is different since a point on the lower surface is passed repeatedly by the slider and there is no frame of reference in which the heating or temperature is steady. This means that flash temperatures, as defined in the last paragraph, do not exist and the problem is more difficult than for uni-directional sliding. The repeated passage of the slider produces, in the steady-state, a local temperature rise over the whole swept area that is in addition to any 'flash' temperature.

A numerical solution of the heat conduction equations for such a case has been made by Hirano and Yoshida (1966). Their solution, in terms of integrals of error functions, gave the steady-state temperature distributions across the slider rather than the contact region on the semi-infinite solid. The results they presented were only for a limited range of contact conditions and geometry, particularly appropriate for fretting contacts.

Archard re-worked the Blok/Jaeger theories of flash temperature, emphasising their physical basis and avoiding much of the mathematical complexities. In the same spirit, this paper presents a more accessible

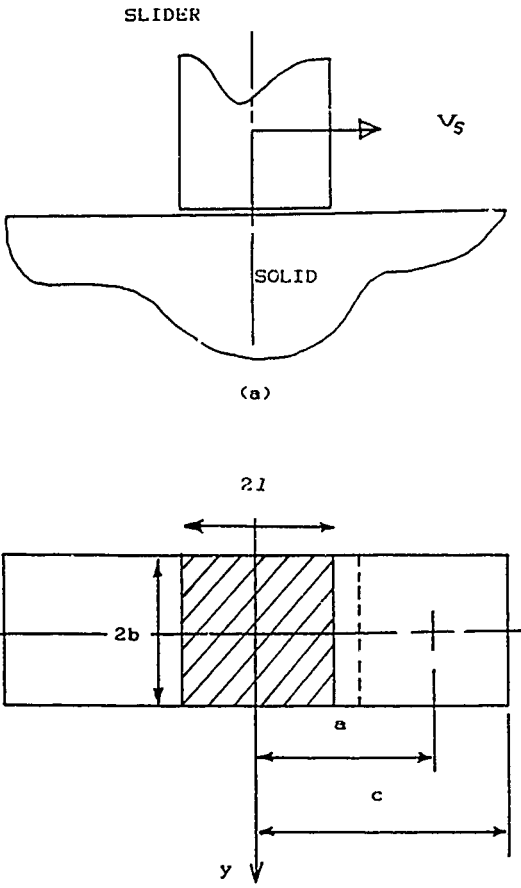

FIGURE 2 Geometry of the reciprocating contact

solution than Hirano and Yoshida's for reciprocating contacts. The enormous advantage of this solution is that temperatures can be calculated easily for any experimental conditions without recourse to re-evaluating the complex numerical solution for every new condition. Hirano and Yoshida's analysis did not and could not easily take into account the partition of heat between the slider and the solid. The analysis in this work starts with the same assumptions as Hirano and Yoshida and then extends the solution by simple means to include partitioning of heat.

1.2 FRAMEWORK AND ASSUMPTIONS

This analysis was carried out using the following simplifying assumptions, see Figure 2:

(i) The slider moves sinusoidally

(ii) The slider is in full contact with the semi-infinite solid and the contact is square or rectangular.

(iii) The slider is adiabatic, and heat loss by convection from the lower surface is negligiole: all heat generated in the contact is conducted away into the lower surface.

(iv) The production of heat is uniform over the area of the slider at any particular instant, and is proportional to the contact pressure, friction coefficient and velocity of sliding:

$$q = \mu p V \qquad (2)$$

The basic geometry is given in Figure 2, i a slider of sides $2\ell \times 2b$ reciprocating with an amplitude a about zero position. The motion of the centre is given by:

$$x_o = a \sin(\omega t) \qquad (3)$$

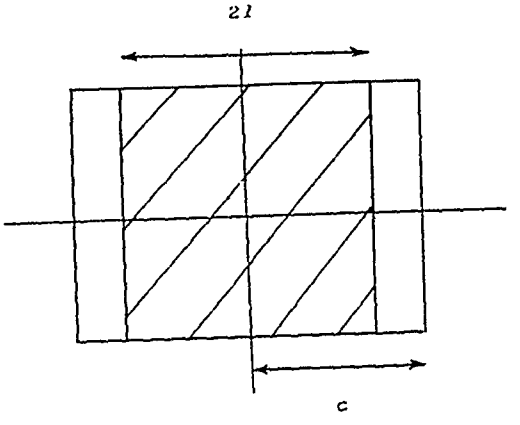

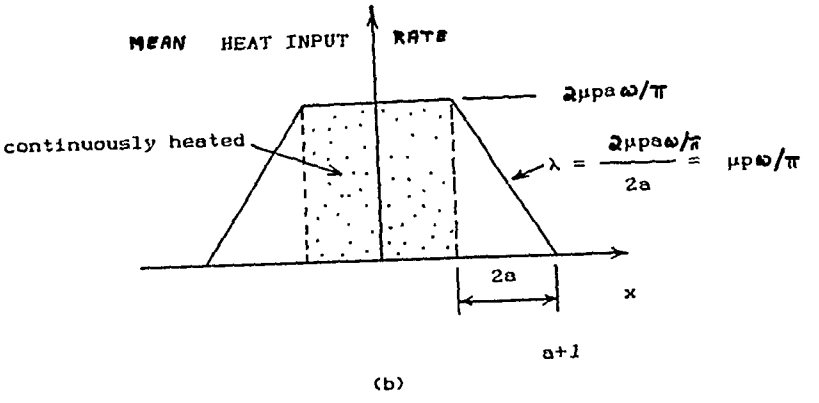

FIGURE 3 Contact geometry and heat input distribution for values of $A \ll 1$.

where a is the amplitude of motion. Blok's speed parameter, $V\ell/2\alpha$, becomes, after non-dimensionalisation, $2M^2A$ where $A = a/\ell$ and $M^2 = (\omega\ell^2/4\alpha)$. This is the non-dimensional form used by Hirano and Yoshida and while, perhaps, not the most appropriate, its adoption allows the results of the two analyses to be compared.

The analysis will be carried out in two stages. We shall first calculate the steady temperatures produced by taking the supply of heat at each point to be constant (and equal to the mean rate at that point). Secondly we shall calculate the temperature fluctuations ('flash temperatures) due to the variation of the heat supply rate at a point about its mean value.

2.1 STEADY TEMPERATURES: SMALL AMPLITUDES ($A \lesssim 1$)

For small values of A, the contact size is greater than the amplitude and the contact geometry is shown in Figure 3a. In this case, some points on the lower surface are always under the slider and are, therefore, continuously heated. For such points, the average rate of heat input is given by:

$$\bar{q} = \frac{2\omega}{\pi} \cdot \int_0^{\pi/2\omega} \mu p a\omega \cos\omega t \cdot dt = 2\,\mu p a\omega/\pi \qquad (4)$$

This is true for all points $-(\ell - a) < x < (\ell - a)$. For points at the ends of the travel $(\ell - a) < x < (\ell + a)$, heating starts at a time after $t = 0$, at $\omega t_o = \sin^{-1}((x - \ell)/a)$ and continues to $\omega t_1 = \pi/2$. The average rate of heat input at such points is given by:

$$\bar{q} = \frac{\omega}{\pi} \cdot \int_{t_o}^{t_1} \mu p a\omega \cos\omega t \cdot dt = \mu p(a - x + \ell)\,\omega/\pi \qquad (5)$$

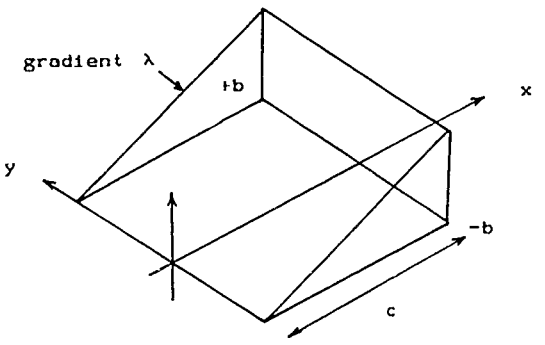

(a)

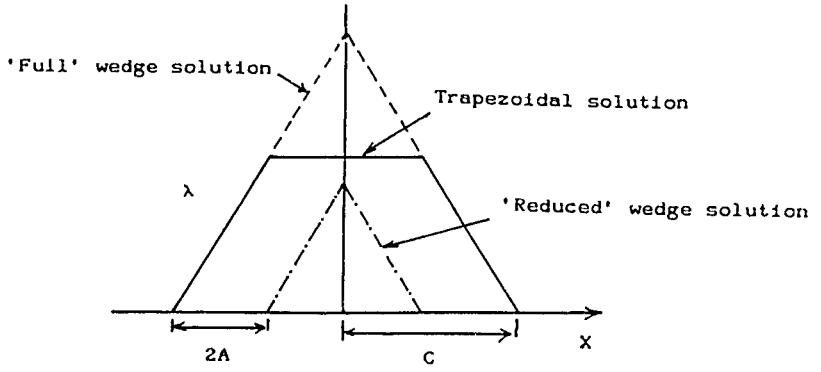

(b)

FIGURE 4 The solution for temperatures due to a trapezoidal heat input: wedge heat inputs (a) are superposed (b). The 'reduced' wedge is subtracted from the 'full' wedge to produce the final trapezoidal solution.

Equations (4) and (5) agree at $x = (\ell - a)$. The heat input to the rectangular contact area on the lower surface is shown in Figure 3b. Note that the slope of the end sections is

$$\lambda = \mu p \omega / \pi \tag{6}$$

The steady temperature rise due to a distributed heat source of rate $q(x',y')$ is known to be

$$\theta(x,y) = \frac{1}{2\pi K} \int\int \frac{q(x',y')\, dx'dy'}{\sqrt{(x - x')^2 + (y - y')^2}} \tag{7}$$

[Francis (1970) points out that this is identical to the expression giving the elastic surface deflection due to a distributed pressure $q(x',y')$ if the thermal conductivity K is replaced by <u>half</u> the plane-strain modulus E' (i.e. $E' \leftrightarrow 2K$), so that answers to steady temperature problems can often be found by consulting texts on elasticity, e.g. Timoshenko and Goodier (1983)).]

The trapezoidal heat input distribution of Figure 3b can conveniently be obtained by superposition of 'pyramid' solutions as shown in Figure 4: a pyramid has width 2b and extends from $x = -c$ to $x = +c$ with slope $\pm\lambda$. It is shown in Appendix 1 that this gives rise to surface temperatures

$$\theta(x) = \frac{\lambda b^2}{2\pi K} \left[F\left[\frac{x + c}{b}\right] - 2F\left[\frac{x}{b}\right] + F\left[\frac{x - c}{b}\right] \right] \tag{8}$$

where $$F(z) = 2z \sinh^{-1} z + z^2 \sinh^{-1}\left[\frac{1}{|z|}\right] - \sqrt{1 + z^2} \tag{9}$$

Hence, by first taking c equal to $(\ell + a)$ and then to $(\ell - a)$ (see Figure 4b), we get

$$\theta(x) = \frac{\lambda b^2}{2\pi K} \left[F\left[\frac{x + \ell + a}{b}\right] + F\left[\frac{x - \ell - a}{b}\right] - \left\{ F\left[\frac{x + \ell - a}{b}\right] + F\left[\frac{x - \ell + a}{b}\right] \right\} \right] \tag{10}$$

where from equation (6) $\lambda = \mu p \omega / \pi$.

We introduce a non-dimensional temperature Φ defined by

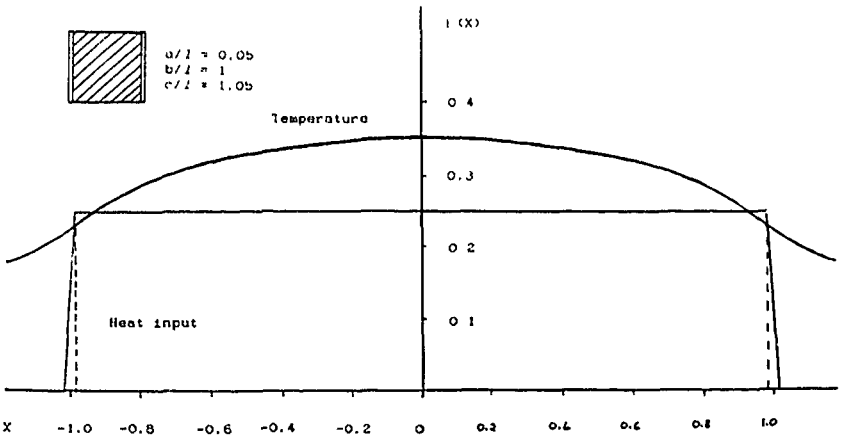

FIGURE 5a Heat input distribution and corresponding temperature solution for A = 0.05.

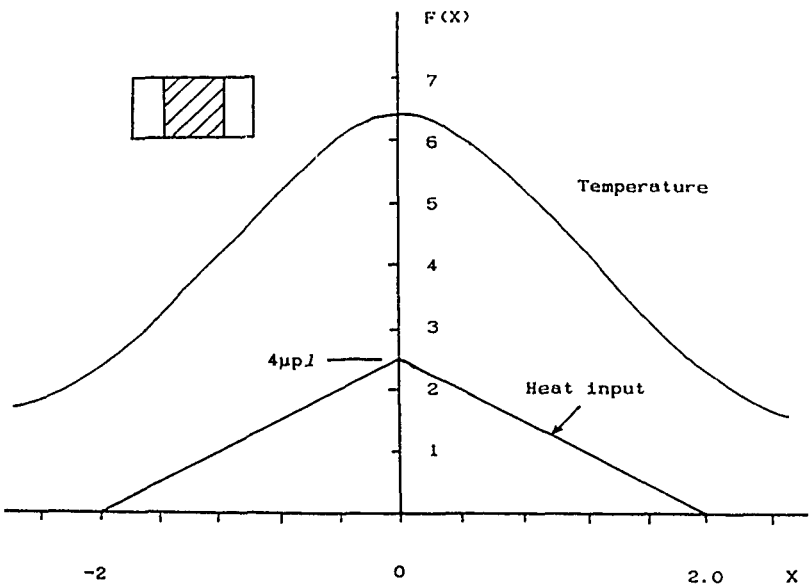

FIGURE 5b Contact geometry, heat input and temperature solution for the case A = 1.

$$\Phi = \frac{K\theta}{\mu_* \alpha} \tag{11}$$

Note that this differs from the Φ used by Hirano and Yoshida, who define $\Phi = \pi^{3/2} K\theta/(2\mu p\alpha)$. Recalling that $M = (\ell/2)\sqrt{\omega/\alpha}$, we can write

$$\Phi(x) = \frac{2}{\pi^2}\left[\frac{b}{\ell}\right]^2 M^2 \left[F\left[\frac{x+\ell+a}{b}\right] + F\left[\frac{x-\ell-a}{b}\right] - F\left[\frac{x+\ell-a}{b}\right] - F\left[\frac{x-\ell+a}{b}\right]\right] \tag{12}$$

Typical examples for $\ell = 1$, $b = 1$, $a = 0.05$ and $a = 1$ are given in Figure 5a,b. The (steady) temperature is a maximum at the middle of the rubbed area; in 5a it is fairly constant up to the edge of the heated zone, while the much more concentrated heat input for $A = 1$ (Figure 5b) gives a more 'peaky' temperature.

2.2 STEADY TEMPERATURES: LARGE AMPLITUDES ($A \geq 1$)

When the amplitude a is greater than the half-length ℓ of the slider, most of the points in the stroke are passed by the slider moving at an approximately constant velocity and this can be treated as a fast-moving heat source. It is only towards the ends of the stroke that this becomes a poor approximation. The essential geometry is shown in Figure 6a, and the total heat received is distributed as shown in Figure 6b. This can be obtained either by the method used in the last section, or as follows. If the source is split into strips of width dx, then each strip heats a point for a time dx/V at a rate μpV and, therefore, supplies $\mu p dx$ to that point. The total heat received by any point in a single pass of the slider is then given by:

$$Q_{TOT} = \mu p \times (\text{width of source that passes the point})$$

and the mean rate of heat input at that point will be $Q_{TOT}/(\pi/\omega)$, i.e.

$$\bar{q} = \frac{\mu p \omega}{\pi} \times (\text{width of the source that passes the point}) \tag{13}$$

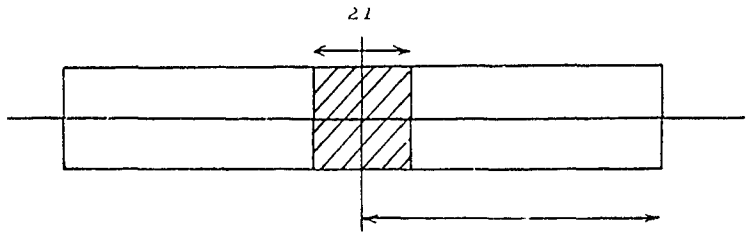

(a)

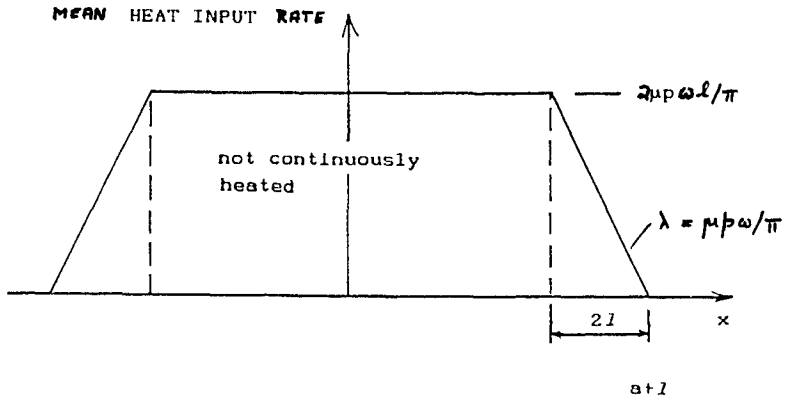

(b)

FIGURE 6 Contact geometry and total heat distribution for values of A > 1.

Thus, for points in the region $0 < |x| < a - \ell$ the mean rate is $\bar{q} = 2\mu p\omega\ell/\pi$, while points in the fringe areas $a - \ell < |x| < a + \ell$ are passed only by $(\ell + a - |x|)$ of the slider, to give,

$$\bar{q} = \frac{2\mu p\omega}{\pi}(\ell + a - |x|) \tag{14}$$

The steady heat input is drawn in Figure 6b, and is seen to be the same as for small amplitudes, except that the height of the plateau is $2\mu p\omega\ell/\pi$ instead of $2\mu p\omega a/\pi$; the end slopes are still $\lambda = \mu p\omega/\pi$ as given in equation (6).

The steady temperature distribution is obtained in the same way as for small amplitudes, except that in superposing the wedge solutions, we subtract those for $c = a - \ell \equiv |\ell - a|$ instead of those for $c = \ell - a$. The final non-dimensional solution for the <u>steady</u> temperature can therefore be written <u>for any value of A</u> as

$$\Phi(x) = \frac{2}{\pi^2}\left[\frac{b}{\ell}\right]^2 \cdot M^2\left[F\left[\frac{x + \ell + a}{b}\right] + F\left[\frac{x - \ell - a}{b}\right] - \left\{F\left[\frac{x + |\ell - a|}{b}\right] + F\left[\frac{x - |\ell - a|}{b}\right]\right\}\right] \tag{15}$$

In all the results presented in this work, the slider was square, i.e. $b = \ell$. Typical values of the non-dimensional temperature at $x = 0$ are tabulated below for $M = 1$.

<u>Table I</u>

A	0.1	0.2	0.5	1	2	5	10
Φ_{steady}	0.286	0.570	1.404	2.619	3.836	5.349	6.476

[For comparison, we note that for uniform heating at a rate $q = (2/\pi)\mu pa\omega$ over a square $2\ell \times 2\ell$, the result is $\Phi_{steady} = 2.858\ M^2A$: clearly the motion has little effect on the steady temperature for $A < 1$.]

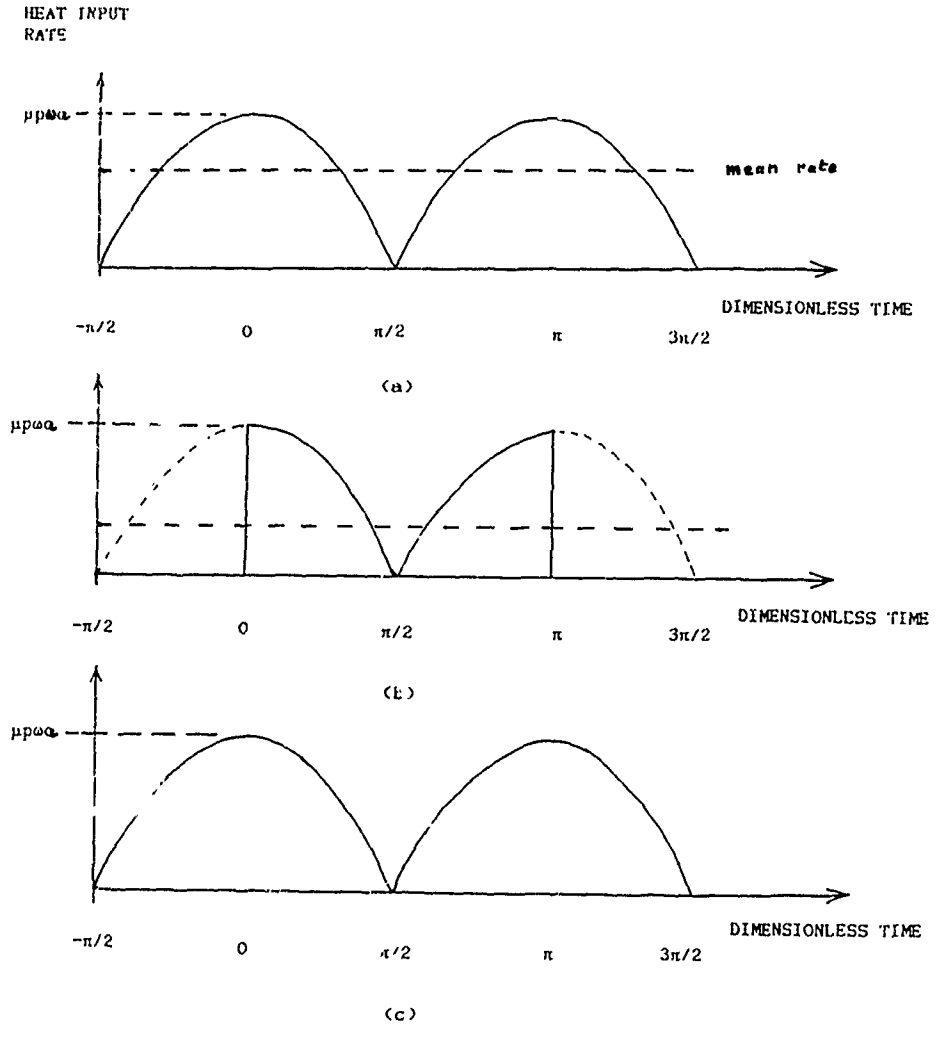

FIGURE 7 Time varying heat inputs to points on the stationary solid (a) at x=0 and (b) at x=*l* and to all points on the slider, (c)

3.1 FLASH TEMPERATURES: $A < 1$

In addition to this steady temperature rise in the contact, there is a transient temperature due to the passage of the slider. All points less than a distance $(\ell - a)$ from the centre of the contact $(x = 0)$ - which for small amplitudes means most of the heated area - are continuously under the slider and so continuously heated, but at a varying rate due to the varying velocity. Thus, the heat input rate is a rectified sine wave as shown in Figure 7a. We have calculated the steady temperature rise due to the mean heat input (shown dashed in Figure 7a): we now wish to estimate the effect of the variation about this mean level.

The surface temperature due to a sinusoidal heat input over the whole surface is given by Carslaw and Jaeger §2.9: $q_A \cos\omega t$ gives rise to

$$\theta = \frac{4q_A}{\pi K}\sqrt{\frac{\alpha}{\omega}}\cos(\omega t - \pi/4) \tag{16}$$

Hence, by Fourier analysis of $q_A|\sin\omega t|$ (dropping the constant term $(2/\pi)q_A$) we get

$$\theta = -\frac{4q_A}{\pi K}\sqrt{\frac{\alpha}{\omega}}\sum_{n\ \text{even}}\frac{1}{\sqrt{n}(n^2 - 1)}\cos(n\omega t - \pi/4) \tag{17}$$

(cf. Carslaw and Jaeger §2.9(vi)). Taking $q_A = \mu p a \omega$ gives

$$\Phi = -\frac{8}{\pi}AM\sum_{n\ \text{even}}\frac{1}{\sqrt{n}(n^2 - 1)}\cos(n\omega t - \pi/4) \tag{18}$$

The series is easily summed by digital computer, and we find

$$\Phi_{max} = 0.549\ A\ M \tag{19}$$

occurring when $\omega t \sim 5\pi/8$, somewhat after the time of greatest heat input, $\omega t = \pi/2$.

When can we regard our rather small heated area as the entire plane surface? Clearly, the answer is when the edges are far enough away. But it

is known that after a time t, the response to a temperature change at one point is small at a distance $2\sqrt{\alpha t}$, but reasonably complete at distances less than $0.5\sqrt{\alpha t}$. We deduce that the temperature at the centre of an area which is heated uniformly with a heating rate varying sinusoidally with frequency 2ω, will be largely independent of the heat input beyond a distance of order $\sqrt{\alpha\pi/\omega}$. Noting that our heat input begins to fall off at a distance $(\ell - a)$ but only falls to zero at $(\ell + a)$, and falls abruptly to zero at a distance ℓ in the lateral direction, we take the effective distance to be equal to ℓ, so that we require $\ell > \sqrt{\alpha\pi/\omega}$, or approximately. $M > 1$.

The exact solution for sinusoidal heating over a circular area on the surface of a semi-infinite solid is easily derived by integrating the solution for a sinusoidal point source, which is given by Carslaw and Jaeger. This is done in Appendix 2, and shows that the above result is pessimistic, and that the centre temperature is close to that for a source covering the whole surface whenever $M > 0.6$, provided that A is appreciably less than 1.

3.1.1 Flash Temperatures: A < 1: M Small

For $M < 0.6$, we cannot assume our heat source to be large. For sufficiently small amplitudes it is clear that the motion is irrelevant, except in so far as it provides the frictional heat: we require the solution for a stationary heat source, with heat input varying as $\mu pa\omega|\sin\omega t|$ - or more generally, as $\Sigma a_n \cos\omega t$. The exact solution for a sinusoidal square (or rectangular) source is not known: but it is easy to extend the analysis for a circle to give a good approximation for a square. According to Appendix 2, the result is

$$q = \cos\omega t \Rightarrow \theta = \frac{1}{K}\sqrt{\frac{\alpha}{\omega}} \cdot \left[\cos\left[\omega t - \frac{\pi}{4}\right] - e^{-z}\cos\left[\omega t - \frac{\pi}{4} - z\right]\right]$$

where $z = M\sqrt{2}$ for a <u>circle</u> of radius ℓ, while for a square of side 2ℓ, approximately $z = 1.587\ M$, which is equivalent to approximating the square by

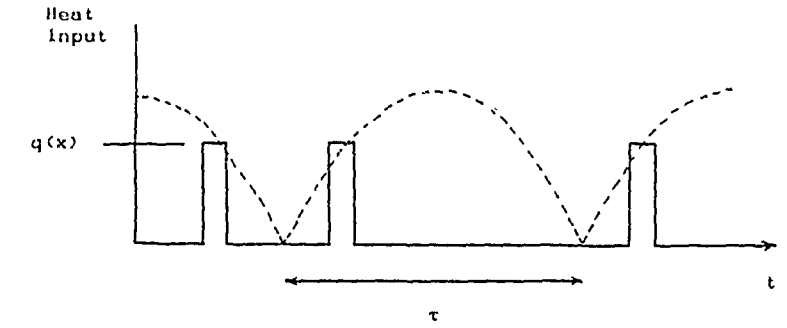

(a)

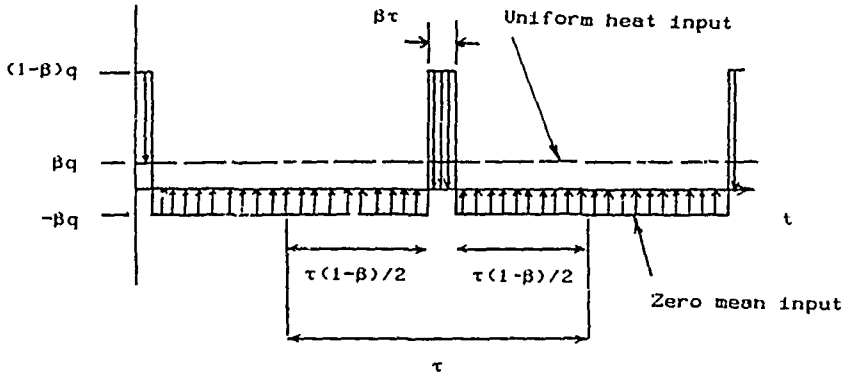

(b)

FIGURE 8 Heat pulses seen by points in the stroke. (a) A general point passed by the slider twice a cycle. (b) The centre point receives heat pulses every half cycle: this can be split into two parts, an averaged or uniform heat input and a zero mean time varying input.

a circle of radius 1.122 ℓ. Hence, from the Fourier analysis of $q = \mu p a\omega|\sin\omega t|$ we get for the largest variation from the steady temperature

$$\Phi = M\,A\,f(M).$$

where

Table II

M	0.1	0.2	0.4	1.0	∞
f(M)	0.1467	0.2639	0.4014	0.5822	0.5492

[The fact that the temperature for a finite disk or square is larger than for an infinite one is due to the time lag in the arrival of heat from distant parts of the source: see Appendix 2.]

3.2 FLASH TEMPERATURES: $A > 1$

For amplitudes greater than the source half-length, the pattern of heat input to any point on the surface is as shown in Figure 8a. The method used for $A < 1$ is inappropriate, but an obvious way is to treat each passage of the slider as an ordinary uni-directional sliding contact. It is clear that the maximum temperature will occur when the velocity is at, or near, its maximum value, so we need not worry about the ends of the stroke where the velocity is small and reverses its direction.

Near the centre of the stroke the velocity will be almost $a\omega$, so that the Blok high-speed solution, equation (1), may be used provided Jaeger's parameter $L = V\ell/2\alpha$ is sufficiently large. Taking $V = a\omega$, we have $L = a\omega\ell/2\alpha = 2AM^2$: Jaeger's condition is that $L > 5$.

At slow speeds, Jaeger shows that the answer for a stationary source, $\theta = 1.1222\ (q\ell/K)$, may be used provided $L < 0.1$.

Thus, we have

$$L > 5,\ \Phi_F = 2.257\sqrt{L}\ ;\ L < 0.1\ ,\ \Phi_S = 2.244\ L\ .$$

Unfortunately in this work we are interested in intermediate values of L. Archard (1959) has proposed an interpolation rule for the average source temperature; but this is not very accurate. If, however, we use a similar rule,

$$\frac{1}{\Phi} \approx \frac{1}{\sqrt{\phi_F^2 + \phi_S^2}}$$

which we simplify to

$$\phi = \frac{2.257\ L}{\sqrt{1 + L}} \qquad (20)$$

comparison with Jaeger's results for intermediate values of L (Table III) shows that we can obtain an acceptable accuracy.

Table III

L	0.1	0.2	0.5	1	2	3	4	5
$\Phi\|_{\text{Jaeger}}$	0.22	0.42	0.89	1.60	2.66	3.44	4.10	4.71
$\Phi\|_{(20)}$	0.214	0.410	0.918	1.591	2.601	3.380	4.033	4.602

We note that Jaeger's condition for the high-speed solution to be valid is rather lenient: at L = 5 it would give 5.05 - noticeably worse than any value in our table.

However, in order to account for the steady temperature rise, we wish to use the solution already obtained (Equation (15)) for the effect of the mean rate of heat input. We need, therefore, to find the transient temperature due to a moving source with zero total heat input, or, what comes to the same thing, to allow for the cooling down from the 'steady' temperature since it was 'topped up' by the last passage of the heat source.

The first method is indicated in Figure 8b: if the time between pulses is T ($\equiv \pi/\omega$) and the pulse length is βT, then we regard this as a moving source of strength q_0 operating from $t + -\frac{1}{2}\beta T$ to $t = +\frac{1}{2}\beta T$, together with a moving source of strength $-\beta q_0$ starting at $t = -(1 - \beta).T/2$.

(This is an adaptation of the normal method of finding the temperature behind a moving heat source by regarding the source as continuing to operate, but to be followed by a negative source of the same strength).

If the speeds are sufficiently high, we may use the Blok/Jaeger high speed solution for both pulses. According to this, the maximum flash temperature occurs as the rear of the source passes the centre point, and is

$$\theta_{flash} = \frac{2}{\sqrt{\pi}} \cdot \frac{q_o}{K} \cdot \sqrt{\alpha} \left\{ \sqrt{\beta T} - \beta \sqrt{\frac{1+\beta}{2}} \cdot T \right\} \qquad (21)$$

where $\beta = \frac{2}{\pi} \sin^{-1} \frac{\ell}{a}$, $T = \frac{\pi}{\omega}$.

If ℓ/a is very small, we can take θ_o to equal the maximum heating rate $\mu pa\omega$; but in this case we could also take $\beta = 2\ell/\pi a$. For moderate values of ℓ/a it seems more consistent to use the mean heating rate while the source passes the centre point. This is $q_o = \mu p\omega\ell/\sin^{-1}(\ell/a)$; so for the flash temperature we get

$$\Phi = \frac{8M}{\pi} \left[\frac{1}{\sqrt{\beta}} - \sqrt{\frac{1+\beta}{2}} \right] ; \qquad \beta = \frac{2}{\pi} \sin^{-1} \frac{1}{A}$$

But the condition for the validity of the high-speed solution is not the same for the real pulse as for the negative one: the negative pulse has far more time available for lateral conduction. It is therefore convenient to separate the two effects: for the flash temperature we replace

$$\Phi = \frac{8M}{\pi\sqrt{\beta}}$$

by the appropriate conversion of equation (20); while for the cooling we replace

$$\Phi_c = \frac{8M}{\pi} \cdot \sqrt{\frac{1+\beta}{2}} ; \qquad \beta = \frac{2}{\pi} \sin^{-1} \frac{1}{A} \qquad (22)$$

by its equivalent for lower speeds.

To convert (20), we note that the definition $L = V\ell/2\alpha$ is slightly

misleading: L appears in the theory as the square of the ratio of the half-length of the source, ℓ, to the diffusion distance $\sqrt{\alpha t}$:

$$L = \frac{\ell^2}{\alpha t} = \frac{V\ell}{2\alpha} \qquad \text{since} \quad t = \frac{2\ell}{V} .$$

Hence for an oscillating contact passing the centre-point of its track, we have $\omega t = 2\sin^{-1}(\ell/a)$ and so we use equation (20) in the form

$$\Phi_{flash} = \frac{2.25\ L}{\sqrt{1 + L}} \qquad \text{with} \quad L = 2M^2/\sin^{-1}(1/A) . \tag{23}$$

3.3 COOLING FROM THE STEADY STATE: $A > 1$

We wish to calculate the reduction below the 'steady' temperature at the time when the source makes its next pass over the centre point: and we have argued that this is due to a source of heat $-\beta q_0$ acting from $t = -(1 - \beta)T/2$ to $t = 0$ as the mid-point of the source passes, or to $t = +\beta T/2$ as the rear edge passes. Now if we take q_0 to be the mean rate while the source passes the centre point, then $\beta q_0 = (2/\pi)\mu p\omega\ell$: which is, of course, exactly the mean heating rate $\bar{q}$ responsible for the steady temperature. That is, we regard the steady heating as ceasing at a time between $-(1 - \beta)T/2$ and $-T/2$ before the time of interest.

We therefore need to study the development of the steady temperature (in order to subtract it from the equilibrium steady temperature). We consider first the simpler case of a rectangle $2a \times 2b$ with a uniform heating rate q_A. The analysis is given in Appendix 3: the final equations were integrated numerically on a digital computer. The important conclusions are:

(i) Initially the temperature grows according to

$$\theta = \frac{2}{\sqrt{\pi}} q_A \sqrt{\alpha t}$$

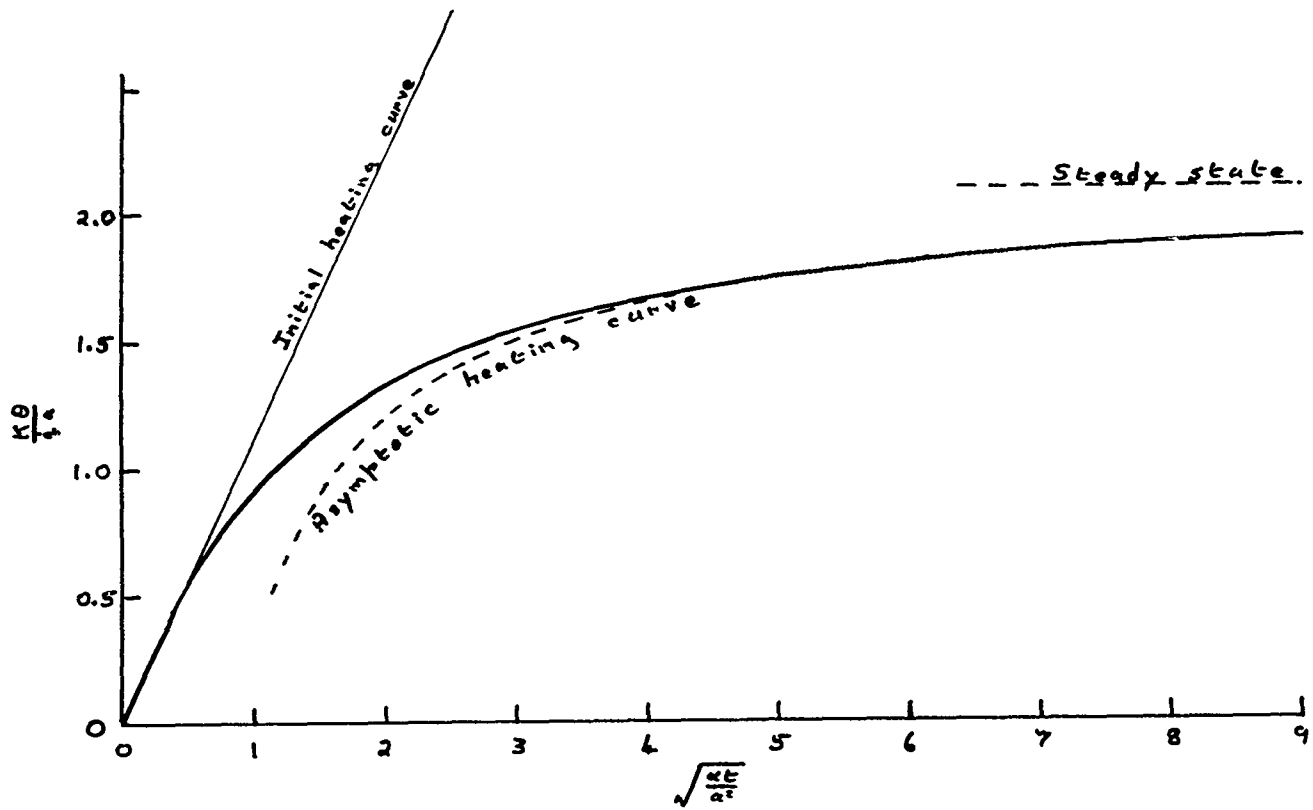

Figure 9: Temperature rise at the centre of a (2a x 5a) rectangle

as if the source covered the entire plane. The temperature is 10% below this value when $\alpha t/b^2 = 0.52$ for any rectangle whose length a is greater than four times its width: for a = 2b the time falls to $\alpha t/b^2 = 0.50$; for a = b it falls more noticeably to $\alpha t/b^2 = 0.33$. Thus, except for A = 1, we can use the Blok formula (22) provided (taking $t = \pi/2\omega$)

$$M^2 > \pi/4 \ .$$

(ii) For long times, the temperature varies as

$$\theta(t) = \theta(\infty) - \frac{Q}{2\pi K} \cdot \frac{1}{\sqrt{\pi\alpha t}} \cdot \left\{1 - \frac{R^2 + k^2}{12\alpha t} + \ldots\right\} \qquad (24)$$

where $\theta(t)$ and $\theta(\infty)$ are the temperatures at any point (x,y,z); $R^2 = x^2 + y^2 + z^2$ is the distance of that point from the centroid of the heat input distribution, k^2 is the 'radius of gyration' of the heat input (borrowing the term from mechanics: the heat input rate q replaces the density), and Q is the total rate of heat input to the plane. We see that whenever $(R^2 + k^2)/12\alpha t$ is small, the temperature deficit, $\theta(\infty) - \theta(t)$, is independent of source geometry and of position: physically we recognise that it represents the heating-up of the distant parts of the half-space: the local temperatures have reached a quasi-equilibrium, but are still rising as a whole because of the distant temperature rise.

The condition that $(R^2 + k^2)/12\alpha t$ be small can easily be interpreted for the actual trapezoidal heat input, equal to $\bar{q}$ for $|x| < a - \ell$, falling to zero at $|x| = a + \ell$. Then $k^2 = \frac{1}{3}(a^2 + b^2 + \ell^2)$, so that for the centre-point R = 0 we require

$$\frac{a^2 + b^2 + \ell^2}{36\alpha t} < 0.11$$

which for $t = \pi/2\omega$ (b = ℓ) becomes

$$M^2(A^2 + 2) < \frac{\pi}{2} \qquad (25)$$

Figure 9 shows the temperature development for a uniformly heated rectangle with a = 5b, together with the initial and final approximations: it is clear that these cover the majority of the range.

We note that where this law is valid, the steady tempearture $\theta(\infty)$ disappears from the final equation for the maximum temperature, to leave

$$\Phi_{max} = \Phi_{flash} + \frac{32\sqrt{2}}{\pi^3} \cdot A M^3 \qquad (26)$$

3.4 FLASH TEMPERATURES: A = 1

We have already estimated the flash temperature for A < 1 by assuming the contact to cover the whole plane, and shown that this is valid for M > 0.6. For A > 1 we can assume the velocity of the slider to be constant (equal to $a\omega$) as it passes the centre point, and so use a form of the Jaeger solution as just described.

For A = 1 we can certainly not assume that the slider velocity is constant: its variation, or rather, the implied heat input rate, is shown in Fig. 7. Each point under the slider experiences a different cycle of heat input, and we note that it is not clear where the maximum temperature will occur. As the slider passes the centre point, it supplies the maximum heating rate, but is moving fast. As it approaches the ends, the heating rate is less, but it heats the surfaces for longer. The centre-point sees a time-varying heat input as shown in Figure 7a and the point $x = \ell$ (half way to the end of the stroke)receives heat as in Figure 7b - with the same maximum heat input rate, but twice as large a deviation above the mean rate (and half as large below - but this does not concern us).

Now, Archard showed that the Blok solution is obtained by ignoring lateral heat conduction: it is therefore equivalent to taking the source to cover the entire half space. But we have already used the solution for a plane source whose intensity varies sinusoidally to obtain the flash temperatures for $A < 1$: we rejected it for $A = 1$ because the source was too small. However, if the speed is high enough to satisfy the Archard criterion $V\ell/2\alpha > 5$, we have an alternative justification: the solution will be valid if

either $M > 0.6$ and $A < 1$ or if $2M^2A > 5$

Thus, as for $A < 1$, we make a Fourier analysis of the heat input, and use the solution for the temperature due to a plane sinusoidal heat input (equation (16)) for each component.

The heat input is easily shown to be

$$\begin{cases} q = \mu pa\omega |\sin n\omega t| & \text{for } -t_1 < t < t_1 \\ q = 0 & \text{otherwise} \end{cases}$$

where for $x > 0$, $\omega t_1 = \cos^{-1}\left(\frac{x - \ell}{a}\right) \equiv \gamma$ say.

$$\left.\begin{aligned} &\text{Hence, } q = \mu pa\omega \sum a_n \cos n\omega t \\ &\text{where } a_n = \frac{1}{\pi}\left[\frac{1 - \cos(\overline{n+1}\,\gamma)}{n+1} - \frac{1 - \cos \overline{n-1}\,\gamma}{n-1}\right] \end{aligned}\right\} \quad (27)$$

The temperature due to $q = a_n \cos n\omega t$ is, as before,

$$\theta = \frac{a_n}{K}\sqrt{\frac{\alpha}{\omega}} \cdot \sum \frac{a_n}{\sqrt{n}} \cos(n\omega t - \pi/4) \quad (28)$$

$$\text{or} \qquad \Phi = 2AM \sum \frac{a_n}{\sqrt{n}} \cos(n\omega t - \pi/4) \quad (29)$$

[Note that on setting $x = 0$, $\ell = a$, we get $\gamma = \pi$ so that $a_n = 0$ when n is odd, and $a_n = -4/(\pi(n^2 - 1))$ when n is even, recovering equation (17) - but with

different conditions for validity.]

Evaluation of equation (29) for different locations gives

Table IV

A = 1	x/ℓ	Φ_{flash}/M	Φ_{steady}/M^2
	0	0.549	2.619
	0.2	0.752	2.48
	0.4	0.98	2.13
	0.6	1.17	1.70
	0.8	1.31	1.28
	1.0	1.28	0.97

The maximum temperature will be the sum of Φ_{flash} and Φ_{steady}, so we give values of Φ_{steady} in the final column. The flash temperatures are valid only for $M > 2.5$, and for this range we see that despite the increase in flash temperature as we leave the centre, the maximum temperature will always occur close to $x = 0$, and its value can be taken as the value there, i.e.

$$\Phi_{max} = 0.55\,M + 2.62\,M^2 \qquad \text{for } A = 1,\ M > 2.5 \tag{30}$$

4.1 MAXIMUM TEMPERATURES

We now collect together the various answers found in the previous sections.

(i) Φ_{steady} is given by Table I (repeated here for convenience)

A	0.1	0.2	0.5	1	2	5	10
Φ_{steady}/M^2	0.286	0.570	1.404	2.619	3.836	5.349	6.476

(ii) $\Phi_{flash} = \dfrac{2.257\,L}{\sqrt{1+L}}$ where $L = \dfrac{2M^2}{\sin^{-1}\left[\frac{1}{A}\right]}$

I <u>For A > 2; M > 0.4</u> $\Phi = \Phi_{steady} - \Phi_{cool} + \Phi_{flash}$

where $\Phi_{cool} = \frac{8M}{\pi}\sqrt{\frac{1+\beta}{2}}$: $\beta = \frac{2}{\pi}\sin^{-1}\left[\frac{1}{A}\right]$.

II For $A > 2$; $M^2(A^2 + 2) < \pi/2$ $\Phi = \Phi_{res} + \Phi_{flash}$

where $\Phi_{res} = 1.480\ AM^2$

III For $A = 1$; $M > 2.5$ $\Phi = \Phi_{steady} + 0.549\ M$

IV For $A < 1$ $\Phi = \Phi_{steady} + AM\ f(M)$

where f(M) is given by Table II (repeated here)

M	0.1	0.2	0.4	1.0	≥ 5
f(M)	0.1467	0.2639	0.4014	0.5822	0.5492

From these equations, we can assemble the maximum temperature chart, Figure 10. In order to reduce the range to be covered, this shows Φ/M^2 rather than Φ. We see that for fretting contacts, defined as those moving less than their width ($A < 1$), the picture is complete: at all frequencies the steady temperature is the major term; at high frequencies, $M \geq 5$, effectively the only term. For reciprocating contacts ($A > 1$), the "flash" temperature dominates at low frequencies - where it is a low-speed flash temperature, not the usual Blok temperature. At higher frequencies we get a Blok flash temperature, but it no longer dominates, and again for $M > (5 - 10)$ effectively only the steady temperature is important. There is a substantial range of frequencies ($0.2 < M < 1$) for which we have no equation; but there seems to be no difficulty in extrapolating the curves across the break.

For the special case $A = 1$, dividing the fretting contacts from reciprocating ones, we have no answers except for $M > 2.5$, where we have the steady temperature plus a small correction. This does not seem to be a particularly important case in practice; but unfortunately it is the principal case for which a comparison with earlier work is possible.

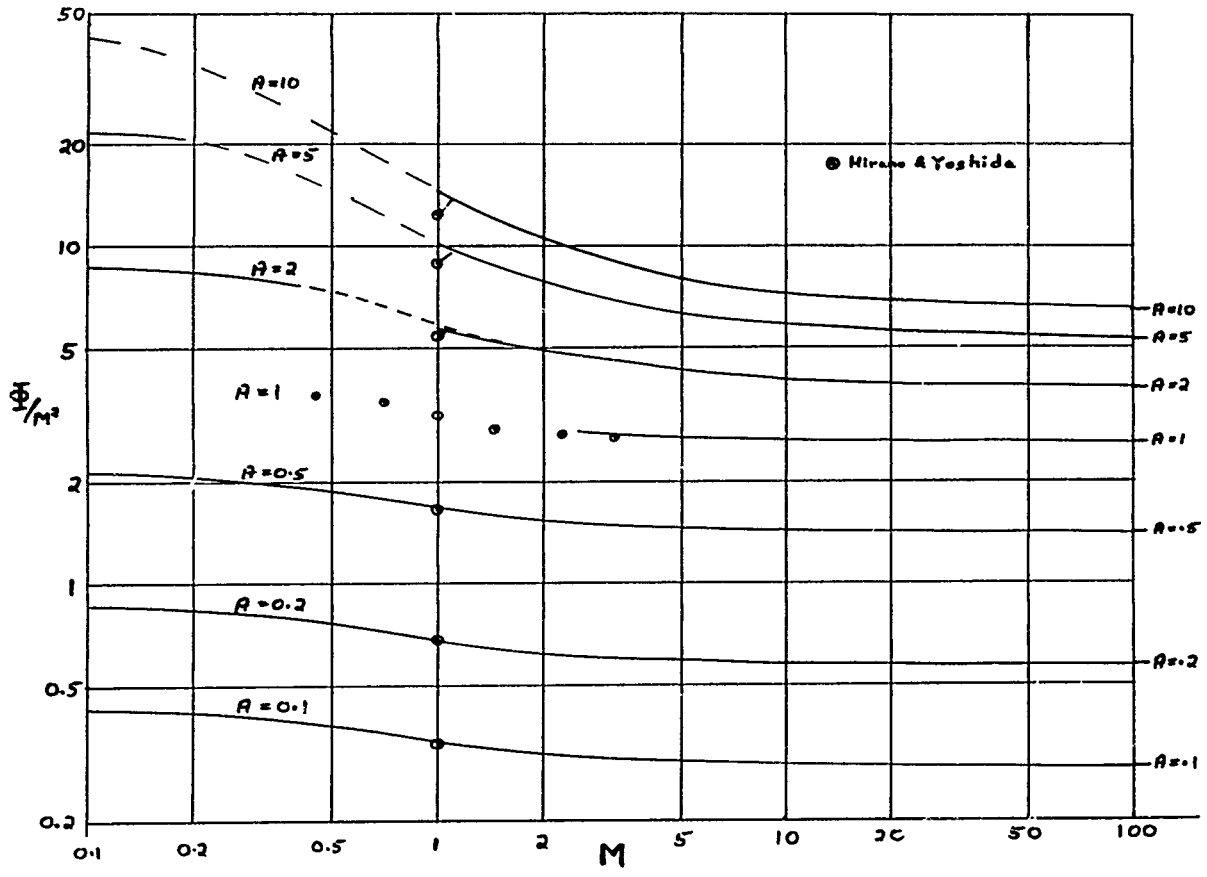

Figure 10: Maximum temperatures in reciprocating contacts.

4.2 COMPARISON WITH PUBLISHED SOLUTION

Hirano and Yoshida's (1966) analytical solution for the temperature over the slider gives answers for A = 1, varying M and M = 1, varying A. Their general conclusions were: (i) the reciprocating contact temperatures were significantly higher than those calculated using a Blok-type solution with uni-directional rubbing, especially at high values of A or M^2. In addition to any flash temperatures, there was, due to the localised continuous heat input into the contact zone on the solid, a significant and time-independent temperature rise. This was a true contact temperature as opposed to what was normally understood as a 'bulk' temperature. (ii) The steady-state temperature variations were set up after only a few cycles of rubbing, (iii) the maximum temperature occurred near the centre of the stroke, (iv) the temperature rise in reciprocating rubbing was nearly proportional to the non-dimensional amplitude A and the parameter M^2. On this last point, Hirano's paper actually quotes proportionality with M not M^2, but this can not be the case for reasons outlined below and must be a typographical error.

Hirano and Yoshida plot dimensionless temperature ($\pi^{3/2}\phi/2$) against A for M = 1, and against M for A = 1. Values read from their figures 8 and 9 have been added to our figure 10 and it is clear that there is substantial agreement. In particular, for M = 1, A < 1 the agreement is 'perfect' - that is, to the accuracy with which values can be read from Hirano's rather small graph.

At large amplitudes, our solution is consistently slightly above Hirano's. If this is not simply due to a plotting or reading error, then this is very difficult to understand. At these amplitudes the contact is a fast-moving heat source with very nearly constant velocity as it passes the centre: the final temperature is the Blok solution plus the contribution due to the mean heat input which we calculate exactly. We can see no reason to distrust these principles in this range: and our calculation is simple enough to be

free from numerical errors. We note that, in contrast, Hirano's results depend on the accurate numerical integration over an infinite range of an oscillating function - and that in any case the difference is small.

Hirano's values for $A = 1$, for which our methods fail unless $M > 2.5$, appear to fit in well, and indeed can be taken as completing our chart. Interestingly, our equation for $A = 1$

$$\Phi = 2.619 + 0.549\ M$$

although only justified for $M > 2.5$, gives exactly Hirano's answer at $M = 1$.

It should be noted that the figure from which Hirano's values are taken has M not M^2 as the ordinate, but we have treated this as a typographical error since it is not consistent with the text of the paper, or the physics of the situation. At the higher values of M the dominant contribution must be due to steady heating: this must be proportional to the mean heating rate, that is, to ω, and so to $M^2 \equiv \omega\ell/4\alpha$.

4.3 COMMENTS ON THE APPROXIMATIONS

Flash temperatures were calculated on the basis that motion had taken place at constant velocity for a time sufficient to give a steady transient solution. Jaeger (1942) described the build-up to the steady solution as a function of time, τ. He gives a plot of the time needed to reach 50% of the final temperature, which is very close to

$$\frac{V^2 t}{2\alpha} = 0.25\ L \qquad (33)$$

(where $L = V\ell/2\alpha$ for a square source $2\ell \times 2\ell$); for small values of L the time is less than this. From other graphs of the development of temperature against time, it appears that a similar result holds for 90% of the final temperature:

$$\frac{V^2 t}{2\alpha} \sim 1.2\ L \qquad (34)$$

These results are more conveniently interpreted in terms of the distance the source slides before the given fraction of the final temperature is achieved: they become

$$d(50\%) = 0.25\ \ell\ ; \qquad d(90\%) = 1.2\ell \qquad (35)$$

Thus, we can assert that once the source has moved its own width, the temperature will be close to the final flash temperature.

Applying this to our reciprocating contact, we note that even for A = 1, the contact has moved its own width when we estimate the flash temperature, although not with a constant velocity; for A = 2 or more the variation in velocity is small. We conclude that, except possibly for A = 1, the maximum temperatures will be close to the calculated ones.

5.1 HEAT PARTITIONING

The analysis so far assumes that all the heat flows into the stationary body and the moving body takes none. This is an acceptable approximation for a fast, uni-directional slider; but is certainly not valid for a reciprocating contact.

We now assume that the sliding body is also a half-space, the square contact area being a slightly raised portion. Heat flow into the slider will again produce a steady temperature and a variable temperature: the only differences from the previous analysis being that for all values of A, there is continuous contact and the heat input varies as in Figure 7c, and that we require the steady temperature for uniform heat input over a square contact. From Jaeger, this is $\Phi_1 = 2.858\ AM^2$.

Accordingly,

$$\Phi_{max} = 2.858\ M^2 + AM\ f(M)$$

where f(M) is given by Table II.

Jaeger's criterion for the partitioning of heat between two bodies is that the average surface temperatures should be the same. It is indeed necessary to match average temperatures since the maximum temperatures of the two bodies will rarely be at the same location - and the temperature redistribution due to placing the bodies in contact will usually bring the maximum temperature down near to the average value.

Despite this, we can obtain an over-estimate of the likely maximum temperature by assuming heat partition leads to equal maximum temperatures. Table V shows the calculation for M = 2.5.

Table V: Heat Partitioning

A	0.1	0.2	0.5	1	2	5	10
Φ_1/M^2	0.31	0.61	1.51	2.82	4.75	7.40	9.70
Φ_2/M^2	0.34	0 68	1.70	3.41	6.82	17.04	34.09
Fraction to Moving Body	0 52	0.53	0.53	0.55	0.59	0.70	0.78
Φ_{max}/M^2	0.16	0.32	0.80	1.54	2.30	5.16	7.55

Generally, we may expect heat partitioning to halve the maximum temperature for low frequencies for all A; at higher frequencies there will be a smaller reduction when A becomes large.

5.2 CONTACT TEMPERATURES UNDER EXPERIMENTAL CONDITIONS

The aim of this analysis was to obtain an estimate of the contact temperatures in our reciprocating rig experiments. Working conditions were:

Frequency	35 Hz	ω = 220 rad/s
Stroke	± 0.5 mm	
Temperature	150°C	
Load	1 kg	μ = 0.1

The steel specimens have thermal constants:

$K = 50$ W/mK

$\alpha = 1.5 \times 10^{-5}$ m/s^2

The worn contact size on the balls were typically 0.15 to 0.4 mm in diameter. For these two contact sizes, calculation and Figure 9 gives

ℓ (mm)	A	M	M^2	$\left[\frac{\mu p \alpha}{K}\right]$	Φ/M^2	Φ	θ
0.07	7.1	.13	.017	20	27	0.46	9.2°C
0.2	2.5	.40	.16	2.4	9.6	1.54	3.7°C

Heat partitioning will approximately halve these temperatures.

Thus, at a contact load of 1 kg, the maximum calculated temperature is 5°C, when partitioning of heat is taken into account. At the increased loads of 5 kg, the contact diameter was of the order 0.2 mm and the total temperature is five times that at 1 kg and 0.2 mm, approximately 10°C.

The conclusion from this analysis is that the total contact temperatures in the reciprocating rig, due to frictional heating, are only a few degrees centigrade. Both flash and steady temperature rises are negligible in size compared to the bulk temperature of the test specimens, typically 200°C. This means that temperature measurements from a thermocouple placed near to the contact gave readings of the contact temperature correct to a few degrees.

jag/rmo/9-1
24 01 89

REFERENCES

J F Archard
The temperatures of rubbing surfaces
Wear, 2 (1959) 438-455

H Blok
Theoretical study of temperature rise at surfaces of actual contact
Proc. I. Mech. E., "General Discussion on Lubrication", 2 (1937), 222-235

H S Carslaw and J C Jaeger
Conduction of Heat in Solids
OUP (1959)

H A Francis
Interfacial temperature distribution within a sliding Hertzian contact
ASLE Trans. 14 (1970) 41-54

F Hirano and S Yoshida
Theoretical study of temperature rise at contact surface for reciprocating motion
Proc. 3rd Int. Heat Transfer Conf., Chicago (1966) p. 127-132

J C Jaeger
Moving sources of heat and the temperature at sliding surfaces
Proc. Roy. Soc. NSW, 66 (1947), 203-224

V Turchina, D M Sanborn and W O Winer
Temperature measurement in sliding EHD point contacts
J. Lub. Tech. (ASME), 96 (1974), 464-471

S Timoshenko and J N Goodier
Theory of Elasticity
McGraw Hill (1951)

Appendix 1

STEADY TEMPERATURES DUE TO A TRAPEZOIDAL HEAT INPUT

It is convenient to use the scheme depicted in Fig. 4b, and obtain the solution for a trapezoidal heat source by superposition of two pyramidal sources, each with slope λ, one extending between $\pm |\ell - a|$, the other between $\pm (\ell + a)$. In applications we shall take $\lambda = \mu p\omega/\pi$.

Pyramidal Heat Source

We take $q = \lambda(c - |x'|)$ per unit time, unit area over $\left.\begin{matrix} -c < x' < c \\ -b < y' < b \end{matrix}\right\}$. The steady temperature at (x,y) due to a point source Q at (x',y') on the surface of a half-space is

$$\theta = \frac{Q}{2\pi K} \cdot \frac{1}{\sqrt{(x - x')^2 + (y - y')^2}}$$

so taking $Q = q\, dx'dy'$ gives

$$\theta(x,y) = \frac{1}{2\pi K} \int_{x'=-c}^{+c} \int_{y'=-b}^{+b} \frac{q\, dx'dy'}{\sqrt{(x - x')^2 + (y - y')^2}}$$

For points on the centre-line this becomes

$$\theta(x) = \frac{1}{\pi K} \int_{x'=-c}^{+c} \int_{0}^{b} \frac{q\, dx'dy'}{\sqrt{(x - x')^2 + y'^2}}$$

Consider first the wedge $0 < x' < c$ for which $q = \lambda(c - x')$. Then

$$\theta(x) = \frac{\lambda}{\pi K} \int_{x'=0}^{+c} \int_{y'=0}^{+b} \frac{(x - x') + (c - x)}{\sqrt{(x - x')^2 + y'^2}}\, dx'\, dy'$$

and the x'-integration gives

$$(c - x)\left[\sinh^{-1}\left[\frac{c - x}{y'}\right] + \sinh^{-1}\left[\frac{x}{y'}\right]\right] - \left[\sqrt{(c - x)^2 + y'^2} - \sqrt{x^2 + y'^2}\right]$$

The contribution from the wedge $-c < x' < 0$ may be obtained by changing the sign of x: so together

$$\theta(x) = \frac{\lambda}{\pi K}\int_{y'=0}^{b}\left\{(c - x)\ \mathrm{sh}^{-1}\left[\frac{c - x}{y'}\right] + (c + x)\ \mathrm{sh}^{-1}\left[\frac{c + x}{y'}\right] - 2x\ \mathrm{sh}^{-1}\left[\frac{x}{y'}\right]\right.$$
$$\left. - \left[\sqrt{(c - x)^2 + y'^2} + \sqrt{(c + x)^2 + y'^2} - 2\sqrt{x^2 + y'^2}\right]\right\} dy'$$

The y'-integration requires

$$\int_0^b \left\{d\ \mathrm{sh}^{-1}\left[\frac{d}{y'}\right] - \sqrt{d^2 + y'^2}\right\} dy'$$

which, noting that it is an <u>even</u> function of d, becomes

$$db\ \mathrm{sh}^{-1}\left[\frac{d}{b}\right] + \frac{1}{2}d^2\ \mathrm{sh}^{-1}\left[\frac{b}{|d|}\right] - \frac{1}{2}b\sqrt{d^2 + b^2}$$

Hence, taking d = (c - x), (c + x), and x in turn,

$$\theta = \frac{\lambda b^2}{\pi K}\left[F\left[\frac{c - x}{b}\right] + F\left[\frac{c + x}{b}\right] - 2F\left[\frac{x}{b}\right]\right] \qquad (A1)$$

where $F(z) = z\ \mathrm{sh}^{-1}z + \frac{1}{2}z^2\ \mathrm{sh}^{-1}\left[\frac{1}{|z|}\right] - \frac{1}{2}\sqrt{1 + z^2}$.

<u>Trapezoidal Heat Source</u>

We now take equation (A1) with $c = a + \ell$ and subtract from it the equation with $c = |a - \ell|$: then

$$\theta = \frac{\lambda b^2}{\pi K}\left[F\left[\frac{a + \ell - x}{b}\right] + F\left[\frac{a + \ell + x}{b}\right] - 2F\left[\frac{x}{b}\right]\right.$$
$$\left. - \left\{F\left[\frac{|a - \ell| - x}{b}\right] + F\left[\frac{|a - \ell| + x}{b}\right] - 2F\left[\frac{x}{b}\right]\right\}\right]$$

i.e. $$\theta = \frac{\lambda b^2}{\pi K}\left[F\left[\frac{a + \ell - x}{b}\right] + F\left[\frac{a + \ell + x}{b}\right] - F\left[\frac{|a - \ell| - x}{b}\right] - F\left[\frac{|a - \ell| + x}{b}\right]\right]$$

which is equation (15).

Appendix 2

TEMPERATURES DUE TO A SINUSOIDAL HEAT INPUT OVER A CIRCLE OF SQUARE

Carslaw and Jaeger (§10.4, VI) give the temperature at a distance R from a sinusoidal point source $Qe^{i\omega t}$ as

$$\theta = \frac{Q}{4\pi KR} \cdot \exp\{-\beta R + i(\omega t - \beta R)\}$$

where $\beta = (\omega/2\alpha)^{\frac{1}{2}}$. For a point source on the surface of a half-space this must be doubled to allow for purely downwards flow, so the temperature at a point <u>on</u> the surface

$$\theta_s = \frac{Q}{2\pi Kr} \exp\{-\beta r + i(\omega t - \beta r)\}$$

where $r^2 = x^2 + y^2$.

Hence, the temperature at the origin due to a disk source of radius b, strength $q_A e^{i\omega t}$/unit area will be

$$\theta_s = \frac{q_A e^{i\omega t}}{2\pi K} \int_{r=0}^{b} \frac{1}{r} \cdot \exp\{-\beta r - i\beta r\} \cdot 2\pi r \, dr \qquad (A1)$$

$$= \frac{q_A}{K} e^{i\omega t} \cdot \frac{1 - e^{-\beta b(1+i)}}{\beta(1 + i)} \qquad (A2)$$

Taking the real part, we get the temperature due to $q_A \cos\omega t$ over $r < b$ as

$$\theta_s = \frac{q_A}{K} \sqrt{\frac{\alpha}{\omega}} \cdot \left[\cos\left(\omega t - \frac{\pi}{4}\right) - e^{-\beta b} \cos\left(\omega t - \frac{\pi}{4} - \beta b\right)\right] \qquad (A3)$$

For (βb) large, this becomes the result for a plane sinusoidal source (Carslaw and Jaeger, §2.6)

$$\theta_s = \frac{q_A}{K} \sqrt{\frac{\alpha}{\omega}} \cdot \cos(\omega t - \pi/4) \qquad (A4)$$

For moderate values of (βb) the amplitude of the oscillations is

$$\frac{q_A}{K}\sqrt{\frac{\alpha}{\omega}}\sqrt{1 - 2e^{-\beta b}\cos(\beta b) + e^{-2\beta b}}$$

so that for βb as small as $\pi/2$ the amplitude differs only by a factor 1.021 from that for the plane source. Surprisingly, it is <u>larger</u> than for the plane source, which indicates that the finite disk cuts out contributions which, because of the time taken to reach the origin, would have been out of phase with the dominant contributions.

The largest variations are when $\beta b \sim 3\pi/4$, when they are 1.07× larger than for the plane source. To this accuracy (± 7%) we can say that disks of any radius $\beta b > 1.2$ give the same answer.

<u>Square Sinusoidal Source</u>

For a square source of side 2ℓ, strength $q_A e^{i\omega t}$, it is easy to see that equation (A1) is replaced by

$$\theta_s = \frac{q_A e^{i\omega t}}{2\pi K} \cdot 8 \int_{\psi=0}^{\pi/4} \int_{r=0}^{\ell \sec\psi} \exp\{-\beta r(1 + i)\} \cdot dr d\psi$$

$$= \frac{4q_A}{\pi K} e^{i\omega t} \int_{\psi=0}^{\pi/4} \frac{\exp\{-\beta\ell(1 + i)\sec\psi\}}{\beta(1 + i)} d\psi$$

For $0 < \psi < \pi/4$, $\sec\psi$ varies only from 1 to $\sqrt{2}$ so we can get an approximate analytical answer by replacing $\sec\psi$ by its mean value, which is 1.1222, i.e. $(4/\pi\ \ell n(1 + \sqrt{2}))$:

$$\theta_s \sim \frac{q_A}{K} \frac{e^{i\omega t}}{\beta(1 + i)} \cdot \exp\{-1.1222\ \beta\ell(1 + i)\}$$

which is seen to be equation (A2) with $b = 1.1222\ell$, that is, a square source of side 2ℓ behaves approximately as a circle of radius $b = 1.1222\ell$.

The advantage of this approximate answer is that with an equation of the form (A3), we can readily find the response to a rectified sine wave,

using the Fourier series

$$|\sin\omega t| - \frac{2}{\pi} = \frac{4}{\pi} \sum_{n \text{ even}} \frac{1}{n^2 - 1} \cos n\omega t$$

Results are given in the text, Table II, and show that the plane source gives answers within 1% for $b\ell > 2$. For a square source this becomes $M > 1.3$.

APPENDIX 3

Development of steady temperatures in a half-space due to surface heating.

a) Uniform surface heating over a rectangle.

From Carslaw and Jaeger §10.2 we find that an instantaneous heat source of strength $Q\rho c$ at a point $(x',y',0)$ on the surface of a half-space gives rise to a temperature at (x,y,z) after a time t equal to:

$$\theta = \frac{Q}{4(\pi\alpha t)^{1/2}} \exp\left[-\frac{R^2}{4\alpha t}\right] \quad \text{where } R^2 = (x-x')^2 + (y-y')^2 + z^2 \qquad \ldots(A1)$$

Hence the effect of instantaneous sources of strength $Q'\rho c$ per unit area distributed over the rectangle $|x'| < a, |y'| < b$ is

$$\theta = \frac{Q'}{4(\pi\alpha t)^{3/2}} \int_{x'=-a}^{+a} \exp\left[-\frac{(x-x')^2}{4\alpha t}\right] dx' \int_{y'=-b}^{+b} \exp\left[-\frac{(y-y')^2}{4\alpha t}\right] dy' . \exp\left[\frac{-z^2}{4\alpha t}\right]$$

which can be shown to equal

$$\theta = \frac{Q'}{4(\pi\alpha t)^{1/2}} \left[\operatorname{erf}\frac{x+a}{2\sqrt{\alpha t}} + \operatorname{erf}\frac{a-x}{2\sqrt{\alpha t}}\right] \left[\operatorname{erf}\frac{y+b}{2\sqrt{\alpha t}} + \operatorname{erf}\frac{b-y}{2\sqrt{\alpha t}}\right] \exp\left[\frac{-z^2}{4\alpha t}\right]$$

Accordingly, the temperature due to heat supplied at a constant rate $\dot{q}$/unit time, unit area for a time t is

$$\theta = \frac{\dot{q}}{4\rho c} \Sigma \int_{\tau=0}^{t} \frac{1}{\sqrt{\pi\alpha t}} \operatorname{erf}\frac{x+a}{2\sqrt{\alpha\tau}} . \operatorname{erf}\frac{y+b}{2\sqrt{\alpha\tau}} \exp\left[-\frac{z^2}{4\alpha\tau}\right] d\tau .$$

where the Σ indicates a set of four terms of which the one given is typical.

Let $u = 2\sqrt{\alpha\tau}/a$; $x = a\xi$, $y = b\eta$, $\lambda = b/a$, $z = a\zeta$

so that $\frac{x+a}{2\sqrt{\alpha\tau}} = \frac{1+\xi}{u}$; $\frac{y+b}{2\sqrt{\alpha\tau}} = \frac{\lambda(1+\eta)}{u.}$

$$\text{Then } \theta = \frac{a\dot{q}}{K} \cdot \frac{1}{4\sqrt{\pi}} \cdot \Sigma \int_{u=o}^{2\sqrt{\alpha\tau}/a} \text{erf } \frac{1+\xi}{u} \cdot \text{erf } \frac{\lambda(1+\eta)}{u} e^{-\zeta^2/u} du \qquad (A2)$$

where the four terms involve obvious combinations of $1 \pm \xi$, $\lambda(1 \pm \eta)$.

For the centre of the rectangle the equation simplifies slightly to:

$$\theta(o,o) = \frac{a\dot{q}}{K\sqrt{\pi}} \cdot \int_{u=o}^{2\sqrt{\alpha\tau}/a} \text{erf } \frac{1}{u} \cdot \text{erf } \frac{\lambda}{u} \cdot du. \qquad (A3)$$

Equation A2 was evaluated by numerical integration, supplemented by analytical integration of the series expansions of erf x for x small (u large). As a check, it was confirmed that the steady state temperatures could be obtained as $t \to \infty$ by an analysis resembling that in Appendix 1. These are found to be:

$$\theta(x,y) = \frac{\dot{q}}{2\pi K}\left[(a-x)\text{sh}^{-1}\frac{b-x}{|a-x|} + (b-y)\text{sh}^{-1}\frac{a-x}{|b-y|} + (a+x)\text{sh}^{-1}\frac{b-y}{|a+x|} + (b-y)\text{sh}^{-1}\frac{a+x}{|b-y|}\right.$$

$$\left. + (a+x)\text{sh}^{-1}\frac{b+y}{|a+x|} + (b+y)\text{sh}^{-1}\frac{a+x}{|b+y|} + (a-x)\text{sh}^{-1}\frac{b+y}{|a-x|} + (b+y)\text{sh}^{-1}\frac{a+x}{|b+y|}\right] \qquad (A4)$$

The result for the centre of the heated area is again very much simpler:

$$\theta(o,o) = \frac{2\dot{q}}{\pi K}\left[a\ \text{sh}^{-1}\frac{b}{a} + b\ \text{sh}^{-1}\frac{a}{b}\right] \qquad (A5)$$

However, it was noted that the steady state took unbelievably long to reach, and an analysis was performed to study this.

b) The approach to the steady state

Consider now a heated area A of any shape on the surface of half-space· the rate of heating q (x',y') may now vary over A.

The temperature at any point (x,y,z) due to a continuous point source $\dot{Q}$ at (x',y') is from equation (A1):

$$\theta(t) = \int_{\tau=0}^{t} \frac{\dot{Q}}{4\, c(\pi\alpha\tau)^{\frac{1}{2}}} \cdot \exp\left[-\frac{R^2}{4\alpha\tau}\right] d\tau$$

where $R^2 = (x-x')^2 + (y-y')^2 + z^2$

The steady temperature at the same point is found by taking the upper limit of the integral to be ∞, so the deficit $\Delta\theta = \theta(\infty) - \theta(t)$ is.

$$\Delta\theta(t) = \frac{\dot{Q}}{4\rho c} \int_{\tau=t}^{\infty} \frac{1}{(\pi\alpha\tau)^{\frac{1}{2}}} \exp\left[-\frac{R^2}{4\alpha\tau}\right] d\tau$$

Put $v^2 = 4\alpha\tau$: then

$$\Delta\theta(t) = \frac{\dot{Q}}{K} \cdot \frac{1}{\pi^{\frac{1}{2}}} \cdot \int_{v=2\sqrt{\alpha t}}^{\infty} \frac{1}{v^2} \cdot \exp\left[-\frac{R^2}{v^2}\right] dv$$

For t large, we can replace the exponential by a series and integrate term-by-term:

$$\Delta\theta(t) = \frac{\dot{Q}}{K\pi^{3/2}} \cdot \int_{v=2\sqrt{\alpha t}}^{\infty} \frac{1}{v^2} \left\{1 - \frac{R^2}{v^2} + \frac{R^4}{2v^4} \ldots\right\} dv$$

$$= \frac{\dot{Q}}{2\pi K} \cdot \frac{1}{\sqrt{\pi\alpha\tau}} \cdot \left| 1 - \frac{R^2}{12\alpha\tau} + \frac{R^4}{160\alpha^2\tau^2} \ldots \right|$$

Now replace $\dot{Q}$ by $\dot{q}(x',y')dx'dy'$ and integrate over A:

$$\Delta\theta(t) = \frac{1}{2\pi K} \cdot \frac{1}{\sqrt{\pi\alpha t}} \cdot \iint_A \dot{\eta}\,(x',y') \left[1 - \frac{(x-x')^2 + (y-y')^2 + z^2}{12kt} + \cdot\right] dx'dy'$$

and we see that the leading term is:

$$\Delta\theta(t) \approx \frac{\dot{Q}_T}{2\pi K} \cdot \frac{1}{\sqrt{\pi\alpha t}} \tag{A6}$$

where $\dot{Q}_T$ is the total rate of surface heating, ignoring the spatial distribution.

For the second term it is convenient to take the origin at the centroid of the heat input distribution, so that:

$$\iint x'\dot{q}\,(x',y')dx'dy' = \iint y'\dot{q}\,(x',y')dx'dy' = 0.$$

We then get:

$$\frac{1}{2\pi K} \cdot \frac{1}{\sqrt{\pi\alpha t}} \cdot \frac{1}{12\alpha t} \cdot \iint \dot{q}\,(x',y') \left[r^2 + x'^2 + y'^2\right] dx'dy'$$

$$= \frac{\dot{Q}_T}{2\pi K} \frac{1}{\sqrt{\pi\alpha t}} \frac{1}{12\alpha t} \cdot \left[r^2 + k_p^2\right] \tag{A7}$$

where $r^2 = x^2+y^2+z^2$; $k_p^2 = \iint \dot{q}(x',y')(x'^2 + y'^2)dx'dy'/\dot{Q}_T$

so that k_p^2 is the "radius of gyration" of the heat input distribution if we interpret $\dot{q}$ as a density and $\dot{Q}_T$ as the mass.

Thus, the leading term describing the temperature rise 'still to come' depends only on the total rate of heat input, and is the same for all locations in the heated body (on the surface or below it!). The next term is of order $t^{-3/2}$ so much smaller when t is large: it depends on a simple overall measure of the size of the heated area, k_p^2: and on the square of the distance from the point considered to the centroid, so that the correction to the leading term is particularly small for compact sources (squares or circles compared to rectangles) and for points near the centre of the source.

Unclassified
SECURITY CLASSIFICATION OF THIS PAGE

REPORT DOCUMENTATION PAGE

Form Approved
OMB No 0704 0188
Exp Date Jun 30 1986

1a REPORT SECURITY CLASSIFICATION Unclassified	1b RESTRICTIVE MARKINGS
2a SECURITY CLASSIFICATION AUTHORITY	3 DISTRIBUTION/AVAILABILITY OF REPORT Approved for public release; distribution unlimited
2b DECLASSIFICATION/DOWNGRADING SCHEDULE	
4 PERFORMING ORGANIZATION REPORT NUMBER(S)	5 MONITORING ORGANIZATION REPORT NUMBER(S) R&D 5305-AN-01
6a NAME OF PERFORMING ORGANIZATION Pembroke College University of Cambridge 6b OFFICE SYMBOL (If applicable)	7a NAME OF MONITORING ORGANIZATION European Research Office USARDSG-UK
6c ADDRESS (City, State, and ZIP Code) Cambridge, CB2 1RF	7b ADDRESS (City, State, and ZIP Code) Box 65 FPO NY 09510-1500
8a NAME OF FUNDING/SPONSORING ORGANIZATION European Research Office USARDSG-UK ARO-E 8b OFFICE SYMBOL (If applicable)	9 PROCUREMENT INSTRUMENT IDENTIFICATION NUMBER DAJA45-86-C-0007
8c. ADDRESS (City, State, and ZIP Code) Box 65 FPO NY 09510-1500	10 SOURCE OF FUNDING NUMBERS PROGRAM ELEMENT NO: 61102A; PROJECT NO: 1L161102BH57; TASK NO: 06; WORK UNIT ACCESSION NO: AR

11 TITLE (Include Security Classification)

(U) Basic Mechanisms of Diesel Lubrication - Correlation of Bench and Engine Tests

12 PERSONAL AUTHOR(S)
Professor A. Cameron Dr J.A. Greenwood

13a TYPE OF REPORT	13b TIME COVERED	14 DATE OF REPORT (Year, Month, Day)	15 PAGE COUNT
FINAL	FROM Dec 85 TO Jan 91	91 MAR 25	226

16 SUPPLEMENTARY NOTATION

17 COSATI CODES			18 SUBJECT TERMS (Continue on reverse if necessary and identify by block number)
FIELD	GROUP	SUB-GROUP	
11	08		(U) Oils, (U) Lubricants, (U) Wear, (U) Friction, (U) Surface
21	07		Roughness, (U) Electrical contact resistance layer
			(U) Temperature effects

19 ABSTRACT (Continue on reverse if necessary and identify by block number)

The lubrication behaviour of a cylinder liner/piston ring contact in a diesel engine has been simulated in a point contact reciprocating rig. When lubricants containing ZDDP additives are used, electrical contact resistance measurements establish that a thick 'reaction film' quickly forms in the rubbed region, protecting the metal surfaces. Electrical capacitance measurements show that the film thickness can vary from 0.1 to 1 μm: the film appears to be a solid organic polymer with a shear strength of 50-100 MPa.

Using segments of diesel engine cylinder liners from various manufacturers in the reciprocating rig, the changes in surface roughness during the running-in process were monitored. The induction time needed for the formation of the reaction film as well as the coherence of the film was studied as a function of load and temperature (in the range 150 - 250°C).

A theoretical analysis of flash temperatures in reciprocating contacts confirms that these are small under the conditions in this rig, so that the measured temperatures are those actually responsible for the reactions.

20 DISTRIBUTION/AVAILABILITY OF ABSTRACT	21 ABSTRACT SECURITY CLASSIFICATION
☑ UNCLASSIFIED/UNLIMITED ☒ SAME AS RPT ☒ DTIC USERS	Unlassified
22a NAME OF RESPONSIBLE INDIVIDUAL Dr. R.E. Reichenbach	22b TELEPHONE (Include Area Code) 071 409 4423
	22c OFFICE SYMBOL AMXSN-UK-RA

DD FORM 1473, 84 MAR 83 APR edition may be used until exhausted
All other editions are obsolete

SECURITY CLASSIFICATION OF THIS PAGE
Unclassified